Mathematical Biology Research Trends

Contributors

Hagit Alon
Gennady Bocharov
Swati DebRoy
S. Dube
Peter Giesl
Zvi Grossman
S. D. Hove-Musekwa
C. Hui
A. Korobeinikov
Tatyana Luzyanina
M. C. Mackey
P. K. Maini
D. G. Mallet
Maia Martcheva
Martin Meier-Schellersheim
Liviu Movileanu
Z. Mukandavire
F. K. Mutasa
G. J. Pettet
Alin Gabriel Popescu
Dumitru Popescu
Dirk Roose
M. Santillán
Robert Sturm
J. M. Tchuenche
Antonio S. Torralba
Heiko Wagner
W. J. Walker
David P. Wilson
Eduardo S. Zeron

Lachlan B. Wilson
Editor

NOVA

MATHEMATICAL BIOLOGY RESEARCH TRENDS

MATHEMATICAL BIOLOGY RESEARCH TRENDS

LACHLAN B. WILSON
EDITOR

Nova Science Publishers, Inc.
New York

LIBRARY OF CONGRESS CATALOGING-IN-PUBLICATION DATA

Mathematical biology research trends / Lachlan B. Wilson (editor).
p. cm.
ISBN 978-1-61668-394-8 (E-Book)
1. Biomathematics. I. Wilson, Lachlan B.
QH323.5.M36373 2007
570.1'51--dc22 2007047433

Published by Nova Science Publishers, Inc. ✣ New York

CONTENTS

PREFACE

Applying mathematics to biology has a long history, but only recently has there been an explosion of interest in the field. Some reasons for this include: the explosion of data-rich information sets, due to the genomics revolution, which are difficult to understand without the use of analytical tools, recent development of mathematical tools such as chaos theory to help understand complex, nonlinear mechanisms in biology, an increase in computing power which enables calculations and simulations to be performed that were not previously possible, and an increasing interest in in silico experimentation due to the complications involved in human and animal research. Applying mathematics to biology has a long history, but only recently has there been an explosion of interest in the field. Some reasons for this include: the explosion of data-rich information sets, due to the genomics revolution, which are difficult to understand without the use of analytical tools, recent development of mathematical tools such as chaos theory to help understand complex, nonlinear mechanisms in biology, an increase in computing power which enables calculations and simulations to be performed that were not previously possible, and an increasing interest in in silico experimentation due to the complications involved in human and animal research.

Chapter 1 presents mathematical models of infectious disease transmission, which add a new dimension of information to assist in public health policy for disease control. They are useful for understanding complex nonlinear systems of transmission and to predict future epidemic trajectories based on different intervention or resource allocation strategies. The science of mathematical and computational population biology that advances this understanding uses various forms of models that vary from deterministic compartmental models, to stochastic models, to dynamically evolving contact networks between individuals. All models require realistic detail and realistic parameter values. For practitioners in this field to make a real-world difference and influence public health policy, policy-makers and/or medical experts must be consulted or heavily involved to ensure realism of model structure and most importantly appropriate parameter estimates. Detailed mathematical analyses are generally of very little real-world importance but uncertainty and sensitivity analyses are a highly under-developed component of current models and must be utilized to a much greater extent (such methodology is clearly presented here in a manner for implementation by any quantitative practitioner). Instead of bringing specific quantitative tools to the research arena, one should determine the important research questions in need of investigation and then use (or obtain) the necessary tools to address the specific key research issues. Additionally, the incorporation of data analysis tools within mechanistic causal models is also important for

future innovative modeling in this field. Above all, the clear and powerful presentation of results in various forms, including effective communication to disseminate results to key authorities, is essential if modeling is to be used insightfully and influentially in designing (or changing) policy decisions.

The theory of metabolism can be subdivided in two main fields: dynamic theory and structural theory. Dynamic theory attempts to produce a description of the systemic dynamic behavior from as little experimental information as possible. Structural theory provides ways of decomposing complex networks in ways that reveal inherent functional relationships between the parts of the system. Since metabolic systems function out of equilibrium, due to the permanent input of material and energetic fluxes, dynamic theory has to deal with non-linearities. On the other hand, structural theory analyses the null-space of a matrix of relationships (usually, the stoichimetric matrix, giving rise to stoichiometric analysis) and therefore it belongs to either linear or convex analysis. Chapter 2 provides a new dynamic theory that generalizes some others, such as Metabolic Control Analysis (MCA) and Biochemical Systems Theory (BST), to time-varying external fluxes of any form, and provides a straighforward way of connecting the non-linear dynamics of metabolic systems to their stoichiometric structure, by means of a set of new properties. In particular, the non-linear response is described in terms of a generalized perturbation theory whose main coefficients are the susceptibilities (much in the same way as in non-linear optics). These coefficients are time-dependent (on one or more perturbation times) and become translationally invariant in time as the system approaches a steady state (the main realistic state of metabolic networks, apart from oscillatory behavior). Hence they can be integrated into constant coefficients, the responsivities, that provide a set of constrains connecting the dynamics and the stoichiometry of the network. As a consequence, the number of stoichiometric degrees of freedom can be reduced because of the dynamics of a specific system. This result, is illustrated by means of examples. The theory presented herein falls in the field of functional analysis, since the susceptibilities are functional derivatives of the response with respect to complete time-courses of the input fluxes, which work as the excitations of the metabolic network and can be manipulated in experiments. Hence, the constraints provided by the theory should help simplify highthroughput experiments.

In Chapter 3, the authors develop a mathematical model describing the haptotactic migration of cells in a pre necrotic avascular tumour. Initially, the model which involves a moving boundary is developed for general three dimensional geometry and then modified for the specific multicell tumour spheroid geometry. A full nondimensionalisation is performed and the model is mapped to a fixed domain to facilitation numerical simulation. Numerically calculated solution profiles are then presented to provide predictions of the behaviour of cells in pre necrotic multicell tumour spheroids. Attention is paid to both passively migrating cells, and cells that respond to gradients in a simultaneously constructed extracellular matrix that is, cells that migrate haptotactically. The model solutions are used to propose biologically relevant hypotheses about the behaviour of cells in pre necrotic avascular tumours and the extracellular matrix in which they reside.

Cholera is a gastrointestinal disease caused by a gram negative coma shaped bacterium of the genus *Vibrio cholerae*. It is often associated with poor hygiene of drinking water, food preparations and waste disposal particularly feaces. It rapidly causes diarrhea, vomiting and dehydration which could be fatal if not medically attended to timeously. The

diarrhea is caused by a toxin produced by the bacterium. This toxin causes the efflux of salts and water into the gastrointestinal tract. Cholera as a disease is a serious public health problem in the developing world, and since the first recorded cases, it has spread rapidly across continents, resulting in numerous deaths. The aim of Chapter 4 is to use mathematical modeling to analyze the dynamics of this disease with and without treatment. Thus, the authors present a single-season deterministic model for cholera transmission dynamics with carriers in a human population and a pool of pathogens. The mathematical features such as the epidemic threshold, equilibria and stabilities are determined. A Lyapunov functional approach is used to analyse the stabilities of equilibria. The authors qualitatively analyse positivity and boundedness of solutions. In the absence of treatment, the trivial equilibrium is shown to be a saddle, while the two biologically meaningful equilibria, namely the disease-free is globally asymptotically stable provided certain conditions are met, and the endemic equilibrium state is only locally stable. The epidemic threshold is used to assess the effectiveness of treatment in controlling cholera in a community. Conditions for cholera containment and persistence are derived using comprehensive analytical and numerical techniques. It is shown from the study that treatment of cholera sufferers reduces the burden of the disease in the community. Further, it is also shown that as long as the pathogen is present in the environment, it will be difficult to eradicate cholera and the existence of carriers may remain a challenge in the control of the epidemic in settings with treatment of cholera sufferers.

The functioning of the immune system involves tightly regulated proliferation, differentiation and death processes of heterogeneous cell populations, including T lymphocytes, B lymphocytes, antigen presenting cells, etc. To quantify the turnover kinetics of specific subsets of immune cells under normal conditions and during infections, labeling techniques (e.g., with fluorescent markers CFSE or BrdU) in conjunction with flow cytometry analysis (FACS) are used in experimental and clinical immunology. To obtain information about the kinetic structure of the cellular responses of heterogenous cell populations from data that in addition to experimental fluctuations (noise) exhibit considerable variation between different study animals, careful computational analysis is needed. The primary objectives of Chapter 5 are: (i) to introduce mathematical models in the form of hyperbolic partial differential equations (PDEs) which allow direct reference to single or double label histograms of cell distributions, (ii) to illustrate the potential of the modeling and parameter identification technology by representative examples from CFSE and BrdU labeled T cell proliferation studies, and (iii) to compare the proposed PDE models with alternative modeling approaches which are based upon the use of ordinary differential equations.

In Chapetr 6 the authors review a number of immunological models of HIV as well as the contribution of mathematical immune modeling of HIV to understanding of HIV. The authors also review a number of epidemiological models, particularly those of HIV. The focus of this review is the development of novel immuno-epidemiological models which link immunological and epidemiological models. The authors first review a simple immunoepidemiological model of transient disease (a disease where infected individuals necessarily recover), and then they introduce an immuno-epidemiological model of HIV. The authors discuss the drawbacks of this simple immuno-epidemiological model as well as methods to address them. They introduce and discuss several other models and their advantages and disadvantages. In the discussion the authors focus on the types of questions

that can be addressed with immuno-epidemiological models and how those can contribute for the development of mathematical biology.

As presented in Chapter 7, the development of physical and mathematical models dealing with the deposition and bronchial clearance of aerosol particles in the human respiratory tract has its origin in the 1970s. Theoretical approaches of this time were usually based on an airway geometry being either approximated by a sequence of straight cylindrical tubes or by a single, variable cross-section channel resembling a trumpet shape. The branching network of lung airways was initially described by a fully symmetrical tree structure (e.g. Weibel's lung model A), within which tubes of the same airway generation were characterized by identical geometric parameters (i.e. diameters, lengths, branching and gravity angles). As a further consequence of this symmetry pathways leading from the trachea to the closing alveolar sacs consisted of the same number of tubes, representing a remarkable simplification for the simulation of deposition and clearance scenarios.

In reality, the human tracheobronchial tree is marked by a significant asymmetry due to the variation of airway geometry within a given generation. Since the end of the 1970s and the early 1980s increased attention was paid to this important fact by the construction of a five-lobe lung model, where intrasubject variation of bronchial geometry was still limited to the first three or four bifurcations. A better approach of the variability of airway properties took place by the formulation of a stochastic model of the human respiratory tract in the middle of the 1980s. With this model both asymmetry and randomness could be well approximated on the basis of available morphometric data. In addition, computation of deposition and bronchial clearance was improved due to a variation in the number of bifurcations leading from the proximal to the distal end of the bronchial pathway.

Currently, stochastic lung models represent the state of the art in simulating deposition and clearance of inhaled particles. In recent years, computation of particle deposition was successively refined by numerical approaches, enabling the determination of exact particle trajectories within single, double, and triple bifurcations. Bronchial clearance was improved by generation-specific variations of mucus thickness and mucus production, causing a remarkable variability of mucus velocity. Additionally, slow bronchial clearance mechanisms were defined, with the help of which particle residence times > 24 hours could be explained.

Chapter 8 starts by introducing a brief review of the history of interdisciplinary research in biology, as well as some of basic concepts from molecular biology. Then, the authors present a survey of the philosophy and goals of a new area of interdisciplinary research: systems biology. Finally, the authors review their efforts of the past few years to understand, via mathematical modeling, the dynamic behavior of one of the most studied gene regulatory networks in bacteria: the tryptophan operon, and offer new results.

In Chapter 9 the authors consider the impacts of two factors, namely the form of the nonlinearity of the infectious disease transmission rate the and mortality associated with a disease, on the dynamics of this infectious disease in a population. The authors consider a very simple discrete-step compartment epidemiological models and a very general form of the nonlinear transmission assuming that the transmission is governed by an arbitrary function constrained by a few biologically feasible conditions. The authors show that when the population size can be considered constant, these models exhibit asymptotically stable steady states. Precisely, the authors demonstrate that the concavity of the disease transmission function with respect to the number of infective individuals is a sufficient condition for this

stability: in this case the models have either an unique and stable endemic equilibrium state, or no endemic equilibrium state at all; in the latter case the infection-free equilibrium state is stable.

The authors demonstrate that under some circumstances the mortality inflicted by the disease is able to destabilise endemic equilibrium state and can lead to a supercritical Hopf bifurcation in the system. However, it appears that for the majority of human infections the threshold for this bifurcation is too high to be realistic.

Human and animal locomotion represent a highly complex control problem. Internal and external disturbances increase these difficulties to maintain or achieve stability in static and dynamic situations. Two kinds of stability can be distinguished: on the one hand the stability is achieved by reflexes and control with neural feedback, and on the other hand stability is based on mechanical properties and the geometrical configuration of muscles and tendons within the musculoskeletal system. The present article is mainly interested in the latter one, which is called selfstability. Biological systems adapt the pure mechanical properties of muscles and passive structures to support stability and to cope with disturbances. In the following, the authors mainly restrict ourselves to one joint with a pair of antagonistic muscles; in particular, the authors will focus on the human elbow joint. The authors describe the most important mechanical properties of muscles and summarize them in a model of a general joint with antagonistic muscles. This model is a system of ordinary differential equations for the joint angle and its angular velocity.

If the antagonistic muscles are activated in a certain relation, then the joint is in an equilibrium state. The definition of stability in the mathematical sense is given using the framework of dynamical systems. The eigenvalues of the linearization at the equilibrium give a detailed characterization of solutions near the equilibrium: real and complex eigenvalues lead to qualitatively different behavior of solutions, and the absolute value of their real part tells us how fast the equilibrium state is approached after a small perturbation.

Can the authors quantify the stability of an equilibrium point? The authors would surely assume the equilibrium point to be the “more stable” the larger its basin of attraction is. The basin of attraction consists of all perturbations which are led back to the equilibrium. Is an equilibrium also the “more stable” the faster small perturbations are corrected? The mathematical analysis will show that the answer depends on the situation.

Besides an overview over the problems and results of mathematical stability analyses in biomechanics, in Chapter 10 the authors apply the theory to a specific situation. More precisely, the authors consider a waiter holding a glass of water. The task is not to spill the water in the glass under perturbations. The question is, whether less water is spilled by a high or a low co-activation of the elbow muscles. The mathematical analysis will show that the answer depends on the position of the upper arm.

There is a great interest for a mechanistic understanding of molecular transport across biological and reconstituted membranes due to its potential applications to the development of news methodologies in medical biotechnology, such as gene therapy and drug delivery. In the first part of Chapter 11, the authors present the behavior of the liposomes under osmotic stress. Because of the mechanical tension induced by osmotic flow, the liposomes expand, triggering transient lipidic pores that fluctuate at the nanoscopic level until their death. The authors report here that this is a periodic process. Such a liposome, also called a pulsatory liposome, is characterized by the number of successive pores, the time interval between two successive pores, and the amount of exchanged material through a single transmembrane

pore. The diffusion of water through the liposomal membrane is analyzed in detail. In the second part of this paper, the authors develop a theoretical model for analyzing experimental data, facilitating information about the diffusion and exchange through spherical interfaces. The effects of experimental parameters, including the bilayer stiffness and the viscosity of the internal fluid, are analyzed and discussed as well.

SHORT COMMUNICATION

In: Mathematical Biology Research Trends
Editor: Lachlan B. Wilson, pp. 3-6
ISBN: 978-1-60456-141-8

BIOLOGICAL COMPLEXITY BY NATURAL SELECTION AND SELF-ORGANIZATION: A GAME OF SURVIVAL

C. Hui
Centre of Excellence for Invasion Biology,
University of Stellenbosch

Since the beginning of biology, a debate has existed between selectionists and neutralists. Fisher (1930) formulized Darwin's idea of natural selection and proved that the fitness of a species will be maximized in a pure-line population. This is equivalent to saying that if the natural selection really happens along billions of years of evolution, polymorphism in species will cause genetic load and therefore should be rare in nature. Counter-intuitively, this is not the case. Haldane (1930) and Wright (1930) at the same time criticized Fisher's arguments by the prevalence of polymorphism in species. According to the neutral theory (Kimura 1983), natural selection is almost futile at the molecular level as most genes are neutral in terms of the fitness of an organism. The result of this debate was the compromise on the unit of natural selection, i.e. at the individual level (although later a theory of group selection also emerged), and further put Darwin's evolution through natural selection into an awkward situation. However, allowed me to postulate: merging of functioning clusters of DNA sequences (gene) could be through the self-organization formed by the positive feedback between its products (protein) and the gene (or other genes) [proteins help genes to make proteins]. This co-evolved process (positive feedback) between particular DNA and protein could be interlinked with other similar processes and self-organized together forming a higher level of complexity, i.e. life itself.

At a larger scale, a similar story was retold. Clements (1916) asserted that under disturbance a community can converge onto a single, stable, mesophytic equilibrium (monoclimax), which determined by the regional climate (a superorganism). In other words, succession in an ecosystem is a universal, orderly process of progressive change. The real king will eventually return. Patten (1971) also regarded the ecosystem as an evolutionary entity. Gleason (1926) rejected this superorganism idea by an individualistic view. Egler (1954) rephrased this individualistic as this: succession is on a high level of sociologic integration, not a matter of individual species, i.e. a (instead of 'the') king will come. Drury

and Nisbet (1973) indicated that the first steps toward theories of succession should be based directly on properties of organisms, rather than emergent properties of ecosystems. My question is: (A) does a community (or an ecosystem) have its own identity or is it just a concoction of millions of individuals with thousands of species? (B) How can we test such an argument?

To test whether a community is a functioning team or a mere conglomerate, two ways lie ahead. One is to judge by its consequences, i.e. the macroecological patterns generated. MacArthur and Wilson (1967) found that the species-area relationship on islands can be largely explained by a colonization-extinction process. Hubbell (2001) also showed the extreme closeness of the abundance rank curve in a neutral community to a real one. Range size distribution and many other patterns in macroecology have found their enlightenments in the neutral theory. However, Tilman (2004) argued that the niche theory (the beloved son of natural selection in ecology) can also perform realistic patterns in community. The debate has far from ended.

The other way to test the 'meaning' of a community has an obvious application in conservation, especially under the pressure of globalization. These early studies identified the characters of a 'pioneer' species as those with great seed production, high speed mobility, high light requirements (for plants) and ability to tolerate disturbed environments, high colonizing and dispersal ability, an opportunist, or a fugitive. All these characters fit the description of a perfect invader, i.e. for an alien species to establish and expand in an endemic community. According to Clements' superorgansim theory, an alien species that has the same trait (or function) as an endemic species will be difficult to invade due to the resilience (or competitive exclusion). Yet, Gleason's and Hubbell's neutral theory implies that an alien species with a similar niche as some endemic species will be easy to invade with the help of disturbance. We can only find out which one is true at the future synthesizing stage of invasion biology.

As far as I am concerned, two processes play an important role in the shaping and emerging of biological patterns (or complexity): natural selection and self-organization. Translated into ecology, these two processes become the niche and the neutral theory. Of course, to observe such a biological pattern, statistic artifacts and sampling prejudice come in and make a picture through our lenses. Like making a movie, the niche theory (natural selection) decides who will be the actors and what role (function) each actor will play. The neutral theory (self-organization) decides what kind of story they will tell and organizes species in a certain way to generate the community pattern. Statistic artifacts and sampling prejudice suggest that each one will have different feelings or responses to the movie. However, let's forget those artifacts and prejudice for a while and only focus on the real patterns beneath.

There are five hierarchies of biological complexity. First, from biochemistry (physics) to life (self-organized replicating molecular system). Natural selection chooses which functioning clusters (of molecules) should interlink or compete with each other. Self-organization (such as crystal formation and reproduction) holds different functioning clusters together and generates the basic "self-replicating" character of life systems. Although the evolution of genetic code (DNA and RNA) and the emerging of advanced function in unicellular organisms could be far more complicated, the key process could be captured by natural selection and self-organization. Second, from simple life unit (cell) to organism. Will a self-organized cell clusters have a greater selection advantage than a single cell? Organism

development and metabolic allometry provide a possible start. Third, the population formation, its behavior and culture. Natural selection surly becomes an obvious process at this level. Behavior, such as altruism, and culture can be formed through ecological imprints and niche construction, accompanied by particular spatial patterns in time and in space. Fourth, speciation and the formation of a community. The species concept is crucial to the study of the evolution of complexity and biodiversity. The ecological interactions, such as resource competition, predation and migration (or dispersal) play an important role in the process of speciation. Meanwhile, evolutionary processes, such as mutation and gene drift, also affect this process. A community could be the necessary consequence of the speciation and ecological process (the evolutionary equilibrium might not be achieved in community). The boundary of a community could be just an artifact, as a community only generates patterns, without a clear function. Finally, the formation of ecosystem function and the self-containing of the whole biosphere. Individuals and species in the community are entangled with all kinds of biological interactions, which give rise to the new properties at the ecosystem and global level. Ecosystem service supports each species (including humans). The earth living system can self-sustain itself (Gaia theory). Energy and matter (such carbon cycle) flow in-and-out and interact with the abiotic sphere on earth. This is the final level of biological complexity.

I would like to end here by describing a game of survival. It simplifies the coevolved biological system by natural selection and self-organization. The game starts with twelve people who don't know each other. During one week of living together (on an isolated island), each one comes to know the others in terms of their personality, common interests, etc. Therefore, friendship begins to make clusters and divisions in these twelve people (a process of self-organization). At the end of each week, one person will be voted out (a process of natural selection), as each one plays double roles in the game, an actor and a judge. Guess who will win in the end. This game perfectly captures the essential characters of an adaptive (or a co-evolved) biological system. If it's a closed system, there will be only one who finally wins the game. Can we predict who will be? If it's an open system (i.e. each week we add a new person in the game), can you predict who will be there after many weeks? It is surly not a random game, but its direction (destiny) is an unfolding one.

References

Clements, F. E. (1916). *Plant succession: an analysis of the development of vegetation*. Washington: Carnegie Institute.

Drury, W. H. & Nesbit, I. C. T. (1973). Succession. *Journal of Arnold Arboretum,* **54**, 331-368.

Egler, F. E. (1954). Vegetation science concepts. I. Initial floristic composition – a factor in old-field vegetation development. *Vegetatio,* **4**, 412-417.

Fisher, R. A. (1930). *The genetical theory of natural selection*. Oxford: Clarendon.

Gleason, H. A. (1926). The individualistic concept of the plant association. *Bulletin of the Torrey Botany Club,* **53**, 1-20.

Haldane, J. B. S. (1930). A note on Fisher's theory the origin of dominance and linkage. *American Naturalist,* **64**, 87–90.

Hubbell, S. P. (2001). *The unified neutral theory of biodiversity and biogeography*. Princeton: Princeton University Press.

Kimura, M. (1983). *The neutral theory of molecular evolution*. Cambridge: Cambridge University Press.

MacArthur, R. H. & Wilson, E. O. (1967). *The theory of island biogeography*. Princeton: Princeton University Press.

Patten, B. C. (1971). *Systems analysis and simulation in Ecology, Vol. I.* New York: Academic Press.

Tilman, D. (2004). Niche tradeoffs, neutrality, and community structure: a stochastic theory of resource competition, invasion, and community assembly. *Proceedings of the National Academy of Sciences USA,* **101**, 10854-10861.

Wright, S. (1930). The genetical theory of natural selection. *Journal of Heredity,* **21**, 349–356.

RESEARCH AND REVIEW STUDIES

In: Mathematical Biology Research Trends
Editor: Lachlan B. Wilson, pp. 9-54
ISBN: 978-1-60456-141-8

Chapter 1

EPIDEMIOLOGICAL MODELING FOR THE REAL WORLD

David P. Wilson*
National Centre in HIV Epidemiology and Clinical Research, Faculty of Medicine
University of New South Wales, Sydney, Australia

Abstract

Mathematical models of infectious disease transmission add a new dimension of information to assist in public health policy for disease control. They are useful for understanding complex nonlinear systems of transmission and to predict future epidemic trajectories based on different intervention or resource allocation strategies. The science of mathematical and computational population biology that advances this understanding uses various forms of models that vary from deterministic compartmental models, to stochastic models, to dynamically evolving contact networks between individuals. All models require realistic detail and realistic parameter values. For practitioners in this field to make a real-world difference and influence public health policy, policy-makers and/or medical experts must be consulted or heavily involved to ensure realism of model structure and most importantly appropriate parameter estimates. Detailed mathematical analyses are generally of very little real-world importance but uncertainty and sensitivity analyses are a highly under-developed component of current models and must be utilized to a much greater extent (such methodology is clearly presented here in a manner for implementation by any quantitative practitioner). Instead of bringing specific quantitative tools to the research arena, one should determine the important research questions in need of investigation and then use (or obtain) the necessary tools to address the specific key research issues. Additionally, the incorporation of data analysis tools within mechanistic causal models is also important for future innovative modeling in this field. Above all, the clear and powerful presentation of results in various forms, including effective communication to disseminate results to key authorities, is essential if modeling is to be used insightfully and influentially in designing (or changing) policy decisions.

* E-mail address: Dwilson@nchecr.unsw.edu.au; Ph: +61 2 9385 0896; Fax: +61 2 9385 0920

1. Brief History of Epidemic Modeling for Public Health

The application of mathematics to the study of infectious disease was initiated by Daniel Bernoulli in 1760, presented at the Royal Academy of Sciences in Paris [1]. Aiming to influence public health policy, he used mathematical techniques to evaluate the potential effectiveness of universal variolation against smallpox [1, 2]. Smallpox was widespread in many parts of Europe where it affected a significant proportion of the population, accounting for large death rates. Bernoulli used Edmund Halley's Life Table 'data' [3] for expected survival (including smallpox mortality) along with his equations to calculate the number of people surviving if smallpox was eradicated. He showed that universal smallpox inoculations would lead to an increase in life expectancy from a mere 26.5 years at the time, during the endemic smallpox epidemic, to approximately 30 years [1, 2]. He was far ahead of his time in terms of utilizing quantitative techniques, and specifically mathematical modeling, to influence public health policy [2, 4]. After Bernoulli, only rare instances of similar techniques were employed (for example, in 1840 William Farr fitted a normal curve to smoothed quarterly data on deaths from smallpox in England and Wales over the period 1837-1839 to track the progress of the epidemic [5]). From the time of Bernoulli it would be approximately 150 years before any significant progress was made in this field. It was not until 1906 that conceptual ideas started to be considered that would form the basis of modern mathematical epidemiology. At that time, Hammer postulated that the course of an epidemic depends on the rate of contact between susceptible and infectious individuals [6]. This notion has become one of the most important concepts in population biology; it is the mass-action principle (sometimes called pseudo-mass action) in which the net rate of spread of infection is assumed to be proportional to the product of the density of susceptible people multiplied by the density of infectious individuals. The law of mass-action was already widely applicable in many areas of science and goes back at least as far as Boyle (*c*. 1674) in the theory of reactant materials in chemistry. The mass-action concept was used by Kermack and McKendrick in 1927 who began to provide a firm theoretical framework for the investigation of observed patterns of the course of an epidemic [7]. Kermack and McKendrick's framework has evolved to become the classic SIR model for studying population biology, and their framework could be considered the birth of modern mathematical epidemiology. The interested reader could refer to Bailey [8] or Anderson & May [9] for more on the development of mathematical frameworks for the spread of epidemics.

In most sciences, research questions are answered from planned repeated experiments. But for infectious diseases, experimenting in communities is not ethical or possible in many instances. Instead, we rely on retrospective epidemiologic data which are neither timely nor capable of predicting future outcomes. Mathematical models for transmission of infection are the most sophisticated and useful tools to aid policy formulation, and have been repeatedly proven to be accurate (although not always). They add a new dimension of information to the control of communicable diseases and provide a dynamic picture of disease transmission. The complex nonlinear systems of epidemics can be understood by models that contain explicit mechanisms linking individual-level behaviors with population-level outcomes (such as incidence and prevalence). These models are used to forecast disease epidemics and trends in disease transmission under various intervention scenarios, and therefore they are highly relevant to planning vaccination programs and predicting the behavior of other interventions

at the population level. Epidemic trajectory forecasting has been particularly used in HIV where the models have been used with varying success [10-16]. The increased trust and popularity of modeling is illustrated by the fact that the World Health Organization responded to the SARS outbreak in 2003 by calling on leading mathematical modelers from the UK to help determine optimal control strategies. Currently, mathematical modelers are key committee members for countless government and other institutions (such as the World Health Organization, the United States Center for Disease Control, the Central Intelligence Agency, etc.). Potential bioterrorism, emerging infectious diseases, current localized and global endemic epidemics, and many more public health problems are being addressed by real-world biomathematical modelers (e.g., [17-27]). Public health decisions, for a wide variety of diseases (e.g., [9, 28-34]) are being made as a direct result of mathematical models of disease transmission. Any discussion of public health policy should include careful evaluation of potential risks. The utility of modeling in public policy is most evident when costs and benefits require balancing or when it must be decided how to focus and administer resources; a tradeoff between positive and negative outcomes in such decision making makes the modeling process more important, and indeed much more interesting in estimating when such potential risks could outweigh the benefits.

Our field owes a lot of the acceptance by the health and medical community over the last few decades to the modern 'godfathers' of the field, Anderson and May. Anderson and May were prominent in effectively bridging the gap between theoretical models and the health/medical/policy communities, bringing about greater insight and influencing change with their models [9, 35-37]. They are still very active in the scientific community. Their influence has spread to other renowned researchers that are not only bridging communities, but making great strides of influence into the mainstream scientific arena. Most notably amongst the more applied modelers are Blower and Garnett (but there are many others). There are various other key 'players' (many of whom are cited in this chapter) and on their theoretical and applied foundations will disease transmission modeling continue to advance and provide bases for more informed influences in health policy decisions.

2. Epidemic Modeling Approaches

2.1. Deterministic Models

In the approach of deterministic models all individuals in the population of interest are generally segmented into various compartments, related to risk factor, disease, or immunological status etc. Schematic flow diagrams illustrate the possible movement of people from one compartment to another. Approximations to the true, integer-valued numbers of individuals involved in an epidemic, allow the derivation of difference or differential equations governing the process to describe this movement and track the number of people in each population segment as a continuous variable over time. If changes in the model population occur as a smooth continuous process then differential calculus is employed, whereas discrete models reflect the change over an entire time step. The interactions allowing the spread of infections occur continuously and so most models are usually continuous. Infection outcomes in these models are not subject to randomness, thus they are "deterministic"; the system develops according to laws similar to those for dynamical

systems. The results of a deterministic process are approximations to the mean of a random process. Mathematical analysis of these underlying stochastic processes that lead to appropriate differential equation models is well illustrated by Diekmann & Heesterbeck [38].

The classical (but still highly relevant) Kermack-McKendrick SIR model [7] considers the total population to be taken as constant, and attempts to describe the spread of infection in a population as a function of time when a small group of infected individuals is introduced. A simple early version of the SIR model is constructed by considering a disease which, after recovery, confers immunity (or if lethal, includes deaths – but dead individuals are still counted). The host population is divided into 3 classes of individuals, namely, susceptible (*S*) who can catch the disease, infected (*I*) who have the disease and can transmit it, and recovered (*R*) who have had the disease and recovered, immune, or isolated from (re)infection. The progress of individuals is schematically represented in Figure 1.

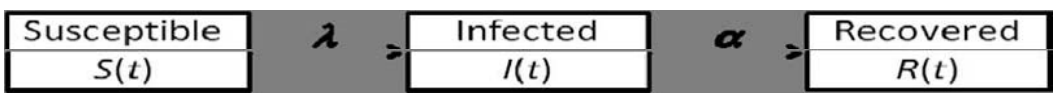

Figure 1. Schematic flow diagram of the simplest form of the SIR model.

This translates into the differential equations:

$$\frac{dS}{dt} = -\lambda S$$

$$\frac{dI}{dt} = \lambda S - \alpha I$$

$$\frac{dR}{dt} = \alpha I ,$$

where the 'force of infection', $\lambda = \beta I$, is the rate at which susceptible people become infected (β is the overall transmission probability per infected person and includes contact rates), and α is the rate of recovery. An SIR model incorporating births and deaths was formulated in 1929 by Soper [39] and extended in 1932 by Kermack and McKendrick [40]. The SIR model and variations of the model have been studied very extensively (for example, [41-43]).

The number and type of categories in these types of models depends on the disease. Usually the modeling process commences, as is demonstrated simplistically above with the SIR model, with the drawing of schematic diagrams to reflect the biology of the particular epidemic and disease progression in infected individuals. Then, differential equations are written to describe the rate of change in the number of people in each compartment. There are countless examples of models in the literature that are based on these approaches. Since this section is not a textbook chapter on developing such models but an overview of the commonly-used approaches, further information and detail will not be provided. Straightforward descriptions of how to construct simple compartmental deterministic models

can be found elsewhere (e.g. [32, 38, 41]). Although individual-level elements are not specifically tracked in these models, individual-level issues must be incorporated in the equations for consistency, especially for sexually transmitted models (for example, balancing the number of male/females partnerships if it is a heterosexual model, including assortative/disassortative partnership mixing, sex budgets, patterns of sexual behavior, and transmission probabilities as they relate to the number of acts and types of protection etc. [9, 44-56]).

2.2. Stochastic Models

The spread of an infectious disease is a random process. In a small group of people in which one has a cold, such as in a classroom or a family, some will become infected while others will not. When the number of individuals is very large, it is customary and most appropriate to characterize the infection process deterministically, but deterministic models are unsuitable for small populations. Stochastic models entered the epidemic modeling arena around the same time as deterministic models (e.g., [39, 57]). The most influential early model was the chain binomial model of Reed and Frost, presented in 1928 but not published until later and was described by others [58-60]. The evolution of this epidemic process is stochastic in the sense that randomness is incorporated and different epidemic trajectories will result from the same initial conditions.

The Reed-Frost model is based on the assumption that, in a group of S_t susceptible people and I_t infected people at times $t = 0,1,2,\ldots$, infection is based on 'adequate' contact of an infectious (infected) person with a susceptible person in a relatively short time interval $(t, t+\Delta t)$ at the beginning of each period. Discrete-time models are appropriate if the infectious period is relatively short in comparison to the latent period, with the latent period as the unit of time. The newly infected individuals I_{t+1} will themselves become infectious in $(t+1, t+1+\Delta t)$, while the current number of infected people I_t will then be removed. Each susceptible individual is assumed to independently have the same probability, p, of not making adequate contact with any one given infected person, or p^{I_t} of not making adequate contact with any of the I_t infected people during $(t, t+\Delta t)$. Therefore, the probability of infection for each susceptible is $1-p^{I_t}$. Assuming independence of each susceptible, the probability that there will be I_{t+1} infected people at time $t+1$ is taken to be the binomial probability:

$$P\left\{S_{t+1}, I_{t+1} \middle| S_t, I_t\right\} = \binom{S_t}{S_{t+1}} \left(1-p^{I_t}\right)^{I_{t+1}} \left(p^{I_t}\right)^{S_{t+1}},$$

where $S_t = S_{t+1} + I_{t+1}$. The structure of an epidemic model path is then

$$\chi = P\left\{S_1, I_1 \middle| S_0, I_0\right\} P\left\{S_2, I_2 \middle| S_1, I_1\right\} P\left\{S_3, I_3 \middle| S_2, I_2\right\} \ldots,$$

that is, the product of a chain of binomials.

The famous Kermack-McKendrick deterministic model was formulated into its general stochastic analog by Bartlett in 1949, and since that time the number of stochastic models has increased very rapidly and become highly popular (see [61, 62] for reviews of such epidemic models). There are numerous ways to allow the events in a stochastic model to be influenced by chance, but the most common approach is Monte Carlo simulation. Here, the possible events that could occur are defined with probabilities associated with them. Random number generators calculate when events will occur and which of the possible events will occur next [63]. These stochastic models allow an exploration of the ability of a model to explain certain observed patterns, with a single set of parameter estimates. Further, stochastic models in continuous time are an extension of the simple discrete time models, in which the main features of the deterministic epidemic model in continuous time also hold. Normally the processes involved are simplistically assumed to be Markovian. The reader is referred to other sources for a description of this approach [64-70].

2.3. Other Approaches

An important distinction in modeling of infectious diseases is whether the population is represented by various compartments with rates of progression through the different compartmental states or whether individuals and their contacts are explicitly tracked; these are the two extremes of model approaches. Discrete individuals rather than continuous populations are the basic units of analysis in individual-level models. Based on a distribution of properties for each person, stochastic events are simulated. As an extension, network models posit fixed relationships during which contacts that transmit infection occur. In the simplest of network models, every individual has a fixed number of linkages to other individuals, and contacts that can transmit infection occur within those linkages at a constant rate. Tracking individuals provides a potentially powerful tool in which microstructures of the dynamic network of contacts is included through which infections spread [71-76]. This could provide a more thorough identification of risks for acquiring and also transmitting infection. Analysis of network models is yielding basic theory just like the basic theory of deterministic compartmental models [77-79]. One example of the new concepts coming out of network models is that of partnership concurrency or the existence of simultaneous linkages with multiple individuals in which transmission can occur. This concept is foreign to deterministic compartmental models. Concurrency of partnerships has been shown to be highly important [73, 80]. Another important effect captured by network models that is not captured well by compartmental models is the influence of social networks that can have powerful effects on the speed and extent of infection dissemination in a population [81]. However, the potential of this approach can rarely be achieved, and if it actually can it is unlikely to be in a timely and meaningful fashion. The quality of data on network structures will always be limited and biased. It is also extremely difficult to identify and to obtain parameter values for individual-level network models.

There is no restriction on the type of approaches that can be used. Quantitative techniques have been applied to a very diverse set of applications in other fields. There is no reason why many of these techniques cannot be brought across into infectious disease epidemiology if they will adequately represent the specific problem and context in question. For example, Kaplan and colleagues have used a variety of methods, such as operations research and economic modeling, to address diverse and important infectious disease transmission questions [19, 27, 82-86]. Operations research techniques have also been applied to important resource allocation problems in HIV research [87-89]. The discipline of operations research incorporates mathematical modeling, statistics, queuing theory, decision analysis, and computer science and are usually used in contexts to optimize profit, output, or performance of operations within an industry, production line, or organization [90-92] but can be extended to dynamic optimal control problems associated with disease [93-95]. Nonlinear and dynamic programming [96] are among the techniques often used in optimization [97, 98]. These numerical methods are appropriate in many real-world problems that cannot be solved analytically as they contain non-linear dependencies and the problems often have various constraints that must be taken into consideration. Adopting operations research approaches is one of the most exciting developments in quantitative population biology and epidemiology. Game theory has also been used in recent years and has provided valuable and interesting insights, especially in terms of vaccination strategies [99-101]. This is another approach that could be utilized more frequently. Problems can be simplified and investigated with risk equations [102]. There is no limit in the diversity of innovative methods that can be extended in the field of quantitative epidemiology or introduced to the field, but new angles at looking at interesting problems can sometimes be restricted by practitioners. Instead of bringing specific quantitative tools to the research arena, one should determine the important research questions in need of investigation and then use (or obtain) the necessary tools to address the specific key research issues. Look at important problems from novel perspectives; for example in geographical models of disease, instead of modeling the conventional spatial diffusion of disease, model the spatial diffusion of treatment to the locations of disease [88]; be creative and willing to go outside conventional boxes and develop new approaches that will be most appropriate to address the most interesting and important research questions.

2.4. Which Approach Should Be Taken?

Deterministic compartmental modeling is by far the most common approach to theoretical population biology. These models are simple to develop and they enable the use of a powerful set of analytic tools (such as elegant algebraic relationships). Although deterministic compartmental models are often adequate and are probably the most appropriate approach in most circumstances of established epidemics, these models have their limitations and inappropriate assumptions [103]. They are certainly not appropriate for addressing circumstances for which there are only a ‘handful’ of individuals or when individual-level intervention strategies (such as contact tracing) is the focal question for investigation. There are times in which the stochastic elements are essential to be modeled explicitly. Recently an intermediate step between continuous deterministic compartmental models and discrete individual models has been developed that maintains compartments, and notions of random mixing, but discrete individuals are the basic entities. Stochastic compartmental models retain

all the compartmental structure of deterministic compartmental models. But if there are large populations and the epidemic is well-established, the stochastic models do not provide any more insight than deterministic models, except they provide more variability in the outcome trajectories.

The trade-off between using simple or complex models for investigating transmission dynamics, and which approaches should generally be adopted, is highly contentious. Most models are constructed using radically simplifying assumptions so that they can stand on their own and provide insight to broad audiences. These models are widely criticized for being unrealistically simple. But such simple model analyses have been largely informative, including the small selected subset [13, 28, 35, 36, 104-122]. Using only simple models may limit the growth of infection transmission science [103], and also the inclusion of many of the realistic and important details necessary to reflect the situation being modeled. Various questions can only be addressed through detailed and complex models. Complex models have recently also usefully addressed a diversity of infection control problems [52, 123-126].

In areas where there are many very intelligent academics that hold strongly opposing views it is wise not to stick too strongly to a closed view and assert definitively that one approach is best. Most practitioners have their preferred approach, including myself. I have strong preference for simple models and good reasons for maintaining this approach to address most practical real-world problems (although the best approach should always to be evaluated on a case-by-case basis for each research problem). Basically, it is extremely difficult as it is to obtain reliable parameter estimates for simple models, let alone for complex ones. In the complex models there are many-fold more parameters to be estimated and many of them cannot be linked easily to an actual biologically or socially measurable outcome. For the majority of parameters that are epidemiologically meaningful, there is often no reliable data available for obtaining appropriate estimates. Furthermore, the complex models essentially become ‘computer games’ – there are thousands upon thousands of lines of code implementing the model and no one knows how the program really works, or can explain the mechanisms and reasons for the observed specific simulated scenarios. It is difficult to ascertain how a given output is a function of any input variable. Also because the models are computationally expensive, it is unwieldy and somewhat infeasible to explore a large input parameter space. For many of these models small numbers of scenario analyses are run with just specific point parameters. Yet these models actually require a much more extensive parameter uncertainty analysis. Because of the large investment in development and implementation of the complex models, the practitioners are less likely to adapt or start afresh to meet new research problems but desire to use their existing model and find a problem to which it could be applied. Although there are many considerations that must be evaluated when one is developing a model, one must choose the approach that is most appropriate for the situation at hand. There is not a single approach that is best in all circumstances; each approach has value for different purposes. One should identify the fundamental and important research questions and then decide on the best way to address the problem. It must be ensured that there is sufficient detail in the model to adequately reflect the situation but that the model is tractable enough to sufficiently analyze it and explore the complete relevant parameter space.

As a final word regarding simple models, consider the main aims of epidemic modeling: to better understand the mechanisms by which diseases spread; to predict the future course of the epidemic; and to understand how we may control the spread of an epidemic. The simplest

models can usually address these aims; for example, the simple Kermack-McKendrick model showed us that (i) the initial number of susceptible must exceed the relative removal rate for an epidemic to grow, (ii) if $S_0 = \rho + \nu$ is the number of susceptible at the start of the epidemic and $\nu << \rho$ (where $\rho = \alpha/\beta$ is the relative removal rate), then we can expect approximately $S_\infty = \rho - \nu$ susceptible people at the end of the epidemic and a total of 2ν affected individuals, (iii) reducing the number of susceptible people, by immunization for example, to below ρ would reduce the epidemic considerably in size.

3. Meaningless Mathematics

Some readers may consider this section a little cynical, and in some respects it is intended as such. But I believe that the message of this section is desperately required to reach into the depths of all the university basements containing mathematicians that consider themselves 'applied', and jolt them toward more purposeful 'applied' research pursuits. This section may be irrelevant to many other readers that already have a real world applied approach to population biology.

Almost every time I present my research within a mathematics department, including applied mathematics departments mind you, one of the first questions I am asked is something along the lines of 'Have you performed detailed mathematical analysis on the equations or can you include more nonlinear terms to find any interesting anomalies and features of the model'? In my opinion, this exemplifies the entirely incorrect mindset of many 'applied' mathematicians. Frankly, I ensure that my model equations do not have any 'mathematically interesting' phenomena. Applied mathematicians will sometimes look for 'blips' in their models under certain limits or perturbations and present these 'big results' as possibly explaining strange phenomena that should occur in the biology (if one looked hard enough). Six, twelve, eighteen months of research time could be spent analyzing such a model, resulting in a publication in the *Journal of Biomathematical Meaningless* or whichever similar journal, never to be read by a single 'real-world' biologist or public-health policy maker. If one looks through the results sections of journals containing such papers, one would continually find integral equations. I am sorry to state that equations containing integrals are not results! At least not results of any utility or meaning to a non-mathematician. If a paradoxical result is presented in some of these biomathematical papers and a biologist happens to come across it and enquires as to how such a seemingly paradoxical result occurs, the response is often some esoteric and obscure mathematical description, alienating the biologist even further from this field. Although the model may have been useful in entertaining the mathematician analyzing it, more than likely the model was simply incorrect – not representing the real biology, investigated only in the vicinity of unrealistic parameter values, or presented in an way that appears unapproachable, rendering it entirely unhelpful in influencing any scientific experimentation or public health policy.

A biological concept familiar to epidemiologists and modelers of disease transmission is the basic reproduction number, symbolized simply as R_0. The basic reproduction number is ''the average number of secondary infections produced when one infected individual is introduced into a host population where everyone is susceptible''[9]. This quantity sounds

like it is something that can be measured from models and actually means something in the real world. Further, if modeling could show how R_0 could be reduced below unity, one would have a theoretical intervention strategy to eradicate the epidemic in question. Consequently, most dynamic transmission models are analyzed in an attempt to obtain a closed-form mathematical expression for R_0. The dominant tradition in infection transmission modeling pursues simple models designed to make clear the nature of nonlinear dynamics. The crowning achievement of such analyses are simple relational expressions such as $R_0 = \beta cD$ [9], which translates as the number of transmissions that an infected individual generates over the course of their infection, when all of their contacts are susceptible, equals the product of the contact rate of individuals, their transmission probability, and the duration of their infection. In the pursuit of such elegance, detailed, realistic data affected by a myriad of peculiarities in the situation where the data are collected is viewed as obscuring that essence. Countless articles, books, and entire PhD theses have been written addressing the calculation of R_0. Of course, the more complex the model, the more complicated the expression for R_0. Expressions for R_0 for many models are often unwieldy and just plain daunting. Every model will have a different representation for R_0.

Bifurcation analysis of the ODE models yield threshold parameters [127] (often presented as R_0). These 'R_0' parameters are *only* valid to determine the threshold (when R_0 =1); that is, the break-even point between an endemic epidemic and one that fizzles out [9, 128]. According to the definition of R_0, it is a measure at the individual level, not at a population level: R_0 is the average number of infections produced per individual person. But the typical population-level differential equation models describe the dynamics (disease transmission and progression rates) of the number of people in various disease stages and do not track individuals. The parameters of the ODE models may have a complex relationship to individual-level processes or the relationships are unknown. Further, population-level data cannot verify individual-level modeling assumptions. As Breban and colleagues [128, 129] have shown us, it is possible to establish individual-level models that identically reflect population-level dynamic models but the way that the rules are set up in the individual models can vary extensively, each yielding different values for R_0. The individual-level and the population-level approaches may produce very different values for R_0. Individual-level approaches calculate R_0, whilst population-level models calculate the value of a threshold parameter. The issue of how well they match has been previously studied [130, 131] and it has been shown that R_0 values obtained from different individual-level models do not necessarily agree with those obtained from mean-field ODE models. Essentially, the actual value of 'R_0' for a dynamic ODE model is irrelevant if it is above one, the importance of the 'R_0' is just that it is above one. A larger R_0 for one disease relative to another also does not necessarily mean anything, because they will have different durations of infection. An R_0 of approximately 2 for HIV over an entire infectious duration of approximately 10 years, is quite different to an R_0 of 2 or 3 for influenza or SARS over an infectious period of a couple of weeks [17, 18, 132, 133]. Regardless of the disease or method for estimating R_0, all estimates in the literature of R_0 for most diseases will almost always be reported to be around the same of 2-3 anyway! Further, how is an expression of 'R_0'= complex function of model parameters going to change policy? It is argued that if we know this expression, then we can determine how much we need to reduce certain key parameters in order to eliminate an epidemic. There is certainly value in this, and I do not want to denounce this line of investigation, but there is

also a lot of uncertainty, heterogeneity and other variation in the parameters to start with, and unless this variation is dealt with appropriately in a meaningful parameter space of the real uncertainty the result is less helpful. But I also implore practitioners to stop obsessing about 'R_0'! 'R_0' is emphasized disproportionately in our field. Instead, there are direct comparisons of policies and interventions that could be investigated with much greater thoroughness and this will prove to be much more directly useful in influencing public health policy.

In order to understand what questions are of greatest importance and interest for investigation, move outside the mathematics department. Ask the real-world policy makers; get them involved in the process as expert consultants for parameter ranges and the structure of the model. Include public health experts, clinicians, field officers etc., as middle authors in manuscripts as required to obtain more credibility in the real world and to obtain the expert information necessary for supporting the model. But of course the more practitioners, the more complex the discussions could become. It is important that the practitioners have some understanding and appreciation of modeling and will be synergistic. Additionally, choose to work with the best people, the people most recognized for their knowledge in the application. Another avenue modeling practitioners must pursue further is to attend the leading conferences in the application area and gain an appreciation for the current most important questions that need addressing or pre-empt such questions.

Mathematical biology, by virtue of the fundamental tool (mathematics), is inclined to be largely theoretical. It is very important to understand the properties of the models, to understand their stability and threshold conditions. But once one is satisfied that the model does not behave strangely and that the model adequately describes the epidemic in question, with appropriate parameter estimates, that is all the mathematical analysis that is required. The mathematical analysis is not necessarily a result; not a result of any utility to influence public policy, but only a preliminary step in the model development process prior to its use in investigation. Occasionally, there are a few instances where simple models that have exact mathematical solutions can provide powerful insight into the relation between parameter values and results and such relationships can be the most precise and elegant conceptual understanding; this is exemplified by some models of the impact of vaccines [134-136]. But most of the time parameter relationships as a mathematical expression are not terribly informative.

It is of utmost importance that modeling projects always have the bigger public health goals in mind and clearly present the important practical results to the appropriate community of influence, without esoteric rhetoric of mathematical details. Simply, it is important that models do not have strange phenomena but accurately reflect the actual epidemic being modeled. Also, as models increase in complexity, only numerical solutions are possible. This leads into the very important topic of model calibration and estimating parameter values.

4. Parameter Estimation

One of the greatest torments in mathematical modeling is that parameter values are rarely known precisely [2]. Typically, one of the longest components of any modeling exercise (from the conception of the first model design through to preparing results, writing and submitting a manuscript) is the process of parameterization. This is also probably the most important part of the process. It cannot be over-emphasized how important realistic parameter

values are in using a model appropriately. Consequently, this part of the process cannot be taken lightly. Data must be incorporated wherever it is possible, but with or without data models will always require calibration to ensure they reflect realism as much as possible. There are many different definitions of validation, verification and calibration in the literature [137-140]. Irrespective of the precise definitions, models should be tested (either formally or informally) for realism in parameter estimates and in the output they generate. Since there are likely to be considerable unknowns in parameter estimates, an appropriate uncertainty analysis should always be considered and not scenario analyses.

4.1. Incorporating Data

One of the most elementary ways of making projections in a population is to fit some theoretical curve to the known empirical data and then extrapolate this curve to predict new cases in the next one or two years. This involves no epidemic model of infection: the theoretical model is chosen because it seems likely to fit the data. Practically speaking, the prediction can only be made for a short period of time ahead, since the conditions which have held in the past for the known data may alter over a longer period, and the statistical curve-fitting has no mechanistic basis and considers no conditions for saturation or other limiting factors. Analyzing surveillance data and trends with curve-fitting models or other statistical techniques to handle data has considerable value. But such models shed little light upon the specific causes of spread and do not include the detail required to provide insight into interventions. Mathematical models can never replace good surveillance data, but they can be used as a framework for certain data analysis exercises. More importantly mathematical models can help to explain underlying mechanistic reasons for the observed data. It is extremely rare to come across a mechanistic model that incorporates available epidemiological surveillance data. Data analysis and inference methods using models of nonlinear infection transmission dynamics only appear sporadically in the literature [141-145]. There is a much greater need to incorporate more real data in transmission models. This is a future direction in the field requiring expansion. The fault for the disconnect between causal models and data-analysis models lies as much (or more) on infection transmission modeling traditions as it does on the data analysis traditions of epidemiologists. The gap must be bridged. Although good data can be difficult to come by, the primary reason for not incorporating data in causal models is probably not the lack of data but an attitude of approach that considers the exercise to be a purely theoretical modeling one. However, if for example there is data on the number of new diagnoses over time, there is no need to model a variable of the number of new diagnoses – that data is already available. One could incorporate a statistical interpolating function of the diagnoses data into the rest of the modeling framework, obviating the need to include additional variables and parameters that will undoubtedly not truly reflect what is currently known or been measured. Data should be used as much as possible within transmission models.

If time course data cannot be used directly in epidemic models, it is essential to know how well the models will fit the available data. This is particularly important if reliable predictions are to be made. Example accounts of the fitting of various models to data for epidemics are given in [8, 9, 141, 146]. The standard method is to minimize the sum of squares of the differences between the observed and model estimates of the outcome of

interest, to fit for unknown parameter values. Calibration techniques used in transmission modeling commonly include maximum likelihood, Bayesian techniques, and basic regression techniques. Also, using a variety of assumptions, Generalized Linear Models have been employed for parameter estimation [17, 141], or to estimate HIV incidence and prevalence [147-149]. Bayesian methods are increasingly being used for parameter estimation. Under the Bayesian framework, all parameters of interest (known and unknown) are considered to be random variables described using probability distributions [150]. According to prior knowledge these distributions are initially specified, and then they are updated with epidemic data and a model to more accurately specify the (posterior) distributions. This method allows one to make probability statements about model parameters. The Bayesian approach has been applied to various disease transmission models [151-155] and within-host models [156, 157]. Rigorous Bayesian statistics to estimate uncertainty in model parameters (as carried out by Elderd et al. [145],for example), will be the way of the future. Likelihood based approaches are also gaining in popularity in population dynamic models [147, 158]. To obtain an accurate estimate of the probability distribution for certain parameters, bootstrapping approaches are also becoming more common [159, 160]. Bootstrapping provides a reliable way to construct a confidence interval for a parameter by resampling from the original data to create replicate datasets.

In order to calibrate a model (particularly complex ones) one often needs detailed empirical data. If the necessary data are limited or unavailable, sensitivity analyses should be used to determine the impact of parameter estimation uncertainty on results [161]. Although data fitting should be incorporated much more in transmission models, care must be taken with estimating parameters by fitting to data. Local minima in the sum of squares may produce a set of estimates for unknown parameters that are not representative of the true values of the parameters – multiple sets of parameter values in different regions of parameter space may produce similar (minimal) sum of square errors but only one set (or none of them) may reflect the true values. Furthermore, the fact that the model fits the data does not necessarily validate the model. By just adding extra parameters to be fitted for, it is possible to fit almost any data [162]. As John von Neumann once famously stated, “With four parameters I can fit an elephant and with five I can make him wiggle his trunk [163].” A model might provide an excellent fit to the data at hand, but because its parameter estimates are quite variable the model will generalize poorly to novel data sets. Hence, inference from unparsimonious, over-fitted models is hazardous and should be avoided. Of course, a model that captures relatively little structural information (that is, an under-fitted model) is also not well suited for inference. Ideally, inference should be based on simple models that describe the data well.

4.2. Model Calibration and Validation

It is highly important to obtain realistic parameter ranges from whatever empirical sources and clinical experience as possible. But there will almost always be some parameters that are unknown. The key is to estimate them appropriately. There are many instances in which no data is available in which to fit the model to determine parameter estimates. It is likely that there are a few different regions in parameter space that will fit the data appropriately. But this does not mean that each of these parameter regions is correct. With more parameters

there is also more uncertainty in the model and the less meaning each one will have. Thus, it is highly important to spend considerable time calibrating the model and checking that input parameters appear appropriate and that outcomes are realistic and match the (measured or expected) reality. Calibration is this process of using a model with its input and output information to adjust or estimate input parameters for which data are typically poor or unavailable [146]. One must typically adjust (or "calibrate") model inputs to observed outcomes in most models. Even when parameter estimates are based on the best available data, calibration procedures can be used to reduce parameter uncertainty. That is, although uncertainty analysis is a separate process to calibration, they should be conducted simultaneously [164]. Calibration is an iterative process involving feedbacks to assist refine the uncertainty analysis. Calibration can be conducted formally statistically [164-166] but often it is not possible or feasible and thus calibration must be done informally as a check that the output uncertainty matches approximately what is expected in the modeled population. Simulations could also be checked against certain predefined criteria (such as population prevalence must be between x% and y%) and if any simulation fails to pass such a criterion it is rejected [167]. If simulations are rejected, analysis of the parameter conditions that lead to passing/failing the criteria is worth investigating (especially to ensure that the parameter sets remaining are not biased due to the removals). This is known as Monte Carlo filtering [168, 169]. Essentially, calibration searches for regions of the constrained parameter space that yield model outputs consistent with predefined criteria and observations [170].

In order to make reasonable predictions and develop methods of control, one must be confident that the model captures the essential features of the course of an epidemic. Thus, it becomes very important to validate models, whether deterministic or stochastic, by checking whether they fit the observed data (or by forcing them to fit the data by fitting a parameter). Validation determines the degree to which a model accurately represents the "real-world", in terms of the intended uses of the model [137-139]. It is important to define how models will be validated, even though there is no single, accepted statistic or test of model validity. Model structure is inextricably linked to the purpose of the model and to knowledge about the processes being modeled. Therefore, it is essential to collaborate with infectious disease experts to ensure biological and medical correctness of the processes modeled. Assumptions of the models should be checked against available empirical data and by consulting with experts. Data quality and input parameters are made explicit. Models are constructed to provide an adequate picture of reality, consider all relevant aspects, and omit those that do not alter results or conclusions significantly. Absence of data is not a justification for simplifying important issues [137]. In the cases where useful data is not available, thorough and convincing explanations of the causes of results, important factors, assumptions, and parameter estimates that contributed to the results will often have to suffice. Assumptions should be made explicit so that they can be challenged, and the impact of any assumptions explored. Often the data available to decisions makers are inadequate, as for example in the case of interventions for HIV/AIDS in Africa or South East Asia. Yet policies still need to be formulated, even if only on the basis of rough qualitative measures. Accurate data may be impossible to obtain, but one should always be in a position to minimize the cost of a policy or to compare one policy to another, however approximately.

There is still much to understand with respect to the determinants of infection. To understand these determinants further, disease transmission scientists must gather more varied and extensive empirical data and integrate it effectively with theory. Sometimes important

insight can be gained from model analyses that use minimal amounts of data. But without data, progress will be limited. The future of the field will involve the incorporation of the best data analysis techniques with mechanistic models. The dominant data-analysis models, such as stratified comparison of risks, logistic regression, and proportionate hazards models, estimate parameters that relate exposure to disease to individuals. Transmission models, in contrast, relate individuals to each other using parameters that express contact rates or transmission probabilities. The data models assume that contact rate and transmission probability parameters have a value of zero – they assume that the outcome in one individual is independent of the outcome in other individuals. Therefore, although the techniques need to be integrated much more extensively, great care should be taken before extensive use so that the same individual-level/population-level problems that have occurred with parameter definitions such as R_0 do not carry across to interpretation of population-level parameters from individual-level data analysis.

Biomathematics is, by nature, interdisciplinary between biology and mathematics. Therefore, one would be foolish not to explore interdisciplinary collaborations to obtain outside expertise for the modeling projects. This will not only provide better parameter estimates but also assure realism and relevance to the community for which the work is intended to impact. One should try to associate with the best people, who understand the medical, biological, clinical, and public health literature as well as possible but who also can appreciate the approach of theoretical modeling. Of course, connecting in a productive working relationship is also essential. But even through tapping into the best expertise available, it is almost invariably the case that all model parameters will either have only been estimated imprecisely or not known at all. The way in which mathematical modelers now deal with these difficulties is to use sophisticated uncertainty and sensitivity analyses. These analyses explore parameter ranges rather than simply focusing on specific parameter values. Each input parameter can be defined to have an appropriate probability density function associated with it. Then, the model can be simulated by sampling one value from each parameter's distribution. Many simulations should then be run, producing variable output variable values. The variation in the output can then be explored as it relates to the variation in the input.

5. Uncertainty Analyses

Sally Blower has pioneered the use of transmission models as health policy and predictive tools by coupling them with uncertainty and sensitivity analyses [13, 15, 102, 108, 109, 161, 171-183]. This is necessary in exploring the behavior of many complex models due to the complexity in their structure and the large degree of uncertainty or heterogeneity in values of many input parameters. Uncertainty analyses assess the variability in the outcome variables due to the variability in the input parameters [184]. Little attention has been given to how uncertainty in parameter estimates might affect model predictions. The real uncertainty in parameter estimates due to lack of data, heterogeneity, and other unknowns or confounders has important implications for intervention strategies and formal uncertainty estimation should play a key role in planning for epidemics. One approach to establishing an uncertainty analysis is to use a full factorial sampling design; this sampling scheme uses every value of each parameter and forms every possible combination of parameter values. This approach has

the best possible advantage of exploring the entire parameter space, but this method is extremely computationally inefficient and time-consuming. This is not feasible for basically every model. If there are M parameters and each one has N values (or its distribution is divided into N equiprobable intervals), then the total number of parameter sets and model simulations is N^M (even just 100 samples per distribution and 20 parameters would result in 10^{40} unique combinations, entirely unfeasible for all models). At the other extreme, one could fix M-1 parameters and vary the Mth parameter over a specified range. This type of univariate sensitivity analysis is highly efficient but has some major flaws, as only one dimension of the M-dimensional parameter space is explored and each of the fixed parameters are required to be estimated with a high degree of precision. Ideally one should vary all parameters simultaneously in the M-dimensional parameter space but in an efficient manner. The first obvious approach is to randomly sample each parameter N times independently from its respective distribution. This generally leads to vast sampling improvements over both univariate approaches and full factorial designs, but it is not the most efficient way to sample the parameter space. More efficient and refined statistical techniques have been applied to sampling in a variety of fields. Currently, the standard sampling technique employed is Latin Hypercube Sampling and was introduced to epidemiology modeling by Blower [185]. Latin Hypercube Sampling is a type of stratified Monte Carlo sampling [186, 187] that is an extension of Latin Square sampling [188, 189]. Although McKay et al. originally proposed the concept [190], it was Iman et al. [184, 186, 187] who developed and introduced this method. Probability density functions (pdfs) are defined for each parameter; each of these pdfs is then stratified (into N equiprobable intervals) and the value of each input parameter is randomly chosen. But each input value is used only once in the entire sampling analysis and so this is a very efficient sampling design [184, 185, 191, 192]. Distributions of the outcome variables can then be derived directly by running the model N times with each of the sampled parameters.

The minimum number of simulations required to be performed has not been determined. Most practitioners currently use N=1000 (as done by Blower in most of her analyses). However, if the model has additional complexity I suggest that 10,000 simulations be performed. The number carried out is arbitrary, but it is important to ensure that a sufficient number are run to capture the appropriate distribution in the outcome variables and relate it to the variability in input distributions.

The algorithm for the Latin Hypercube Sampling methodology is described clearly by Blower & Dowlatabadi [185], complete with an example from HIV epidemic modeling. For completeness of this chapter, a brief description of the algorithm is given here. Each parameter's distribution is divided into N equiprobable serial intervals and each interval is assigned an index. The limits of each interval $\left(\alpha^i_{\min}, \alpha^i_{\max}\right)$ are to be determined. If the pdf of parameter α is $f(\alpha)$, and $F(\alpha)$ is the integral of $f(\alpha)$, the function should be normalized such that $F\left(\alpha_{\max}\right) - F\left(\alpha_{\min}\right) = 1$, where $\alpha_{\max}$ is the upper bound on α's definition and $\alpha_{\min}$ is the lower limit. Since the area of each equiprobable interval is 1/N,

$$1/N = \int_{\alpha^i_{\min}}^{\alpha^i_{\max}} f(\alpha)\, \mathrm{d}\alpha = F\left(\alpha^i_{\max}\right) - F\left(\alpha^i_{\min}\right), \quad \forall i.$$

Therefore, the upper limit of each interval can be calculated based on the calculation of the previous interval (acknowledging that the upper limit of the previous interval becomes the lower limit of the following interval and the lower limit of the first interval is the lower limit of the distribution). The upper limit of each interval is calculated by

$$\alpha_{\max}^{i} = F^{-1}\left(F\left(\alpha_{\min}^{i}\right)+1/N\right).$$

This is demonstrated schematically in Figure 2 for the case of two sample parameters and N=10 samples. Once the intervals are established for all parameters, N iterations are performed, each randomly selecting an interval of each parameter without replacement. Therefore, each and every interval will be chosen once for each parameter (see Figure 3). The specific parameter value to be used in the computational simulations from each interval can be chosen as the mid-point of the interval, the median of the interval, or a randomly selected value from the interval (the latter has been chosen for illustrative purposes in Figures 2 and 3 and this is generally what is done in practice).

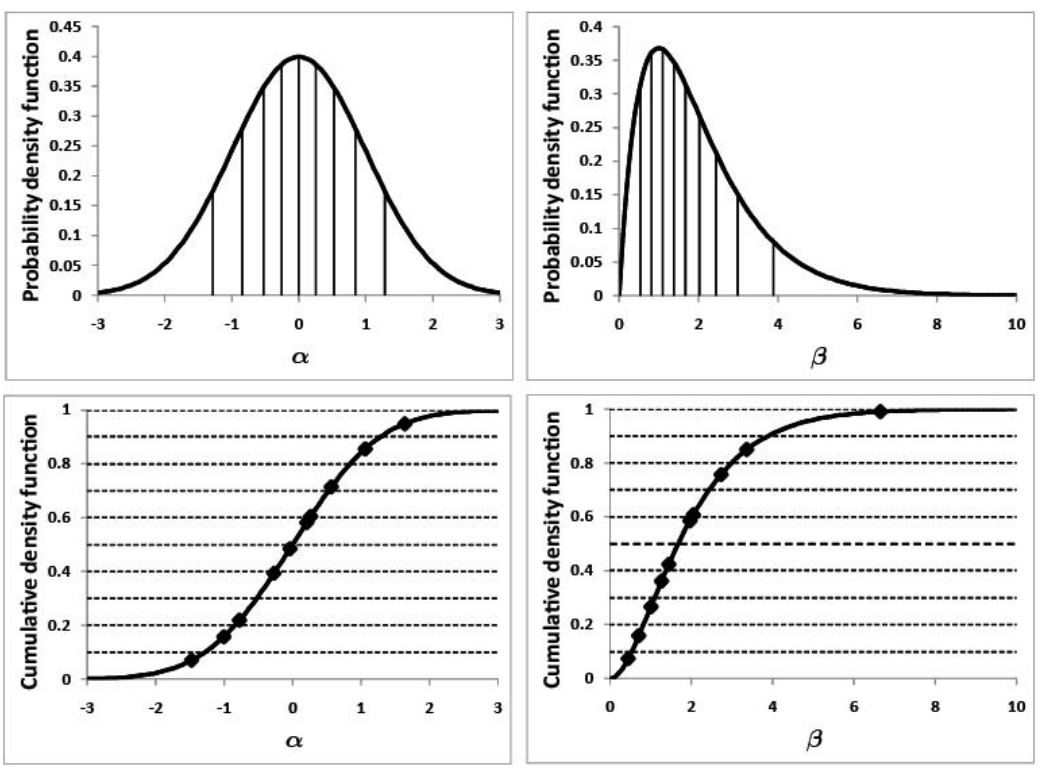

Figure 2. Schematic Diagram of the Method of Latin Hypercube Sampling. Here, two parameter distributions are defined: all as a Gaussian distribution with mean ($\mu = 0$) and standard deviation ($\sigma = 1$), and beta as a Gamma distribution with shape parameter ($k = 2$) and scale parameter ($\theta = 1$). The probability density functions and cumulative density functions are shown and their division into N=10 equiprobable intervals. A computer-generated Latin hypercube sampling scheme is indicated by the diamond points.

Given an appropriate number of parameter sets from Latin Hypercube Sampling, or another sampling technique, and model calibration has been performed, the parameter sets should each be used in model simulations to generate outcome variables. According to the variability in the input, there will be variability in the output. The simulated data can be treated like real measured/observed data and standard statistical methods can be used to investigate the relationships between the input parameters and the outcome variables. This is the essence of sensitivity analyses.

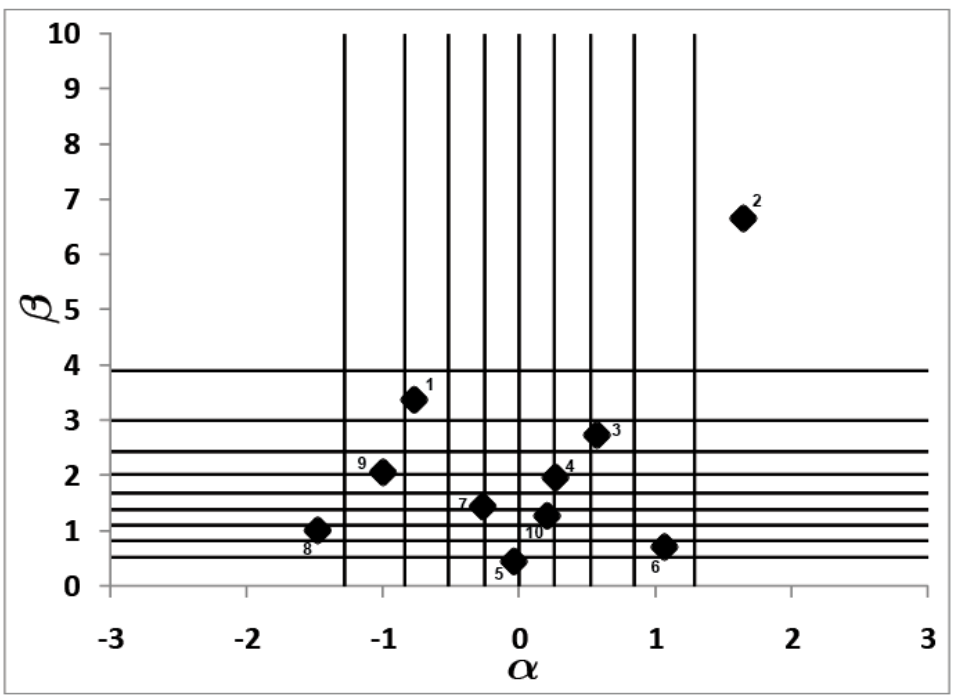

Figure 3. The resulting computer-generated N=10 samples from the 2-dimensional parameter space as defined in Figure 2. The sampled parameter sets are random ordered and indicated by ordinal counts.

6. Sensitivity Analyses

Sensitivity analysis is the study of how the uncertainty in the output of complex models can be apportioned to sources of uncertainty in the model inputs [185, 193]. It has been argued that sensitivity analyses are not required for analytical solutions where the influence of changing a parameter is explicit within the model solution [32]. An equation may well describe the full extent of influence but generally such equations are meaningless (unless they are extremely simple) to most people. Equations are also uninformative without the definition of the parameter space over which the equations are valid. Sensitivity analysis involves investigating how an outcome variable responds to changes in input variables. Formal sensitivity analyses (statistically) evaluate how important each parameter is in influencing model outcomes. The simplest form of sensitivity is scenario analyses, in which illustrative results are shown with very specific point estimates of single parameter sets. All parameters

are fixed as constants and one parameter is changed in value and the changed trajectories are plotted or different outcomes compared. This is an awful way of carrying out a sensitivity analysis, especially if there is a lot of heterogeneity and uncertainty in numerous model parameters. However, it does demonstrate differences in single epidemic trajectories for changes in, usually a single parameter but can be any number of changes in, specific model parameters. Such univariate sensitivity analyses apply only to that very specific set of parameter values and results outside these parameter estimates cannot be determined accurately. These trajectories are also heavily dependent on the structure of the transmission model.

A good sensitivity analysis will extend an uncertainty analysis by identifying which parameters are important (due to the variability in their uncertainty) in contributing to the variability in the outcome variable [184]. These analyses allow identification of the models' parameters and processes that exert the most leverage on the models' outputs [161]. As Hornberger and Spear [194] mention:

> *"…most simulation models will be complex, with many parameters, state-variables and nonlinear relations. Under the best circumstances, such models have many degrees of freedom and, with judicious fiddling, can be made to produce virtually any desired behaviour, often with both plausible structure and parameter values."*

It is therefore essential to determine the underlying assumptions in parameter estimates and key influencing factors and interaction effects by conducting a thorough sensitivity analysis. Different understandings of sensitivity analysis are used in different modeling communities (e.g. [195-202]). Methodology for implementing some of the standard sensitivity analyses currently within epidemic modeling is now presented, along with the presentation of some new methodologies from other disciplines that could be usefully brought across to the field of epidemic modeling.

6.1. Pearson, Spearman, and Partial Rank Correlation Coefficients

We are often concerned with the association, or relationship, between two different kinds of measurements. The standard measure of ascertaining such associations is the correlation coefficient. A correlation coefficient is a number between -1 and 1 which measures the degree to which two variables are linearly related. If the relationship is perfectly linear (such that all data points lie perfectly on a straight line), the correlation coefficient is 1 if there is a positive correlation/slope and the correlation coefficient is -1 if the line has a negative slope. A correlation coefficient of zero means that there is no linear relationship between the variables. It must also be noted that the existence of a significant correlation between two factors does not in itself necessarily imply a direct causal link. Scientific significance can be determined once statistical significance is obtained but it cannot be automatically assumed. There are various means of determining the appropriate correlation coefficient, dependent upon the type of data (and distribution of the data).

The normal (or Gaussian) distribution is often a fair representation of particular kinds of data, and there are theoretical reasons for expecting this distribution to turn up in practice. Similarly, when there are two variables, we often find that a bivariate normal distribution is a reasonable description of the data. Again, there are theoretical reasons for expecting this

distribution to occur, at least approximately. The analog of the normal curve, $z(x) = \frac{1}{\sigma\sqrt{2\pi}} \exp\left(-\frac{(x-\mu)^2}{2\sigma^2} \right)$, is the bivariate normal surface, and its expression (in variates *X* and *Y*) is given by:

$$z(x,y) = \frac{1}{2\pi\sigma_x\sigma_y\sqrt{1-\rho^2}} \exp\left(-\frac{1}{2(1-\rho^2)} \left[\frac{(x-\mu_x)^2}{\sigma_x^2} - \frac{2\rho(x-\mu_x)(y-\mu_y)}{\sigma_x\sigma_y} + \frac{(y-\mu_y)^2}{\sigma_y^2} \right] \right),$$

with means μ_x and μ_y, and variances σ_x^2 and σ_y^2. Here, the parameter ρ is the correlation coefficient between *X* and *Y*. Note, that intrinsic in the definition of this correlation coefficient is the assumption that both data sets can be assumed to be normally distributed. This correlation coefficient is known as the Pearson product-moment correlation coefficient (PCC). Given data (x_i, y_i), the Pearson correlation coefficient ρ is estimated by the statistic

$$r = \frac{\sum (x_i - \overline{x})(y_i - \overline{y})}{\sqrt{\sum (x_i - \overline{x})^2 \sum (y_i - \overline{y})^2}}.$$

This formula is equivalent to the sum of the products of the standard scores of the two measures divided by the degrees of freedom:

$$r = \frac{\sum z_x z_y}{n-1}.$$

Although there are various ways of interpreting the meaning of a correlation coefficient in absolute terms, it is firstly important to know whether the value is significantly different from zero. This is highly important for real data, especially when sample sizes are relatively small. For simulated data from mathematical or computational algorithms in which very large numbers of simulations can be run, the correlation coefficient will almost certainly be significantly different from zero (extremely small p-value) and thus the significance test is of little importance in this case. To test the hypothesis that the correlation coefficient is equal to zero, the Student's *t*-test with $n-2$ degrees of freedom is used with the test statistic

$$t = \frac{r\sqrt{n-2}}{\sqrt{1-r^2}}.$$

As an extension for the measure of the association between *X* and *Y*, the coefficient of determination (R^2) is determined; it is the proportion of the variability in the data set that is

accounted for by the statistical model. For example, if r=0.9, then r^2=81% of the variance of Y can be accounted for by changes in X and the linear relationship between X and Y.

As noted above, the PCC is only valid if the two variables are jointly approximately normally distributed. When this assumption is not justified, a non-parametric measure such as the Spearman Rank Correlation Coefficient (SRCC) [203, 204] may be more appropriate. Additionally, the PCC can be misleadingly small when there is a relationship between the variables but it is a nonlinear one, whereas the SRCC may also be a better indicator that a relationship exists between two variables if the relationship is nonlinear. This is also usually calculated when it is not convenient or possible to allocate actual values to variables but only to assign a rank order to instances of each variable. By assigning ranks to data (positioning each datum point on an ordinal scale in relation to all other data points), any outliers can also be incorporated without heavily biasing the calculated relationship. The SRCC assesses how well an arbitrary *monotonic* function could describe the relationship between two variables, without making any assumptions about the frequency distribution of the variables. Any standard statistical software package will evaluate the full product-moment form, but an accepted short-cut (assuming no tie) is to determine the differences d between the ranks of each paired observation of the two variables and then the SRCC is given by

$$r = 1 - \frac{6\sum d_i^{\,2}}{n\left(n^2 - 1\right)}.$$

To test whether the SRCC is significantly different from zero, a permutation test is performed to calculate the probability that ρ would be greater than or equal to r, given the null hypothesis. However, if the data set is very large so that a permutation test is not computational realistic, traditional methods can be used involving tables (if available) or alternatively using the approximation to the Student's t-distribution. For sample sizes greater than approximately 30, the test statistic is the essentially the same as that for the PCC.

These methods for determining correlation are extremely powerful when only a single pair of variables is to be investigated. However, quite often measurements of different kinds will occur in batches. This is especially the case in the analysis of epidemic models that have many input parameters and various outcome variables. Here, the relationship between each input parameter with each outcome variable is desired. Specifically, each relationship should be ascertained whilst also acknowledging that there are various other contributing factors (input parameters). Simple correlation or regression analyses could be carried out by taking the variables two at a time, but it would be unwieldy and would fail to reveal more complicated patterns of relationships that might exist between several variables simultaneously. Therefore, an extension of previous methods is required. The appropriate extension for handling groups of variables is partial correlation.

Firstly, some notation will be designated. The true correlation coefficient between two variables, ρ_{12}, can be estimated by r_{12} (using the methods above). This correlation coefficient is the total coefficient (as distinct from 'partial' coefficients). If one is interested in the correlation of factors A and B, irrespective of any influence factor C might have, the total coefficient (r_{12}) is calculated. However, one may want to know how A was related to B when the effect of C had been specifically excluded. For this, the calculation of a partial correlation

coefficient (PCC) is required (and represented here by $\rho_{12,3}$). The PCC, $r_{12,3}$, is determined by first calculating the total correlation coefficients for the various pairing combinations of variables (r_{12}, r_{13}, and r_{23}) and then evaluated by

$$r_{12,3} = \frac{r_{12} - r_{13}r_{23}}{\sqrt{\left(1-{r_{13}}^2\right)\left(1-{r_{23}}^2\right)}}.$$

If two factors are to be specifically excluded then the calculation is extended to

$$r_{12,34} = \frac{r_{12,4} - r_{13,4}r_{23,4}}{\sqrt{\left(1-{r_{13,4}}^2\right)\left(1-{r_{23,4}}^2\right)}}.$$

This can similarly be extended for the exclusion of >2 factors. The PCCs should also be tested for significance and this is done with the test statistic:

$$t = \frac{r\sqrt{n-m-1}}{\sqrt{1-r^2}},$$

using the Student's *t*-distribution with $n-m-1$ degrees of freedom, where m is the number of independent variables in the analysis. This methodology is valid under the assumption that the variables follow (at least approximately) a multivariate normal distribution.

Because normality cannot be assumed for some variables or the variables could have outliers that may act as highly influential points to distort the correlation, often partial rank correlation coefficients (PRCCs) are calculated. Here, the variable values are replaced by their numerical rank for the variable and the methodology for calculating PCCs is employed. Calculating PRCCs is currently the best method for determining statistical association between two sets of variables in a large system (such as the relation between one input parameter (out of many input parameters) on a particular outcome variable) [184, 185, 205]. However, usually there are a reasonably large set of parameters and also potentially a large number of outcome variables of interest in computational and mathematical models. Calculating separate PRCCs for each input-output variable pairing can become unwieldy. In such cases, PRCCs can be determined for each input variable and each outcome variable by the following algorithm. Firstly, assign an $n \times m$ matrix (A) of input parameters, where 'm' is the number of input variables (each with 'n' values, for the n simulations or data points). For PRCCs, the values in the matrix will be the ordinal numbers representing the rank (1 to n) of each value relative to each other value for that variable (column). Secondly, rank the n values of the outcome variable of interest and augment a vector of these outcome values as an $\left(m+1\right)^{\text{th}}$ column to the matrix. Thirdly, define the $(m+1)\times(m+1)$ symmetric matrix B as

$$b_{ij} = \frac{\sum_{t=1}^{n}\left(a_{ti}-\Lambda\right)\left(a_{tj}-\Lambda\right)}{\sqrt{\sum_{t=1}^{n}\left(a_{ti}-\Lambda\right)^2\sum_{s=1}^{n}\left(a_{sj}-\Lambda\right)^2}}, \qquad i,j=1,2,\ldots,\left(m+1\right)$$

where $\Lambda = \left(n+1\right)/2$ is the average rank; the leading diagonal of B are all ones. Lastly, define the matrix C as the inverse of B; $B = C^{-1}$. Then, the PRCCs $\left(\omega_{iy}\right)$ between the i^{th} parameter and the k^{th} outcome variable is defined as

$$\omega_{ik} = \frac{-c_{i,m+1}}{\sqrt{c_{i,i}c_{m+1m+1}}}.$$

The test of significance is the same as for PCCs.

The method of calculating PRCCs for the purpose of sensitivity analysis was first developed for risk analysis in various systems [186-189, 206]. Blower pioneered its application to deterministic transmission models [161, 171, 172, 175-180]. It is now standard to calculate the PRCC between each independent parameter, and each outcome variable of interest that have been simulated during the uncertainty analysis, or evaluated from derived analytically calculated equilibrium outcomes [161]. Because the outcome variables can often be time-dependent, PRCCs can be calculated over the outcome timecourse and determined whether they change substantially with time. This is a tool that allows identification of monotonic relationships. Thus, it is also important to examine scatterplots of each model parameter versus each predicted outcome variable to check for monotonicity and discontinuities [161, 188, 207]. PRCCs are useful for identifying the most important parameters but not for identifying the significance of how much change in parameters contributes to change in outcomes. PRCCs are also useful for identifying monotonic relationships but not for non-monotonic. These issues can be explored with regression and response hypersurfaces.

6.2. Regression and Response Hypersurfaces

Correlation coefficients are useful in determining associations when the relationship between variables is monotonic, but they will not always be adequate. This is the case if the relationship is non-monotonic, or one of the measurements is arbitrarily or irregularly distributed. In such circumstances regression analysis is more appropriate. Regression analysis also provides further information, and is especially useful if the behavior of a second measurement in relation to the first is of primary importance. If relationships are monotonic, PRCCs can be used in conjunction with regression analysis. PRCCs can determine the most important explanatory variables (input parameters) and then these variables can be fed into the regression analysis to make it more tractable. Alternatively, regression analyses can be built by themselves as a sensitivity analysis. A regression equation provides an expression of

the relationship between two (or more) variables algebraically and indicates the extent to which a dependent variable can be predicted by knowing the values of other variables, or the extent of the association with other variables. Multiple linear regression aims to find a linear relationship between a response variable and several potential predictor variables, and nonlinear regression aims to describe a nonlinear relationship. One of the values of regression analysis is that results can be appreciated to a greater extent *visually*. If there is only a single explanatory (or predictor) input variable, then the regression equation can be plotted graphically as a curve; if there are two explanatory variables then a three dimensional surface can be plotted. For greater than two explanatory variables the resulting regression equation is a hypersurface. Although hypersurfaces cannot be shown graphically, contour plots can be generated by taking level slices, fixing certain parameters. However, obtaining the values of the coefficients of the regression equation can also prove to be quite insightful. Another benefit of regression analysis is that the resulting equation can provide more meaningful sensitivity than correlation coefficients; it can be shown that an x% decrease in one parameter can be offset by a y% increase/decrease in another, simply by exploring the regression equation. Further, complex relationships and interactions between outputs and input parameters are simplified in an easily interpreted manner [208, 209]. Cross-products of input parameters reveal interaction effects of model input parameters, and squared or higher order terms allow curvature of the hypersurface.

Regression analysis comprises a group of statistical techniques for empirical model building and model exploitation. It seeks to relate a response, or output variable, to a number of predictors, or input variables, that affect it. Although higher-order polynomial expressions can be used, constructing quadratic response surfaces is recommended. This is in order to include direct effects of each input variable and also variable cross interactions and nonlinearities. The generalized form of the full second-order response surface models is:

$$Y = \beta_0 + \sum_{i=1}^{m} \beta_i X_i + \sum_{i=1}^{m} \beta_{ii} X_i^{\,2} + \sum_{i=1}^{m-1} \sum_{j=i+1}^{m} \beta_{ij} X_i X_j \,,$$

where Y is the dependent response variable, the X_i's are the predictor (input parameter) variables, and the β's are unstandardized regression coefficients.

In order to calculate the unstandarized regression coefficients, generally a linear least squares approach is adopted. The quadratic terms in the regression equation can be transformed to linear terms by defining new variables (for example, $Z_i = X_i^{\,2}$ and $W_{ij} = X_i X_j$). For a system of m variables, there will be $M = \left(1 + 2m + m(m-1)/2\right)$ coefficients to determine. The least squares methodology is used to find the values b_0, b_1, …, b_{M} that minimize:

$$F\left(\beta_0, \beta_1, \beta_2, \ldots, \beta_M\right) = \sum_{i=1}^{N} \left(Y_i - \left[\beta_0 + \beta_1 X_1 + \beta_2 X_2 + \ldots \beta_M X_M\right]\right)^2 ,$$

which are the solutions to the M+1 normal equations,

$$b_0 N + b_1 \sum X_{i1} + b_2 \sum X_{i2} + \ldots + b_M \sum X_{iM} = \sum Y_i$$

$$b_0 \sum X_{i1} + b_1 \sum {X_{i1}}^2 + b_2 \sum X_{i1} X_{i2} + \ldots + b_M \sum X_{i1} X_{iM} = \sum X_{i1} Y_i$$
$$\vdots$$
$$b_0 \sum X_{iM} + b_1 \sum X_{iM} X_{i1} + b_2 \sum X_{iM} X_{i2} + \ldots + b_M \sum {X_{iM}}^2 = \sum X_{iM} Y_i \,.$$

In matrix notation,

$$\boldsymbol{Y} = \boldsymbol{X}\boldsymbol{b} + \boldsymbol{\varepsilon},$$

where $\boldsymbol{Y} = \left[Y_1, Y_2, \ldots, Y_N\right]^T$, $\boldsymbol{b} = \left[b_0, b_1, \ldots, b_k\right]^T$, $\boldsymbol{\varepsilon} = \left[\varepsilon_1, \varepsilon_2, \ldots, \varepsilon_N\right]^T$ and

$$\boldsymbol{X} = \begin{bmatrix} 1 & X_{11} & X_{12} & \cdots & X_{1M} \\ 1 & X_{21} & X_{22} & \cdots & X_{2M} \\ 1 & X_{31} & X_{32} & \cdots & X_{3M} \\ \vdots & \vdots & \vdots & \ddots & \vdots \\ 1 & X_{N1} & X_{N2} & \cdots & X_{NM} \end{bmatrix}.$$

Then,

$$\boldsymbol{b} = \left(\boldsymbol{X}^T \boldsymbol{X}\right)^{-1} \boldsymbol{X}^T \boldsymbol{Y}.$$

In most circumstances it is inefficient and memory intensive to calculate the inverse of a matrix such as $\boldsymbol{X}^T \boldsymbol{X}$. Therefore, LU-, QR-decomposition, or some other form of Gaussian elimination is recommended. The usual test of the significance of the fitted regression equation is a test of the null hypothesis that all values of b_i (except b_0) are zero, versus at least one value of b_i is not zero. Assuming normality of the errors, the test statistic is

$$F = \frac{\text{mean square regression}}{\text{mean square residual}} = \frac{SSR/\left(M-1\right)}{SSE/\left(N-M\right)},$$

where $\mathrm{SSE} = \boldsymbol{Y}^{\mathrm{T}}\boldsymbol{Y} - \boldsymbol{b}^{\mathrm{T}}\boldsymbol{X}^{\mathrm{T}}\boldsymbol{Y}$ is the sum of squares of the residuals, $\mathrm{SSR} = \sum_i \left[\left(\boldsymbol{X}\boldsymbol{b}\right)_i - \overline{Y}\right]^2$ (where $\overline{Y}$ is the mean of Y) is the sum of squares due to regression, and $\mathrm{SST} = \mathrm{SSE} + \mathrm{SSR}$ is the total sum of squares. The test statistic is compared with the F-distribution with M - 1 and N - M degrees of freedom on the numerator and denominator, respectively ($F_{\alpha, p-1, N-p}$).

The proportion of the variability in the data set that is explained by the fitted model, the coefficient of determination, is calculated by

$$R^2 = \frac{\text{SSR}}{\text{SST}};$$

but some people prefer the adjusted R^2 statistic

$$R_A^{\,2} = 1 - \frac{\text{SSE}/(N-M)}{\text{SST}/(\text{N-1})} = 1 - \left(1 - R^2\right)\left(\frac{N-1}{N-M}\right).$$

Although regression analysis can be useful to predict a response based on the values of the explanatory variables, the coefficients of the regression expression are not meaningful nor do they indicate which parameters are most influential in affecting the outcome variable. This is due to differences in the magnitudes of values, different amounts of variability, and also different units in the explanatory variables. A regression analysis run on original, unstandardized variables yields unstandardized coefficients. The same analysis can be performed from the original variables, but standardized so that they have variances of one, producing standardized coefficients [210]. Before fitting the multiple regression equation, all variables (predictor and response) can be standardized by subtracting the mean and dividing by the standard deviation. The standardized coefficients represent the change in the response variable that result from a change of one standard deviation in the corresponding explanatory variable. However, it must be noted that this is somewhat deceptive in that there is no reason why a change of one standard deviation in one variable should be comparative to one standard deviation in another variable. But whereas the unstandardized coefficients cannot be compared directly or easily, the standardized coefficients determine the order of importance of each parameter (in much the same way as PRCCs). A standardized coefficient of +1 means that the predictor variable perfectly describes the response variable and a value of zero means that the predictor variable has no influence in predicting the response variable (just in the same ways as PRCC value of +1 and zero, respectively). This should not be confused as equivalence of standardized regression coefficients and PRCCs. They both are evaluated on the same range, can be used to determine parameter importance, and have similar interpretations at the extremes but they are evaluated differently and measure different quantities. Consequently, their values will differ when analyzing the same data. Standardized regression coefficients will typically be lower than PRCCs and should not solely be used when there are large numbers of explanatory variables.

6.3. Logistic Regression

Binomial logistic regression is a form of regression which is used when the response variable is dichotomous (but the independent predictor variables can be of any type). Logistic regression is used very extensively in the medical, biological, and social sciences [211-215]. Any dichotomous response (0/1) can use logistic regression analysis; for example, whether or

not disease or death occurs (or analyzing rejected simulations from the process of model calibration). In an epidemic model with large uncertainty ranges, one could examine the set of parameters that lead to an endemic epidemic versus no epidemic. Other response outcomes could include outputs above/below a certain threshold or when an outcome variable is better for women than for men, for example. In logistic regression, one calculates the probability of an event occurring, given the values of various predictors. The logistic regression analysis determines the importance of each predictor in influencing the particular outcome.

The 'odds' of an event is defined as the ratio of the probability that an event occurs to the probability that it fails to occur. Thus,

$$\text{Odds(indicator=1)} = \frac{\text{Pr(indicator=1)}}{1-\text{Pr(indicator=1)}}.$$

Probabilities are constrained to lie between 0 and 1, with 1/2 as a neutral value for which both outcomes are equally likely. The constraints at 0 and 1 make it impossible to construct a linear equation for predicting probabilities. The odds lie between 0 and ∞, with 1 as the neutral value. Taking the (natural) logarithm of the odds (the 'log odds') will result in a range of possible values between -∞ and ∞. Then, the coefficients of a normal regression equation on the log odds can be interpreted in the usual way, namely, they represent the change in log odds of the response per unit change in the predictor. Logistic regression is a generalized linear model that uses the logit link function,

$$\text{logit}\left(p_i\right) = \ln\left(\frac{p_i}{1-p_i}\right) = \beta_0 + \beta_1 X_{1,i} + \beta_2 X_{2,i} + \ldots + \beta_m X_{m,i},\ i = 1\ldots n,$$

where $p_i = E\left(Y \middle| X_i\right) = \Pr\left(Y_i = 1\right)$ and the X's are the covariates. This is equivalent to the model:

$$\text{Pr(event)} = p_i = \frac{1}{1+\exp\left[-\left(\beta_0 + \beta_1 X_{1,i} + \beta_2 X_{2,i} + \ldots + \beta_m X_{m,i}\right)\right]}.$$

As with normal multiple regression analysis, it is also possible to test a range of models by applying stepwise inclusion or elimination of predictors. The β coefficients are to be found that maximize the conditional log-likelihood of the model given the data:

$$l\left(\boldsymbol{\beta}\right) = \sum_{i=1}^{N}\left[Y_i \log p_i + \left(1-Y_i\right)\log\left(1-p_i\right)\right].$$

In order to maximize $l\left(\boldsymbol{\beta}\right)$, the first order partial derivatives of $l\left(\boldsymbol{\beta}\right)$ are set to zero and solved according to Newton-Raphson iterations. In matrix notation, this is solved by:

$$\boldsymbol{\beta}^{new} = \boldsymbol{\beta}^{old} + \left(\boldsymbol{X}^T \boldsymbol{W} \boldsymbol{X}\right)^{-1} \boldsymbol{X}^T \left(\boldsymbol{Y} - \boldsymbol{p}\right)$$
$$= \left(\boldsymbol{X}^T \boldsymbol{W} \boldsymbol{X}\right)^{-1} \boldsymbol{X}^T \boldsymbol{W} \boldsymbol{z}$$

where $\boldsymbol{z} = \boldsymbol{X}\beta^{old} + \boldsymbol{W}^{-1}\left(\boldsymbol{Y} - \boldsymbol{p}\right)$, $\boldsymbol{p} = p\left(\boldsymbol{X}_i \middle| \beta^{old}\right)$, and W is defined as an $N \times N$ diagonal matrix of weights with the i^{th} element $p\left(\boldsymbol{X}_i \middle| \beta^{old}\right)\left(1 - p\left(\boldsymbol{X}_i \middle| \beta^{old}\right)\right)$. Here, if z is viewed as a response and X is the input matrix then $\boldsymbol{\beta}^{new}$ is the solution to a weighted least squares problem:

$$\boldsymbol{\beta}^{new} \leftarrow \min_{\boldsymbol{\beta}} \left(\boldsymbol{z} - \boldsymbol{X}\boldsymbol{\beta}\right)^{T\rightarrow} \left(\boldsymbol{z} - \boldsymbol{X}\boldsymbol{\beta}\right);$$

$\boldsymbol{z}$ is referred to as the adjusted response and the algorithm is referred to as iteratively reweighted least squares.

There is no precise way to calculate R^2 for logistic regression models. There are various measures for a pseudo-R^2, with no real consensus on preferred methods. They are not percent of variance explained, but rather an attempt to measure strength of association. These pseudo-R^2 values for logistic regression are typically always low in magnitude and this is a problem when reporting to audiences accustomed to seeing linear regression values. Thus, one must interpret the pseudo-R^2 more carefully and appropriately, or do not report them at all as Hosmer and Lemeshow suggest [215]. Cox and Snell's R^2 is an attempt to imitate the interpretation of the ordinary least squares R^2 based on the likelihood, but its maximum is usually less than one [216]. Nagelkerke's R^2 is a further modification of the Cox and Snell coefficient to ensure that it can vary from 0 to 1, by dividing the Cox and Snell R^2 by its potential maximum [217]. Among other alternatives, one could also carry out bivariate regression on the observed dependent values and predicted values and use the R^2 from this ordinary regression [218].

6.4. Smirnov Test

Like binomial logistic regression, the Smirnov two-sample test (two-sided version) [194, 219-221] can also be used when the response variable is dichotomous or upon dividing a continuous or multiple discrete response into two categories. It is applicable when a qualitative definition of a model outcome can be defined in two different categories, e.g. through a set of constraints, thresholds, or ceilings. All model outputs are classified according to the specification of the 'acceptable' model behavior; each simulation is allocated to either set A if the model output lies within the specified constraints, and set to A' otherwise. The Smirnov two-sample test (two-sided version) is performed for each predictor variable independently, analyzing the maximum distance $d_{\max}$ between the cumulative distributions of the A and A' sets (see Figure 4). The test statistic is $d_{\max}$ and is used to test the null

hypothesis that the distribution functions of the populations from which the samples have been drawn are identical. Formally,

$$H_0 : f\left(x_i \middle| A\right) = g\left(x_i \middle| A'\right)$$
$$H_1 : f\left(x_i \middle| A\right) \neq g\left(x_i \middle| A'\right)$$

and $d_{\max}\left(x_i\right) = \sup\left\|F\left(x_i \middle| A\right) - G\left(x_i \middle| A'\right)\right\|$, where F and G are marginal cumulative probability functions and f and g are the empirical density functions.

P-values for the test statistics are calculated by permutation of the exact distribution whenever possible [221-223]. All values of x_i, from $A \cup A'$, are randomly sorted (without replacement) into two groups B and B', equivalent in respective sizes to A and A'. The maximum distance between the cumulative distributions of B and B' is determined, $d^j_{\max}\left(x_i\right)$; index j denotes the j^{th} permutation. This procedure is then repeated over every possible permutation for sorting x_i values into B and B'. Then, the p-value is calculated by

$$p = 1 - \Pr\left(d^j_{\max}\left(x_i\right) < d_{\max}\left(x_i\right)\right).$$

The smaller the p-value (or equivalently the larger $d_{\max}\left(x_i\right)$), the more important is the parameter, x_i, in driving the behavior of the model. Despite some limitations, such as possible lack in statistical power [224] and that any covariate structure is not detected by the univariate $d_{\max}$ statistic, the Smirnov test is useful for distinguishing the importance of parameters in contributing to dichotomous outcomes.

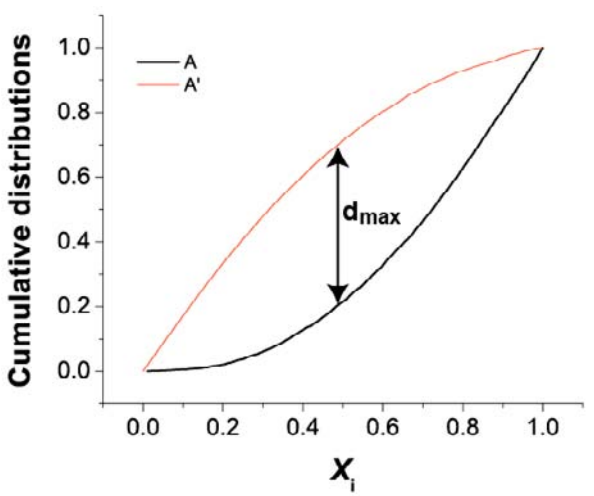

Figure 4. Graphical representation of the Smirnov test for checking the separation of the distributions under the A and A' sets.

6.5. Factor Prioritization by Reduction of Variance

Factor prioritization is a broad term denoting a school of statistical methodologies to rank the importance of variables in contributing to particular outcomes. There are many statistical measures that could be used in defining factors of importance, each measure producing its own ranking. These different measures should result in similar rankings, but not always identical. To avoid confusion, the practitioner of sensitivity analyses should decide beforehand what definition of factor importance is relevant for the analysis in question. Variance-based measures are some of the most popular in sensitivity analyses of other fields [195-202] and are appropriate for the output of uncertainty analyses of disease transmission models. However, as far as I am aware, variance-based measures have never been used in performing sensitivity analysis for disease models. Practitioners of other disciplines have come up with various measures of sensitivity or sensitivity indices related to these variance statistics [225, 226].

The objective of reduction of variance is to identify the factor which, if determined (that is, fixed to its true, albeit unknown, value), would lead to the greatest reduction in the variance of the output variable of interest, and then the second most important factor in reducing the outcome is determined etc., until all independent input factors are ranked. The concept of importance is thus explicitly linked to a reduction of the variance of the outcome. Reduction of variance can be described conceptually by the following question: for a generic model,

$$Y = f\left(X_1, \ldots, X_M\right),$$

what would happen to the uncertainty in Y if a particular independent variable X_i could be fixed as a constant? This resultant variation is defined as $V_{\mathbf{X}_{\sim i}}\left(Y \middle| X_i = x_i^*\right)$. One could expect that having fixed one source of variation $\left(X_i\right)$, the resulting variance $V_{\mathbf{X}_{\sim i}}\left(Y \middle| X_i = x_i^*\right)$ would be smaller than the total or unconditional variance $V\left(Y\right)$. Hence, $V_{\mathbf{X}_{\sim i}}\left(Y \middle| X_i = x_i^*\right)$ could be used as a measure of the importance of X_i ; the smaller $V_{\mathbf{X}_{\sim i}}\left(Y \middle| X_i = x_i^*\right)$, the more X_i is influential. However, this is based on sensitivity as a measure from the position of a single point $X_i = x_i^*$ for each input variable, and also it is possible to design a model for which $V_{\mathbf{X}_{\sim i}}\left(Y \middle| X_i = x_i^*\right)$ at particular x_i^* values is greater than the unconditional variance, $V\left(Y\right)$ [227].

In general, it is also not possible to obtain a precise factor prioritization, as this would imply knowing the true value of each factor. The purpose of the reduction of variance methodology is then to allow a rational choice of ranking importance under uncertainty. Since the true value is not known, the factor of greatest importance is chosen as the one which, on average, causes the greatest reduction in variance. “On average” specifies in this case that the variation of the outcome factor should be averaged over the defined distribution of the

specific input factor, removing the dependence on x_i^*. This is written as $E_{X_i}\left(V_{\mathbf{X}_{\sim i}}\left(Y\middle|X_i\right)\right)$ and will always be less than or equal to $V(Y)$; in fact,

$$E_{X_i}\left(V_{\mathbf{X}_{\sim i}}\left(Y\middle|X_i\right)\right)+V_{X_i}\left(E_{\mathbf{X}_{\sim i}}\left(Y\middle|X_i\right)\right)=V(Y) \text{ [226].}$$

A small $E_{X_i}\left(V_{\mathbf{X}_{\sim i}}\left(Y\middle|X_i\right)\right)$, or a large $V_{X_i}\left(E_{\mathbf{X}_{\sim i}}\left(Y\middle|X_i\right)\right)$ will imply that X_i is an important factor. Note that $V_{X_i}\left(E_{\mathbf{X}_{\sim i}}\left(Y\middle|X_i\right)\right)\le V(Y)$. Then, a first order sensitivity index of X_i on Y can be defined as

$$S_i=\frac{V_{X_i}\left(E_{\mathbf{X}_{\sim i}}\left(Y\middle|X_i\right)\right)}{V(Y)}.$$

The sensitivity index is conveniently between 0 and 1. A high value of S_i implies that X_i is an important variable. Variance based measures, such as the sensitivity index just defined, are concise, easy to understand and to communicate. This is a proper measure of sensitivity to use to rank the input factors in order of importance even if the input factors are correlated [228].

The first order variance and sensitivity can be extended to a general variance decomposition scheme, proposed by Sobol [229] where the total unconditional variance for a model with M factors can be decomposed as:

$$V(Y)=\sum_i V_i+\sum_i\sum_{j>i}V_{ij}+\ldots+V_{123\ldots M},$$

where $V_i=V\left(E(Y\mid X_i)\right)$ are the first order terms, $V_{ij}=V\left(E(Y\mid X_i,X_j)\right)-V_i-V_j$, are second order terms and higher order terms are calculated by the same pattern. If there are M terms of first order, then there are $M(M-1)/2$ second order terms, and a total of 2^M-1 teams. Evaluating every term is unwieldy and typically not done; it has been referred to by Rabitz as "the curse of dimensionality"[230]. Usually just the first order terms are calculated. The second order V_{ij} terms capture that part of the effect of X_i and X_j not described by the first order terms and can be calculated to determine interaction effects on variability. Different versions of variance measures for sensitivity can be found in various reviews [230-232].

One other complementary measure of variance, denoted $V\left(E\left(Y\mid\mathbf{X}_{-j}\right)\right)$, is the total contribution to the variance of Y that is due to all of the variables except X_j [233]. This implies that the difference $V(Y)-V\left(E\left(Y\mid\mathbf{X}_{-j}\right)\right)$ is equal to all the terms in the variance

decomposition that include X_j. The ratio of this difference to the total unconditional variance is known as the total effects sensitivity index, S_j^T. For demonstration, for the case of M=3,

$$S_1^T = \frac{V(Y) - V\left(E\left(Y \mid \mathbf{X}_{-1}\right)\right)}{V(Y)}$$
$$= \frac{E\left(V\left(Y \mid \mathbf{X}_{-1}\right)\right)}{V(Y)} = S_1 + S_{12} + S_{13} + S_{123},$$

where, for example, $S_1 = V\left(E\left(Y \mid X_1\right)\right)\Big/V(Y)$. Similarly, S_2^T and S_3^T can be calculated. The total effects terms can be useful because they give information about the non-additive parts of the model [226].

In terms of practical implementation, the unconditional variance can be easily calculated from the output data of a model. However, the conditional variances based on fixing parameters cannot be calculated as simply. If the model is simple (such as if the output variable can be expressed in a closed mathematical form) then the conditional variances can each be calculated directly from the model. But ideally a sensitivity analysis would be performed purely on the input and output data without need to refer back to the model used to generate the output from the input. In order to generate conditional variances efficiently for this sensitivity analysis, it is appropriate to use a regression model. The regression model must fit the data very well though (a high coefficient of determination R^2); arbitrarily, an R^2 value of at least 0.7 should be obtained from a regression model in order to use it in a reduction in variance sensitivity scheme.

6.7. Concluding Comments about Sensitivity Analyses

In order to simplify model sensitivity analyses, there are times when non-influential factors can be fixed as constants [229]. The objective of this setting is to identify the variable or the subset of input variables that can be fixed at any given value over their range of uncertainty without reducing significantly the output variance. If such a set is identified, then the remaining factors effectively explain almost all of the unconditional variance. The non-influential factors can be fixed anywhere in their range of variation without significant loss of information in the model.

One should also keep in mind that an unpleasant (or pleasant, depending on the viewpoint) feature of sensitivity analysis is that it may falsify the analysis altogether by, for example, showing that the model cannot answer the fundamental research question given the uncertainties, or that the model is irrelevant, or that the variation in the output of interest is insensitive to the available policy options given the uncertainties. An example that shows how sensitivity analysis can falsify a model as applied to policy-making is described in [234]. However, clearly this should not deter anyone from carrying out sensitivity analyses as it is essential in ensuring the science is performed rigorously [235].

7. Presenting Results

Remember that modeling is, by definition, applied science. Basic science has the purpose of pursuing knowledge that is unknown and applied science has a different goal, of attaining greater understanding for the purpose of more immediate and direct applied benefit. In order to make modeling investigations applicable and influence change, nothing is more important than effective communication. Clearly written manuscripts are the most obvious means. My rule of thumb is that an epidemic modeling manuscript should be written so that any intelligent person outside the field (and outside academia) can understand clearly what the investigation did, the basic constructs of how results were obtained, what the key results are, and the reasons behind these results. Effective communication also occurs directly with "real-world" field workers or policy makers throughout, and after, the investigation. But the most effective way of conveying results, around which the text of manuscripts direct dialogue should be based, is the development of high-impact, visual, clear figures.

I once heard a quote from a Professor of Applied Mathematics: "I am a mathematician; I do not draw cartoons". The inference and surrounding opinion was that more pure thought can be represented through mathematics and this was not to be defiled with pictures, figures, or cartoons. However, frankly, this professor is out of touch with reality and his research is very unlikely to influence real public health. Results must be conveyed in the most effective means. This means well thought out illustrations and figures are essential. Otherwise, the best models and results will often be in vain and the message will be much more difficult to receive by people in need of it outside the biomathematics field. A visual representation of an analytical relationship or a good numeric-based figure is valuable in conveying the point of a piece of work. Figures and the discussion around the figures are often the influential aspects of a good scientific manuscript. As the saying goes… a picture is worth a thousand words (or Greek symbols). Lastly, generate figures that are easily understood. For example, to reach the medical community use plots that they are familiar with, such as Kaplan Meier curves for example. The amount of simulated data that can be produced, especially from full uncertainty and sensitivity analyses, is massive. Accordingly, we are able to produce many colorful and descriptive plots. We should do so, but ensure that they are not too cluttered, are easy to understand, and make a clear and powerful point.

Color can also be greatly utilized to distinguish features of the plot. When one prints in black and white, the figures should still be interpretable. Since colorblindness is fairly common (one in twelve Caucasians, one in twenty Asians, and one in twenty-five Africans) [236], it is also essential to take certain colors into consideration to avoid alienating this relatively large group (see http://jfly.iam.u-tokyo.ac.jp/color/); for example, instead of using red-green use magenta-green.

8. Conclusions

Epidemiology of infectious diseases is no longer purely dominated by identifying aetiological agents and risk factors, but has moved more towards understanding the complex mechanisms involved in controlling the distribution of diseases in populations [237]. Mathematical disease transmission models provide an ideal framework for theoretical investigation of these mechanisms. However, the language of mathematics can be intimidating for non-

mathematicians. This can lead to both extremes of reception of modeling investigations: either being ignored, or accepted uncritically. Modelers are required to present the models in a balanced manner somewhere between describing the full complexity of irrelevant details and presenting a "black box" without outlining its critical assumptions. Being interdisciplinary by nature, practitioners of biomathematics require exceptional communication skills in order to effectively convey modeling investigations to the appropriate "real-world" audience where they will hopefully inform, guide, and assist in influencing and changing public health policy.

One of the paradoxes in infectious disease modeling is that although the approach is quantitative in nature, often the results and conclusions that are drawn from investigations can only provide qualitative insights. But valid qualitative insights can assist in the development or changing of public health policy. A primary purpose of modeling is to predict the consequences of changes due to different interventions. Accordingly, the models provide a tool to translate theoretical intervention strategies into meaningful patterns and trends to inform policy-makers. Infection transmission modeling has provided valuable insight into the nonlinear dynamics that spread infection. To further influence public policy, models should (i) improve the intuitions of policy makers to the ways that their decisions affect the behavior of the transmission system; (ii) deal explicitly with all the issues that the policy makers see as important to making their decision; and (iii) allow the policy makers to locate reality as they see it within the model structure so that they feel confident that the results they are looking at are relevant to their decision [103]. Effective modeling should always be an iterative process, with dialogue between modelers, experimentalists, field workers, and policymakers. In order for epidemic models to be investigated most appropriately for application, less emphasis should be placed on the equations and more on the parameters of the model equations. To treat this issue thoroughly, not only should interdisciplinary experts be consulted frequently, but rigorous uncertainty and sensitivity analyses should be conducted. Complete methodologies and algorithms for standard and novel uncertainty and sensitivity analyses have been provided in this chapter. The application of these techniques may have considerable utility in a wide variety of applied mathematical applications. But this current standard set of methods is by no means complete; there is plenty of room for expansion of the suite of tools used in the field, drawing from any quantitative framework (whether it be statistics, economics, computer science, risk analysis, or the plethora of other related disciplines).

References

[1] Bernoulli, D., Essai d'une nouvelle analyse de la mortalit cause par la petite vrole et des advantages de l'inoculation pour la prvenir. *Mem Math Phy Acad Roy Sci Paris*, 1766: p. 1-45.

[2] Blower, S. and D. Bernoulli, An attempt at a new analysis of the mortality caused by smallpox and of the advantages of inoculation to prevent it. 1766. *Rev Med Virol*, 2004. 14(5): p. 275-88.

[3] Halley, E., An Estimate of the Degrees of the Mortality of Mankind, drawn from curious Tables of the Births and Funerals at the City of Breslaw; with an Attempt to

ascertain the Price of Annuities upon Lives. *Phil. Trans. Roy. Soc. Lond*., 1963. 17(196): p. 596-610.

[4] Dietz, K. and J.A. Heesterbeek, Bernoulli was ahead of modern epidemiology. *Nature*, 2000. 408(6812): p. 513-4.

[5] Farr, W., *Progress of epidemics, in Second report of the Registrar General of England.* 1840: London. p. 91-98.

[6] Hammer, W.H., Epidemic disease in England. *The Lancet*, 1906. i: p. 733-739.

[7] Kermack, W.O. and A.G. McKendrick, A contribution to the mathematical theory of epidemics. *Proc. R. Soc.,* 1927. A115: p. 700-721.

[8] Bailey, N.T.J., *The Mathematical Theory of Infectious Diseases and its Applications*. 1975, London: Charles Griffin.

[9] Anderson, R.M. and R.M. May, *Infectious Diseases of Humans*. 1991, Oxford: Oxford University Press.

[10] Anderson, R.M., R.M. May, and A.R. McLean, Possible demographic consequences of AIDS in developing countries. *Nature*, 1988. 332(6161): p. 228-34.

[11] Bongaarts, J., A model of the spread of HIV infection and the demographic impact of AIDS. *Statistics in Medicine*, 1989. 8: p. 103-20.

[12] Chin, J. and S.K. Lwanga, Estimation and projection of adult AIDS cases: a simple epidemiological model. *Bull World Health Organ*, 1991. 69: p. 399-406.

[13] Wilson, D.P., J. Kahn, and S.M. Blower, Predicting the epidemiological impact of antiretroviral allocation strategies in KwaZulu-Natal: the effect of the urban-rural divide. *Proc Natl Acad Sci U S A,* 2006. 103(38): p. 14228-33.

[14] Blower, S.M., R.B. Moss, and E. Fernandez-Cruz, Calculating the potential epidemic-level impact of therapeutic vaccination on the San Francisco HIV epidemic. *AIDScience,* 2003. 3(21).

[15] Blower, S., E.J. Schwartz, and J. Mills, Forecasting the future of HIV epidemics: the impact of antiretroviral therapies & imperfect vaccines. *AIDS Rev*, 2003. 5(2): p. 113-25.

[16] Blower, S.M., A.N. Aschenbach, and J.O. Kahn, Predicting the transmission of drug-resistant HIV: comparing theory with data. *Lancet Infect Dis*, 2003. 3(1): p. 10-1.

[17] Lipsitch, M., et al., Transmission dynamics and control of severe acute respiratory syndrome. *Science,* 2003. 300(5627): p. 1966-70.

[18] Riley, S., et al., Transmission dynamics of the etiological agent of SARS in Hong Kong: impact of public health interventions. *Science,* 2003. 300(5627): p. 1961-6.

[19] Kaplan, E.H., D.L. Craft, and L.M. Wein, Emergency response to a smallpox attack: the case for mass vaccination. *Proc Natl Acad Sci U S A*, 2002. 99(16): p. 10935-40.

[20] Kaplan, E.H., D.L. Craft, and L.M. Wein, Analyzing bioterror response logistics: the case of smallpox. *Math Biosci*, 2003. 185(1): p. 33-72.

[21] Koopman, J., Epidemiology. Controlling smallpox. *Science,* 2002. 298(5597): p. 1342-4.

[22] Longini, I.M., Jr., P.E. Fine, and S.B. Thacker, Predicting the global spread of new infectious agents. *Am J Epidemiol*, 1986. 123(3): p. 383-91.

[23] Becker, N.G., Parametric inference for epidemic models. *Math Biosci*, 1993. 117(1-2): p. 239-51.

[24] Halloran, M.E., et al., Community interventions and the epidemic prevention potential. *Vaccine*, 2002. 20(27-28): p. 3254-62.

[25] Ovaskainen, O.T. and B.T. Grenfell, Mathematical tools for planning effective intervention scenarios for sexually transmitted diseases. *Sex Transm Dis*, 2003. 30(5): p. 388-94.
[26] Kaplan, E.H., Preventing second-generation infections in a smallpox bioterror attack. *Epidemiology*, 2004. 15(3): p. 264-70.
[27] Kaplan, E.H. and L.M. Wein, Smallpox bioterror response. *Science,* 2003. 300(5625): p. 1503-4; author reply 1503-4.
[28] Brisson, M., et al., Modelling the impact of immunization on the epidemiology of varicella zoster virus. *Epidemiol Infect*, 2000. 125(3): p. 651-69.
[29] De Serres, G., N.J. Gay, and C.P. Farrington, Epidemiology of transmissible diseases after elimination. *Am J Epidemiol*, 2000. 151(11): p. 1039-48; discussion 1049-52.
[30] van den Hof, S., et al., Protecting the vaccinating population in the face of a measles epidemic: assessing the impact of adjusted vaccination schedules. *Epidemiol Infect,* 2002. 128(1): p. 47-57.
[31] Blower, S.M., P.M. Small, and P.C. Hopewell, Control strategies for tuberculosis epidemics: new models for old problems. *Science,* 1996. 273(5274): p. 497-500.
[32] Garnett, G.P., An introduction to mathematical models in sexually transmitted disease epidemiology. *Sex Transm Infect*, 2002. 78(1): p. 7-12.
[33] Koopman, J.S., G. Jacquez, and S.E. Chick, New data and tools for integrating discrete and continuous population modeling strategies. *Ann N Y Acad Sci*, 2001. 954: p.268-94.
[34] Hethcote, H.W. and J.A. Yorke, Gonnorrhea transmission dynamics and control, *Lecture notes in Biomathematics*. 1984, New York: Springer.
[35] Anderson, R.M. and R.M. May, Population biology of infectious diseases: Part I. *Nature*, 1979. 280(5721): p. 361-7.
[36] May, R.M. and R.M. Anderson, Population biology of infectious diseases: Part II. *Nature*, 1979. 280(5722): p. 455-61.
[37] Anderson, R.M., et al., A preliminary study of the transmission dynamics of the human immunodeficiency virus (HIV), the causative agent of AIDS. *IMA J Math Appl Med Biol*, 1986. 3(4): p. 229-63.
[38] Diekmann, O. and J.A.P. Heesterbeek, *Mathematical Epidemiology of Infectious Diseases: Model Building, Analysis and Interpretation*. 2000, Chichester, UK: Wiley.
[39] Soper, H.E., Interpretation of periodicity in disease prevalence. *J. Roy. Stat. Soc., Series B,* 1929. 92: p. 34-73.
[40] Kermack, W.O. and A.G. McKendrick, Contributions to the mathematical theory of epidemics, part. II,. *Proc. Roy. Soc. London*, 1932. 138: p. 55-83.
[41] Edelstein-Keshet, L., *Mathematical Models in Biology* (Classics in Applied Mathematics). 2005, Philadelphia: SIAM.
[42] Murray, J.D., *Mathematical Biology*. 1980: Springer-Verlag.
[43] Brauer, F. and C. Castillo-Chavez, *Mathematical Models in Population Biology and Epidemiology*. 2001, New York: Springer-Verlag.
[44] Anderson, R.M., *The transmission dynamics of sexually transmitted diseases: The behavioural component, in Sexual Behaviour and Networking: Anthropological and Socio-Cultural Studies on the Transmission of HIV*. 1992, Derouaux-Ordina Liège.
[45] Hyman, J.M., J. Li, and E.A. Stanley, Threshold conditions for the spread of HIV infection in age-structured populations of homosexual men. *J. Theor. Biol.*, 1994. 166: p. 9-31.

[46] Blower, S.M. and C. Boe, Sex acts, sex partners, and sex budgets: implications for risk factor analysis and estimation of HIV transmission probabilities. *J Acquir Immune Defic Syndr*, 1993. 6(12): p. 1347-52.

[47] Le Pont, F. and S.M. Blower, The supply and demand dynamics of sexual behavior: implications for heterosexual HIV epidemics. *J Acquir Immune Defic Syndr*, 1991. 4(10): p. 987-99.

[48] Anderson, R.M., et al., Age-dependent choice of sexual partners and the transmission dynamics of HIV in Sub-Saharan Africa. *Philos Trans R Soc Lond B Biol Sci*, 1992. 336(1277): p. 135-55.

[49] Blythe, S.P., et al., Toward a unified theory of sexual mixing and pair formation. *Math Biosci*, 1991. 107(2): p. 379-405.

[50] Busenberg, S. and C. Castillo-Chavez, A general solution of the problem of mixing of subpopulations and its application to risk- and age-structured epidemic models for the spread of AIDS. *IMA J Math Appl Med Biol*, 1991. 8(1): p. 1-29.

[51] Garnett, G.P. and R.M. Anderson, Factors controlling the spread of HIV in heterosexual communities in developing countries: patterns of mixing between different age and sexual activity classes. *Philos Trans R Soc Lond B Biol Sci*, 1993. 342(1300): p. 137-59.

[52] Garnett, G.P. and R.M. Anderson, Balancing sexual partnerships in an age and activity stratified model of HIV transmission in heterosexual populations. *IMA J Math Appl Med Biol*, 1994. 11(3): p. 161-92.

[53] Garnett, G.P., et al., Gonococcal infection, infertility, and population growth: II. The influence of heterogeneity in sexual behaviour. *IMA J Math Appl Med Biol*, 1992. 9(2): p. 127-44.

[54] Gupta, S., R.M. Anderson, and R.M. May, Networks of sexual contacts: implications for the pattern of spread of HIV. *Aids*, 1989. 3(12): p. 807-17.

[55] Johnson, A.M., et al., Sexual lifestyles and HIV risk. *Nature*, 1992. 360(6403): p. 410-2.

[56] Rottingen, J.A. and G.P. Garnett, The epidemiological and control implications of HIV transmission probabilities within partnerships. *Sex Transm Dis,* 2002. 29(12): p. 818-27.

[57] McKendrick, A.G., Applications of mathematics to medical problems. *Proc. Edinburgh Math. Soc*., 1926. 14: p. 98-130.

[58] Wilson, E.B. and M.H. Burke, The epidemic curve. *Proc. Nat. Acad. Sci*., 1942. 28: p. 361-367.

[59] Wilson, E.B. and M.H. Burke, The epidemic curve, II. *Proc. Nat. Acad. Sci*., 1943. 29(43-48).

[60] Abbey, H., An examination of the Reed-Frost theory of epidemics. *Hum. Biology*, 1952. 24: p. 201-233.

[61] Dietz, K. and D. Schenzle, *Mathematical models for infectious disease statistics., in A Celebration of Staitistics*, S.E.F. A.C. Atkinson, Editor. 1985, Springer-Verlag: New York. p. 167-204.

[62] Hethcote, H.W., A thousand and one epidemic models. *Lecture Notes in Biomathematics*, 1994. 100: p. 504-515.

[63] Rubinstein, R.Y., *Simulation and the Monte Carlo method*. 1981, New York: John Wiley.

[64] Bailey, N.T.J., The Elements of Stochastic *Processes with Applications to the Natural Sciences*. 1964, New York: John Wiley.
[65] Cox, D.R. and H.T. Miller, *The Theory of Stochastic Processes*. 1965, London: Methuen.
[66] Karlin, S. and H.M. Taylor, *A First Course in Stochastic Processes* (2nd Edition). 1975, New York: Academic Press.
[67] Karlin, S. and H.M. Taylor, *An Introduction to Stochastic Models*. 1984, New York: Academic Press.
[68] Bartlett, M.S., *An Introduction to Stochastic Processes (3rd Edition)*. 1978, Cambridge: Cambridge University Press.
[69] Ross, S.M., *Stochastic Processes*. 1983, New York: John Wiley.
[70] Daley, D.J. and J. Gani, *Epidemic Modelling: An Introduction*. 2005, Cambridge: Cambridge University Press.
[71] Ferguson, N.M. and G.P. Garnett, More realistic models of sexually transmitted disease transmission dynamics: sexual partnership networks, pair models, and moment closure. *Sex Transm Dis*, 2000. 27(10): p. 600-9.
[72] Ghani, A.C. and G.P. Garnett, Risks of acquiring and transmitting sexually transmitted diseases in sexual partner networks. *Sex Transm Dis*, 2000. 27(10): p. 579-87.
[73] Morris, M. and M. Kretzschmar, Concurrent partnerships and the spread of HIV. *Aids*, 1997. 11(5): p. 641-8.
[74] Kretzschmar, M., Y.T. van Duynhoven, and A.J. Severijnen, Modeling prevention strategies for gonorrhea and Chlamydia using stochastic network simulations. *Am J Epidemiol*, 1996. 144(3): p. 306-17.
[75] Ghani, A.C., et al., Sexual partner networks in the transmission of sexually transmitted diseases. An analysis of gonorrhea cases in Sheffield, UK. *Sex Transm Dis*, 1996. 23(6): p. 498-503.
[76] Potterat, J.J., R.B. Rothenberg, and S.Q. Muth, Network structural dynamics and infectious disease propagation. *Int J STD AIDS*, 1999. 10(3): p. 182-5.
[77] Kuperman, M. and G. Abramson, Small world effect in an epidemiological model. *Phys Rev Lett,* 2001. 86(13): p. 2909-12.
[78] Newman, M.E., Spread of epidemic disease on networks. Phys Rev E Stat Nonlin *Soft Matter Phys,* 2002. 66(1 Pt 2): p. 016128.
[79] Newman, M.E., Properties of highly clustered networks. Phys Rev E Stat Nonlin *Soft Matter Phys,* 2003. 68(2 Pt 2): p. 026121.
[80] Kretzschmar, M. and M. Morris, Measures of concurrency in networks and the spread of infectious disease. *Math Biosci*, 1996. 133(2): p. 165-95.
[81] Keeling, M.J., D.A. Rand, and A.J. Morris, Correlation models for childhood epidemics. *Proc Biol Sci*, 1997. 264(1385): p. 1149-56.
[82] Kaplan, E.H. and M. Johri, Treatment on demand: an operational model. *Health Care Manag Sci*, 2000. 3(3): p. 171-83.
[83] Kaplan, E.H. and M.H. Merson, Allocating HIV-prevention resources: balancing efficiency and equity. *Am J Public Health*, 2002. 92(12): p. 1905-7.
[84] Paltiel, A.D. and E.H. Kaplan, The epidemiological and economic consequences of AIDS clinical trials. J Acquir Immune *Defic Syndr*, 1993. 6(2): p. 179-90.
[85] Paltiel, A.D. and E.H. Kaplan, The cost-effectiveness of HIV testing: accounting for differential participation rates. *Med Decis Making*, 1997. 17(4): p. 490-5.

[86] Wein, L.M., D.L. Craft, and E.H. Kaplan, Emergency response to an anthrax attack. *Proc Natl Acad Sci U S A*, 2003. 100(7): p. 4346-51.
[87] Malangu, N., Estimating the number of antiretroviral treatment facilities based on the Wilson-Blower method. *PLoS Med,* 2005. 2(8): p. e270.
[88] Wilson, D.P. and S.M. Blower, Designing equitable antiretroviral allocation strategies in resource-constrained countries. *PLoS Med*, 2005. 2(2): p. e50.
[89] Wilson, D.P. and S.M. Blower, How far will we need to go to reach HIV-infected people in rural South Africa? *BMC Medicine*, 2007. In Press.
[90] Addie, R.G., M. Zukerman, and T.D. Neame, Broadband traffic modeling: simple solutions to hard problems. *Communications Magazine*, *IEEE*, 1998. 36(8): p. 88-95.
[91] Hillier, F.S. and G.J. Lieberman, *Introduction to Operations Research* (Eighth Ed.). 2005, Boston: McGraw-Hill.
[92] Winston, W., *Operations Research: Applications and Algorithms* (Fourth Ed.). 2003: Duxbury Press.
[93] Jung, E., S. Lenhart, and Z. Feng, Optimal control of treatments in a two-strain tuberculosis model. *Discrete and Continuous Dynamical Systems - Series B*, 2002. 2(4): p. 473-482.
[94] Fister, K.R., S. Lenhart, and J.S. McNally, Optimizing chemotherapy in an HIV model. *Electronic J. Differential Equations*, 1998: p. 1-12.
[95] Kirschner, D., S. Lenhart, and S. Serbin, Optimal control of the chemotherapy of HIV. *J Math Biol,* 1997. 35(7): p. 775-92.
[96] Nocedal, J. and S. Wright, *Numerical Optimization*. 2000, New York: Springer.
[97] Bertsekas, D.P., *Dynamic Programming and Optimal Control*. 2007: Athena Scientific.
[98] Robinett, R.D., et al., *Applied Dynamic Programming for Optimization of Dynamical Systems* (Advances in Design and Control). 2005, Philadelphia: SIAM.
[99] Bauch, C.T. and D.J. Earn, Vaccination and the theory of games. *Proc Natl Acad Sci U S A*, 2004. 101(36): p. 13391-4.
[100] Bauch, C.T., A.P. Galvani, and D.J. Earn, Group interest versus self-interest in smallpox vaccination policy. *Proc Natl Acad Sci U S A*, 2003. 100(18): p. 10564-7.
[101] Vardavas, R., R. Breban, and S. Blower, Can influenza epidemics be prevented by voluntary vaccination? *PLoS Comput Biol*, 2007. 3(5): p. e85.
[102] Smith, R.J., et al., Evaluating the potential impact of vaginal microbicides to reduce the risk of acquiring HIV in female sex workers. *Aids*, 2005. 19(4): p. 413-21.
[103] Koopman, J., Modeling infection transmission. *Annu Rev Public Health,* 2004. 25: p. 303-26.
[104] Anderson, D.C., et al., Preventing needlestick injuries. *Bmj*, 1991. 302(6779): p. 769-70.
[105] Anderson, R.M. and R.M. May, Immunisation and herd immunity. *Lancet*, 1990. 335(8690): p. 641-5.
[106] Blower, S., Modeling the potential public health impact of imperfect HIV vaccines. *J Infect Dis,* 2005. 192(8): p. 1494-5; author reply 1495-6.
[107] Blower, S., et al., The antiretroviral rollout and drug-resistant HIV in Africa: insights from empirical data and theoretical models. *Aids*, 2005. 19(1): p. 1-14.
[108] Blower, S.M., et al., Predicting the unpredictable: transmission of drug-resistant HIV. *Nat Med*, 2001. 7(9): p. 1016-20.

[109] Blower, S.M., et al., Live attenuated HIV vaccines: predicting the tradeoff between efficacy and safety. *Proc Natl Acad Sci U S A*, 2001. 98(6): p. 3618-23.
[110] Bonten, M.J., D.J. Austin, and M. Lipsitch, Understanding the spread of antibiotic resistant pathogens in hospitals: mathematical models as tools for control. *Clin Infect Dis*, 2001. 33(10): p. 1739-46.
[111] Earn, D.J., et al., A simple model for complex dynamical transitions in epidemics. *Science,* 2000. 287(5453): p. 667-70.
[112] Grenfell, B.T., O.N. Bjornstad, and J. Kappey, Travelling waves and spatial hierarchies in measles epidemics. *Nature*, 2001. 414(6865): p. 716-23.
[113] Gupta, S., J. Swinton, and R.M. Anderson, Theoretical studies of the effects of heterogeneity in the parasite population on the transmission dynamics of malaria. *Proc Biol Sci*, 1994. 256(1347): p. 231-8.
[114] Halloran, M.E., M. Haber, and I.M. Longini, Jr., Interpretation and estimation of vaccine efficacy under heterogeneity. *Am J Epidemiol*, 1992. 136(3): p. 328-43.
[115] Hethcote, H.W., Measles and rubella in the United States. *Am J Epidemiol*, 1983. 117(1): p. 2-13.
[116] Kretzschmar, M., et al., Vaccination against hepatitis B in low endemic countries. *Epidemiol Infect*, 2002. 128(2): p. 229-44.
[117] Lipsitch, M., et al., Effects of antiviral usage on transmission dynamics of herpes simplex virus type 1 and on antiviral resistance: predictions of mathematical models. *Antimicrob Agents Chemother*, 2000. 44(10): p. 2824-35.
[118] Nokes, D.J. and R.M. Anderson, Measles, mumps, and rubella vaccine: what coverage to block transmission? *Lancet*, 1988. 2(8624): p. 1374.
[119] Stilianakis, N.I., A.S. Perelson, and F.G. Hayden, Emergence of drug resistance during an influenza epidemic: insights from a mathematical model. *J Infect Dis*, 1998. 177(4): p. 863-73.
[120] Vardavas, R. and S. Blower, The Emergence of HIV Transmitted Resistance in Botswana: "When Will the WHO Detection Threshold Be Exceeded?" *PLoS ONE,* 2007. 2: p. e152.
[121] Yorke, J.A., H.W. Hethcote, and A. Nold, Dynamics and control of the transmission of gonorrhea. *Sex Transm Dis*, 1978. 5(2): p. 51-6.
[122] Ziv, E., C.L. Daley, and S.M. Blower, Early therapy for latent tuberculosis infection. *Am J Epidemiol*, 2001. 153(4): p. 381-5.
[123] Diekmann, O., J.A. Heesterbeek, and J.A. Metz, On the definition and the computation of the basic reproduction ratio R0 in models for infectious diseases in heterogeneous populations. *J Math Biol,* 1990. 28(4): p. 365-82.
[124] Finkenstadt, B. and B. Grenfell, Empirical determinants of measles metapopulation dynamics in England and Wales. *Proc Biol Sci,* 1998. 265(1392): p. 211-20.
[125] Keeling, M.J. and C.A. Gilligan, Metapopulation dynamics of bubonic plague. *Nature*, 2000. 407(6806): p. 903-6.
[126] Keeling, M.J. and B.T. Grenfell, Understanding the persistence of measles: reconciling theory, simulation and observation. *Proc Biol Sci*, 2002. 269(1489): p. 335-43.
[127] van den Driessche, P. and J. Watmough, Reproduction numbers and sub-threshold endemic equilibria for compartmental models of disease transmission. *Math Biosci*, 2002. 180: p. 29-48.

[128] Breban, R., R. Vardavas, and S. Blower, Theory versus Data: How to Calculate R(0)? *PLoS ONE,* 2007. 2: p. e282.
[129] Breban, R., R. Vardavas, and S. Blower, Linking population-level models with growing networks: a class of epidemic models. *Phys Rev E Stat Nonlin Soft Matter Phys*, 2005. 72(4 Pt 2): p. 046110.
[130] Green, D.M., I.Z. Kiss, and R.R. Kao, Parameterization of individual-based models: comparisons with deterministic mean-field models. *J Theor Biol,* 2006. 239(3): p. 289-97.
[131] Keeling, M.J. and B.T. Grenfell, Individual-based perspectives on R(0). *J Theor Biol*, 2000. 203(1): p. 51-61.
[132] Mills, C.E., J.M. Robins, and M. Lipsitch, Transmissibility of 1918 pandemic influenza. *Nature*, 2004. 432(7019): p. 904-6.
[133] May, R.M. and R.M. Anderson, The transmission dynamics of human immunodeficiency virus (HIV). *Philos Trans R Soc Lond B Biol Sci*, 1988. 321(1207): p. 565-607.
[134] McLean, A.R. and S.M. Blower, Imperfect vaccines and herd immunity to HIV. *Proc Biol Sci,* 1993. 253(1336): p. 9-13.
[135] McLean, A.R. and S.M. Blower, Modelling HIV vaccination. *Trends Microbiol*, 1995. 3(12): p. 458-62.
[136] Smith, R.J. and S.M. Blower, Could disease-modifying HIV vaccines cause population-level perversity? *Lancet Infect Dis,* 2004. 4(10): p. 636-9.
[137] McCabe, C. and S. Dixon, Testing the validity of cost-effectiveness models. *Pharmacoeconomics*, 2000. 17(5): p. 501-13.
[138] Sendi, P.P., et al., Systematic validation of disease models for pharmacoeconomic evaluations. Swiss HIV Cohort Study. *J Eval Clin Pract*, 1999. 5(3): p. 283-95.
[139] Weinstein, M.C., et al., Principles of good practice for decision analytic modeling in health-care evaluation: report of the ISPOR Task Force on Good Research Practices--Modeling Studies. *Value Health*, 2003. 6(1): p. 9-17.
[140] Weinstein, M.C., et al., Modeling for health care and other policy decisions: uses, roles, and validity. *Value Health*, 2001. 4(5): p. 348-61.
[141] Becker, N., *Analysis of Infectious Disease Data*. 1989, New York: Chapman and Hall.
[142] Brookhart, M.A., et al., Statistical estimation of parameters in a disease transmission model: analysis of a Cryptosporidium outbreak. *Stat Med,* 2002. 21(23): p. 3627-38.
[143] Longini, I.M., Jr., A.S. Monto, and J.S. Koopman, Statistical procedures for estimating the community probability of illness in family studies: rhinovirus and influenza. *Int J Epidemiol*, 1984. 13(1): p. 99-106.
[144] O'Neill, P.D., A tutorial introduction to Bayesian inference for stochastic epidemic models using Markov chain Monte Carlo methods. *Math Biosci*, 2002. 180: p. 103-14.
[145] Elderd, B.D., V.M. Dukic, and G. Dwyer, Uncertainty in predictions of disease spread and public health responses to bioterrorism and emerging diseases. *Proc Natl Acad Sci U S A*, 2006. 103(42): p. 15693-7.
[146] Spear, R.C., et al., Disease transmission models for public health decision making: toward an approach for designing intervention strategies for Schistosomiasis japonica. *Environ Health Perspect*, 2002. 110(9): p. 907-15.

[147] Deuchert, E. and S. Brody, Plausible and implausible parameters for mathematical modeling of nominal heterosexual HIV transmission. *Ann Epidemiol*, 2007. 17(3): p. 237-44.
[148] Gray, R.H., et al., Increased risk of incident HIV during pregnancy in Rakai, Uganda: a prospective study. *Lancet*, 2005. 366(9492): p. 1182-8.
[149] Napravnik, S., et al., Triple-class antiretroviral drug resistance: risk and predictors among HIV-1-infected patients. *AIDS*, 2007. 21(7): p. 825-34.
[150] Gelman, A., et al., *Bayesian Data Analysis*. 2004, London: Chapman and Hall.
[151] Streftaris, G. and G.J. Gibson, Bayesian analysis of experimental epidemics of foot-and-mouth disease. *Proc Biol Sci*, 2004. 271(1544): p. 1111-7.
[152] Sweeting, M.J., D. De Angelis, and O.O. Aalen, Bayesian back-calculation using a multi-state model with application to HIV. *Stat Med*, 2005. 24(24): p. 3991-4007.
[153] Tan, W.Y. and Z. Ye, Estimation of HIV infection and incubation via state space models. *Math Biosci*, 2000. 167(1): p. 31-50.
[154] Tanaka, M.M., et al., Using approximate Bayesian computation to estimate tuberculosis transmission parameters from genotype data. *Genetics*, 2006. 173(3): p. 1511-20.
[155] McBryde, E.S., A.N. Pettitt, and D.L. McElwain, A stochastic mathematical model of methicillin resistant Staphylococcus aureus transmission in an intensive care unit: predicting the impact of interventions. *J Theor Biol*, 2007. 245(3): p. 470-81.
[156] Putter, H., et al., A Bayesian approach to parameter estimation in HIV dynamical models. *Stat Med,* 2002. 21(15): p. 2199-214.
[157] Wu, H., et al., Modeling and estimation of replication fitness of human immunodeficiency virus type 1 in vitro experiments by using a growth competition assay. *J Virol*, 2006. 80(5): p. 2380-9.
[158] Raftery, A.E., G.H. Givens, and J.E. Zeh, Inference from a deterministic population dynamics model for bowhead whales. *Journal of the American Statistical Association*, 1995. 90(430): p. 402-16.
[159] Davison, A.C.H., D.V., *Bootstrap Methods and their Application*. 1997, New York: Cambridge University Press.
[160] Carpenter, J. and J. Bithell, Bootstrap confidence intervals: when, which, what? A practical guide for medical statisticians. *Stat Med*, 2000. 19(9): p. 1141-64.
[161] Blower, S.M. and H. Dowlatabadi, Sensitivity and uncertainty analysis of complex models of disease transmission: an HIV model, as an example. *Internat Stat Rev*, 1994. 2: p. 229-243.
[162] Burnham, K.P., Anderson, D. R., Model selection and multimodel inference: a practical information-theoretic approach (2nd Edition). 2002, New York: Springer-Verlag.
[163] Dyson, F., A meeting with Enrico Fermi. *Nature*, 2004. 427(6972): p. 297.
[164] Campbell, K., Statistical calibration of computer simulations *Reliability Engineering & System Safety,* 2006. 91: p. 1358-1363.
[165] Higdon, D., et al., Combining field data and computer simulations for Calibration and Prediction. *Siam J Sci Comput* 2004. 26: p. 448–466.
[166] Kennedy, M.C. and A. O'Hagan, Bayesian calibration of computer models. *J R Stat Soc B* 2001. 63: p. 425–464.

[167] Spear, R.C. and G.M. Hornberger, Eutrophication in Peel Inlet: II. Identification of critical uncertainties via a generalized sensitivity analysis. *Water Research*, 1980. 14: p. 43-9.
[168] Rose, K.A., et al., Parameter sensitivities, monte carlo filtering, and model forecasting under uncertainty. *Journal of Forecasting*, 1991. 10: p. 117-133.
[169] Fedra, K., G. Van Straten, and M.B. Beck, Uncertainty and arbitrariness in ecosystems modeling: A lake modeling example. *Ecological Modelling*, 1981. 13: p. 87-110.
[170] Eisenberg, J.N., et al., Quantifying water pathogen risk in an epidemiological framework. *Risk Anal*, 1996. 16(4): p. 549-63.
[171] Blower, S.M., et al., Drugs, sex and HIV: a mathematical model for New York City. *Philos Trans R Soc Lond B Biol Sci*, 1991. 331(1260): p. 171-87.
[172] Blower, S.M., et al., The intrinsic transmission dynamics of tuberculosis epidemics. *Nat Med*, 1995. 1(8): p. 815-21.
[173] Blower, S.M., T.C. Porco, and G. Darby, Predicting and preventing the emergence of antiviral drug resistance in HSV-2. *Nat Med*, 1998. 4(6): p. 673-8.
[174] Lietman, T., et al., Global elimination of trachoma: how frequently should we administer mass chemotherapy? *Nat Med*, 1999. 5(5): p. 572-6.
[175] Porco, T.C. and S.M. Blower, Quantifying the intrinsic transmission dynamics of tuberculosis. *Theor Popul Biol*, 1998. 54(2): p. 117-32.
[176] Sanchez, M.A. and S.M. Blower, Uncertainty and sensitivity analysis of the basic reproductive rate. Tuberculosis as an example. *Am J Epidemiol*, 1997. 145(12): p. 1127-37.
[177] Blower, S. and L. Ma, Calculating the contribution of herpes simplex virus type 2 epidemics to increasing HIV incidence: treatment implications. *Clin Infect Dis*, 2004. 39 Suppl 5: p. S240-7.
[178] Blower, S., et al., Predicting the impact of antiretrovirals in resource-poor settings: preventing HIV infections whilst controlling drug resistance. *Curr Drug Targets Infect Disord*, 2003. 3(4): p. 345-53.
[179] Blower, S.M. and T. Chou, Modeling the emergence of the 'hot zones': tuberculosis and the amplification dynamics of drug resistance. *Nat Med*, 2004. 10(10): p. 1111-6.
[180] Breban, R., et al., Modeling the potential impact of rectal microbicides to reduce HIV transmission in bathhouses. *Mathematical Biosciences and Engineering*, 2006. 3(3): p. 459-466.
[181] Blower, S. and P. Volberding, What can modeling tell us about the threat of antiviral drug resistance? *Curr Opin Infect Dis*, 2002. 15(6): p. 609-14.
[182] Blower, S.M., H.B. Gershengorn, and R.M. Grant, A tale of two futures: HIV and antiretroviral therapy in San Francisco. *Science,* 2000. 287(5453): p. 650-4.
[183] Velasco-Hernandez, J.X., H.B. Gershengorn, and S.M. Blower, Could widespread use of combination antiretroviral therapy eradicate HIV epidemics? *Lancet Infect Dis*, 2002. 2(8): p. 487-93.
[184] Iman, R.L. and J.C. Helton, An Investigation of Uncertainty and Sensitivity Analysis *Techniques for Computer Models. Risk Analysis*, 1988. 8(1): p. 71-90.
[185] Blower, S.M. and H. Dowlatabadi, Sensitivity and uncertainty analysis of complex-models of disease transmission - an HIV model, as an example. *International Statistical Review*, 1994. 62(2): p. 229-243.

[186] Iman, R.L., J.C. Helton, and J.E. Campbell, An Approach To Sensitivity Analysis Of Computer-Models .1. Introduction, Input Variable Selection And Preliminary Variable Assessment. *Journal Of Quality Technology*, 1981. 13(3): p. 174.

[187] Iman, R.L., J.C. Helton, and J.E. Campbell, An approach to sensitivity analysis of computer-models .2. Ranking of input variables, response-surface validation, distribution effect and technique synopsis. *Journal of Quality Technology*, 1981. 13(4): p. 232.

[188] Iman, R.L. and J.C. Helton, An Investigation Of Uncertainty And Sensitivity Analysis Techniques For Computer-Models. *Risk Analysis*, 1988. 8(1): p. 71.

[189] McKay, M.D., R.J. Beckman, and W.J. Conover, A comparison of three methods for selecting values of input variables in the analysis of output from a computer code. *Technometrics*, 2000. 42(1): p. 55.

[190] McKay, M.D., W.J. Conover, and R.J. Beckman, A Comparison of Three Methods for Selecting Values of Input Variables in the Analysis of Output from a Computer Code. *Technometrics* 1979. 21: p. 239-245.

[191] Stein, M., Large sample properties of simulations using Latin Hypercube Sampling. *Technometrics*, 1987. 29: p. 143-151.

[192] Handcock, M.S., *Latin Hypercube Sampling to Improve the Efficiency of Monte Carlo Simulations: Theory and Implementation in ASTAP*, IBM Research Division, TJ Watson Research Center, RC 14546. 1989.

[193] Saltelli, A., Sensitivity Analysis for Importance Assessment. *Risk Analysis*, 2002. 22(3): p. 579-590.

[194] Hornberger, G.M. and R.C. Spear, An approach to the preliminary analysis of environmental systems. *Journal of Environmental management*, 1981. 12: p. 7-18.

[195] Turanyi, T. and H. Rabitz, Local methods and their applications, in Sensitivity Analysis, A. Saltelli, K. Chan, and M. Scott, Editors. 2000, John Wiley: New York.

[196] Varma, A., M. Morbidelli, and H. Wu, Parametric Sensitivity in Chemical Systems. 1999, Cambridge: Cambridge Series in Chemical Engineering.

[197] Goldsmith, C.H., Sensitivity Analysis, in *Encyclopedia of Biostatistics*, P. Armitage and T. Colton, Editors. 1998, John Wiley.

[198] Campolongo, F., et al., The Role of Multiphase Chemistry in the Oxidation of Dimethylsulphide (DMS). *A Latitude Dependent Analysis Journal of Atmospheric Chemistry*,, 1999. 32: p. 327-356.

[199] Campolongo, F., S. Tarantola, and A. Saltelli, Tackling quantitatively large dimensionality problems. *Computer Physics Communications*, 1999. 117: p. 75-85.

[200] Kioutsioukis I., et al., Uncertainty and global sensitivity analysis of road transport emission estimates. *Atmospheric Environment*, 2004. 38: p. 6609-6620.

[201] Crosetto, M. and S. Tarantola, Uncertainty and sensitivity analysis: tools for GIS-based model implementation *International Journal of Geographic Information Science,* 2001. 15(4): p. 415-437.

[202] Pastorelli, R., et al., Design of surface Brillouin scattering experiments by sensitivity analysis Surface *Science,* 2000. 468: p. 37-50.

[203] Spearman, C., The proof and measurement of association between two things. *American Journal of Psychology*, 1904. 15: p. 72-101.

[204] Spearman, C., Demonstration of formulae for true measurement of correlation. *American Journal of Psychology*, 1907. 18: p. 161-169.

[205] Rosner, B., *Fundamentals of Biostatistics* (6th Ed.). 2006, Duxbury Press: Boston. p. 538-543.
[206] Iman, R.L. and W.J. Conover, Small Sample Sensitivity Analysis Techniques For Computer-Models, With An Application To Risk Assessment. Communications In *Statistics Part A-Theory And Methods*, 1980. 9(17): p. 1749.
[207] Kleijnen, J.P.C. and J.C. Helton, Statistical analyses of scatterplots to identify important factors in large-scale simulations, 1: Review and comparison of techniques. *Reliability Engineering & System Safety*, 1999. 65(2): p. 147.
[208] Seaholm, S.K., Software systems to control sensitivity studies of Monte Carlo simulation models. *Comput Biomed Res,* 1988. 21(6): p. 531-50.
[209] Seaholm, S.K., J.J. Yang, and E. Ackerman, Order of response surfaces for representation of a Monte Carlo epidemic model. *Int J Biomed Comput*, 1988. 23(1-2): p. 113-23.
[210] Schroeder, L.D., D.L. Sqoquist, and P.E. Stephan, *Understanding regression analysis*. 1986, Sage Publications. p. 31-32
[211] Tabachnick, B. and L. Fidell, *Using Multivariate Statistics* (Third Edition). 1996: Harper Collins.
[212] McCullagh, P. and J.A. Nelder, *Generalized Linear Models* (2nd Edition). 1990: Chapman & Hall/CRC Press.
[213] Bender, R. and U. Grouven, Ordinal logistic regression in medical research. *J R Coll Physicians Lond*, 1997. 31(5): p. 546-51.
[214] Hall, G.H. and A.P. Round, Logistic regression--explanation and use. *J R Coll Physicians Lond*, 1994. 28(3): p. 242-6.
[215] Hosmer, D. and S. Lemeshow, *Applied Logistic Regression* (2nd Edition). 2000, New York: John Wiley and Sons, Inc.
[216] Cox, D.R. and E.J. Snell, *Analysis of binary data* (2nd Edition). 1989, London: Chapman & Hall.
[217] Nagelkerke, N.J.D., A note on a general definition of the coefficient of determination. *Biometrika*, 1991. 78(3): p. 691-692.
[218] Menard, S., Applied logistic regression analysis (2nd Edition). 2002, Sage Publications: Thousand Oaks, CA. p. p. 23.
[219] Conover, W.J., *Practical nonparametric statistics*. 1971, New York: John Wiley.
[220] Massey, F.J., The Kolmogorov-Smirnov Test for Goodness of Fit. *Journal of the American Statistical Association*, 1951. 46: p. 68-77.
[221] Conover, W.J., *Practical Nonparametric Statistics* (3rd edition). . 1999, New York: Wiley.
[222] Nikiforov, A.M. and A.S. Algorithm, Exact Smirnov two-sample tests for arbitrary distributions. *Applied Statistics*, 1994. 43: p. 265-284.
[223] Kim, P.J. and R.I. Jennrich, Tables of the exact sampling distribution of the two-sample Kolmogorov-Smirnov criterion, in *Selected Tables in Mathematical Statistics* (Vol 1). 1973, American Mathematical Society Providence.
[224] Spear, R.C., T.M. Grieb, and N. Shang, Factor Uncertainty and Interaction in Complex Environmental Models. *Water Resources Research*, 1994. 30: p. 3159-3169.
[225] Chan, K., et al., Variance based methods, in *Sensitivity Analysis*, A. Saltelli, K. Chan, and M. Scott, Editors. 2000, John Wiley: New York. p. 385-397.

[226] Saltelli, A., S. Tarantola, and K. Chan, A quantitative, model independent method for global sensitivity analysis of model output. *Technometrics*, 1999. 41(1): p. 39-56.
[227] Saltelli, A., et al., Sensitivity analysis practices: Strategies for model-based inference. *Reliability Engineering & System Safety*, 2006. 91: p. 1109-1125.
[228] Saltelli, A. and S. Tarantola, On the relative importance of input factors in mathematical models: Safety assessment for nuclear waste disposal. *Journal of the American Statistical Association*, 2002. 97(459): p. 702-709
[229] Sobol, I.M., Sensitivity estimates for nonlinear mathematical models. *Matematicheskoe Modelirovanie* (*Mathematical Modelling and Computational Experiment*), 1990. 2: p. 112-118.
[230] Rabitz, H. and O.F. Ali, Managing the tyranny of parameters in mathematical modelling of physical systems, in *Sensitivity Analysis*, A. Saltelli, K. Chan, and M. Scott, Editors. 2000, John Wiley: New York. p. 385-397.
[231] Rabitz, H., Efficient input-output model representations. Computer Physics Communications, 1999. 117: p. 11-20.
[232] Archer, G., A. Saltelli, and I.M. Sobol, Sensitivity measures, ANOVA like techniques and the use of bootstrap. *Journal of Statistical Computation and Simulation*, 1997. 58: p. 99-120.
[233] Homma, T. and A. Saltelli, Importance measures in global sensitivity analysis of model output. *Reliability Engineering & System Safety*, 1996. 52(1): p. 1-17.
[234] Tarantola, S., J. Jesinghaus, and M. Puolamaa, Global sensitivity analysis: a quality assurance tool in environmental policy modelling, in *Sensitivity Analysis*, A. Saltelli, K. Chan, and M. Scott, Editors. 2000, John Wiley: New York. p. 385-397.
[235] Rabitz, H., System analysis at molecular scale. *Science,* 1989. 246: p. 221-226.
[236] Holden, C., Breaking the Color Barrier. *Science,* 2002. 298: p. 1551.
[237] Halloran, M.E., Concepts of infectious disease epidemiology, in *Modern epidemiology*, K.J. Rothman and S. Greenland, Editors. 1998, Lippincott-Raven: Philadelphia. p. 529-54.

In: Mathematical Biology Research Trends
Editor: Lachlan B. Wilson, pp. 55-79
ISBN 978-1-60456-141-8

Chapter 2

STRUCTURE-DYNAMICS RELATIONSHIPS OF METABOLIC NETWORKS: THE SUSCEPTIBILITY-RESPONSIVITY CONNECTION OF ENZYMES

Antonio S. Torralba
Department of Physics and Astronomy, University College London,
Gower Street, London WC1E 6BT, United Kingdom

Abstract

The theory of metabolism can be subdivided in two main fields: dynamic theory and structural theory. Dynamic theory attempts to produce a description of the systemic dynamic behavior from as little experimental information as possible. Structural theory provides ways of decomposing complex networks in ways that reveal inherent functional relationships between the parts of the system. Since metabolic systems function out of equilibrium, due to the permanent input of material and energetic fluxes, dynamic theory has to deal with non-linearities. On the other hand, structural theory analyses the null-space of a matrix of relationships (usually, the stoichimetric matrix, giving rise to stoichiometric analysis) and therefore it belongs to either linear or convex analysis. This paper provides a new dynamic theory that generalizes some others, such as Metabolic Control Analysis (MCA) and Biochemical Systems Theory (BST), to time-varying external fluxes of any form, and provides a straighforward way of connecting the non-linear dynamics of metabolic systems to their stoichiometric structure, by means of a set of new properties. In particular, the non-linear response is described in terms of a generalized perturbation theory whose main coefficients are the susceptibilities (much in the same way as in non-linear optics). These coefficients are time-dependent (on one or more perturbation times) and become translationally invariant in time as the system approaches a steady state (the main realistic state of metabolic networks, apart from oscillatory behavior). Hence they can be integrated into constant coefficients, the responsivities, that provide a set of constrains connecting the dynamics and the stoichiometry of the network. As a consequence, the number of stoichiometric degrees of freedom can be reduced because of the dynamics of a specific system. This result, is illustrated by means of examples. The theory presented herein falls in the field of functional analysis, since the susceptibilities are functional derivatives of the response with respect to complete time-courses of the input fluxes,

which work as the excitations of the metabolic network and can be manipulated in experiments. Hence, the constraints provided by the theory should help simplify high-throughput experiments.

1. Introduction

Metabolic networks operate far from equilibrium, due to the existence of permanent input fluxes, while, at the same time, avoiding explosive accumulation of metabolites and achieving homeostasis. For modelling purposes, the input fluxes are often considered to be either constant or such that they consume a so-called external metabolite whose concentration is constant. The latter case is usually a good approximation when the substrate of a metabolic pathway proceeds from an inexhaustible source of material. These two extreme approximations, although frequently correct, are not universal. For example, predators often feed discontinuously, only when preys can be found. Because of this, it is essential to understand metabolic responses to variable fluxes of material.

Several approaches to the modelling of the dynamics of metabolic networks exists that can, in principle, be applied when fluxes vary. Models based on differential balance equations are widespread and are considered to be fundamental, as they contain very detailed information of enzyme rates and parameters. However, this is not only their strength, but also their weakness, since practical experimental determination of kinetic parameters is often difficult if not impossible. A known problem is that parameters measured in vitro are often unreliable when used in the context of the network, because of the many interations present in vivo that disappear when dealing with isolated enzymes [1].

An alternative, frequently encountered in metabolic engineering, is to use black-box approaches, in which only the relationships between inputs and selected outputs are considered. The problem then is not of parameter measurement, but of system identification. Usually, extremely general transfer functions are defined, that can be determined experimentally. Transfer functions allow, by applying appropriate operators, to convert inputs into outputs as if the fluxes were nothing more than chemical signals, transformed through metabolic filters [2–4]. The relationships between transfer functions for different responses can then be analysed, in order to gain some insight into the internal structure of the network.

Yet another possibility is to use some perturbative approach. The goal is to obtain general purpose sensitivity coefficients that can be used as parameters of a simplified model. A successful theory based on this idea is Biochemical Systems Theory (BST) [5–7]. There are several flavors of the theory. Particularly useful are S-systems [8, 9], as they group all terms producing a given metabolite and all those consuming it in two respective mass-action-like rates, thus making the treatment of the differential equations extremely simple in a logarithmic space. The theory is, essentially, a linearization with respect to fractional variations (hence the logarithmic space).

The main goal of BST is to describe the dynamics of the network. A related approach with a different aim is Metabolic Control Analysis (MCA) [10, 11]. In this theory, the foremost goal is to understand control and regulation. For reviews, see [12, 13]. The main sensitivity coefficients of the theory are the control coefficients. For example, the flux control coefficients are

$$C_{ij}^{J0} = \frac{e_j^0}{J_j^0} \frac{\mathrm{d}J_i}{\mathrm{d}e_j}, \tag{1}$$

where J_i is a steady state flux through reaction rate i, e_j is the enzyme concentration for enzyme j and 0 denotes a reference state. The control coefficients express the sensitivity of some observable with respect to a parameter. They satisfy summation theorems, under certain assumptions, particularly homogeneity of the reaction rates with respect to enzyme concentrations and constant concentration of initial and final metabolites of the pathways. Some of the assumptions can be lifted, leading to more general expressions for the theorems [14].

Control coefficients are global quantities, as they quantify variations of systemic properties, like fluxes. Other coefficients of the theory, the elasticities,

$$\varepsilon_{ij}^{x0} = \frac{x_j^0}{J_j^0} \frac{\partial v_i}{\partial x_j}, \tag{2}$$

where x is a concentration and v is a reaction rate, are local properties, since they refer to rates of particular reactions in the network. Control coefficients and elasticities are related by what is known as connectivity theorems. The exponents in the mass-action-like rates of BST are identical to the elasticities in MCA. Both theories are, therefore, closely related.

Dynamics is only one of the two fundamental aspects of metabolic networks. The other one is the network structure. Both aspects are tightly intertwined, as a seminal paper by Reder showed [15] in the context of MCA. The structure of the network is frequently represented by the stoichiometric matrix, i.e. the matrix of coefficients of the balance equations in differential equation models. Since metabolic networks remain, as already mentioned, in a homeostatic state, there is special interest in understanding the space of possible steady states, which depends strongly on the structure. This question has been answered by Metabolic Pathway Analysis [16–19], among other approaches. By using convex analysis, a unique set of elementary modes, that appears to be related to metabolic funcion [20], can be obtained. A more basic approach is to use conventional linear analysis. Convex analysis has some advantages over linear analysis. First, the basis of possible flux distributions is unique, so interpretation is straightforward. Second, irreversibility can be dealt with in a natural way. Nevertheless, linear analysis is the fundamental technique to find the set of admissible steady states, so it is still useful to derive fundamental theorems.

Despite all the available theories, there are fundamental problems that have not been solved yet. In particular, both MCA and BST are linear approximations (in logarithmic spaces) and, although some non-linear extensions of MCA exist [21, 22], the coefficients do not allow the calculation of transient responses to finite time-dependent excitations. For this, a more general approach is needed in which the sensitivity coefficients are not constant but time-dependent. This idea is in line with black-box approaches. The main purpose of this chapter is to show how the concept of transfer function can be extended to non-linear dynamics of metabolic systems. For this, susceptibility functions, analogous to those found in non-linear optics [23], will be used.

A second problem presently found is that stoichiometric analysis of metabolic networks produces the set of admissible steady state fluxes, but does not provide a way of predict-

ing what the coefficients of the linear combinations of flux modes will be under particular excitations and for specified network kinetics. To deal with this, we will introduce the responsivities of the system. These are sensitivity coefficients related to the dynamic susceptibilities.

The organization of the chapter is as follows. In section 2., the dynamic part of the theory will be presented. First, a general way of dealing with excitations in terms of fluxes of concentrations will be discussed, in section 2.1.. Next, a representation of responses using functional analysis will be proposed and the susceptibilities will be defined. The linear approximation will be used in section 2.3. to compare the present approach and MCA coefficients. A practical algorithm for computing susceptibilities will be given in section 2.4.. It will be illustrated by a simple analytical calculation of the first two susceptibilities of an irreversible Michaelis enzyme. The connection of the susceptibilities with stoichiometric analysis will be derived in section 3.1., where the responsivities of metabolic systems will be defined. The constraints that the network structure imposes on the responsivities will be obtained in section 3.2.. They will be applied to two simple examples of unbranched (section 3.3.1.) and branched (section 3.3.2.) networks. The chapter will conclude with some general comments about the advantages and limitations of the approach, and with an appendix where functionals are briefly introduced for non-mathematicians.

2. Dynamic Responses

2.1. Excitations

We start be showing that input fluxes are a general way of representing material excitations in metabolic networks. It is useful to consider the case of instantaneous variations of concentrations. Suppose first that the metabolic network was originally subject to some excitation that keeps it out of equilibrium and at a steady state. We call this state the reference state and label it as "ref". An experimenter has access to w metabolites, via variations of the fluxes that the system was already receiving at its reference state. Let these input flux variations be $\Delta J^i_{\text{in}}(t), i = 1, \ldots, w$, or simply $\Delta J_i(t)$. These fluxes represent all the freedom that the experimenter has to influence the behavior of the system. Input fluxes will be a completely general form of excitation if any perturbation of the system can be represented using them.

The simplest possible perturbation is the instantaneous change of the concentration of a metabolite i, ΔS^0_i at time t_0. In terms of differential equations, it can be written as:

$$\frac{\mathrm{d}\Delta S_i}{\mathrm{d}\Delta t} = 0 \quad \text{with} \quad \Delta S_i(t_0) = \Delta S^0_i, \tag{3}$$

where $\Delta S(t_0)$ is the variation of concentration of the external metabolite S at "initial" time, t_0, with $\Delta t = t - t_0$. This is a typical initial-concentration experiment, like those used to determine kinetic parameters of enzymes and, apparently, it does not involve fluxes.

However, the same experiment can be represented, using an input flux, as:

$$\frac{d\Delta S}{dt} = \Delta S_0 \delta(t - t_0) \quad \text{with} \quad \Delta S(t_0) = 0. \tag{4}$$

where $\delta(t-t_0)$ is a Dirac's delta. In this representation, there is no explicit variation of the concentration. Instead, the reference input flux is changed by means of an impulse. This approach is harder to implement in practice, but nevertheless there is an exact mathematical equivalence between Eqs. (3) and (4). To prove it, it suffices to check that both equations share the same Laplace transform (s is the conjugate variable of time),

$$s\mathscr{L}[S] = \Delta S_0 e^{t_0 s}, \tag{5}$$

and therefore have the same solution. The linearity of the Laplace operator guarantees that the equivalence is true for any system in which external fluxes are additive.

Moreover, using the sifting property of Dirac's delta, *any* time-dependent excitation, $\Delta J_{\text{in}}(t)$, can be represented in terms of impulses,

$$\Delta J_{\text{in}}(t) = \int_0^t \Delta J_{\text{in}}(\tau)\delta(t-\tau)d\tau. \tag{6}$$

2.2. Responses

The equivalence between initial-concentration and impulse-perturbation experiments opens a way to the generalization of perturbation theory that we are pursuing: Eqs. (3) and (4) relate impulses to finite changes of concentration at specified times, and eq. (6) shows a connection between excitations of any form and impulse excitations. We would like to be able to obtain responses to those excitations.

For example, the basic experiment of MCA, the determination of a control coefficient, consists of changing (infinitesimally) the concentration of an enzyme and measuring the change of flux that results. This is exactly what Eq. (3) represents, but, of course, the consequences of such a change will be highly non-linear, due to the kinetics of metabolic systems. More generally, we would like to know what the response of the system would be if, instead of changing the enzyme concentration by a constant value at a given time, we allow it to be time-dependent. Suppose, for instance, that there are fluxes of synthesis and degradation of the enzyme that must be accounted for. This problem is harder than just introducing time-dependence in the values of the parameters (in this MCA example, an enzyme concentration), because the response of the network to changes is, in general, not instantaneous, even if the excitation is.

The response to the excitations $\Delta J_i(t)$ can be stated, very formally, as a transformation $\mathscr{F}$, such that the variation of a variable of interest, $\Delta V(t)$ is

$$\Delta V(t) = \mathscr{F}[\Delta J_1(t), \ldots, \Delta J_w(t)]. \tag{7}$$

Mathematically, $\mathscr{F}$ is a functional (see Appendix A.). In most applications of biochemical interest, $\mathscr{F}$ is non-linear and a closed form solution is not known.

For the particular case of impulse excitations, $\Delta S_k \delta(t-t_0^k)$, with k the index of a perturbed metabolite, the functional reduces to an ordinary function of the impulse intensities, ΔS_k, and of the times elapsed since the perturbation, $\Delta t_k = t - t_0^k$,

$$\Delta V_\delta(t) = f(\Delta S_1, \ldots, \Delta S_w; \Delta t_1, \ldots, \Delta t_w) \tag{8}$$

This function is the progress curve of the variable V (usually, a rate, v, or a concentration, S) resulting from a typical initial velocity experiment, when the system is allowed to relax completely to the reference state. Therefore, it is generally accessible from experiment. In fact, similar data are routinely used to determine kinetic parameters of enzymes.

If the system has linear kinetics, which is a common approximation when enzymes operate well below the saturation point, the form of functional $\mathscr{F}$ is just the linear superposition law

$$\Delta V(t) = \sum_{i=1}^{w} \int_0^t \chi_i^{(1)}(t;t_1)\Delta J_i(t_1)\mathrm{d}t_1, \tag{9}$$

where $\chi_i^{(1)}(t;t_1)$ is the first order susceptibility, defined as the functional derivative of the functional $\mathscr{F}$ with respect to the input flux of metabolite i:

$$\chi_i^{(1)}(t;t_1) \equiv \left.\frac{\delta\Delta\mathscr{F}[\Delta J_i(t)]}{\delta\Delta J_i(t_1)}\right|_{\Delta J_i(t_1)=0} \tag{10}$$

The susceptibilities are evaluated at the reference state and are, therefore, sensitivity coefficients of the system at that state. The significance of Eq. (9) is that, in linear systems, it produces the transition from the initial state to any other state induced by the *finite* excitations, $\Delta J_i(t)$. The integration limits in Eq. (9) reflect the fact that meaningful systems are causal. In systems whose behavior doesn't change in time, i.e. if the implicit kinetic parameters remain constant, the susceptibilities have the time-independence property:

$$\chi_i^{(1)}(t;t_1) = \chi_i^{(1)}(t-t_1;0) \tag{11}$$

In general, in a non-linear metabolic system there is no known closed-form equivalent of Eq. (9). Therefore, approximations are needed. The generalization of the concept of susceptibility to higher orders leads to a functional Taylor expansion, which can be used to obtain such approximations. For a system with only one input, the series is

$$\begin{aligned}\Delta V(t) &= \int_0^t \chi^{(1)}(t;t_1)\Delta J_{\mathrm{in}}(t_1)\mathrm{d}t_1 \\ &+ \int_0^t\int_0^t \chi^{(2)}(t;t_1,t_2)\Delta J_{\mathrm{in}}(t_1)\Delta J_{\mathrm{in}}(t_2)\mathrm{d}t_1\mathrm{d}t_2 \\ &+ \cdots\end{aligned} \tag{12}$$

with nonlinear susceptibilities of the form

$$\chi^{(\rho)}(t;t_1,\ldots,t_\rho) \equiv \frac{1}{\rho!}\left.\frac{\delta^{(\rho)}\Delta\mathscr{F}[\Delta J_{\mathrm{in}}(t)]}{\delta\Delta J_{\mathrm{in}}(t_1)\cdots\delta\Delta J_{\mathrm{in}}(t_\rho)}\right|_{\substack{\Delta J_{\mathrm{in}}(t_i)=0 \\ i=1,\ldots,\rho}} \tag{13}$$

Before writing the general expansion for several inputs, it is important to note that, in Eqs. (12) and (13), the nonlinear terms contain several evaluations of the same excitation, ΔJ_{in}, at as many perturbation times as the order of the corresponding term, ρ, rather than several different excitations. In the general case, when several external metabolites exist, the

susceptibilities can be defined with respect to different orders for each separate input. This slighly complicates the notation and it is essential to understand it fully before proceeding further. The most general expression for the susceptibilities of metabolic systems is

$$\chi^{(\rho)}_{p_1,\ldots,p_w}(t;t_1,\ldots,t_\rho) \equiv \frac{1}{\rho!}\frac{\delta^{(\rho)}\Delta\mathscr{F}[\Delta J_1(t),\ldots,\Delta J_w(t)]}{\delta\Delta J_1(t_1)\cdots\delta\Delta J_1(t_{p_1})\cdots\delta\Delta J_w(t_{\rho-p_w+1})\cdots\delta\Delta J_w(t_\rho)}\Bigg|_{\substack{\Delta J_i(t_j)=0\\ i=1,\ldots,w\\ j=1,\ldots,\rho}}, \quad (14)$$

where the vector of metabolite orders, $\mathbf{p} \equiv (p_i,\ldots,p_w)$, is one of the non-negative integer solutions to the equation $\sum_{i=1}^{w} p_i = \rho$. Because some p_i can be zero, not all external metabolites need to take part in a particular susceptibility. For instance, the second order susceptibilities of a two-input system are $\chi^{(2)}_{2,0}$, $\chi^{(2)}_{1,1}$ and $\chi^{(2)}_{0,2}$, i.e. the second-order susceptibility with respect to metabolite 1, the first-order one in both 1 and 2, and the second-order one in 2, respectively. Thus, the total number of ρ-th order susceptibilities in a system with w inputs is $S_{\rho,w} = (w+\rho-1)!/[(w-1)!\rho!]$.

Each perturbation time is associated with a single impulse perturbation, and each may correspond to a different external metabolite. For instance, in a system with three external metabolites, in the 4-th order susceptibility $\chi^{(4)}_{2,1,1}(t;t_1,t_2,t_3,t_4)$, the first two perturbation times correspond to metabolite 1, whereas the last two correspond to metabolites 2 and 3, respectively. This has implications on the intrinsic symmetry of the function [24]: interchanging times t_1 and t_2 leaves $\chi^{(4)}_{2,1,1}$ unchanged, but all other times cannot be interchanged without affecting the value of the susceptibility.

With the aid of Eq. (14), the general functional Taylor expansion for a metabolic system with w inputs is

$$\begin{aligned}\Delta V(t) &= \sum_{\rho=1}^{\infty}\sum_{\mathbf{p}}\int_0^t\cdots\int_0^t \chi^{(\rho)}_{\mathbf{p}}(t;t_1,\ldots,t_\rho)\\ &\times \Delta J_1(t_1)\cdots\Delta J_1(t_{p_1})\cdots\Delta J_w(t_{\rho-t_w+1})\cdots\Delta J_w(t_\rho)\mathrm{d}t_1\ldots\mathrm{d}t_\rho \quad (15)\end{aligned}$$

In this representation of the functional, the susceptibilities characterize the system, and they allow to evaluate the response to arbitrary inputs. From the definition, Eq. (14), it would seem that each susceptibility requires data from a different type of experiment, namely, double impulse perturbation experiments for a second-order susceptibility, et cetera. Fortunately, it will be shown below (section 2.4.) that composition of responses can reduce the amount of necessary experimental data significantly.

2.3. Linear Approximation and the Connection to Elasticities

Eqs. (9), (12) and (15) are finite increments with respect to the reference state. Thus, they represent finite responses. In order to make a comparison of the present approach and other metabolic theories, such as MCA and BST, let us consider the first-order infinitesimal variation of a rate instead. The appropriate differential expression is analogous to Eq. (9), but it is valid also in non-linear systems:

$$\delta\Delta v_i(t) = \sum_j \int \left.\frac{\delta\Delta\mathscr{F}_{v_i}[\Delta J_1,\ldots,\Delta J_w](t)}{\delta\Delta J_j(t')}\right|_{\text{ref}} \delta\Delta J_j(t')\mathrm{d}t', \tag{16}$$

$\Delta\mathscr{F}_{v_i}$ is the representation of the i-th rate as a functional of the input fluxes. Both the functional and the fluxes are still finite variations with respect to the reference state, but the functional derivative must be evaluated at ref for the expression to hold.

Rates depend on the vector of concentrations (again, variations with respect to the reference state), which depend themselves on the external fluxes, and hence the functional derivative can be rewritten as

$$\left.\frac{\delta\Delta\mathscr{F}_{v_i}[\Delta J_1,\ldots,\Delta J_w](t)}{\delta\Delta J_j(t')}\right|_{\text{ref}} = \sum_k \int \left.\frac{\delta\Delta\mathscr{F}_{v_i}(t)}{\delta\Delta S_k(t'')}\frac{\delta\Delta S_k(t'')}{\delta\Delta J_j(t')}\right|_{\text{ref}} \mathrm{d}t'', \tag{17}$$

In the particular case in which rates can be expressed as functions of the instantaneous concentrations at real time t (the most frequent situation in practice), it holds that

$$\begin{aligned}
&\left.\frac{\delta\Delta\mathscr{F}_{v_i}[\Delta J_1,\ldots,\Delta J_w](t)}{\delta\Delta J_j(t')}\right|_{\text{ref}} \\
&= \sum_k \int \left.\frac{\partial\Delta\mathscr{F}_{v_i}(\Delta S_1,\ldots,\Delta S_w)}{\partial\Delta S_k(t'')}\delta(t-t'')\frac{\delta\Delta S_k(t'')}{\delta\Delta J_j(t')}\right|_{\text{ref}} \mathrm{d}t'' \\
&= \sum_k \left.\frac{\partial\Delta\mathscr{F}_{v_i}(\Delta S_1,\ldots,\Delta S_w)}{\partial\Delta S_k(t)}\frac{\delta\Delta S_k(t)}{\delta\Delta J_j(t')}\right|_{\text{ref}}
\end{aligned} \tag{18}$$

The factors

$$\varepsilon^*_{i,j} \equiv \left.\frac{\partial\Delta\mathscr{F}_{v_i}}{\partial\Delta S_j}\right|_{\text{ref}} \tag{19}$$

are unscaled elasticity coefficients of the rate i with respect to the concentration j. Thus, Eq. (18) shows how the functional differential Eq. (16) is connected to MCA and BST, through common coefficients of all three theories.

If the reference state is a steady state, the elasticities, Eq. (19), are constant coefficients. If, on the other hand, the reference is a time-dependent transition, time-dependent coefficients result, much in the same way as in previous theories [25]. The other factors,

$$\chi^S_{i,j}(t,t') \equiv \frac{\delta\Delta S_i(t)}{\delta\Delta J_j(t')}, \tag{20}$$

are concentration susceptibilities of metabolite i with respect to a flux through metabolite j. They express a complete time-course of the concentration after a perturbation at time t', not just the immediate response at the excitation time.

If $i = j$, i.e. if the external flux and the measured concentration correspond to the same metabolite, and if, in addition, the metabolite is not consumed in any reaction, Eq. (20) is a step function, i.e. the concentration remains constant after the initial perturbation. This

is the usual situation when dealing with the susceptibilities of enzymes in the context of MCA. In this particular case, $\varepsilon_{i,j}\chi^S_{j,j}(t,t') \propto \varepsilon_{i,j}$ for $t \geq t'$, with a proporcionality constant equal to one in most cases. This reduces many of the terms in Eq. (18) to the equivalent MCA elasticity coefficient, but the functional differential contains cross-terms as well, that account for the sensitivity of a rate to metabolite concentrations which do not immediately participate in a particular reaction. Such delayed responses make the present theory immediately time-dependent and, as such, it is a generalization of previous approaches.

2.4. Computation of Susceptibilities by an Iterative Procedure

Before computing a susceptibility, appropriate excitations have to be specified. There is no loss of generality in always choosing fluxes, rather than concentrations or other variables, because, as section 2.1. shows, material excitations in metabolic systems can always be represented as input fluxes of metabolites. Furthermore, dimensional analysis of one of the definitions of the functional derivative, Eq. (62), shows that, if the excitation is a flux, the impulses necessary to disturb the system must have dimensions of concentration. This is convenient because concentrations are easily accessible experimentally, whereas rates are not. On the other hand, the response (i.e. the functional), unlike the excitations, can be any variable of interest, regardless of its dimensions. The two most frequent instances are concentrations and rates, which depend on one another. For instance, Eq. (18) shows a relationship between rate and concentration susceptibilities (to a first order approximation).

Although the formal definition of the susceptibilities is given in Eq. (62), a practical method for obtaining them from experimental data is necessary. A general method of computation as multivariate partial derivatives has been proposed [24], but that basic approach is extremely expensive. It requires determining a great number of multidimensional functions of the impulse intensities. The amount of required experimental data grows combinatorially, even for a single input. The purpose of this section is to show that impulses exerted on the same metabolite concentration are indeed not independent. This reduces the experimental effort enormously.

To see how experimental data can be reused, consider the case of a system with a single input. The corresponding susceptibilities are given by Eq. (13). If the derivatives are computed directly, a discretization of the ρ-th order susceptibility in τ time-intervals would require $R\prod_{i=1}^{\rho}\frac{(\tau-1)!}{(i-1)!(\tau-i)!}\frac{(\rho-1)!}{(i-1)!(\rho-i)!}\prod_{j=1}^{i}(p_j+1)$ separate multiple perturbation experiments, with R a constant factor depending on the numerical method used to compute partial derivatives, and with p_j including all possible solutions of $\sum_{j=1}^{i}p_j$ (for details, see [24]). In other words, the unrefined problem scales combinatorially with the time discretization and with the time order, and polynomially with the partial-derivative orders.

Suppose, however, that time-independence properties like Eq. (11) hold. This is the case when the implicit parameters of the system do not depend in time. In differential-equation-based models, this is equivalent to say that the coefficients do not depend on time. We observe that, under such premise, the responses to multiple-perturbation experiments can be composed, as shown in Fig. 1, from single-perturbation data.

The line of argument which leads to this conclusion is as follows. The definition of the susceptibilities, Eq. (13), implies that, in order to determine a second-order response, the system must be perturbed twice, at times t_1 and t_2, with impulses of intensities ΔS_1

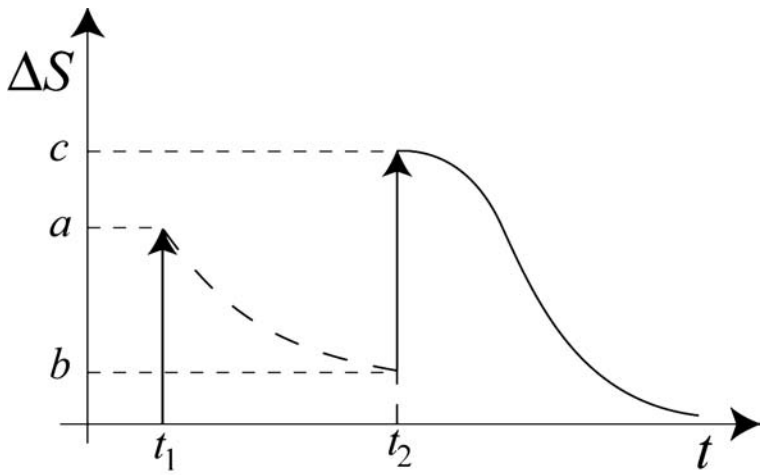

Figure 1. Composition of responses for determining susceptibilities. At time t_1, a first impulse of intensity a is introduced. The system then relaxes (dashed line) until, at time t_2, a second impulse of intensity $c - b$ is applied. The final relaxation (solid line) can be used for computing a second-order functional derivative with respect to the two intensities. The procedure can be extended to higher-order derivatives.

and ΔS_2, respectively. If the response of a concentration to impulses, denoted ΔS_δ after Eq. (8), is known, and provided that $t_1 \leq t_2$, it holds that $\Delta S_\delta(t_2) = \Delta S_\delta(\Delta S_1; t_2 - t_1)$. Consequently, at the time the second impulse is introduced, the concentration of the external metabolite is made of two terms: the intensity of the second impulse and the concentration remaining after the first one, $\Delta S_2 + \Delta S_\delta(\Delta S_1; t_2 - t_1)$. As a result, the response after t_2 can be expressed as

$$\Delta S_\delta(\Delta S_2 + \Delta S_\delta(\Delta S_1; t_2 - t_1); t - t_2). \tag{21}$$

The second-order susceptibility results from taking partial derivatives with respect to ΔS_1 and ΔS_2. Such a procedure can be trivially extended to third- and higher-order derivatives by simple iteration of the response to impulses. If the response of interest is an enzyme velocity, Δv, Eq. (21) would change to

$$\Delta v_\delta(\Delta S_2 + \Delta S(\Delta S_1; t_2 - t_1); t - t_2). \tag{22}$$

where the response of the velocity to impulses Δv_δ is used only at the most external iteration level.

Since the susceptibilities can be expressed as partial derivatives of expressions like Eqs. (21) and (22), they will obviously depend only on the partial derivatives of the responses to impulses. The amount of data that a numerical computation will require is therefore proportional to the order of the susceptibility, with the same constant factor R, dependent on the differentiation algorithm, as above. One may wonder how it is possible that the basic algorithm, of combinatorial complexity, has been reduced to a linear-scaling algorithm. The answer is that the explicit development of the susceptibilities in terms of derivatives of

ΔS_δ, et cetera, produces expressions of growing complexity. It is well known that partial derivatives are related to partition problems [26]. The first few derivatives of iterated expressions of the form of Eq. (21) have been given elsewhere [27] and are reproduced here for completeness:

$$\begin{aligned}
\chi^{(1)}_{\mathscr{F}}(t;t_1) &= \partial\mathscr{F}_1 && (23)\\
\chi^{(2)}_{\mathscr{F}}(t;t_1,t_2) &= \left(\partial S_1\partial^2\mathscr{F}_2\right)/2! && (24)\\
\chi^{(3)}_{\mathscr{F}}(t;t_1,t_2,t_3) &= \left[\partial S_1\left(\partial S_2\right)^2\partial^3\mathscr{F}_3\right.\\
&+ \left.\partial S_1\partial^2 S_2\partial^2\mathscr{F}_3\right]/3! && (25)\\
\chi^{(4)}_{\mathscr{F}}(t;t_1,t_2,t_3,t_4) &= \left[\partial S_1\left(\partial S_2\right)^2\left(\partial S_3\right)^3\partial^4\mathscr{F}_4\right.\\
&+ 3\partial S_1\left(\partial S_2\right)^2\partial S_3\partial^2 S_3\partial^3\mathscr{F}_4\\
&+ \partial S_1\partial^2 S_2\left(\partial S_3\right)^2\partial^3\mathscr{F}_4\\
&+ \partial S_1\left(\partial S_2\right)^2\partial^3 S_3\partial^2\mathscr{F}_4\\
&+ \left.\partial S_1\partial^2 S_2\partial^2 S_3\partial^2\mathscr{F}_4\right]/4! && (26)\\
\cdots &\quad \cdots
\end{aligned}$$

where the notation

$$\partial^r\mathscr{F}_n \equiv \left.\frac{\partial^r\Delta F_\delta(\Delta S_0,\Delta t_n)}{\partial\Delta S_0}\right|_{\text{ref}}, \qquad (27)$$

has been used. $\mathscr{F}$ indicates that the notation is valid for the functional representation of any variable of interest, and ΔF_δ shows that responses to impulses (functions, not functionals) are used. The dummy subscript n refers to the index of the corresponding perturbation time (always an increment with respect to the first impulse in the equivalent multiple impulse experiment) that must be used in Eqs. (23)-(26).

These expressions are universally correct, for systems with one input and for terms in the multiple-input expansion Eq. (15) other than the cross-terms, and do not depend on the nature of either the system, the excitation or the response. Because they only depend on the partial derivatives of responses to impulses, they emphasize the fundamental importance of this kind of experiments, well-known in linear systems theory, but less recognized in non-linear theory. Thus, in biochemistry, initial-concentration and initial-rate experiments are essential, not only in equilibrium theory, to determine kinetic parameters, but also in far-from-equilibrium conditions.

It should be mentioned that Eqs. (23)-(26) are extensions of existing standard Faà di Bruno formulas [28], but a general formula for the multiply iterated problem has not been found yet. Cross-terms in multiple impulse systems also depend on impulse responses, but more general functions, of the form of Eq. (8), must be used to iterate and take derivatives.

2.4.1. Example

Let us compute the first two susceptibilities of the rate of an irreversible Michaelis-Menten enzyme, $v = VS/(K+S)$, with respect to the input of the substrate S. The parameters

of the enzyme are the maximum velocity, V, and the half-saturation Michaelis constant, K. For simplicity, we restrict ourselves to the empty reference state, so that $S^{\mathrm{ref}} = 0$. Consequently, the notation can be simplified by omitting the $\Delta' s$.

A comprehensive derivation was given elsewhere [27], but the method there was exact for the expression of ΔS_δ. Here, we derive a much simpler expression of the impulse response, valid only to obtain the first two susceptibilities, with the aim of clarifying the significance of the iterative procedure. The computation of the first susceptibilities presented below is, however, exact, as can be checked by comparison with the comprehensive method. Whereas that method is frequently not affordable analytically in most systems, the simplified approach used in this section should be feasible more generally, although it can produce only the first few sensitivities.

We start with the corresponding differential equation for the system:

$$\frac{dS}{dt} = J_{\mathrm{in}} - \frac{VS}{K+S}. \tag{28}$$

This equation cannot be integrated explicitly in terms of usual functions, as is the case in most metabolic systems, due to non-linearities . Fortunately, the computation of the first two susceptibilities only requires a second-order solution. Therefore, the rate can be expanded in a Taylor series, so that

$$\frac{dS}{dt} \simeq J_{\mathrm{in}} - \frac{VS}{K} + \frac{VS^2}{K^2}. \tag{29}$$

The impulse response of the concentration corresponds exactly to the solution of an initial concentration problem, that is, of Eq. (29) with $J_{\mathrm{in}} = 0$. After rearrangement, the formal solution

$$\frac{K}{V}\int_{S_1}^{S} \left(S' - S'^2/K\right)^{-1} dS' \simeq -\Delta t = t_1 - t \tag{30}$$

results. The initial concentration has been labelled S_1 for convenience. Eq. (30) can be integrated, after decomposition in fractions of polynomials, to yield

$$S(S_1;\Delta t) \simeq \frac{S_1 K \exp\left(-V\Delta t/K\right)}{K - S_1\left\{1 - \exp\left(-V\Delta t/K\right)\right\}}. \tag{31}$$

The key simplification here has been the expansion of the original rate equation in series, and truncation beyond order two, so that an integral could be calculated, whose solution could be rearranged to yield the explicit concentration decay. A second expansion of the implicit solution (up to order two) would also contain all the information necessary to calculate the first two susceptibilities and could be attempted in other systems, when it is not possible to express the solution explicitly.

Taking partial derivatives of Eq. (31), the first-order susceptibility of the enzyme rate results:

$$\chi^{(1)}(t;t_1) \;=\; \left.\frac{\delta v(t)}{\delta J_{\mathrm{in}}(t_1)}\right|_{J_{\mathrm{in}}(t_1)=0}$$

$$\begin{aligned} &= \left.\frac{\partial v}{\partial S}\frac{\partial S}{\partial S_1}\right|_{S_1=0} \\ &= (V/K)\exp(-V\Delta t/K),\ t \geq t_1 \end{aligned} \tag{32}$$

Note that the second line is an expression of the form of Eq. (18), where the first factor is an unscaled elasticity and the second, a concentration susceptibility, has been replaced by the corresponding partial derivative of the initial concentration decay. Even when the enzyme rate is known, as in this example, this factor should be determined, in general, from experiment, because it can be affected by network connectivities.

The derivation of the second-order susceptibility is more interesting. As mentioned in the previous section, it requires data from double-impulse experiments, that is, the excitation must be of the form $J_{\text{in}}(t) = S_1\delta(t-t_1) + S_2\delta(t-t_2)$, with $t_2 \geq t_1$.

As usual, it is preferable to consider that $J_{\text{in}}(t) = 0$ and to introduce the excitation as finite variations of the concentration. As explained above, this is achieved by iterating Eq. (31), so that the evolution of the concentration *after* t_2 is $S(S_1, S_2; t-t_2) = S(S_2 + S(S_1; t_2 - t_1); t - t_2)$.

The second-order susceptibility is now easy to compute:

$$\begin{aligned} \chi^{(2)}(t; t_1, t_2) &= \left.\frac{1}{2}\frac{\delta^2 v(t)}{\delta J_{\text{in}}(t_1)\delta J_{\text{in}}(t_2)}\right|_{\substack{J_{\text{in}}(t_i)=0,\\ i=1,2}} \\ &= \left.\frac{1}{2}\frac{\partial^2 v}{\partial S_1 \partial S_2}\right|_{S_1=S_2=0} \\ &= (V/K^2)\left\{\exp\left[-V\Delta t/K\right]\right. \\ &- \left. 2\exp\left[-V(2\Delta t - \Delta t_1)/K\right]\right\} \end{aligned} \tag{33}$$

The time increments are $\Delta t = t - t_1$ and $\Delta t_1 = t_2 - t_1$, with $t \geq t_2 \geq t_1 \geq 0$. The fact that the susceptibilities can be expressed as functions of time increments with respect to the first perturbation time, t_1, means that the system is time-invariant. In other words, the kinetic parameters do not depend on time. (For a more rigorous general definition, see [24].)

The susceptibilities (32) and (33) can now be used to find approximations to the response of the enzyme rate, Δv. Let $\Delta\mathscr{V}$ be the functional representation of the response and $\Delta\mathscr{V}^{(\rho)}$ its ρ-th order contribution. Since the perturbation times have been chosen to follow a fixed, ordered sequence, the general term of Eq. (12) can be computed as

$$\begin{aligned} \Delta\mathscr{V}^{(\rho)} &= \rho! \int_0^t dt_1 \int_{t_1}^t dt_2 \cdots \int_{t_{\rho-1}}^t dt_\rho \chi^{(\rho)}(t; t_1, \ldots, t_\rho) \\ &\times \Delta J_{\text{in}}(t_1)\cdots\Delta J_{\text{in}}(t_\rho). \end{aligned} \tag{34}$$

It should be noted that the lower integration limits are no longer zero, but are limited by the previous perturbation time. Thus, the integral corresponds to just one permutation of the perturbation times. To account for all permutations, the prefactor $\rho!$ has to be introduced.

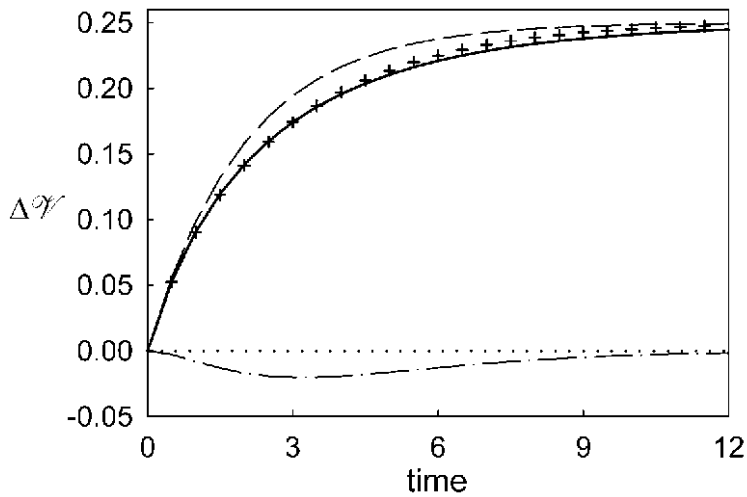

Figure 2. Response of an irreversible Michaelis-Menten enzyme ($V = 1.0$, $K = 2.0$) for $J_{\rm in} = 0.25$, starting at the empty state. Thick solid-line: exact (numerical) response; crosses: second-order approximation; dashed line: first-order contribution; dashed-dotted line: second-order contribution.

A simple computation yields the first two contributions to the enzyme rate for a constant excitation $J_{\rm in}(t) = J$, namely

$$\Delta\mathscr{V}^{(1)} = J\left[1 - \exp(-V\Delta t/K)\right] \tag{35}$$

and

$$\begin{aligned}\Delta\mathscr{V}^{(2)} &= 2J^2\left[\left(V^{-1} - K^{-1}\Delta t\right)\exp(-V\Delta t/K)\right. \\ &- \left. V^{-1}\exp(-2V\Delta t/K)\right].\end{aligned} \tag{36}$$

An example of application of Eqs. (35) and (36) is displayed in Fig. 2. As shown, the prediction of the response is quite good, even for large excitations (e.g. 25% V and is improved by using the second-order term of the functional series. Third- and higher-order terms would improve the approximation even further and may be necessary when the enzyme is close to the maximum velocity, in which limit the expansion is expected to diverge, since at saturation a steady state can not be achieved.

3. Stoichiometric Analysis

3.1. Responsivities and Asymptotic Behavior

As the excitations approach asymptotically a constant value, $\Delta J_i^{\rm ss}$, realistic metabolic networks, that is, those adapted to preserve homeostasis, will approach a steady state (ss) or, if

the concentrations oscillate, their average will. In the limit $t \to \infty$, a necessary condition for a steady state to be possible is that the susceptibilities become time-invariant, i.e. that the times $t, t_1, t_2, \ldots$ can be replaced by time increments, $\Delta t = t - t_1,\ \Delta t_i = t_{i+1} - t_1$, where t_1 is the first perturbation time. This is required even if the network is not time-invariant in the transient regime. In the time-invariant limit, the susceptibilities can be written as $\chi^{(\rho)}(\Delta t; \Delta t_1, \ldots, \Delta t_{\rho-1})$ and the functional Taylor expansion reduces to the algebraic series. For example, in a single-input system, Eq. (12) becomes

$$\Delta v^{\text{ss}} = \sum_i \mathscr{R}^{(i)} \times \left(\Delta J_{\text{in}}^{\text{ss}}\right)^i . \tag{37}$$

The notation Δv^{ss} indicates that the steady state is no longer a functional, but a function (of the asymptotically steady input fluxes). The constant coefficients of the asymptotic expansion,

$$\begin{aligned} \mathscr{R}^{(\rho)} &= \int_0^\infty d\Delta t \int_0^\infty d\Delta t_1 \cdots \int_0^\infty d\Delta t_{\rho-1} \\ &\times \chi^{(\rho)}(\Delta t; \Delta t_1, \ldots, \Delta t_{\rho-1}), \end{aligned} \tag{38}$$

are the responsivities of the system (mathematically, the hypervolumes under the susceptibilities). They provide a way of relating external fluxes, accessible to the experimentalist, to internal variables at steady state.

In simple situations, e.g. an unbranched pathway without feedback, the ratio $\Delta v^{\text{ss}}/\Delta J_{\text{in}}^{\text{ss}}$ is determined only by the overall stoichiometry of the pathway and is therefore usually constant. This implies that the non-linear responsivities are zero, $\mathscr{R}^{(\rho)} = 0,\ \rho > 1$. It can be checked, by integrating the susceptibilities of section 2.4.1., that this is the case, for instance, for the rate of an isolated Michaelis-Menten enzyme with respect to the input of substrate. This is true even though the enzyme has non-linear kinetics. In a complex network, however, the nonlinear responsivities of each enzyme depend on those of the rest. As shown in the next section, the values that the responsivities can take are determined by the stoichiometric properties of the network, but also by the kinetics.

3.2. Network Analysis

The dynamics of metabolic networks are usually represented, in terms of differential equations, as

$$\frac{d\mathbf{s}}{dt} = \mathbf{N}\mathbf{v}, \tag{39}$$

where $\mathbf{s}$ and $\mathbf{v}$ are the vectors of concentrations and velocities, respectively, and $\mathbf{N}$ is the stoichiometric matrix.

We are interested in finding the constraints that the network stoichiometry imposes on the responsivities. Because the external fluxes can be manipulated at will, the constraints should depend on them. To see how, let us split the vector of velocities in the partition $\mathbf{v} = \begin{bmatrix} \mathbf{j} \\ \mathbf{r} \end{bmatrix}$, where $\mathbf{r}$ is the vector of internal rates, with m components, and $\mathbf{j}$ is the vector of

external fluxes, with n components. Consequently, the stoichiometric matrix can be split as $\mathbf{N} = \left[\mathbf{N^j}\ \mathbf{N^r}\right]$.

The partition of velocities allows to express $\mathbf{r^{ss}}$ (a flux distribution) in terms of the inputs $\mathbf{j^{ss}}$ and of the responsivities. This is done by integrating Eq. (15) in the limit $t \to \infty$, which yields:

$$r_i^{\mathrm{ss}} = \sum_{\rho=1}^{\infty} \sum_{j=1}^{S_{\rho,n}} \mathscr{R}_{i,j}^{(\rho)} \times (\Delta J_1^{\mathrm{ss}})^{p_1} \cdots (\Delta J_n^{\mathrm{ss}})^{p_n} \,. \tag{40}$$

This equation expresses the steady state internal rates in terms of external fluxes, as desired. Notably, there is no need to assume a particular model in order to obtain this relationship. Here, $r_i^{\mathrm{ss}},\ i = 1, ..., m$, is the i-th element of $\mathbf{r^{ss}}$ and $\Delta J_k^{\mathrm{ss}},\ k = 1, ..., n$, is the k-th element of $\mathbf{j^{ss}}$. The exponents p_k satisfy the usual condition $\sum_{k=1}^{n} p_k = \rho$, which generates $S_{\rho,n} = (n + \rho - 1)!/[(n-1)!\rho!]$ combinations (hence the second sum). Finally, the ρ-th order responsivity $\mathscr{R}_{i,j}^{(\rho)}$ belongs to the i-th rate and the j-th combination of input fluxes.

Letting $q_j^{(\rho)}$ be the j-th element of the vector $\mathbf{q}^{(\rho)}$ of products of the form $(\Delta J_1^{\mathrm{ss}})^{p_1} \cdots (\Delta J_n^{\mathrm{ss}})^{p_n}$ and $\mathbf{R}^{(\rho)}$ the matrix of ρ-th order responsivities, Eq. (40) can be written as $\mathbf{r^{ss}} = \sum_{\rho=1}^{\infty} \mathbf{R}^{(\rho)}\mathbf{q}^{(\rho)}$. At steady state, $\mathbf{N}\mathbf{v^{ss}} = \mathbf{0}$, and consequently

$$\left[\mathbf{N^j}\ \mathbf{N^r}\right] \begin{bmatrix} \mathbf{j^{ss}} \\ \mathbf{R}^{(1)}\mathbf{j^{ss}} + \sum_{\rho=2}^{\infty} \mathbf{R}^{(\rho)}\mathbf{q}^{(\rho)} \end{bmatrix} = \mathbf{0}. \tag{41}$$

This is a polynomial equation and should, in principle, be solved as such, for a set of specified input fluxes. However, the susceptibilities, and hence the responsivities, depend only on the reference state and not on the excitations. Therefore, if the system achieves steady states for a continuous range of fluxes, as is usually the case, Eq. (41) will have a solution only if the coefficients are identically zero. For this reason, the constraints that metabolic systems satisfy are

$$\delta_{1\rho}\mathbf{N^j} + \mathbf{N^r}\mathbf{R}^{(\rho)} = \mathbf{0}, \tag{42}$$

where δ_{ij} is the usual Kronecker's delta.

Eq. (42) shows that the first order responsivities obey special relationships, different from those of the rest of the orders. This is of paramount importance when determining how many degrees of freedom a network actually has. Eq. (42) states that the non-linear responsivities belong to the kernel of $\mathbf{N^r}$, whereas the linear ones are solutions of an inhomogeneous equation that involves the stoichiometry of the inputs. As the examples below will show, it is entirely possible that a system with non-linear kinetics (and therefore with non-trivial susceptibilities) has nevertheless null responsivities. This usually implies that the network has less degrees of freedom than the stoichiometry would suggest.

3.3. Examples

3.3.1. Unbranched Pathway

As a first example, consider an unbrached metabolic pathway composed of three metabolites and three enzymes (Fig. 3). Assuming that inputs are allowed through metabolites 1

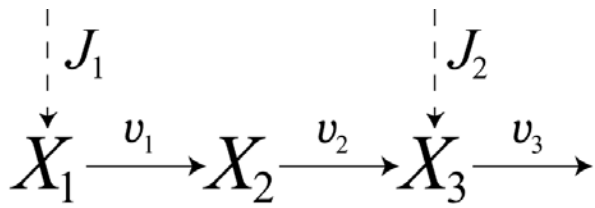

Figure 3. Unbranched metabolic pathway with two inputs (dashed lines, J_1 and J_2), three metabolites (X) and three internal rates (solid lines, v). Rates may be reversible.

and 3, the stoichiometric matrices are

$$\mathbf{N^j} = \begin{pmatrix} 1 & 0 & 0 \\ 0 & 0 & 0 \\ 0 & 0 & 1 \end{pmatrix}, \quad \mathbf{N^r} = \begin{pmatrix} -1 & 0 & 0 \\ 1 & -1 & 0 \\ 0 & 1 & -1 \end{pmatrix}. \tag{43}$$

The dimension of the null space of $\mathbf{N^r}$ is zero and, as a result, the nonlinear responsivities are also zero, irrespective of the kinetics. The linear responsivities are

$$\mathbf{R^{(1)}} = \begin{pmatrix} 1 & 0 & 0 \\ 1 & 0 & 0 \\ 1 & 0 & 1 \end{pmatrix}. \tag{44}$$

The first column is the relative flux distribution of the pathway when the flux excites the system through metabolite 1. Similarly, the third column shows that, when the excitation enters through metabolite 3, only the third rate is non-trivial. The implication is that, in that case, enzymes 1 and 2 will reach equilibrium. Importantly, this is true regardless of the reversibility of the enzymes. The second column is zero, of course, as no input is allowed via metabolite 2. This is a very fundamental example that shows how the linear responsivities in particular are related to other theories, like stoichiometric analysis.

3.3.2. Branched Pathway

Let us consider the network shown in Fig. 4. It consists of three external metabolites and five enzymes, only one of which is external. Metabolites 2 and 3 share the same input flux. This is similar to the aldolase reaction in glycolysis, where glyceraldehyde 3-phosphate and dihydroxyacetone phosphate are both produced from fructose 1,6-bisphosphate and are interconverted by triose phosphate isomerase. The stoichiometric matrices for this system are

$$\mathbf{N^j} = \begin{pmatrix} 1 & 0 & 0 \\ 0 & 1 & 0 \\ 0 & 1 & 0 \\ 0 & 0 & 1 \end{pmatrix} \tag{45}$$

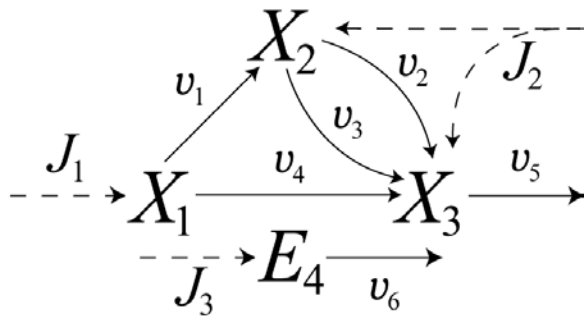

Figure 4. Branched metabolic pathway with three inputs (dashed lines, J), three metabolites (X) and six internal enzymatic rates (solid lines, v). One of the inputs (J_2) affects two metabolites and the external "metabolite" for another (J_3) is an enzyme (E_4). Enzymes 2 and 3 are isoenzymes. Rates may be reversible.

and

$$\mathbf{N^r} = \begin{pmatrix} -1 & 0 & 0 & -1 & 0 & 0 \\ 1 & -1 & -1 & 0 & 0 & 0 \\ 0 & 1 & 1 & 1 & -1 & 0 \\ 0 & 0 & 0 & 0 & 0 & -1 \end{pmatrix}. \tag{46}$$

From Eq. (42), the matrix of first order responsivities results. It is of the form

$$\mathbf{R^{(1)}} = \begin{pmatrix} \mathscr{R}_{11}^{(1)} & \mathscr{R}_{12}^{(1)} & \mathscr{R}_{13}^{(1)} \\ \mathscr{R}_{21}^{(1)} & \mathscr{R}_{22}^{(1)} & \mathscr{R}_{23}^{(1)} \\ \mathscr{R}_{11}^{(1)} - \mathscr{R}_{21}^{(1)} & 1 + \mathscr{R}_{12}^{(1)} - \mathscr{R}_{22}^{(1)} & \mathscr{R}_{13}^{(1)} - \mathscr{R}_{23}^{(1)} \\ 1 - \mathscr{R}_{11}^{(1)} & -\mathscr{R}_{12}^{(1)} & -\mathscr{R}_{13}^{(1)} \\ 1 & 2 & 0 \\ 0 & 0 & 1 \end{pmatrix} \tag{47}$$

In this example, the dimension of $\mathrm{Ker}(\mathbf{N^r})$ is two. This is, in principle, the number of degrees of freedom of the unexcited system. One possible basis for the kernel is $\mathbf{k_1}^T = (1,\ 0,\ 1,\ -1,\ 0,\ 0)$ and $\mathbf{k_2}^T = (0,\ -1,\ 1,\ 0,\ 0,\ 0)$. In this basis, the coefficients of a vector of ρ-th order responsivities, with $\rho \geq 2$, are the responsivities of enzymes 1 and 2, so that the columns of $\mathbf{R}^{(\rho)}, \rho \geq 2$ have the following structure:

$$\left(\mathscr{R}_{1i}^{(\rho)},\ \mathscr{R}_{2i}^{(\rho)},\ \mathscr{R}_{1i}^{(\rho)} - \mathscr{R}_{2i}^{(\rho)},\ -\mathscr{R}_{1i}^{(\rho)},\ 0,\ 0\right)^T \tag{48}$$

Eqs. (47) and (48) express the maximum freedom of the system compatible with the stoichiometric constraints. Hence, they establish a link between the dynamics of the network,

described by the susceptibilities, and its stoichiometry, determined by the stoichiometric matrix. In this example, out of a maximum of 18 responsivities per order, only 6 (dimension of the kernel $\times$ number of input fluxes) are independent and need to be measured.

Let us now specify an example of kinetics, so that the responsivities can be evaluated numerically. Suppose that the rates of the network are as follows:

$$v_1 = \frac{V_1 X_1^2}{K_1^2 + X_1^2} \tag{49}$$

$$v_2 = \frac{V_2 X_2}{K_2 + X_2} \tag{50}$$

$$v_3 = \frac{V_3 X_2}{K_3 + X_2} \tag{51}$$

$$v_4 = \frac{V_4 X_1}{K_4 + X_1} \tag{52}$$

$$v_5 = k_{out} X_3 \tag{53}$$

$$v_6 = k_{deg} E_4 \tag{54}$$

with the parameters $V_1 = 5$,$V_2 = 3$, $V_3 = 2$, $V_4 = 2$, $K_1 = 2$, $K_2 = 1$, $K_3 = 1$, $K_4 = 2$, $k_{out} = 10$ and $k_{deg} = 5$ (arbitrary units). Concentrations are denoted with the symbol for the corresponding species. Eq. (49) is a Hill equation and corresponds to a cooperative enzyme. Eqs. (50)-(52) are simple Michaelis enzymes. Eq. (53) is the output rate of the network and is non-saturable. Finally, Eq. (54) is the degradation rate of enzyme 4. The reference state in all calculations is the steady state obtained by integrating the balance equations

$$\frac{\mathrm{d}X_1}{\mathrm{d}t} = J_1 - v_1 - v_4 \tag{55}$$

$$\frac{\mathrm{d}X_2}{\mathrm{d}t} = J_2 + v_1 - v_2 - v_3 \tag{56}$$

$$\frac{\mathrm{d}X_3}{\mathrm{d}t} = J_2 + v_2 + v_3 + v_4 - v_5 \tag{57}$$

$$\frac{\mathrm{d}E_4}{\mathrm{d}t} = J_3 - v_6 \tag{58}$$

with the fluxes $J_1 = 0.5$, $J_2 = 0$ and $J_3 = 25$. We restrict ourselves to independent excitations through single input fluxes, so as to ignore cross-terms. The first- and second-order responsivities of the velocities with respect to each input flux, calculated using the code described in [24], are compiled in Table 1.

It is straightforward to check that, except for small numerical errors, the responsivities satisfy Eqs. (47) and (48). However, the most interesting details of this example are the second-order responsivities with respect to J_2 and the null value of the first-order responsivity for v_5 with respect to J_3.

We discuss the responsivities with respect to J_2 first. It is a somewhat surprising result that a whole column of the non-linear responsivities is zero, when Eq. (48) allows for much greater variability. In particular, since all enzymes have non-linear kinetics, it would

Table 1. Responsivities of the branched network shown in Fig. 4

	$\rho = 1$			$\rho = 2$		
	J_1	J_2	J_3	J_1	J_2	J_3
v_1	0.047	0	-3.7×10^{-4}	0.105	0	2.9×10^{-5}
v_2	0.028	0.6	-2.2×10^{-4}	0.063	0	1.7×10^{-5}
v_3	0.019	0.4	-1.5×10^{-4}	0.042	0	1.2×10^{-5}
v_4	0.952	0	3.7×10^{-4}	-0.105	0	-2.9×10^{-5}
v_5	1	2	0	0	0	0
v_6	0	0	1	0	0	0

be reasonable to expect that the non-linear responsivities for v_2 and v_3 would be non-null. They are zero, however, because the Michaelis constants of these two enzymes are identical and therefore the rates are proportional to each other at all times. The transient behavior (not shown) is clearly non-linear. For example, the response times [29] increase as the input flux approaches saturation. However, if a steady state is achieved, it depends only on the first-order responsivities. The parameters of this example were chosen specifically to illustrate the point that, although the stoichiometric analysis provides an upper limit for the flexibility of the system, much less freedom might happen in practice due to what could be called kinetic locking. As the example illustrates, this should be expected in branched pathways with simple Michaelis kinetics at the branching point and with Michaelis constants of similar magnitude. In fact, it has been observed before that Michaelian enzymes, although formally non-linear, display clearly linear features in aspects like oscillation transmission [30], even for large variations of the fluxes. In particular, branched pathways are often equivalent to unbranched pathways when oscillations are present [31]. Notice, however, that enzymes v_1 and v_4 have non-zero non-linear responsivities, because, althouh they also have the same Michaelis constants, v_1 is allosteric. Therefore, in this case one could expect to be able to control the ratio of fluxes through each branch by simply modifying the input flux of X_1.

As to the responsivity $\mathscr{R}^{(1)}_{53}$, it is equivalent to a control coefficient in that it reflects the infinitesimal (first-order) variation of a flux as a consequence of the infinitesimal variation of the concentration of an enzyme (E_4). However, the coefficient is zero, and the same result would have been obtained if the concentration of any of the other enzymes had been considered external. This is an example in which MCA cannot be applied directly, since all control coefficients are zero and summation theorems do not hold. It could be argued that, due to the degradation flux, v_6, the enzyme does not accumulate in the long term (for an impulse perturbation, like the ones used to calculate susceptibilities), thus explaining the null coefficient. In fact, MCA was developed for persistent, though infinitesimal, variations of enzyme concentrations (or other parameters). However, it should be emphasized that the coefficient is identically zero under any kinetics, as shown in Eq. (48), meaning that a persistent change of the enzyme concentration would have no effects on the overall steady

state flux either. The reason why MCA does not hold in this example is the following. An implicit assumption of that theory is that the external concentrations are kept constant. Conversely, here, and in many practical situations, it is the flux, rather than the concentration, that is kept constant (or even variable). Due to the stoichiometric constraints, the overall output flux is independent of the enzyme levels. However, this is not the case for other rates (see, for example, v_1 and v_4). Such robust response of metabolic networks *to fluxes* is likely to have played a role in the achievement of homeostasis and could in fact be related to the observation that most experimental measurements of control coefficients yield very low values [32].

To summarize, this example illustrates how the present perturbative approach is able to connect stoichiometry and kinetics. In particular, stoichiometric analysis provides a set of admissible steady state fluxes, but leaves the coefficients of the linear combinations unsolved. Thus, the responsivities complement stochiometric analysis by providing such coefficients as a function of external perturbations and, implicitly, of the internal kinetics.

4. Conclusion

This chapter presents a sensitivity analysis that can be applied to study and characterize metabolic responses. It has several advantages over previously existing approaches. First, because it uses functional analysis, time-dependent excitations can be dealt with in a very natural way. Furthermore, there is no need to choose time-dependent reference states, as done in other sensitivity theories, notably, in extensions to MCA [25, 33]. As a consequence, transients can be studied with reference to steady states, which are usually easier to achieve and measure, and are more reproducible. A second advantage is that approximations are systematically improvable by simply keeping extra terms of a generalized Taylor series. Non-linear extensions of other approaches, notably MCA [21, 22], exist, but each new improvement has to be worked out separately.

The main coefficients of the theory are the susceptibilities. These are multidimensional functions of increasing order but, as this chapter shows, they can be determined from simple initial-concentration experiments, in which one or more concentrations are taken out of the reference state and left to decay. By composition of responses, it is possible to reduce the amount of required experimental data to be proportional to the order of the approximation. It should be mentioned that robust algorithms exist to calculate accurate derivatives from noisy data, such as the Savitzky-Golay filters [34].

The susceptibilities have connections with MCA quantities. In particular, the susceptibilities of rates are global quantities, whose value depends, in principle, on the properties of the whole system. This is similar to control coefficients. The example in section 3.3.2. shows that, when the external "metabolite" is an enzyme, the interpretation of the susceptibilities relates to that of (unscaled) flux control coefficients. However, susceptibilities are more general in that they describe transient behavior and in that they do not require an assumption of constant affinity, i.e. of constant concentration of the external metabolites. Without this assumption, there are situations in which the summation theorems of MCA do not hold, but the present approach can still be used. Another connection between the susceptibilities and MCA and BST is the relationship between rate and concentration

susceptibilities, Eqs. (18) and (19). Factors appear that are equivalent to elasticities, and relate global (susceptibilities) and local (rate equations) properties of the metabolic network. However, it must be emphasized that the present approach is not a control theory, since the aim is to reproduce responses, rather than to analyze the regulation. In that sense, it complements but does not replace MCA.

One limitation of the representation of responses as functional Taylor expansions is that bifurcations in the phase space are represented by non-invertible functionals [35], so that expansions are not possible at or through bifurcation points. This limitation is common to many sensitivity analyses [21]. The use of functionals to represent responses is, however, completely general. Thus, a future line of research is to find alternative approximations to the functional that can account for transitions through unstable states, such as the transition from steady states to and oscillatory, or even chaotic, regime.

The other important coefficients of the present theory are the responsivities. They connect the dynamics of a metabolic network and its stoichiometric structure. It has been shown that, whereas stoichiometric analysis and other related theories give an upper bound of the admissible space of steady state fluxes, the responsivities can in fact be more restrictive. Since they are defined from the susceptibilities, they implicitly contain kinetic information, but must also satisfy stoichiometric constrains. They are, therefore, a very interesting new tool for analysing the degrees of freedom of a metabolic network. As such, they should be useful in reducing the amount of experimental effort in high-throughput experiments.

This work was partially supported by a grant from DGICYT, Ministerio de Ciencia y Tecnología, Spain, BMC2000-0554. The author was a recipient of a fellowship from the FPU program of the Ministerio de Educación, Cultura y Deporte of Spain. Additional support from the Ramón Areces Foundation is also gratefully acknowledged. Marcel O. Vlad and John Ross participated in helpful discussions.

A. Functionals and Functional Derivatives

A functional $\mathscr{F}$ can be viewed as a generalization of a multivariate function, $f(j_1, \ldots, j_N)$, when the number of variables, N, tends to infinity. The argument of $\mathscr{F}$, say $J_{\text{in}}(t)$, is, therefore, a *function* of time, corresponding to the continuous version of the vector $(j_1, \ldots, j_i, \ldots, j_N)$, whose index i becomes real time t in the continuous limit. In addition to $J_{\text{in}}(t)$, $\mathscr{F}$ may depend explicitly on time, in which case it can be denoted as $\mathscr{F}[J_{\text{in}}; t]$. Moreover, the functional may accept several arguments, i.e. $\mathscr{F}[J^1_{\text{in}}, \ldots, J^w_{\text{in}}; t]$, where, in the context of this chapter, w is the number of independent excitations.

The generalization of the derivative of a function to that of a functional is a functional derivative. A definition of the latter results from the total differential of a multivariate function about a reference point, ref,

$$df = \left.\frac{\partial f}{\partial j_1}\right|_{\text{ref}} dj_1 + \cdots + \left.\frac{\partial f}{\partial j_N}\right|_{\text{ref}} dj_N, \tag{59}$$

which can be rewritten, by trivially introducing a time increment, Δt, as

$$\sum_{i=1}^{N} \left(\frac{1}{\Delta t} \frac{\partial f}{\partial j_i} \right)_{\text{ref}} dj_i \, \Delta t. \tag{60}$$

As N tends to infinity, f tends to $\mathscr{F}$, j_i to $J_{\text{in}}(t)$, total and partial differentials to a functional differential, $\delta J_{\text{in}}(t')$, and Δt to dt. In the limit, partial derivatives lead to the notation of the *functional derivative*,

$$\frac{1}{\Delta t} \frac{\partial f}{\partial j_i} \rightarrow \frac{\delta \mathscr{F}[J_{\text{in}}(t)]}{\delta J_{\text{in}}(t')}, \tag{61}$$

where the differential of time that comes from Δt remains implicit. This should be taken into account in dimensional analysis. Note that the functional differential of the function, δJ_{in}, is evaluated at time t', not t. This means that functional differentiation introduces a new variable.

Alternatively, putting $\partial j_i = \lim_{\lambda \rightarrow 0} \lambda / \Delta t$ in Eq. (61), the standard definition of a partial derivative leads to

$$\left. \frac{\delta \mathscr{F}[J_{\text{in}}(t)]}{\delta J_{\text{in}}(t')} \right|_{\text{ref}} = \left. \frac{\partial \mathscr{F}[J_{\text{in}}^{\text{ref}}(t) + \lambda \delta(t - t')]}{\partial \lambda} \right|_{\lambda = 0}. \tag{62}$$

Eq. (62) involves impulse perturbations, so that λ is the intensity of the excitation. For dimensional consistency, if the perturbation is a metabolic flux, λ is a concentration. Eq. (60) leads naturally to the functional differential of the functional $\mathscr{F}$:

$$\begin{aligned} \delta \mathscr{F} &= \mathscr{F}[J_{\text{in}}^{\text{ref}} + \delta J_{\text{in}}] - \mathscr{F}[J_{\text{in}}^{\text{ref}}] \\ &\equiv \int \left. \frac{\delta \mathscr{F}[J_{\text{in}}(t)]}{\delta J_{\text{in}}(t')} \right|_{\text{ref}} \delta J_{\text{in}}(t') dt' \end{aligned} \tag{63}$$

By repeated differentiation, functional derivatives of higher orders can be obtained. From them, the generalized functional Taylor expansion results, either in one excitation, Eq. (12), or in several, Eq. (15). It should be noted that, in functional Taylor expansions, all functional differentials are replaced by increments, in exact correspondence to the usual algebraic Taylor expansions.

References

[1] Teusink B, Passarge J, Reijenga CA, Esgalhado E, van der Weijden CC, Schepper M, et al. Can yeast glycolysis be understood in terms of in vitro kinetics of the constituent enzymes? Testing biochemistry. *Eur J Biochem.* 2000;267:5313–5329.

[2] Kremling A, Jahreis K, Lengeler JW, Gilles ED. The organization of metabolic reaction networks: a signal-oriented approach to cellular models. *Metab Eng.* 2000;2: 190–200.

[3] Kremling A, Gilles ED. The organization of metabolic reaction networks. II. Signal processing of hierarchical structured functional units. *Metab Eng.* 2001;3:138–150.

[4] Kremling A, Bettenbrock K, Laube B, Jahreis K, Lengeler JW, Gilles ED. The organization of metabolic reaction networks. III. Application for diauxic growth on glucose and lactose. *Metab Eng.* 2001;3:362–379.

[5] Savageau MA. Biochemical systems analysis. I. Some mathematical properties of the rate law for the component enzymatic reactions. *J Theor Biol.* 1969;25:365–369.

[6] Savageau MA. Biochemical systems analysis. II. The steady-state solutions for an n-pool system using a power-law approximation. *J Theor Biol.* 1969;25:370–379.

[7] Savageau MA. Biochemical systems analysis. III. Dynamic solutions using a power-law approximation. *J Theor Biol.* 1970;26:215–226.

[8] Schwake JH, Voit EO. Improved methods for the mathematically controlled comparison of biochemical systems. *Theor Biol Med Model.* 2004;1.

[9] Ervadi-Radhakrishnan A, Voit EO. Controllability of non-linear biochemical systems. *Math Biosci.* 2005;196:99–123.

[10] Kacser H, Burns JA. The control of flux. *Symp Soc Exp Biol.* 1973;32:65–104.

[11] Heinrich R, Rapoport TA. A linear steady-state treatment of enzymatic chains. General properties, control and effector strength. *Eur J Biochem.* 1974;42:89–95.

[12] Fell DA. Metabolic Control Analysis: a survey of its theoretical and experimental development. *Biochem J.* 1992;286:313–330.

[13] Visser D, Heijnen JJ. The mathematics of metabolic control analysis revisited. *Metab Eng.* 2002;4:114–123.

[14] Ehlde M, Zacchi G. A general formalism for Metabolic Control Analysis. *Chem Eng Sci.* 1997;52:2599–2606.

[15] Reder C. Metabolic control theory: a structural approach. *J Theor Biol.* 1988;135:175–201.

[16] Schuster S, Dandekar T, Fell DA. Detection of elementary flux modes in biochemical networks: a promising tool for pathway analysis and metabolic engineering. *Trends Biotechnol.* 1999;17:53–60.

[17] Schilling CH, Schuster S, Palsson BO, Heinrich R. Metabolic pathway analysis: basic concepts and scientific applications in the post-genomic era. *Biotechnol Prog.* 1999;15:296–303.

[18] Schuster S, Pfeiffer T, Moldenhauer F, Koch I, Dandekar T. Exploring the pathway structure of metabolism: decomposition into subnetworks and application to *Mycoplasma pneumoniae*. *Bioinformatics*. 2002;18:351–361.

[19] von Kamp A, Schuster S. Metatool 5.0: fast and flexible elementary modes analysis. *Bioinformatics*. 2006;22:1930–1931.

[20] Stelling J, Klamt S, Bettenbrock K, Schuster S, Gilles ED. Metabolic network structure determines key aspects of functionality and regulation. *Nature*. 2002;420: 190–193.

[21] Höfer T, Heinrich R. A second-order approach to metabolic control analysis. *J Theor Biol.* 1993;164:85–102.

[22] Hatzimanikatis V. Nonlinear metabolic control analysis. *Metab Eng*. 1999;1:75–87.

[23] Stoller P, Reiser KM, Celliers PM, Rubenchik AM. Polarization-modulated second harmonic generation in collagen. *Biophys J.* 2002;82:3330–3342.

[24] Torralba AS. Susceptibility of non-linear systems as an approach to metabolic responses. *Bioinformatics*. 2003;19:2428–2435.

[25] Mauch K, Arnold S, Reuss M. Dynamic sensitivity analysis for metabolic systems. *Chem Eng Sci.* 1997;52:2589–2598.

[26] Yang WC. Derivatives are essentially integer partititons. *Discrete Math*. 2000;222:235–245.

[27] Torralba AS, Rodríguez Y. Susceptibilities of an irreversible Michaelis-Menten enzyme. *Bull Math Biol.* 2006;68:1335–1353.

[28] Hérnandez-Encinas L, Muñoz Masqué J. A short proof of the generalized Faá de Bruno's formula. *Appl Math Lett.* 2003;16:975–979.

[29] Torralba AS, Rodríguez Y, Montero F. Phenomenological definition of response times with application to metabolic reactions. *J Theor Biol.* 2003;221:475–489.

[30] Rodríguez Y, Torralba AS, Montero F. Periodic signal transmission through metabolic pathways with Michaelian kinetics. *J Phys Chem B.* 2002;106:5536–5542.

[31] Rodríguez Y, Torralba AS, Montero F. Equivalence of branched and unbranched Michaelian pathways concerning periodic signal transmission. *Mol Biol Rep.* 2002;29:63–66.

[32] Mazar JP, Reder C, Letellier T. Why are most flux control coefficients so small? *J Theor Biol*. 1996;182:253–258.

[33] Ingalls BP, Sauro HM. Sensitivity analysis of stoichiometric networks: an extension of metabolic control analysis to non-steady state trajectories. *J Theor Biol.* 2003;222: 23–36.

[34] Press WH, Teukolsky SA, Vetterling WT, Flannery BP. Numerical Recipes in C. *The Art of Scientific Computing.* Cambridge University Press; 1992.

[35] Ambrosetti A. *A Primer of Nonlinear Analysis.* Cambridge: Cambridge University Press; 1993.

In: Mathematical Biology Research Trends
Editor: Lachlan B. Wilson, pp. 81-107
ISBN 978-1-60456-141-8

Chapter 3

HAPTOTAXIS IN PRE-NECROTIC AVASCULAR TUMOURS

D.G. Mallet and G.J. Pettet
School of Mathematical Sciences
Queensland University of Technology

Abstract

We develop a mathematical model describing the haptotactic migration of cells in a pre necrotic avascular tumour. Initially, the model which involves a moving boundary is developed for general three dimensional geometry and then modified for the specific multicell tumour spheroid geometry. A full nondimensionalisation is performed and the model is mapped to a fixed domain to facilitation numerical simulation. Numerically calculated solution profiles are then presented to provide predictions of the behaviour of cells in pre necrotic multicell tumour spheroids. Attention is paid to both passively migrating cells, and cells that respond to gradients in a simultaneously constructed extracellular matrix that is, cells that migrate haptotactically. The model solutions are used to propose biologically relevant hypotheses about the behaviour of cells in pre necrotic avascular tumours and the extracellular matrix in which they reside.

1. Introduction

In this chapter a mathematical model is developed to provide a description of the haptotactic migration of cells in a pre-necrotic avascular tumour. Initially, the model is developed for general three-dimensional geometry before more considering the more specific geometry of a multicell tumour spheroid. Numerically calculated solution profiles are then presented to provide predictions of the behaviour of cells in a pre-necrotic avascular tumour. Attention is paid to both passively migrating cells, and cells that respond to gradients in a simultaneously constructed extracellular matrix — that is, cells that migrate haptotactically. Finally, the model solutions are used to propose hypotheses about the behaviour of cells in pre-necrotic avascular tumours and the extracellular matrix in which they reside.

As stated above, two classes of cells are considered in the model — those deemed to be in a proliferative state that migrate due to passive mechanisms only and are henceforth

known as *proliferating cells*, and those whose proliferation has been stalled due to a lack of nutrient and undergo active migration mediated by the extracellular matrix. Cells of this second type will be referred to as the *migrating cells*. The diffusion and consumption of a generic nutrient are also considered in the model, along with the production of the extracellular matrix by the two types of tumour cells. In particular, the nutrient species is considered in a similar way to Greenspan [2], Byrne and Chaplain [1], Thompson and Byrne [14], Pettet et al. [12], and Landman and Please [5], using a quasi-steady diffusion equation where the nutrient is consumed by the cells.

Also considered in this model are two possibilities for the production of the extracellular matrix — production by the proliferating cells, and production by actively migrating cells. The experimental literature indicates that the type of cell, proliferating or migrating, responsible for the production of the extracellular matrix is actually cell-line specific. As such both are considered and their respective effects are investigated.

Appropriate kinetic functions are proposed to model conversion between the two cell types and also for the processes of cell death and mitosis. Similarly to Pettet et al. [12], the rates of cell death, mitosis and cell-type conversions are taken to depend on the local nutrient levels. The migratory behaviour of the two cell types is also considered and a distinct treatment offered for the migrating cells by specifying an altered cell velocity. While the proliferating cell velocity is influenced by cell death and loss, the haptotactically-migrating cells are assumed to undergo a further response, that due to gradients in the extracellular matrix density, modelling their haptotactic migration. Finally, it is also assumed that the outer boundary of the avascular tumour is moving with the same velocity as the actively migrating cells on the outer rim of the tumour.

The model is used to consider the behaviour of cells and the effect of the extracellular matrix for multicell tumour spheroids. After specifying the model in spherically symmetric geometry and nondimensionalising the model equations, the problem is mapped to a fixed domain to allow numerical solutions to be calculated. Numerical solutions are presented for a variety of parameter specifications to demonstrate the applicability of the model to describing haptotaxis in avascular tumours. Comments are made on the distribution throughout the tumour of the two cell types for the different extracellular matrix production sources. The evolution of tumours to steady state is considered and related to the system parameters. The different velocity profiles of the two cell types are also considered.

Numerous unusual observations are made when investigating the numerical solutions of the model. Particularly, it is shown that it is possible for the tumour to contract when the extracellular matrix is produced by the actively migrating cells. For such tumours, it is shown that a proportion of the proliferating cells that initially dominate just the outer regions of the tumour, may be displaced to the centre of the tumour by the migrating cells, effectively splitting the proliferating cell population. The model is also capable of simulating the usual behaviour of pre-necrotic avascular multicell spheroids. That is, an outer rim of proliferating cells and in inner region of cells in a quiescent state, with the tumour evolving to a steady state size after periods of exponential and then slowed linear growth.

2. Mathematical Model for Haptotaxis in Avascular Tumours

The model developed in this section describes the haptotactic migration of cells in avascular tumours of arbitrary three dimensional geometry consisting entirely of cell matter with no void space or extracellular water. Also present in the system are extracellular matrix fibres and nutrients such as oxygen, which are assumed to occupy negligible space in the avascular tumour. Figure 1 shows a rough schematic of the biological situation of interest.

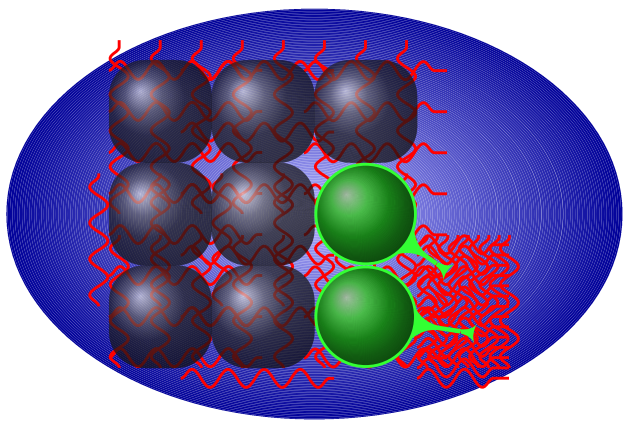

Figure 1. Schematic of the biological components in the model. Shown are two types of cells with a background matrix of ECM fibres and a continuous field of nutrient and extracellular water.

Introducing $E(\mathbf{x}, t)$ and $C(\mathbf{x}, t)$ to represent the density of the extracellular matrix and the local oxygen concentration at some spatial position $\mathbf{x}$ and at some time t, respectively, the following conservation equations are proposed:

$$\frac{\partial E}{\partial t} = -\nabla \cdot \mathbf{J}_E + f_E, \tag{1}$$

$$\frac{\partial C}{\partial t} = -\nabla \cdot \mathbf{J}_C + f_C, \tag{2}$$

where $\mathbf{J}_E$ and $\mathbf{J}_C$ represent the ECM and nutrient flux terms, and f_E and f_C represent as yet unspecified functions governing the production and degradation of ECM and the production and consumption of the nutrient, respectively.

The ECM is assumed to be a large immobile matrix of proteins and as such, migration of the extracellular matrix is neglected in equation (1) to give

$$\frac{\partial E}{\partial t} = f_E. \tag{3}$$

Furthermore, it is assumed that the nutrient undergoes passive migration due to Fickian diffusion only, and that this diffusion is rapid when compared with the rate of growth of the tumour. Thus equation (2) may be reduced to the quasi-steady equation

$$0 = D\nabla^2 C + f_C, \tag{4}$$

where D is the constant diffusion coefficient for the nutrient species.

In this study of haptotactic migration in multicell spheroids, we consider two distinct sub-populations of cells which combine to form the spheroid. First, denote by $\kappa(\mathbf{x}, t)$ the volume fraction of haptotactically migrating, non-proliferating cells at some spatial position $\mathbf{x}$ and at some time t. Then denote by $\psi(\mathbf{x}, t)$ the volume fraction of actively proliferating cells at some spatial position $\mathbf{x}$ and at some time t. These cells are assumed to display no haptotactic response.

In a manner similar to Pettet et al. [12], it is assumed that all cells are in either one of the two aforementioned states, or are dead cells that occupy no space. It is further assumed that all live cells are incompressible and closely packed. Given that the entire tumour consists of cells with no void space, the total volume fraction of all cells, denoted $N(\mathbf{x}, t)$ is then governed by

$$N(\mathbf{x}, t) = \kappa(\mathbf{x}, t) + \psi(\mathbf{x}, t). \tag{5}$$

Since the tumour consists of tightly packed cells, the total volume fraction of cells at a point does not change spatially, or over time, regardless of whether or not the tumour expands or contracts. That is

$$\begin{aligned} \nabla N(\mathbf{x}, t) = 0, \ \text{ and} \\ \frac{\partial N}{\partial t} = 0, \end{aligned} \tag{6}$$

and hence equation (5) becomes

$$N_0 = \kappa(\mathbf{x}, t) + \psi(\mathbf{x}, t), \tag{7}$$

where N_0 is the constant, total volume fraction of cells.

Conservation equations are now introduced for the volume fraction of each type of cell. The conservation equation for haptotactically-migrating cells is given by

$$\frac{\partial \kappa}{\partial t} + \nabla \cdot (\mathbf{u}_\kappa \kappa) = f_\kappa, \tag{8}$$

where f_κ represents any source or sink of migrating cells and $\mathbf{u}_\kappa$ is the migrating cell velocity.

For proliferating cells the equation takes the form

$$\frac{\partial \psi}{\partial t} + \nabla \cdot (\mathbf{u}_\psi \psi) = f_\psi, \tag{9}$$

where f_ψ represents any source or sink of proliferating cells and $\mathbf{u}_\psi$ is the proliferating cell velocity.

In this model, the two subpopulations of cells undergo distinctly different migratory processes. Essentially, it is assumed that proliferating cells are subject to passive migration processes only. Passive migration occurs due to, for example, pressure differences throughout the tumour mass. Here, this passive migration is caused by proliferation and death of cells. Actively migrating cells also undergo passive migration, but since they are not actively involved in proliferation, they are also able to respond to gradients in the extracellular

matrix density and thus undergo haptotactic migration. To reflect this difference in cell subpopulation velocities it is assumed that the velocity of actively migrating cells is equal to the sum of the proliferating cell velocity and a haptotactic term, such that

$$\mathbf{u}_\kappa = \mathbf{u}_\psi + \eta \nabla E, \tag{10}$$

where η is the haptotactic coefficient which here is assumed to be constant. The haptotactic term is taken to be of the form of similar terms in the cell fluxes of other haptotaxis models such as those due to Maini [6] and Murray [8], and is of a similar form to the chemotaxis term employed in the multicell spheroid model of Pettet et al. [12] where cells respond to gradients in nutrient concentration.

Differentiating equation (7) with respect to time gives

$$\frac{\partial \kappa}{\partial t} = -\frac{\partial \psi}{\partial t}. \tag{11}$$

Adding equations (8) and (9), and using (7) and (11) gives

$$\nabla \cdot (\mathbf{u}_\psi N_0 + \eta(N_0 - \psi)\nabla E) = f_\kappa + f_\psi.$$

By applying the divergence operator above, the above equation may be expanded and rearranged to give

$$\nabla \cdot \mathbf{u}_\psi = \frac{1}{N_0}\left(f_\kappa + f_\psi\right) - \frac{\eta}{N_0}\nabla \cdot \left((N_0 - \psi)\nabla E\right). \tag{12}$$

Since the tumour may be growing or shrinking, it is necessary to define a condition for the outer boundary of the tumour. It is assumed that the outer boundary will move at the same velocity as the cells located at the boundary. To derive a condition on the outer boundary position, first consider the following equation for the conservation of total cell volume:

$$\frac{\partial N}{\partial t} + \nabla \cdot (\mathbf{u}_N N) = f_N, \tag{13}$$

where $\mathbf{u}_N$ is the cell velocity and f_N is an unspecified source/sink of cells.

All cells are in either a proliferative or actively migrating state, and thus any source or sink in the total cell volume will be given by the sum of the source/sink functions of the two cell types. That is

$$f_N = f_\psi + f_\kappa.$$

Using the above equation, along with equations (5) and (6), and substituting into equation (13) gives

$$\nabla \cdot (\mathbf{u}_N(\psi + \kappa)) = f_\psi + f_\kappa. \tag{14}$$

Also, adding equations (8) and (9) and using equation (11) gives

$$\nabla \cdot (\mathbf{u}_\psi \psi + \mathbf{u}_\kappa \kappa)) = f_\psi + f_\kappa. \tag{15}$$

Hence, comparing equations (14) and (15) and rearranging gives

$$\mathbf{u}_N = \frac{\mathbf{u}_\psi \psi + \mathbf{u}_\kappa \kappa}{\psi + \kappa}.$$

Using equation (10) to replace the migrating cell velocity produces

$$\mathbf{u}_N = \mathbf{u}_\psi + \eta \frac{\kappa}{N_0} \nabla E.$$

Finally, since the outer boundary of the tumour moves at the same velocity as the cells located there, the equation of motion is given by

$$\frac{dB(t)}{dt} = u_\psi(B(t), t) + \eta \frac{\kappa}{N} \nabla E \Big|_{\mathbf{x}=B(t)}, \tag{16}$$

along with some initial tumour size

$$B(0) = B_0,$$

where $B(t)$ is the position of the boundary at time t.

At this point the model is complete, with the exception of appropriately assigned boundary and initial conditions which generally speaking, depend on the geometry of the spatial domain. The solution of the model requires the solution of equation (3) for the extracellular matrix density, equation (4) for the nutrient concentration, equation (12) for the velocity of the proliferating cells, and equation (9) for the distribution of proliferating cells. Equations (7) and (10) may then be used to determine the distribution of migrating cells and their velocity, respectively.

In the sections to follow, we consider the application of the model to the geometry of the multicell tumour spheroid. The model is nondimensionalised and mapped to a fixed spatial domain to allow for the calculation of numerical solutions. Variations in the model parameters are made and the resulting effects on the solution behaviour are explained. In particular, the effects of different sources of ECM production on the internal characteristics and growth of the tumour will be considered.

3. Haptotaxis in a Spherical Tumour

In this section, the model developed in Section 2. is used to describe the migration of cells in a tumour with geometry that is assumed to be spherically symmetric. In this way a description of cell migration in a multicell spheroid is given where it is assumed that the dependent variables vary only with distance from the tumour centre. This is similar to the models of McElwain and Pettet [7], Please et al. [13], Pettet et al. [12], and Landman and Please [5]. A schematic of the spherically symmetric tumour geometry is given in Figure 2. Below, the governing equations are stated for spherically symmetric geometry with spatial coordinate r, before a nondimensionalisation and fixed domain mapping are performed. Numerical solutions are then presented to demonstrate the ability of the model to predict the behaviour of cells in multicell spheroids.

It is unclear which type of cells (proliferating or migrating) is active in producing the extracellular matrix. The scarce sources in the literature seem to suggest that the production may at least depend on the cell type in question. For example, Nederman *et al*. [9] claim that for U-118MB cells the ECM is denser towards the core of a tumor, while for HTh-7 the matrix is roughly uniform throughout the tumor. Kelm [3] also discusses an extensive ECM associated with lab-grown multicell spheroids, particularly at the spheroid surface.

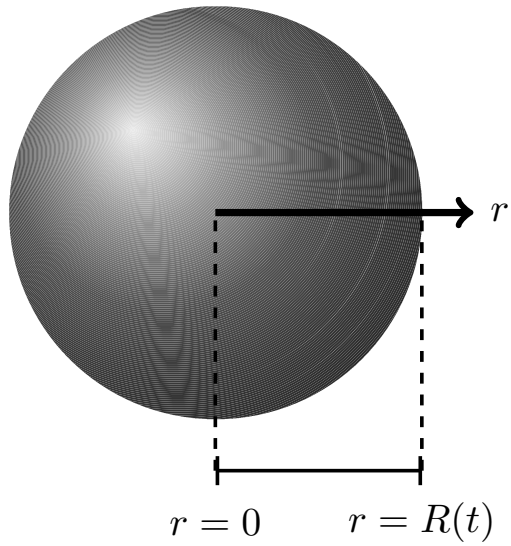

Figure 2. Schematic of a spherically symmetric tumour. Variations are assumed to occur only with distance from the centre of the tumour. The distance from the centre of the tumour is denoted r and the outer radius of the tumour, which may vary over time, is denoted $R(t)$.

With such conflicting evidence related to the cell type responsible for ECM production, it is first assumed in applying the model of Section 2. to a multicell spheroid, that both migrating and proliferating cells may form ECM but at varying rates, k_1 and k_2 respectively, and up to the maximum level of ECM, denoted by $\hat{E}$. Thus for the spherical tumour, equation (3) becomes

$$\frac{\partial E}{\partial t} = k_1(N_0 - \psi)(\hat{E} - E) + k_2\psi(\hat{E} - E).$$

Furthermore, it is assumed that initially the ECM is distributed according to the condition

$$E(r, 0) = E_0(r),$$

where r is the radial coordinate representing distance from the centre of the tumour.

With all cells consuming nutrient at a rate proportional to the local nutrient concentration, for a spherically symmetric tumour, equation (4) becomes

$$\frac{1}{r^2}\frac{\partial}{\partial r}\left(r^2\frac{\partial C}{\partial r}\right) = \frac{k_3 N_0}{D}C,$$

where k_3 is the constant rate of nutrient consumption. Furthermore, the boundary conditions are given by

$$\frac{\partial C}{\partial r}(0, t) = 0, \tag{17}$$

$$C(R(t), t) = C_0, \tag{18}$$

with equation (17) indicating that, due to spherical symmetry, nutrient cannot flow through the centre of the tumour at $r = 0$. Equation (18) represents the assumption that the spheroid is growing in a nutrient-rich medium, where the nutrient concentration outside of the tumour is $C = C_0$. $R(t)$ is introduced to denote the position of the outer boundary of the tumour, which may expand or shrink over time.

The following forms for the kinetic functions, f_ψ and f_κ, are now introduced. The birth of new cells and the conversion of migrating cells to proliferating cells are taken to be proportional to the nutrient level with rate constants k_B and k_ψ, respectively. Further, the rates of nutrient-related cell death and conversion from the proliferating to the haptotactically migrating cell type are assumed to be large for low nutrient concentrations, while the rates decrease linearly to zero for the external nutrient level $C = C_0$, with rate constants k_D for cell death and k_κ for cell-type conversion. Hence the kinetic functions take the form

$$f_\kappa = k_\kappa(C_0 - C)\psi - k_\psi C\kappa - k_D\,(C_0 - C)\,\kappa, \tag{19}$$

$$f_\psi = k_B C\psi - k_\kappa(C_0 - C)\psi + k_\psi C\kappa. \tag{20}$$

It should be noted that in the absence of cell type conversion, the tumour will undergo unbounded growth due to the presence of the proliferation term in the proliferating cell kinetics without any compensating cell death term. Furthermore, with rates proportional to the difference between the local nutrient level and that at the outer boundary, it is assumed that cell death and conversion occur throughout the tumour. It is possible to specify other forms for these rates that do not depend on the external nutrient level, although these are not considered here for the sake of clarity and so as not to introduce further assumptions to the model.

In spherically symmetric geometry and assuming the kinetic forms given by equations (19) and (20), equation (12) may be written as

$$\frac{1}{r^2}\frac{\partial}{\partial r}(r^2 u_\psi) = \frac{1}{N_0}\left(k_B C\psi - k_D\,(C_0 - C)\,(N_0 - \psi)\right) - \frac{\eta}{N_0}\frac{1}{r^2}\frac{\partial}{\partial r}\left(r^2(N_0 - \psi)\frac{\partial E}{\partial r}\right),$$

where u_ψ represents the velocity of proliferating cells, with a positive velocity indicative of motion away from the centre of the tumour. Due to symmetry, cells cannot move across the centre of the spheroid at $r = 0$, and as such the proliferating cells have a zero velocity at $r = 0$. That is

$$u_\psi(0, t) = 0.$$

In spherically symmetric geometry and again assuming the same kinetic forms given by equations (19) and (20) for the one-dimensional tumour, the proliferating cell conservation equation becomes

$$\frac{\partial \psi}{\partial t} + \frac{1}{r^2}\frac{\partial}{\partial r}\left(r^2 u_\psi \psi\right) = k_B C\psi - k_\kappa(C_0 - C)\psi + k_\psi C(N_0 - \psi).$$

It is assumed that initially, the volume fraction of proliferating cells is given by

$$\psi(r, 0) = \psi_0(r).$$

Again, due to symmetry at the centre of the spheroid, there is no flux of proliferating cells at $r = 0$. This gives the boundary condition

$$\frac{\partial \psi}{\partial r}(0,t) = 0.$$

Equation (16) is used to determine the position of the outer radius of the tumour. Hence, given the velocity of the proliferating cells, the following equation may be used to determine the position of the outer radius of the tumour

$$\frac{dR(t)}{dt} = u_\psi(R(t),t) + \eta \left(\frac{N_0 - \psi}{N_0}\right) \frac{\partial E}{\partial x}\bigg|_{r=R(t)},$$

where initially the outer boundary of the tumour is given by

$$R(0) = R_0.$$

Finally, equations (7) and (10) may be rewritten as

$$\kappa(r,t) = N_0 - \psi(r,t),$$
$$u_\kappa(r,t) = u_\psi(r,t) + \eta \frac{\partial E}{\partial r},$$

allowing for the calculation of the migrating cell distribution and velocity.

3.1. Nondimensionalisation

To proceed with the solution of the model for haptotaxis in a multicell tumour spheroid, the governing equations are now nondimensionalised. The equations are scaled by a timescale, T, associated with cell proliferation at the outer surface and a length scale, L, associated with the diffusion of the nutrient. That is,

$$T = \frac{1}{k_B C_0}, \quad L = \sqrt{\frac{D}{k_3 N_0}}.$$

This scaling gives the following dimensionless variables

$$E^* = \frac{E}{\hat{E}}, \quad C^* = \frac{C}{C_0}, \quad N^* = \frac{N}{N_0}, \quad \psi^* = \frac{\psi}{N_0},$$
$$r^* = \frac{r}{L}, \quad R^* = \frac{R}{L}, \quad t^* = \frac{t}{T}, \quad u_\psi^* = \frac{u_\psi T}{L},$$

where asterisks denote dimensionless variables.

Upon dropping the asterisks for notational simplicity, a dimensionless model formed by the following equations and conditions is obtained. First, for the extracellular matrix

$$\frac{\partial E}{\partial t} = \overline{k}_1(1-\psi)(1-E) + \overline{k}_2 \psi (1-E),$$

where initially

$$E(r,0) = \frac{1}{\hat{E}} E_0(r).$$

For the concentration of the nutrient

$$\frac{1}{r^2}\frac{\partial}{\partial r}\left(r^2\frac{\partial C}{\partial r}\right) = C,$$

where at the centre of the tumour

$$\frac{\partial C}{\partial r}(0,t) = 0,$$

and on the outer radius of the tumour

$$C(R(t),t) = 1.$$

For the velocity of the proliferating cells

$$\frac{1}{r^2}\frac{\partial}{\partial r}(r^2 u_\psi) = C\psi - \overline{k}_D(1-C)(1-\psi) - \overline{\eta}\frac{1}{r^2}\frac{\partial}{\partial r}\left(r^2(1-\psi)\frac{\partial E}{\partial r}\right),$$

where the cell velocity is zero at the centre of the tumour. That is

$$u_\psi(0,t) = 0.$$

In terms of dimensionless variables, the volume fraction of proliferating cells is governed by

$$\frac{\partial \psi}{\partial t} + \frac{1}{r^2}\frac{\partial}{\partial r}(r^2\psi u_\psi) = C\psi - \overline{k}_\kappa\psi(1-C) + \overline{k}_\psi C(1-\psi),$$

where initially

$$\psi(r,0) = \frac{1}{N_0}\psi_0(r),$$

and at the centre of the spherically symmetric tumour

$$\frac{\partial \psi}{\partial r}(0,t) = 0.$$

Finally, the outer boundary of the tumour is determined using

$$\frac{dR(t)}{dt} = u_\psi(R(t),t) + \overline{\eta}(1-\psi)\frac{\partial E}{\partial r}\bigg|_{r=R(t)},$$

where

$$R(0) = \sqrt{\frac{k_3 N_0}{D}}R_0.$$

In the above equations for a spherical tumour, the dimensionless parameters are given by

$$\overline{k}_1 = \frac{k_1 N_0}{k_B C_0},\ \ \overline{k}_2 = \frac{k_2 N_0}{k_B C_0},\ \ \overline{\eta} = \frac{\eta N_0 k_3 \hat{E}}{C_0 k_B D},$$
$$\overline{k}_D = \frac{k_D}{k_B},\ \ \overline{k}_\kappa = \frac{k_\kappa}{k_B},\ \ \overline{k}_\psi = \frac{k_\psi}{k_B},$$

where $\overline{k}_1$ and $\overline{k}_2$ are the rates of ECM production relative to the rate of cell mitosis at the outer radius, due to actively migrating and proliferating cells, respectively. The dimensionless haptotaxis coefficient is represented by $\overline{\eta}$, while the rates of cell death and conversion between cell types, relative to the mitosis rate, are represented by $\overline{k}_D$, $\overline{k}_\kappa$ and $\overline{k}_\psi$, respectively.

3.2. Landau Transformation

In order to produce numerical solutions it is necessary to map the moving boundary problem to a fixed domain using the method of Landau [4] . Hence the following change of variables is introduced

$$\xi = \frac{r}{R(t)},$$
$$\tau = t,$$

such that ξ represents the distance from some point in the tumour to the spheroid centre, scaled by the outer radius of the tumour at that point in time.

Upon changing variables, the conservation equation for the ECM density becomes

$$\frac{\partial E}{\partial \tau} - \frac{\xi}{R}\frac{dR}{d\tau}\frac{\partial E}{\partial \xi} = \overline{k}_1(1-\psi)(1-E) + \overline{k}_2\psi(1-E), \tag{21}$$

where initially

$$E(\xi, 0) = \frac{1}{\hat{E}}E_0(\xi). \tag{22}$$

For the concentration of the nutrient

$$\frac{1}{\xi^2}\frac{\partial}{\partial \xi}\left(\xi^2\frac{\partial C}{\partial \xi}\right) = CR^2, \tag{23}$$

where at the centre of the tumour

$$\frac{\partial C}{\partial \xi}(0, \tau) = 0,$$

and at the outer surface, $\xi = 1$,

$$C(1, \tau) = 1.$$

For the velocity of the proliferating cells

$$\frac{1}{\xi^2}\frac{\partial}{\partial \xi}(\xi^2 u_\psi) = R\left(C\psi - \overline{k}_D(1-C)(1-\psi)\right) - \frac{\overline{\eta}}{R}\frac{1}{\xi^2}\frac{\partial}{\partial \xi}\left(\xi^2(1-\psi)\frac{\partial E}{\partial \xi}\right), \tag{24}$$

where the cell velocity is zero at the centre of the tumour. That is

$$u_\psi(0, \tau) = 0.$$

The volume fraction of proliferating cells is governed by

$$\frac{\partial \psi}{\partial \tau} - \frac{\xi}{R}\frac{dR}{d\tau}\frac{\partial \psi}{\partial \xi} + \frac{1}{R}\frac{1}{\xi^2}\frac{\partial}{\partial \xi}(\xi^2\psi u_\psi) = C\psi - \overline{k}_\kappa\psi(1-C) + \overline{k}_\psi C(1-\psi), \tag{25}$$

where initially

$$\psi(\xi, 0) = \frac{1}{N_0}\psi_0(\xi),$$

and at the centre of the tumour

$$\frac{\partial \psi}{\partial \xi}(0, \tau) = 0.$$

Finally, the outer radius of the tumour is determined as before, using the ordinary differential equation

$$\frac{dR(\tau)}{d\tau} = u_\psi(1,\tau) + \overline{\eta}(1-\psi)\frac{\partial E}{\partial \xi}\bigg|_{\xi=1}, \tag{26}$$

along with the initial condition

$$R(0) = \sqrt{\frac{k_3 N_0}{D}} R_0.$$

3.3. Numerical Simulations

The simulations presented in this section are calculated using NAG routine D03PCF [11] to solve, at each time step, equations (21), (23), (24), and (25) for the ECM density, nutrient concentration, velocity and volume fraction of proliferating cells. An Euler scheme is then used to solve equation (26) and hence, update the position of the tumour boundary, also at each time step. The NAG routine is again implemented with a timestep of $\delta\tau = 0.1$ and mesh size $\Delta\xi = 0.005$.

Unless otherwise noted, the model parameters are given by

$$\overline{k}_\psi = 0.05, \quad \overline{k}_D = 0.3, \quad \overline{k}_\kappa = 0.9, \quad R_0 = 1, \quad \overline{\eta} = 1.$$

This typical parameter set is similar to that used by Pettet et al. [12] in their description of chemotaxis in multicell spheroids, and will therefore be of particular relevance in the next section of this chapter. Pettet et al.make a number observations of likely relationships in selecting their parameters. In particular, they state that the cell death rate is expected to be small compared with the proliferation rate, and that the cells are expected to convert from the proliferative state to the migrating state more quickly than the reverse. The parameter values are also based on general time- and length-scales associated with the problem and this is discussed in detail by Pettet et al.. For example, the time-scale is associated with the cell cycle time of cells in the proliferative state which is known to be between 8 and 24 hours [15]. Hence, while the exact values for the parameters are unknown, these values are taken to be reasonable given the limited information.

Considered below are the effects on the numerical solutions of varying the system parameters. Since there is little information available regarding the distribution and source of production of the extracellular matrix in multicell spheroids, variations in the parameters of equation (21) are made so as to form predictions regarding the resulting ECM distributions. In particular, spheroids in which proliferating cells secrete the extracellular matrix are considered, and then the different behaviour exhibited by spheroids in which the matrix proteins are secreted by actively migrating cells is also examined. The effects of varying the cell death and conversion parameters, as well as the initial spheroid size and haptotactic migration coefficient, will also be outlined.

3.3.1. ECM Production by Proliferating Cells

The secretion of ECM proteins is first considered to be carried out by those cells which are in the proliferative state. That is, in equation (21) $\overline{k}_1$ is set to zero and $\overline{k}_2$ is varied to

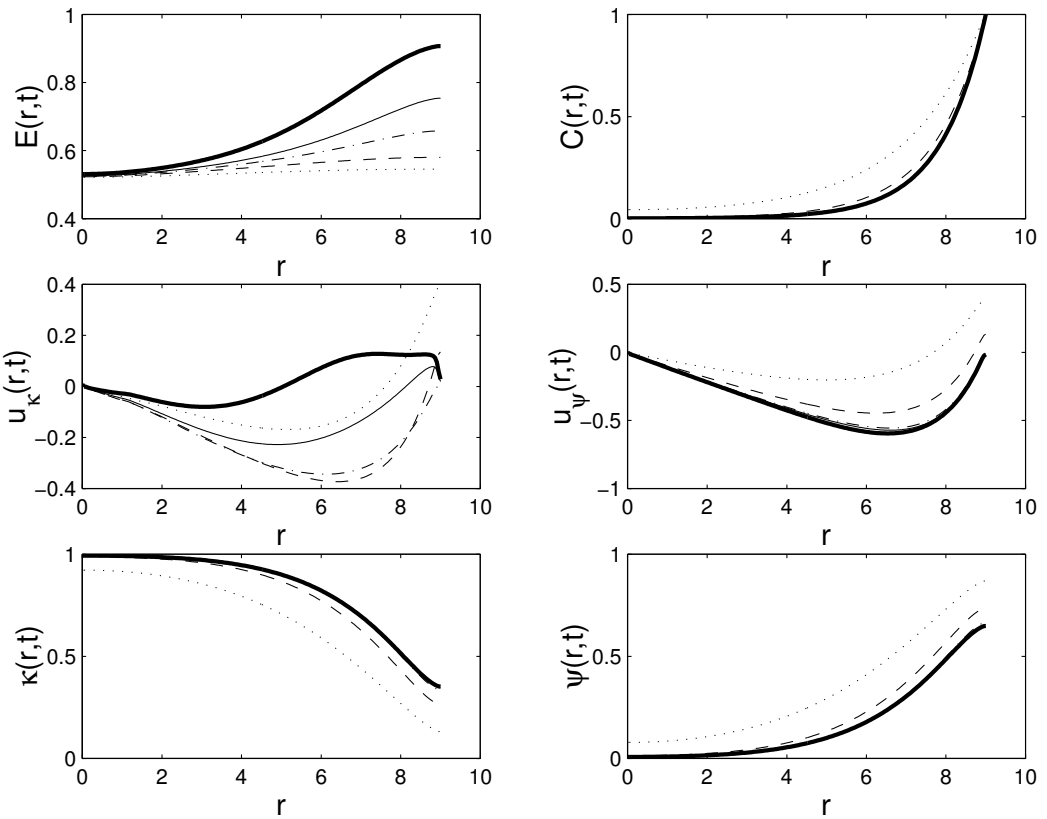

Figure 3. Haptotaxis in a multicell spheroid with low ECM production by proliferating cells for dimensionless times $t = 25$ ($\cdot\cdot\cdot\cdot$), $t = 50$ (– – – –), $t = 100$ (– $\cdot$ – $\cdot$ – –), $t = 200$ (———), $t = 250$ (thick ———). Parameter values used are $\overline{k}_1 = 0$, $\overline{k}_2 = 0.01$, $\overline{k}_\psi = 0.05$, $\overline{k}_D = 0.3$, $\overline{k}_\kappa = 0.9$, $\overline{\eta} = 1$, $R(0) = 1$. Initial conditions used are $E(r,0) = 0.5$ and $\psi(r,0) = 1$.

consider the effects of different levels of extracellular matrix production. Also considered below are the effects of different initial ECM profiles on the size of the spheroid and the solution profiles for the cell populations and velocities. All simulations shown below use the initial condition

$$\psi(r,0) = 1,$$

although very little variation in the solutions of the model is observed with the initial population of proliferating cells set to zero.

With an initially constant extracellular matrix profile, condition (22) becomes

$$E(r,0) = a,$$

where a is a positive constant, and for the numerical simulations carried out here, $a = 0.5$.

For early times, as shown in Figure 3, the migrating and proliferating cell populations undergo rapid changes from the initial conditions. Due to the form of the nutrient profile, a high population of migrating cells resides in the inner regions of the spheroid where

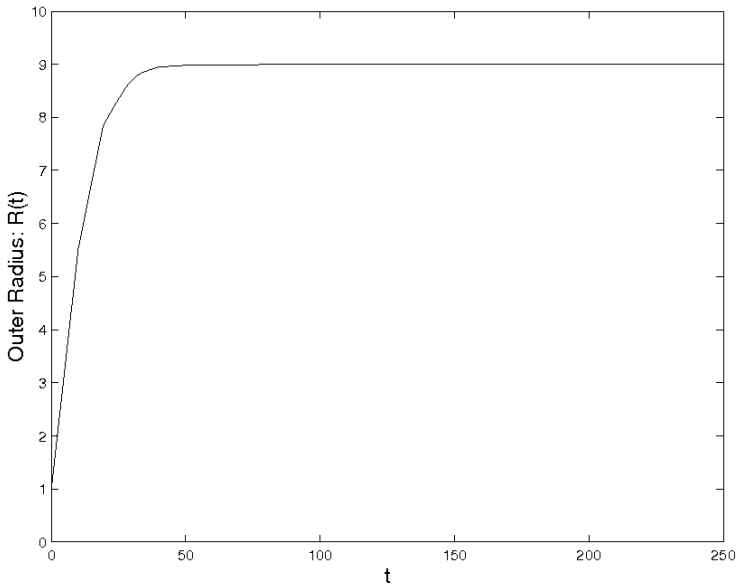

Figure 4. Evolution of the outer radius of a multicell spheroid with low ECM production by proliferating cells,for dimensionless time $t = 0$ to $t = 250$. Parameter values and initial conditions used as in Figure 3.

nutrient levels are low, while at the outer edges where there is a high level of nutrient, the proliferating cells dominate. This arrangement of the two cell populations persists over time and leads to the increased production of ECM proteins at the outer regions of the spheroid and the subsequent creation of a positive ECM gradient.

Considering the plot of $u_\kappa(r,t)$, early in the development of the spheroid, the matrix gradient is slight, and causes only a small amount of haptotactic migration. Hence, for small t, the velocities of migrating and proliferating cells are similar. As the ECM gradient becomes greater, the outward migration due to haptotaxis dominates the inward migration, particular towards the outer boundary of the tumour, resulting in the more positive velocity for actively migrating cells throughout the spatial domain.

Figure 4 shows the evolution of the outer radius of the spheroid with the same parameters as Figure 3. The spheroid appears to follow the same three phase growth described by Greenspan [2]. There is an initial phase of rapid growth, followed by a slowed, linear growth phase, and finally a dormant phase where the spheroid has attained a steady-state size. In this simulation, the dimensionless steady-state spheroid radius is $R_s \approx 9$.

Using the same initial conditions as above and varying the extracellular matrix production coefficient leads to only slight changes in the solution profiles. In fact, the steady-state radius is relatively unaffected by such changes, although it is attained more slowly than for the low production rate (where haptotactic migration aids the tumour in attaining its dormant size). The final distributions of actively migrating and proliferating cells also appear similar to those in Figure 3. Increasing the ECM production coefficient results in changing the position of the positive ECM gradient and this, in turn, causes the actively migrating cells to respond to the matrix at different spatial locations throughout the spheroid. As

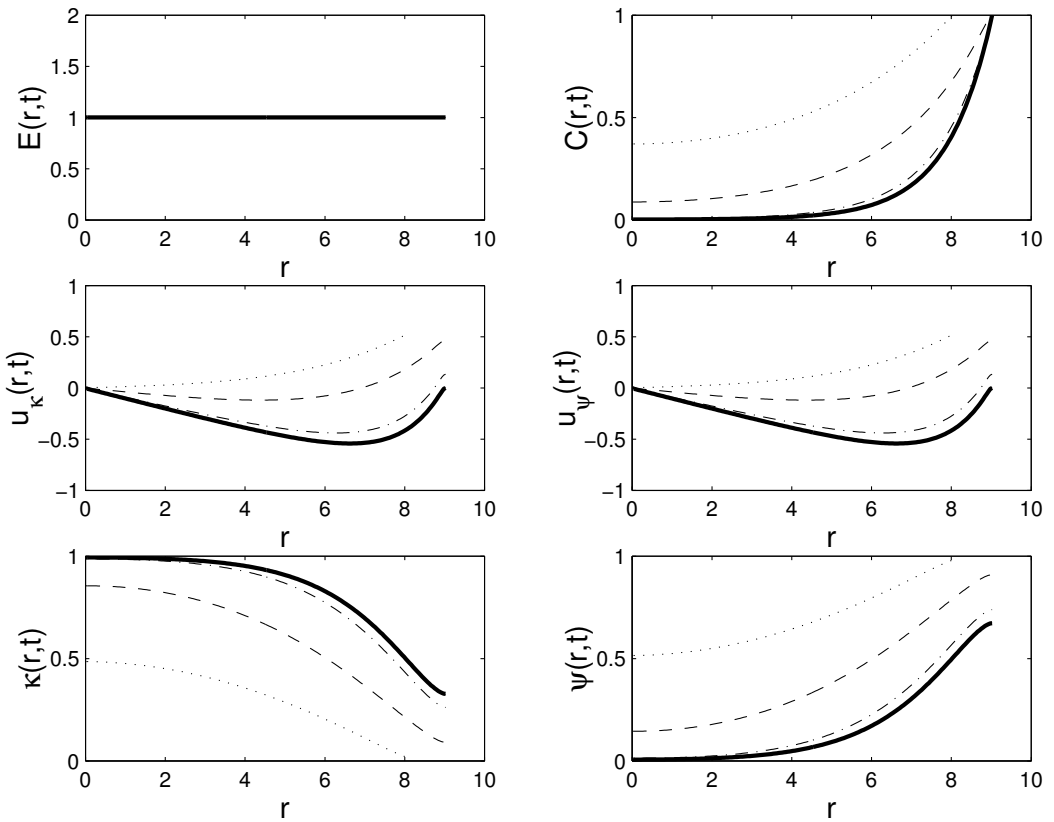

Figure 5. Haptotaxis in a multicell spheroid with high ECM production by proliferating cells for dimensionless times $t = 20$ ($\cdots\cdots$), $t = 40$ (– – – –), $t = 60$ (– · – · –), $t = 80$ (———), $t = 100$ (thick ———). Parameter values used are $\overline{k}_1 = 0$, $\overline{k}_2 = 10$, $\overline{k}_\psi = 0.05$, $\overline{k}_D = 0.3$, $\overline{k}_\kappa = 0.9$, $\overline{\eta} = 1$, $R(0) = 1$. Initial conditions used are $E(r,0) = 0.5$ and $\psi(r,0) = 1$.

shown in Figure 5, when the value of $\overline{k}_2$ is large enough (here $\overline{k}_2 = 10$), the ECM is quickly constructed to its carrying capacity of $E(r,t) = 1$, and there is no gradient in the matrix density. This results in a population of actively migrating cells which cannot undergo haptotactic migration, and the model reduces to considering two cell populations with identical migratory responses (as demonstrated in the plots of u_κ and u_ψ) — a situation similar to that considered by Ward and King who discussed cell populations with identical velocities and differing kinetic functions [16]. Note that in Figure 6, the tumour takes longer to reach its eventual steady state size when compared with the case shown in Figure 4 where the cells are able to migrate haptotactically.

An initially linear extracellular matrix profile with a slight positive gradient has also been considered. Under this assumption, equation (22) becomes

$$E(r,0) = br + a,$$

where a and b are positive constants, and for the numerical simulations carried out here, $a = 0.5$ and $b = 0.02$.

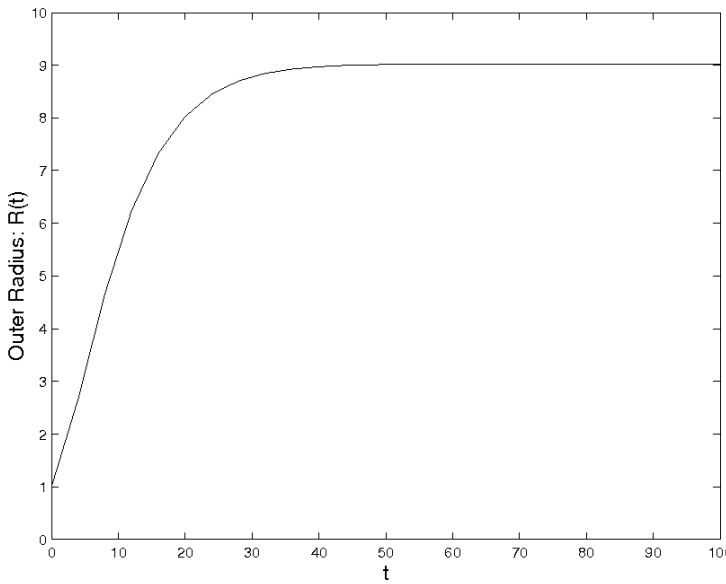

Figure 6. Evolution of the outer radius of a multicell spheroid with high ECM production by proliferating cells,for dimensionless time $t = 0$ to $t = 100$. Parameter values and initial conditions used as in Figure 5.

Comparing the ECM profile of Figure 7 with that of Figure 3, the inner spheroid regions now demonstrate a relatively steep, positive ECM density gradient. This results in the actively migrating cells undergoing dominantly haptotactic migration throughout the development of the spheroid. As shown in Figure 8, this leads to an increase in the steady-state radius to $R_s \approx 9.8$.

When the extracellular matrix production coefficient is increased to $\overline{k}_2 = 0.1$, an interesting effect is noticed in a plot of the outer radius location, $R(t)$. Initially, similar growth to that shown in Figures 7 and 8 is exhibited, where the spheroid grows towards $R(t) \approx 9.8$. However, as the proliferating cells continue to produce extracellular matrix, the ECM distribution throughout the spheroid begins to resemble that of a spheroid where the initial ECM distribution is uniform. As a result, the velocity due to proliferative pressure begins to dominate that due to haptotaxis and the actively migrating cells at the outer radius begin to move towards the interior of the spheroid. This continues until the haptotactic and proliferative pressure-related velocities balance, and the steady-state radius of $R_s \approx 9$ is again reached. That is, initially the tumour exceeds its eventual steady-state radius, before settling back to the smaller dormant size, $R_s \approx 9$.

Finally, the case where the initial ECM profile takes on a negative gradient was considered. In particular, equation (22) becomes

$$E(r, 0) = -br + a,$$

where a and b are positive constants, and again for the numerical simulations carried out here, $a = 0.5$ and $b = 0.02$.

Figure 11 shows the evolution of the ECM density, nutrient concentration, proliferating

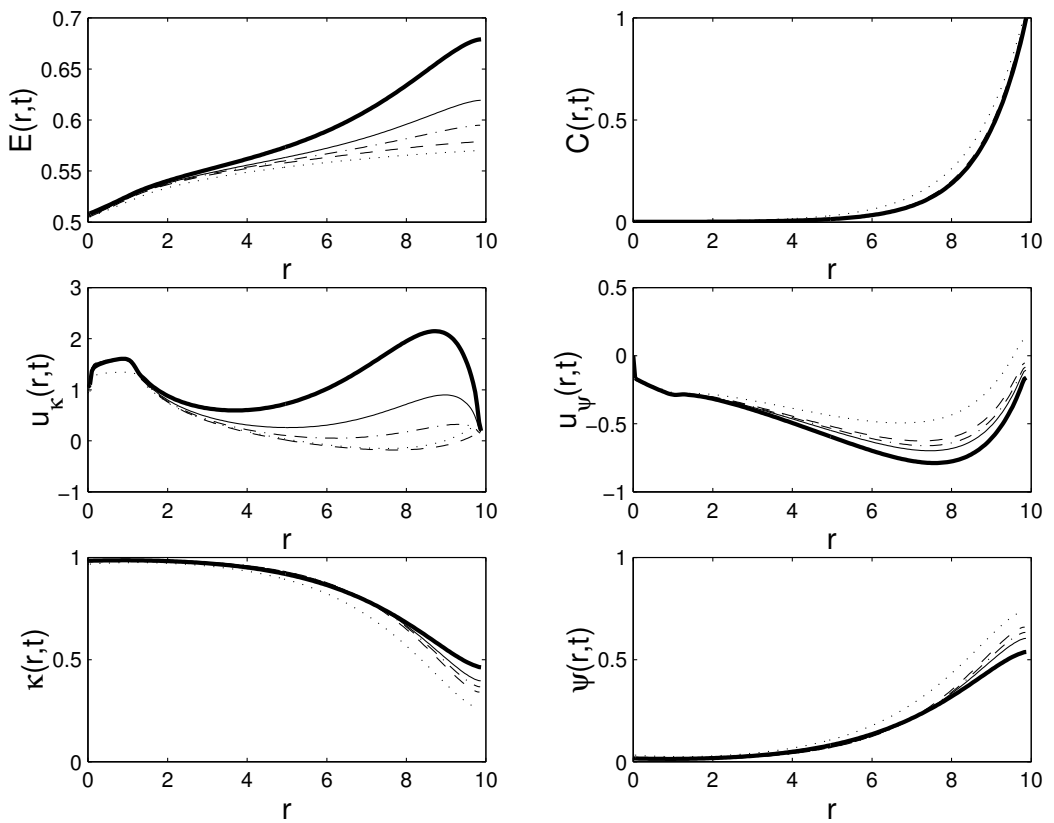

Figure 7. Haptotaxis in a multicell spheroid with low ECM production by proliferating cells for dimensionless times $t = 50$ ($\cdots\cdots$), $t = 100$ (– – – –), $t = 200$ (– · – · –), $t = 400$ (———), $t = 500$ (thick ———). Parameter values used are $\overline{k}_1 = 0$, $\overline{k}_2 = 0.001$, $\overline{k}_\psi = 0.05$, $\overline{k}_D = 0.3$, $\overline{k}_\kappa = 0.9$, $\overline{\eta} = 10$, $R(0) = 1$. Initial conditions used are $E(r,0) = 0.02r + 0.5$ and $\psi(r,0) = 1$.

and actively migrating cell velocities and populations, for a spheroid with the low ECM production coefficient $\overline{k}_2 = 0.001$, and an initially linear ECM distribution with a slight negative gradient. This case predicts that the ECM density for such a tumour evolves to a distribution with high levels of ECM at the outer edge and inner regions of the spheroid — indicating that it may be possible for haptotactic migration to lead to a splitting of the population of actively migrating cells. Given that, for a majority of the time over which the spheroid grows the migrating cell velocity is negative, the resulting dormant spheroid size is smaller than for any of the previous simulations. In fact, for this case $R_s \approx 8.2$. Furthermore, when comparing the cell volume fractions in Figure 11 with those in Figure 9, there is not such a distinct separation between the two cell types. Further investigation may confirm that measurements of the separation of the cell types can be used to predict the potential size of the tumour.

Note that for higher extracellular matrix production rates, the ECM distribution is quickly built to a form which is qualitatively similar to that for an initially constant ECM profile. Hence, simulations with negative-gradient, linear, initial ECM profiles and large $\overline{k}_2$

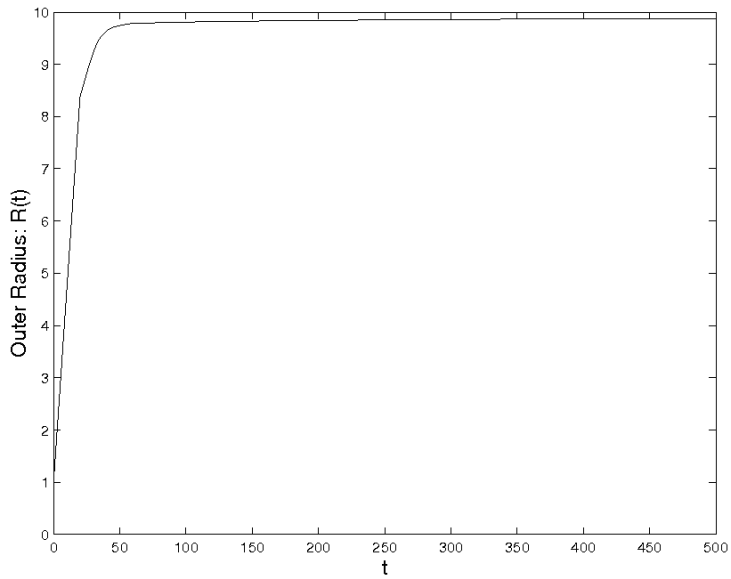

Figure 8. Evolution of the outer radius of a multicell spheroid with low ECM production by proliferating cells,for dimensionless time $t = 0$ to $t = 500$. Parameter values and initial conditions used as in Figure 7.

values produce spheroids with dormant sizes that are similar to those produced by simulations using an initially constant ECM profile.

3.3.2. ECM Production by Actively Migrating Cells

Now, consider the secretion of ECM proteins to be carried out by those cells which are haptotactically migrating. That is, in equation (21), $\overline{k}_2 = 0$ and $\overline{k}_1$ is varied to consider the effects of different levels of extracellular matrix production. Again considered below are the effects of different initial ECM profiles on the size of the spheroid and the solution profiles for the cell populations and velocities. All simulations shown below use the initial condition

$$\psi(r, 0) = 1.$$

The solutions of the model here with the initial proliferating cell volume fraction set to zero are again similar to those observed with an initial volume fraction of one.

With an initially constant extracellular matrix profile, equation (22) becomes

$$E(r, 0) = a,$$

where a is a positive constant, and for the numerical simulations carried out here, $a = 0.5$.

Initially, as shown in Figures 13 and 14, the spheroid size increases toward the steady-state level observed in Figures 4 and 6. As the production of the extracellular matrix by the actively migrating cells continues, mainly in the inner regions of the spheroid, the ECM density gradient becomes increasingly negative. As a result, the actively migrating cells undergo inward migration resulting in a contraction of the spheroid radius. The above

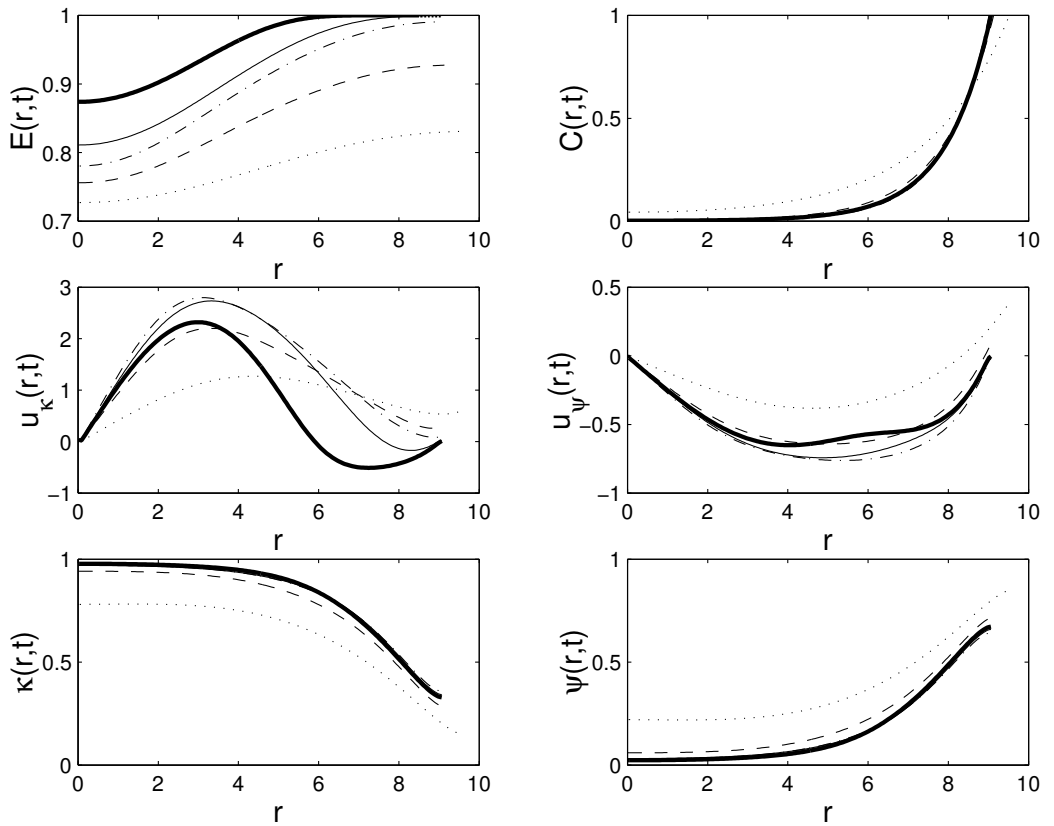

Figure 9. Haptotaxis in a multicell spheroid with low ECM production by proliferating cells for dimensionless times $t = 40$ ($\cdots\cdots$), $t = 80$ (– – – –), $t = 120$ (– · – · –), $t = 200$ (———), $t = 250$ (thick ———). Parameter values used are $\overline{k}_1 = 0$, $\overline{k}_2 = 0.1$, $\overline{k}_\psi = 0.05$, $\overline{k}_D = 0.3$, $\overline{k}_\kappa = 0.9$, $\overline{\eta} = 10$, $R(0) = 1$. Initial conditions used are $E(r,0) = 0.02r + 0.5$ and $\psi(r,0) = 1$.

behaviour is also observed when the ECM production coefficient is increased and when considering a spheroid with an initially linear ECM density with a negative gradient. As the ECM density reaches its maximum level, the effects of haptotaxis diminish, the velocities of the two cell types balance at the outer boundary, and the tumour reaches a dormant size.

When considering an initially linear ECM density with a positive gradient, the production of the ECM by migrating cells results in solution profiles such as those shown in Figure 15. The spheroid radius grows quickly towards $R = 12.5$ before undergoing significant contraction, as shown in Figure 16. Also, there is unusual behaviour in the plots of $\psi(\xi, t)$ and $\kappa(\xi, t)$. As was discussed earlier, by considering haptotaxis it may be possible to observe the splitting of one of the cell populations into two distinct regions of high density. As a result of the shape of the ECM profiles shown in Figure 15, actively migrating cells on the left-side of the maximum-ECM-density location attempt to migrate up the gradient in extracellular matrix, while those to the right are converted to proliferating cells due to the high nutrient levels. This results in the formation of a "hump" of actively migrating cells around the location of the ECM maximum. This causes an increase in the volume fraction

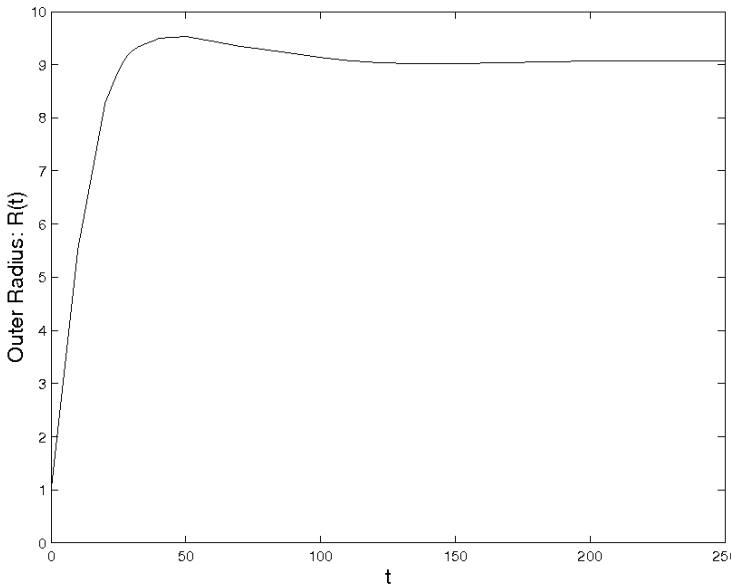

Figure 10. Evolution of the outer radius of a multicell spheroid with low ECM production by proliferating cells,for dimensionless time $t = 0$ to $t = 250$. Parameter values and initial conditions used as in Figure 9.

of proliferating cells at both the outer rim and, unusually, towards the centre of the spheroid. That is, the population of proliferating cells has been split into two almost distinct regions — one at the outer rim of the spheroid, and the other towards the centre.

The splitting of the cell population occurs here and not in such earlier situations as shown in Figures 7 and 9 due to the source of ECM production. The location of the migrating cells and their subsequent production of ECM, leads to the ECM profile that allows for bidirectional haptotactic migration. When the proliferating cells are producing the ECM, it is not possible to form an ECM gradient of this structure.

In a study of the growth characteristics of glioblastoma spheroids, Nirmala et al. describe experiments that resulted in the contraction of the spheroid and subsequent appearance of proliferating cells in the inner regions of the spheroid [10]. Such an observation is predicted in Figures 15 and 16 and suggests that the spheroids considered in the Nirmala et al. experiments were comprised of cells which produced extracellular matrix fibres when they were in a migrating state, and then responded haptotactically to gradients in the extracellular matrix.

3.3.3. The Effects of Variations in Other Model Parameters

While the primary focus of the numerical investigation of the multicell spheroid haptotaxis model is to elucidate the effects on MCS growth of different sources of extracellular matrix production, the effects of varying other system parameters are also considered. Throughout the discussion below, it is assumed that $\overline{k}_\psi = 0.05$, $\overline{k}_D = 0.3$, $\overline{k}_\kappa = 0.9$, $\overline{\eta} = 1$, $R_0 = 1$, $\overline{k}_1 = 0$ and $\overline{k}_2 = 0.01$, unless otherwise noted. These parameters are considered as they

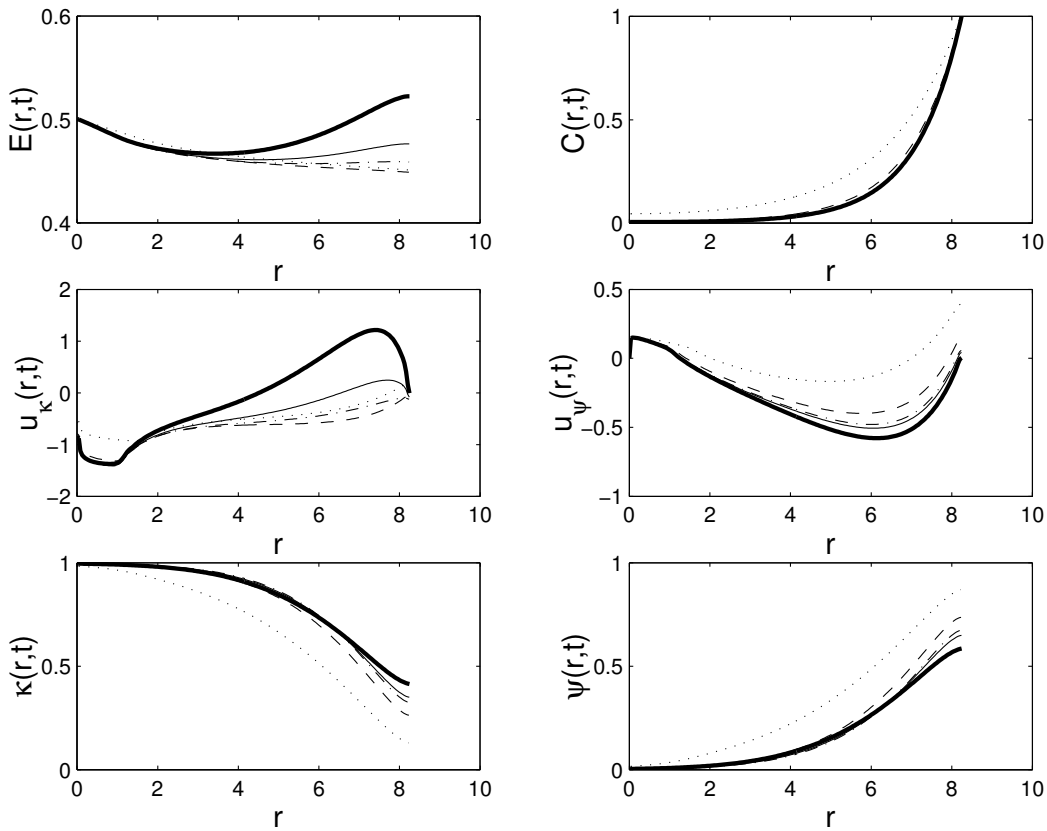

Figure 11. Haptotaxis in a multicell spheroid with low ECM production by proliferating cells for dimensionless times $t = 25$ ($\cdots\cdots$), $t = 50$ (– – – –), $t = 100$ (– · – · –), $t = 200$ (———), $t = 250$ (thick ———). Parameter values used are $\overline{k}_1 = 0$, $\overline{k}_2 = 0.001$, $\overline{k}_\psi = 0.05$, $\overline{k}_D = 0.3$, $\overline{k}_\kappa = 0.9$, $\overline{\eta} = 10$, $R(0) = 1$. Initial conditions used are $E(r,0) = -0.02r + 0.5$ and $\psi(r,0) = 1$.

allow for reproduction of spheroid growth similar to the classical spheroid development discussed by Greenspan [2]. The numerical solutions shown in Figure 3, calculated using the aforementioned parameter set, are also used as a reference point for the simulations using altered parameters discussed below.

Increasing the coefficient of the cell death rate, $\overline{k}_D$, causes a decrease in the steady-state tumour size, while lower $\overline{k}_D$ values result in larger spheroids. Increasing the cell death rate coefficient from the reference value of $\overline{k}_D = 0.3$ also increases the level of proliferating cells throughout the spheroid, and hence increases the rate of ECM production. This increased ECM production and the subsequent decrease in the period of time over which haptotactic migration may occur explains the decrease in the steady-state tumour radius for high cell death rates.

Increases in the migrating-to-proliferating cell conversion coefficient lead to larger tumour sizes and increases in the growth rate towards the steady-state. The volume fraction of proliferating cells at the outer radius is also increased, giving more evidence for the hy-

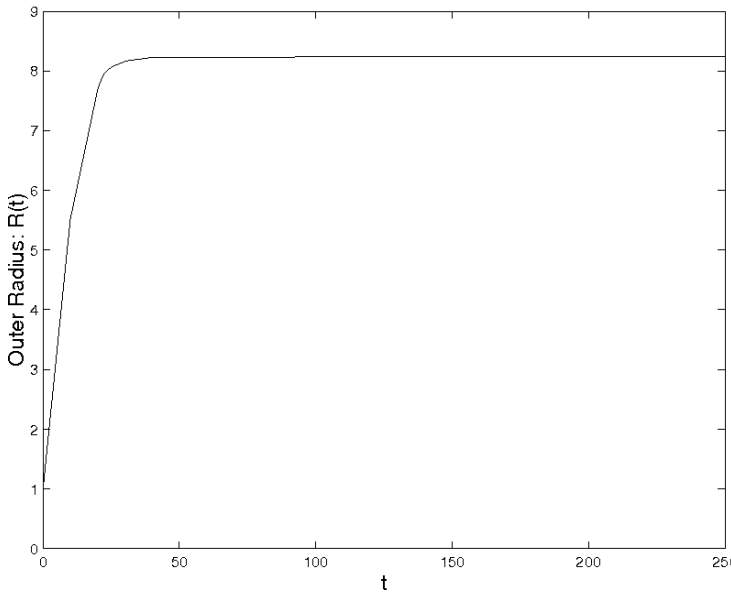

Figure 12. Evolution of the outer radius of a multicell spheroid with low ECM production by proliferating cells,for dimensionless time $t = 0$ to $t = 250$. Parameter values and initial conditions used as in Figure 11.

pothesis that the level of proliferating cells at the outer boundary of the tumour is directly related to the steady-state tumour size. For decreased values of $\overline{k}_\psi$, the steady-state radius shows little variation from that shown in Figure 4, although the growth rate is decreased.

Increasing the proliferating-to-migrating cell conversion coefficient has the opposite effect to that described above. For larger values of $\overline{k}_\kappa$, the dormant tumour size is decreased, as is the proportion of proliferating cells at the outer boundary. Decreasing the parameter results in larger spheroids and an increase in the proliferating cell population in the outer regions of the tumour.

Altering the haptotactic coefficient, $\overline{\eta}$, results in similar effects to those discussed for the one-dimensional application of the cell migration model. That is, the steady-state tumour radius is not changed, while the internal behaviour of the spheroid cells, in particular the velocity of the actively migrating cells, does change. This change in cell velocity involves the greater positive migration response of actively migrating cells, to the gradient in the extracellular matrix density. Furthermore, variations in the initial tumour radius also make no effect on the resulting dormant spheroid size. The growth rate is simply altered so as to decrease the outer radius, in the case of large initial tumour sizes, and increase the outer radius, in the case of small initial tumour sizes.

4. Conclusions

In this chapter, a mathematical model has been presented that describes the haptotactic migration of cells in pre-necrotic avascular tumours. As in previous models (see for example [2], [5], [7], [12], [14]), the model includes a quasi-steady diffusion equation for the

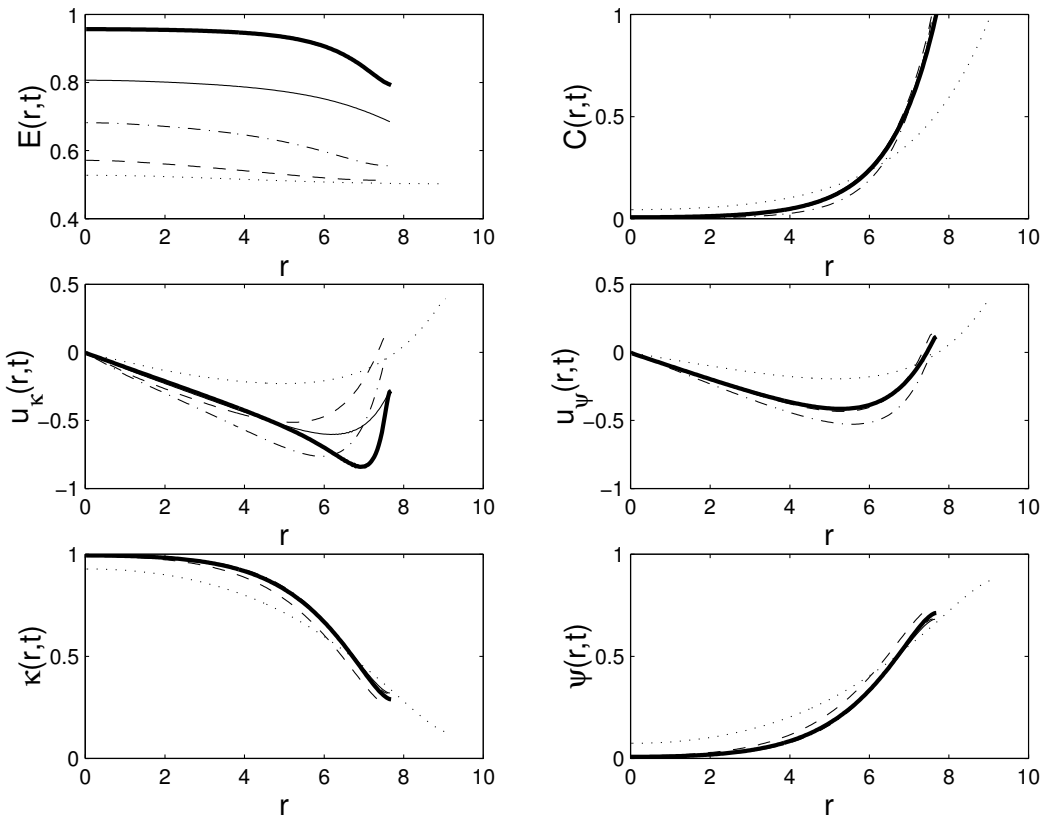

Figure 13. Haptotaxis in a multicell spheroid with low ECM production by actively migrating cells for dimensionless times $t = 50$ ($\cdot\cdot\cdot\cdot$), $t = 100$ ($-\,-\,-\,-$), $t = 150$ ($-\cdot-\cdot-$), $t = 200$ (———), $t = 250$ (thick ———). Parameter values used are $\overline{k}_1 = 0.01$, $\overline{k}_2 = 0$, $\overline{k}_\psi = 0.05$, $\overline{k}_D = 0.3$, $\overline{k}_\kappa = 0.9$, $\overline{\eta} = 1$, $R(0) = 1$. Initial conditions used are $E(r,0) = 0.5$ and $\psi(r,0) = 1$.

nutrient species, with a sink of the nutrient concentration due to consumption by cells. Two cell types — proliferating and migrating — are considered to comprise the tumour mass, with dead cells occupying no space. The two cell types have different velocities due to the haptotactic response of the migrating cells to gradients in the extracellular matrix density. Appropriate kinetic functions are also specified to describe conversion between the two cell types, as well as birth and death of cells, all of which depend on the local nutrient concentration. Finally, the density of the extracellular matrix is described using a conservation equation with ECM sources dependent on the concentrations of proliferating and migrating cells.

Using spherically symmetric geometry, it was possible to use the model to describe the migration of cells due to haptotaxis in multicell spheroids. It was possible to simulate pre-necrotic tumours that follow the familiar structure of a proliferating rim coupled with a predominantly quiescent interior as shown in Figure 5. Similarly, the usual three growth phases of multicell spheroids were shown in Figure 6, with an initial exponential growth phase due to the high rate of cell proliferation in the small, nutrient-rich spheroid. The

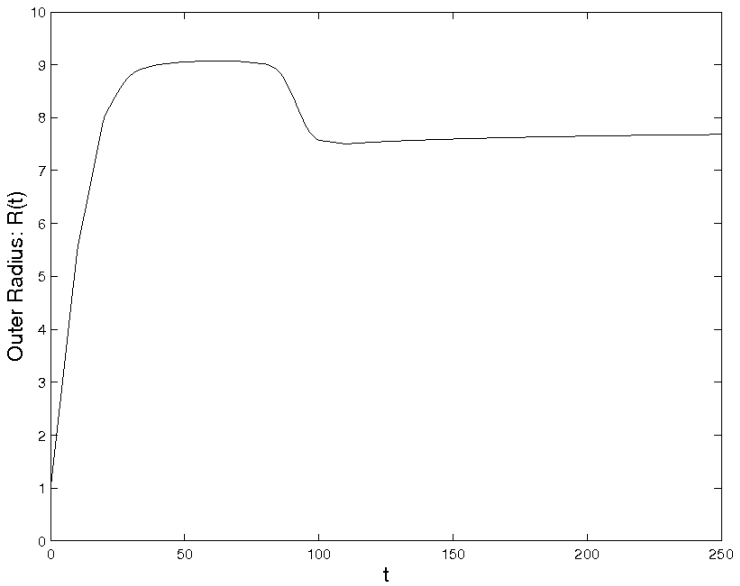

Figure 14. Evolution of the outer radius of a multicell spheroid with low ECM production by actively migrating cells,for dimensionless times $t = 0$ to $t = 200$. Parameter values and initial conditions used as in Figure 13.

exponential growth phase is followed by a phase of slowed linear growth, as the nutrient level in the centre of the spheroid drops, and subsequently the rate of proliferation falls. Finally, when proliferation, death and haptotactic migration are in balance, the outer boundary reaches a steady state and a period of dormancy follows.

While the usual tumour behaviour was predicted, as mentioned above, other unusual observations were also made. In Figure 10, it is shown that when the initial ECM profile is linearly distributed with a positive gradient, it is possible for the tumour radius to initially overshoot the steady-state radius before settling back down to its eventual dormant size.

Considering the extracellular matrix to be produced by migrating cells rather than by proliferating cells leads to quite novel observations also, as demonstrated in Figures 13–16. In particular, the model predicts that while the tumour will initially increase in size due to the abundance of nutrient and associated high proliferation levels, the development of a negatively-sloped ECM profile leads to contraction of the tumour due to haptotactic migration towards the centre of the tumour.

When the initial ECM profile is a positively-sloped linear function, not only does the tumour contract, but the proliferating cell distribution also appears to split into two almost distinct bands of high density. That is, the usual band of proliferating cells on the outer boundary, and another population of proliferating cells in the centre of the tumour. While low nutrient levels earlier in the tumour development imply that this high density of proliferating cells at the tumour centre would not be possible, the tumour shrinkage allows for higher levels of nutrient to exist throughout the spheroid. Furthermore, the outward migration of actively-migrating cells due to the positive ECM gradient displaces proliferating cells towards the outer-most and inner-most regions of the spheroid. These observations are

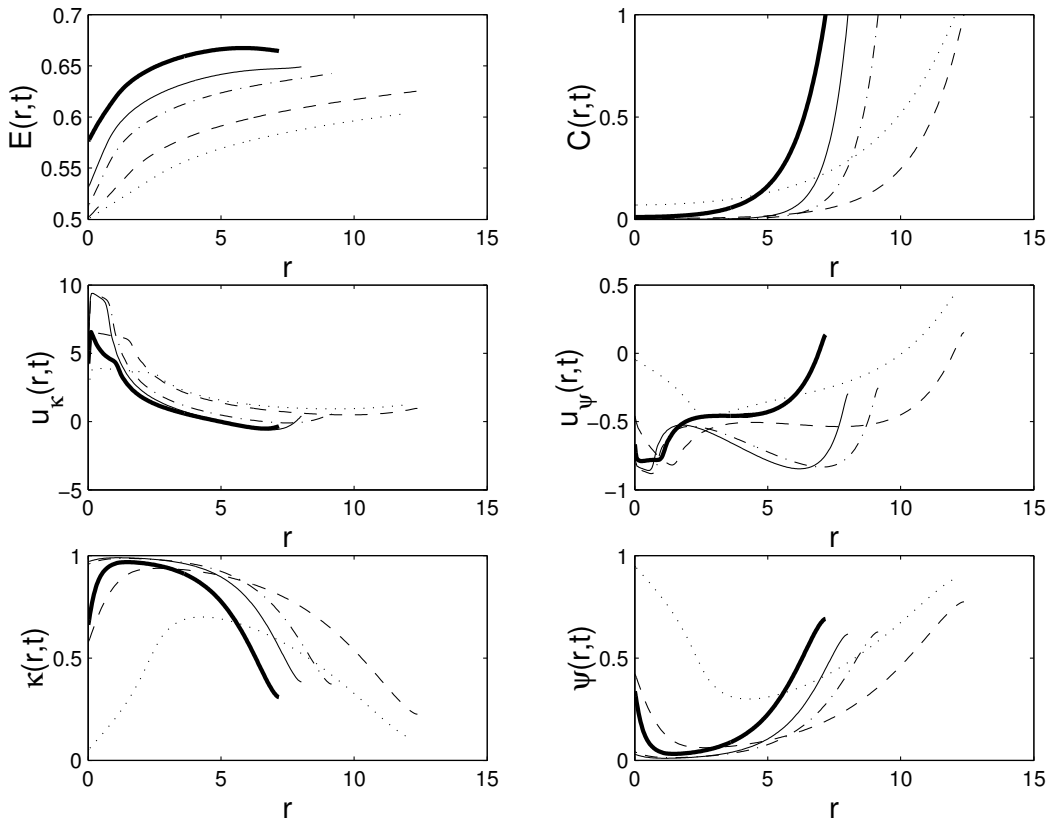

Figure 15. Haptotaxis in a multicell spheroid with low ECM production by actively migrating cells for dimensionless times $t = 20$ (·····), $t = 50$ (– – – –), $t = 100$ (– · – · –), $t = 150$ (———), $t = 200$ (thick ———). Parameter values used are $\overline{k}_1 = 0.001$, $\overline{k}_2 = 0$, $\overline{k}_\psi = 0.05$, $\overline{k}_D = 0.3$, $\overline{k}_\kappa = 0.9$, $\overline{\eta} = 10$, $R(0) = 1$. Initial conditions used are $E(r,0) = 0.02r + 0.5$ and $\psi(r,0) = 1$.

similar to experimental results due to Nirmala et al. which describe the growth of glioblastoma spheroids, that at some point in their development, contracted and developed centrally located proliferating cells [10].

Finally, this model provides a useful experimental tool for judging which cells in a particular tumour produce the extracellular matrix. That is, given an extracellular matrix distribution obtained through an examination of the internal structure of a multicell spheroid, this could then be compared with simulations of the multicell spheroid haptotaxis model developed in this chapter. By varying the source of the ECM in the model simulations and making the appropriate comparisons, the source of the ECM in the experimental spheroid could then be identified.

The model developed in this research is currently being extended to investigate the effects of haptotaxis on the internalisation of cells at the spheroid surface. Importantly, this is related to the possible internalisation of treated cells or microspheres which may aid in eliminating or decreasing the size of spheroids.

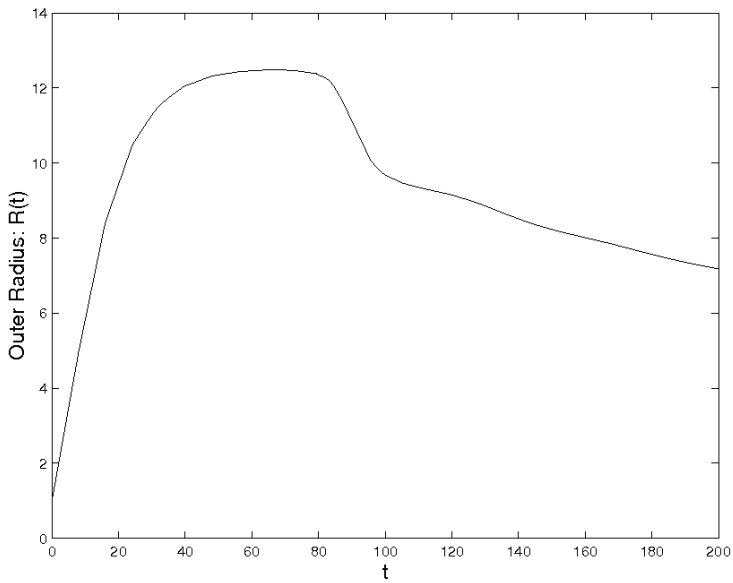

Figure 16. Evolution of the outer radius of a multicell spheroid with low ECM production by actively migrating cells,for dimensionless time $t = 0$ to $t = 200$. Parameter values and initial conditions used as in Figure 15.

References

[1] H.M. Byrne and M.A.J. Chaplain. Modelling the role of cell-cell adhesion in the growth and development of carcinomas. *Mathl. Comput. Modelling*, **24**(12):1–17, 1996.

[2] H.P. Greenspan. Models for the growth of a solid tumor by diffusion. *Studies in Applied Mathematics*, **51**:317–338, 1972.

[3] J.M. Kelm, N.E. Timmins, C.J. Brown, M. Fussenegger, and L.K. Nielsen. Method for generation of homogeneous multicellular tumor spheroids applicable to a wide variety of cell types. *Biotechnol Bioeng.*, **83**:173–180, 2003.

[4] H.G. Landau. Heat conduction in a melting solid. *Q.J. Appl. Math.*, **8**:81–94, 1950.

[5] K.A. Landman and C.P. Please. Tumour dynamics and necrosis: surface tension and stability. *IMA Journal of Mathematics Applied in Medicine and Biology*, **18**:131–158, 2001.

[6] P.K. Maini. Spatial and spatio-temporal patterns in a cell-haptotaxis model. *Journal of Mathematical Biology*, **27**:507–522, 1989.

[7] D.L.S. McElwain and G.J. Pettet. Cell migration in multicell spheroids: Swimming against the tide. *Bulletin of Mathematical Biology*, **55**(3):655–674, 1993.

[8] J. Murray. *Mathematical Biology*. Springer Verlag, 1989.

[9] T. Nederman, B. Norling, B. Glimelius, J. Carlsson, and U. Brunk. Demonstration of an extracellular matrix in multicellular tumor spheroids. *Cancer Research*, **44**:3090–3097, 1984.

[10] C. Nirmala, J.S. Rao, A.C. Ruifrok, L.A. Langford, and M. Obeyesekere. Growth characteristics of glioblastoma spheroids. *International Journal of Oncology*, **19**:1109–1115, 2001.

[11] Numerical Algorithms Group. *The NAG Fortran Library Manual, Mark 19*.

[12] G.J. Pettet, C.P. Please, M.J. Tindall, and D.L.S. McElwain. The migration of cells in multicell tumor spheroids. *Bulletin of Mathematical Biology*, **63**:231–257, 2001.

[13] C.P. Please, G.J. Pettet, and D.L.S. McElwain. Avascular tumour dynamics and necrosis. *Mathematical Models and Methods in Applied Sciences*, **9**(4):569–579, 1999.

[14] K.E. Thompson and H.M. Byrne. Modelling the internalization of labelled cells in tumour spheroids. *Bulletin of Mathematical Biology*, **66**:601–623, 1999.

[15] M. Tubiana. The kinetics of tumour cell proliferation and radiotherapy. *Br. J. Radiol.*, **44**:325–347, 1971.

[16] J.P Ward and J.R. King. Mathematical modelling of avascular-tumour growth. *IMA Journal of Mathematics Applied in Medicine and Biology*, **14**:36–69, 1997.

In: Mathematical Biology Research Trends
Editor: Lachlan B. Wilson, pp. 109-145
ISBN 978-1-60456-141-8

Chapter 4

MATHEMATICAL ANALYSIS OF A CHOLERA MODEL WITH CARRIERS: ASSESSING THE EFFECTS OF TREATMENT

Z. Mukandavire*[1]*, F.K. Mutasa*[1]*, S.D. Hove-Musekwa*[1]*,
***S. Dube*[2] *and J.M. Tchuenche*[3]**
[1]Department of Applied Mathematics,
Modelling Biomedical Systems Research Group,
National University of Science and Technology,
Box AC 939 Ascot, Bulawayo, Zimbabwe
[2]Department of Applied Biology/Biochemistry,
National University of Science and Technology,
Box AC 939, Bulawayo, Zimbabwe
[3]Mathematics Department, University of Dar es Salaam,
P.O.Box 35062, Dar es Salaam, Tanzania

Abstract

Cholera is a gastrointestinal disease caused by a gram negative coma shaped bacterium of the genus *Vibrio cholerae*. It is often associated with poor hygiene of drinking water, food preparations and waste disposal particularly feaces. It rapidly causes diarrhea, vomiting and dehydration which could be fatal if not medically attended to timeously. The diarrhea is caused by a toxin produced by the bacterium. This toxin causes the efflux of salts and water into the gastrointestinal tract. Cholera as a disease is a serious public health problem in the developing world, and since the first recorded cases, it has spread rapidly across continents, resulting in numerous deaths. The aim of this chapter is to use mathematical modeling to analyze the dynamics of this disease with and without treatment. Thus, we present a single-season deterministic model for cholera transmission dynamics with carriers in a human population and a pool of pathogens. The mathematical features such as the epidemic threshold, equilibria and

*E-mail address: zmukandavire@nust.ac.zw or zmukandavire@gmail.com; Corresponding author: Department of Applied Mathematics, Modelling Biomedical Systems Research Group, National University of Science and Technology, Box AC 939 Ascot, Bulawayo, Zimbabwe

stabilities are determined. A Lyapunov functional approach is used to analyse the stabilities of equilibria. We qualitatively analyse positivity and boundedness of solutions. In the absence of treatment, the trivial equilibrium is shown to be a saddle, while the two biologically meaningful equilibria, namely the disease-free is globally asymptotically stable provided certain conditions are met, and the endemic equilibrium state is only locally stable. The epidemic threshold is used to assess the effectiveness of treatment in controlling cholera in a community. Conditions for cholera containment and persistence are derived using comprehensive analytical and numerical techniques. It is shown from the study that treatment of cholera sufferers reduces the burden of the disease in the community. Further, it is also shown that as long as the pathogen is present in the environment, it will be difficult to eradicate cholera and the existence of carriers may remain a challenge in the control of the epidemic in settings with treatment of cholera sufferers.

MSC: 92D30, 34K20.

Key words: *Vibrio cholerae,* cholera, stability, persistence, treatment, epidemic threshold.

1. Introduction

Cholera is a gastrointestinal disease characterized by vomiting, dehydration and diarrhea in which the stools are rice like in appearance. It is caused by a coma shaped bacterium of the genus *Vibrio cholerae*. *V. cholerae* is naturally found in aquatic plankton particularly copepods. Water from copepod infested sources if taken by susceptible humans becomes the cause of the disease [27]. Cholera is rarely spread directly from person to person but the resulting diarrhea allows bacteria to spread under unsanitary conditions. Cholera is thus transmitted through ingestion of faecal matter contaminated with the bacterium. The contamination usually occurs when untreated sewage is released into waterways or into groundwater, affecting the supply, any foods washed in the water and shellfish living in the affected waterways [34]. The ability of *V. cholerae* to cause disease is engineered by a filamentous phage virus CTXΦ. Any *V. cholerae* not infected by this virus does nor cause cholera [22]. *V. cholerae* colonizes the gastrointestinal tract, where it adheres to villous absorptive cells via pili, and secretes a binary toxin, called cholera toxin (CT) which is made of two subunits A and B. The A subunit is catalytic and the B subunit is a membrane penetration unit of five subunits. The A chain catalyzes the ADP-ribosylation of key signal-coupling protein, leading to persistent activation of adenylate cyclase. The pentameric B subunit binds a ganglioside GM_1 the cell-surface receptor for this toxin and enables the A chain to enter the cytosol. The ADP ribosylation of the G_s protein blocks its capacity to hydrolyze GTP to GDP and so impairs the deactivation device. The G_s protein is locked in an active form and hence the adenylate cyclase stays persistently activated leading to a hundred fold build up of cyclic AMP which stimulate the active transport of ions and leads to very large efflux of Na^+ and water into the gut resulting in diarrhea [1, 30].

CT is encoded by the ctxAB genes on a specific filamentous bacteriophage CTXF. Transduction of this phage is dependent upon bacterial expression of the Toxin Coregulated Pilus (TCP), which is encoded by the *V. Cholerae* pathogen city island (VPI). VPI is generally only present in virulent strains and is laterally transferred. VPI was originally thought to encode a filamentous phage responsible for transfer. This theory was discredited

by a study of 46 diverse *V. cholerae* isolates, which found no evidence of VPI phage production. The generalized transduction phage CP-TI has been shown to transduce the entire VPI, which is integrated at the same chromosomal location [34]. Also, VPI has been shown to excise and circularize to produce pVPI via a specialized mechanism involving VPI-encoded recombinases. It is not known whether pVPI is involved in CP-TI transduction or if it is perhaps a component of an alternative VPI mobilization mechanism. Theoretically, any mutation on the ctxAB gene can result in the bacterium being non pathogenic but should the mutation revert to the wild type then such bacterium would become pathogenic again.

Cholera causes serious health problem in many parts of the world, especially in the developing world where sewage and water treatment systems are barely adequate. It is an epidemic with seasonal outbreaks occurring mainly during the dry season when water becomes scarce or when there is excessive rains in poor hygiene communities. Outbreaks are generally associated with contaminated food and water supplies, and poor hygiene. *V. cholerae* was first isolated as the cause of cholera by an Italian anatomist Filippo Pacini in 1854. It is a gram negative bacterium, which resembles Enterobactericae, but it does not belong to this group. Coastal cholera outbreaks typically follow zooplankton blooms and this makes cholera a typical zoonosis. If left untreated, it can cause a mortality rate ranging from 25% to 50%, where those infected often die of dehydration. Infected individuals whether symptomatic or not can carry and transmit the bacterium up to four weeks after infection, while a small number of individuals can remain carriers for several months. While a number of factors conspire to cause a cholera outbreak such as poor hygiene conditions, overcrowding and lack of safe drinking water, stopping the spread of the disease and treating patients requires more resources to be mobilized quickly in the communities affected, a challenging task to the developing world.

The history of cholera outbreak is well documented [34]. Some historical brief cases are presented here. In Bangladesh, cholera outbreaks occur twice a year with sudden outbreaks starting simultaneously in many different sites. Cholera has been endemic on the Indian sub-continent for centuries, with the Ganges River likely serving as a contamination reservoir. It spread by trade routes (land and sea) to Russia, then to Western Europe, and from Europe to North America. It is now no longer considered an issue in Europe and North America, due to filtration and chlorination of the water supply. In 1816-1826 the first cholera pandemic began in Bengal, and then spread across India by 1820. It extended as far as China and the Caspian Sea before receding. The second pandemic reached Europe between 1829-1851, London and Paris in 1832. In London, it claimed 6536 victims; in Paris, 20,000 succumbed (out of a population of 650,000 with 100,000 victims in all of France). It reached Russia, Quebec, Ontario and New York in the same year and the Pacific coast of North America by 1834. The third pandemic, which occurred between 1852 and 1860 mainly, affected Russia, with over a million deaths. In 1853-1854, London's epidemic claimed 10,738 lives and in 1854 an outbreak of cholera in Chicago took the lives of 5.5 % of the population. The Soho outbreak in London was stopped by blocking of the Broad Street pump by John Snow, who is mostly acclaimed to be the first person to diagnose the disease as associated with water. The fourth pandemic which occurred from 1863-1875 spread mostly in Europe and Africa. In London, a localized epidemic in the East claimed 5,596 lives and in 1892 8,616 people died in Hamburg, causing a major political upheaval, as control over the City was removed from the City Council which had not updated water

supplies. The sixth pandemic from 1899-1923 had little effect in Europe because of advances in public health, but Russia was badly affected again. The seventh pandemic called El Tor began in Indonesia in 1961-1970, and reached Bangladesh in 1963, India in 1964, and the USSR in 1966. From North Africa it spread into Italy by 1973. In the late 1970s there were small outbreaks in Japan and in the South Pacific. From January 1991 to September 1994, there was an outbreak in South America, apparently initiated by discharged ballast water. In Peru there were 1.04 million identified cases and almost 10,000 deaths. *Vibrio cholerae* serogroup O1 had been considered the only causative agent of epidemic cholera until the emergence of *V. cholerae* serogroup O139 Bengal in 1992 in southern India. O139 cholera rapidly spread and caused explosive epidemics throughout Bangladesh, India, and neighboring countries. *V. cholerae* O139 can disseminate widely, causing severe watery diarrhea that is clinically indistinguishable from that caused by *V. cholerae* O1 strains. Prior immunity to *V. cholerae* O1 does not provide protection against infection caused by *V. cholerae* O139. In 1993, the first outbreak caused by serogroup O139 strains occurred in Xinjiang, China, where 200 cases were reported. In 1994, outbreaks of *V. cholerae* O139 were reported in six Chinese provinces. Although this newly recognized pathogen has not caused large-scale epidemics, as seen for El Tor, regions in China where sporadic cases are reported each year have been expanding: a total of 628 cases were reported up to 1999. Unlike the epidemics seen in Bangladesh and India, where explosive epidemics and reemergence following transient disappearance were observed, O139 cholera in China appeared to have only rare outbreaks [27].

1.1. Management and Control of the Cholera Epidemic

When a cholera epidemic occurs in a community, three basic disease control measures that need to be implemented are:

(a) hygienic disposal of human faeces, use of latrines and toilets and covering them from flies,

(b) an adequate supply of clean drinking water that has been boiled or treated with disinfectants,

(c) good food hygiene, and effective food hygiene measures include: cooking food thoroughly and eating it while still hot; preventing cooked foods from being contaminated by contact with raw foods, including water and ice, contaminated surfaces and flies; avoiding raw fruits and vegetables unless they are first peeled; and washing hands after defecation and especially before handling food or drinking water is equally important.

It has been demonstrated that treatment of a community with antibiotics has no effect on the spread of cholera, nor does restricting travel and trade between countries or between different regions of a country. Mass chemoprophylaxis with antibiotics has never succeeded in limiting the spread of cholera, this is because:

(a) infection spreads rapidly, before mass treatment can be organized,

(b) the effects of the antibiotic only last for $1-2$ days, after which time the person is once again fully susceptible to infection,

(c) the entire population at risk would need to be treated simultaneously. However, even such simultaneous treatment does not prevent reinfection from environmental sources such as contaminated water, and

(d) it is difficult to persuade all members of a community to take medication, especially when most of them are in good health.

WHO discourages mass chemoprophylaxis as a mechanism to control cholera [33]. Since cholera is spread from place to place largely by infected persons, most of whom have no signs of illness, the so-called "carriers", there is no practical way of identifying all carriers and it is not feasible to prevent the movement of people. Furthermore, travel restrictions are very disruptive and often have adverse economic consequences for normal trade and tourism. In 1973, WHO deleted from the International Health Regulations the requirement for presentation of a cholera vaccination certificate and currently, no country requires proof of cholera vaccination as a condition of entry [33]. It may be appropriate, however, to discourage large gatherings for events such as funerals, fairs and markets when cholera threatens an area. Infection can spread rapidly during such events through contaminated food or water and is then further disseminated when the infected person returns home. If such events do take place, it is essential to institute safe disposal of excreta, safe practices for food preparation and to ensure a safe supply of drinking water.

1.2. Signs and Symptoms of Cholera

Infection with cholera has a short incubation period, from less than one day to five days and produces an enterotoxin that causes a copious, painless, watery diarhhoea that can, in a matter of a few hours, result in profound, rapidly progressive dehydration and death if treatment is not initiated promptly. Vomiting also occurs in most patients. In severe cases, stool volume can exceed $250ml/kg$ body weight in the first 24 hours. If fluids and electrolytes are not replaced, hypovolaemic shock and death ensue. Muscle cramps due to electrolyte disturbances are common. The stool has a characteristic appearance; a nonbilious, grey, slightly cloudy fluid with flecks of mucous, no blood and a sweet, inoffensive odour. It has been called "rice-water" stool because of its resemblance to the water in which rice has been washed. Clinical symptoms of cholera parallel those of volume depletion (see [26]):

(a) at 3-5 % loss of normal body weight and thirst develops,

(b) at 5-8 % loss of normal body weight, postural hypotension, weakness, tachycardia and decreased skin turgor occur, and

(c) at 10 % or more loss of normal body weight oliguria, weak or absent pulses, sunken eyes (and in infants, sunken fontanelles), wrinkled skin, somnolence and coma can occur.

Complications of cholera occur from the effects of volume and electrolyte depletion and may include renal failure, coma and death. Therefore, if the patient is adequately

treated with fluid and salt, the complications can be averted and the disease process is self-limiting, resolving in a few days. However, since fluid losses occur extremely rapidly, fluid replacement needs to be aggressive and be initiated early. It is recommended to start fluid replacement while taking the patient to the nearest clinic, doctor or hospital.

1.3. Use of Mathematical Models

Mathematical models are powerful tools for the development of epidemiological studies [3]. They can synthesize the current empirical knowledge about the disease into a coherent mechanistic framework and often provide answers to the following questions: what demographic, environmental and sociological factors drive disease dynamics? The purpose of the mathematical modeling is to:

(a) understand what factors govern outbreaks of infectious diseases,

(b) take facts about the disease as inputs and to make predictions about the number of infected and uninfected people over time as outputs,

(c) develop understanding of the interplay between the variables that determine the course of, for example, the infection within an individual and the variables that control the pattern of infections within the communities of people,

(d) to facilitate the indirect assessment of, for example, certain epidemiological parameters,

(e) to clarify what data are required to predict future trends,

(f) to give an insight into what happens in the real world,

(g) help identify the groups of the population at highest risk,

(h) help in planning of intervention programs, and

(i) help governments, public-health agencies and health care providers to determine how best to allocate scarce resources for say cholera treatment and prevention.

A model is a set of functions that describe the relationships between different variables. Types of variables are, decision variables (independent variables), input variables, state variables, exogenous variables (parameters or constants), random variables, and output variables. Mathematical models can be classified as:

(i) Deterministic or stochastic: a deterministic model is based on the premise that if complete information on the system is known at a specific time, then its future behaviour can be predicted exactly whereas a stochastic model incorporates probabilistic behaviour, that is, future behaviour is not completely determined but that there are a number of possible results and each has a certain probability of occurring.

(ii) Dynamic or static: dynamic models are typically represented by differential or difference equations, whereas static models do not account for time.

(ii) Linear or nonlinear: a linear model is one in which the operators in the model are linear. If not linear it is considered as nonlinear.

In the modeling of infectious diseases, deterministic models have the advantage that they can be more complex than stochastic models but still possible to analyze, at least when numerical solutions are adequate yet for a stochastic epidemic model to be mathematically manageable it has to be quite simple and thus not entirely realistic. When analysis of stochastic models is possible there are several reasons to suggest that stochastic models are to be preferred. Firstly, the most natural way to describe the spread of disease is stochastic; one defines the probability of disease transmission between two individuals, rather than stating with certainty whether or not transmission will occur. Deterministic models describe the spread of disease under the mass action law, thus relying on the law of large numbers [12]. Secondly, there are phenomena which are genuinely stochastic and do not satisfy the law of large numbers. Thirdly, knowledge about uncertainty in estimates requires stochastic models, and an estimate is not much of use without some knowledge of its uncertainty. Lastly, stochastic models also provide more information, for example, means, variances and covariances. Stochastic models have the disadvantage that, no matter how much one knows about the system at a given time, it is impossible to determine with absolute certainty the nature of the system for future times. Models must be developed based on detailed understanding of the components of the disease dynamics. Predictions and recommendations for control stem from the mathematical and numerical analysis of models. Being able to make predictions about disease dynamics is really helpful for public health. If we know there will be an outbreak, we can prepare for it and alternatively, if we have a reliable model, we can study how to prevent an outbreak and save lives by changing the factors we can control using public health means. Some of the factors include education, quarantine regulations and health treatment strategies.

Mathematical models go back to 1760 when Daniel Bernoulli used mathematical methods to study techniques of protection against smallpox [4]. Further concepts on mathematical modeling of epidemics were developed by Ronald Ross [28] and his students Kermack and Mackendrick [18–20, 23]. The 1927 *SIR* (Susceptible-Infectives-Removed) model in [18] used to understand the cholera epidemic was and is still famous among researchers. Here, the form of the mathematical model is a system of ordinary differential equations which track the levels of each of the susceptible, exposed, infective and the pathogen population. The model is a Susceptible-Exposed-Infected model (for the human population) coupled to an aquatic population of *V.cholerae*. The objective of this chapter is to carry out detailed qualitative mathematical analysis of a single-season deterministic cholera model with carriers and assessing the effects of treatments of cholera sufferers using comprehensive analytical and numerical techniques. The role of the aquatic reservoir on the persistence of the endemic cholera as well as conditions for the development of epidemic and endemic cholera will be established. An epidemic is a disease that affects many individuals in a population and is generally defined as a widespread disease. It can be endemic or non-endemic depending on the time period it occurs. An epidemic is endemic if it persists in a population in the long term without reintroduction of the disease from outside, during which there is a renewal of susceptibles by birth or recovery from temporary or permanent immunity and is non-endemic if it occurs for a short period of time and it is called a pandemic if it is widely distributed in space. There has not been much studies on cholera

models, at least from the mathematical world. Nevertheless, this disease demands a high level of interest and contribution from both the epidemiology as well as the mathematics communities in order to combine efforts in determining conditions under which the disease will die out. Since cholera is mainly a disease related to hygiene, awareness is therefore paramount to the spread or reduction of an outbreak. In this regard, the contribution of each individual to the population of *V.cholerae* is a bio-social parameter which cannot be easily measured, but if regarded as the awareness factor, heuristic values can be assigned to it. Thus, the model includes parameters related to the behavioral pattern of individuals. In the last decades, attention to cholera epidemiology increased as cholera epidemics became a worldwide health problem. Detailed investigation of *V.cholerae* interactions with its host and with other organisms in the environment suggests that cholera dynamics is much more complex than previously thought.

2. Basic Model

The basic cholera model divides the human population into three classes: $S(t)$ denoting the population density of susceptible individuals, this compartment contains individuals who are not infected with the bacterium, $E(t)$ denoting the population density of exposed individuals, this compartment contains individuals who are infected with the bacterium but are asymptomatic and not yet suffering from the disease (*referred to as carriers in this chapter*), $I(t)$ denoting the population density of infected individuals, this class contains individuals who are infected with the bacterium and are symptomatic and suffering from the disease (*referred to as sufferers in this chapter*), and the pathogen population, i.e., the *V.cholerae pool* is denoted by $P(t)$. According to [4], a major complication of many diseases is the existence of the so-called "carriers" that are individuals who although apparently healthy themselves are already infected and are capable of transmitting the infection to others. In fact, they are not themselves usually recognized as actual cases.

It is assumed that, at any moment in time, new individuals enter the susceptible human population at a rate $\eta(1 - \frac{S(t)}{K})$ proportional to individuals in that class where $\eta > 0$ is the constant intrinsic growth and $K > 0$ is the environmental carrying capacity of humans. Susceptible individuals, acquire infection at a time dependent rate $\frac{aP(t)}{H+\epsilon P(t)}$, where $a > 0$ is the maximal rate of exposure, H is the half saturation constant, and ϵ is the limitation of the growth velocity of *V.cholerae* with the increase of cases (exposed and sufferers) [16]. In the absence of the pathogen, the human population follows a logistic growth, while the functional response of the susceptibles to the pathogen given by $\frac{P(t)S(t)}{H+\epsilon P(t)}$ is of the modified Holling's type-II response (also known as the Michaelis-Menten function when $\epsilon = 1$), and the response refers to the change in density of the susceptibles per unit time per pathogen as the susceptible population density changes. Upon becoming infected with the bacterium, a proportion p of the infected individuals move into the class of carriers, $E(t)$ and the complimentary proportion $(1 - p)$ move into class $I(t)$ of infected individuals. Carriers can eventually suffer from cholera and enter the class $I(t)$ of individuals suffering from the disease at a rate $\phi > 0$. It is assumed that carriers and infectives can recover naturally at constant rates $\gamma_1 > 0$ and $\gamma_2 > 0$ respectively and become susceptible again. The natural death rate of humans in each class is assumed to be $\mu_H > 0$ and infected individuals have

an additional disease-induced (cholera-induced) mortality rate, $\delta > 0$. The growth rate of *V.cholerae* is assumed to be a constant $c > 0$ and proportional to $P(t)$. Susceptibles, infected and exposed individuals contribute to pathogen population growth at rates $\sigma_1, \sigma_2, \sigma_3$ respectively with $\sigma_1 < \sigma_2 < \sigma_3$ suggesting that carriers contribute more to the growth of the pathogen population than other classes. The natural death rate of the pathogen is assumed to be $\mu_P > 0$. Transmission of infection is assumed to be only through the environment. The model does not account for interactions between susceptible and exposed, susceptible and infective individuals as the etiological agent infects susceptibles through a third party (namely, contaminated food or water). The model structure, which greatly improves on the work of Codeco [9], is shown in Figure 1. In Figure 1, the dashed arrows indicate the indirect contribution of the human population in the growth of the pathogen.

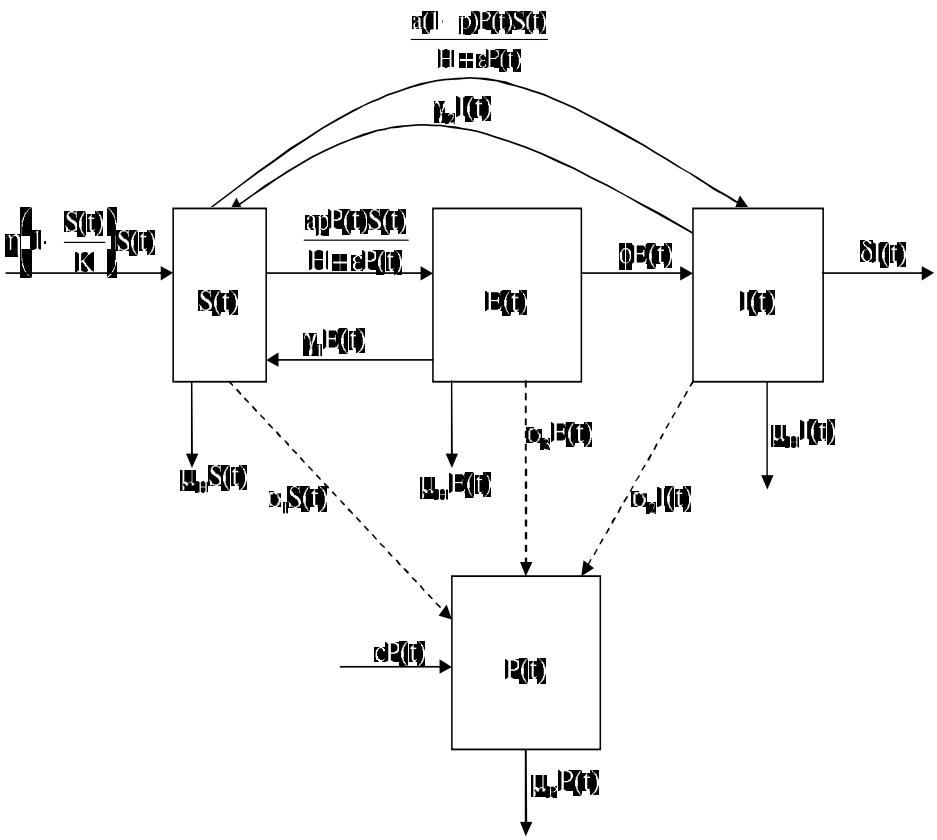

Figure 1. Flow diagram of the basic cholera model.

Putting the above formulations and assumptions together gives the following system of

differential equations (where a dot represents differentiation with respect to time),

$$\begin{aligned}
\dot{S(t)} &= \eta(1-\tfrac{S(t)}{K})S(t) + \gamma_1 E(t) + \gamma_2 I(t) - \tfrac{aP(t)S(t)}{H+\epsilon P(t)} - \mu_H S(t),\\
\dot{E(t)} &= ap\tfrac{P(t)S(t)}{H+\epsilon P(t)} - (\mu_H + \phi + \gamma_1)E(t),\\
\dot{I(t)} &= a(1-p)\tfrac{P(t)S(t)}{H+\epsilon P(t)} + \phi E(t) - (\mu_H + \delta + \gamma_2)I(t),\\
\dot{P(t)} &= cP(t) + \sigma_1 S(t) + \sigma_2 I(t) + \sigma_3 E(t) - \mu_P P(t).
\end{aligned} \tag{1}$$

The initial condition for system (1) is given by,

$$\begin{cases}
S(\theta) = \varphi_1(\theta), E(\theta) = \varphi_2(\theta),\\
I(\theta) = \varphi_3(\theta), P(\theta) = \varphi_4(\theta),\\
\varphi_i(\theta) \geq 0, \varphi_i(0) > 0, i = 1,2,3,4.
\end{cases} \tag{2}$$

We define,

$$\mathbf{\Omega} = \Big\{(S,E,I,P) \in \mathbb{R}^4 | S \geq 0, E \geq 0, I \geq 0, P \geq 0\Big\}, \tag{3}$$

to be the epidemiologically and mathematically feasible region.

2.1. Positivity of Solutions

Model system (1) describes the dynamics of a human population and a pathogen population, therefore it is very important to prove that the susceptibles, exposed, infected and pathogen populations are positive for all time, thus in this section we prove solutions of model system (1) with positive initial data will remain positive for all $t > 0$.

Theorem 1. *Let the initial data be $S(t) \geq 0, E(t) \geq 0, I(t) \geq 0, P(t) \geq 0$. Then, solutions of $S(t)$, $E(t)$, $I(t)$, $P(t)$ of system (1) are positive for all $t \geq 0$.*

Proof. The plane $S = 0$ of $\mathbb{R}^4$ is invariant for model system (1). Considering the variable $P(t)$ in $[0,T]$, then for $t \in [0,T]$ the fourth equation of model system (1) can be written as,

$$\dot{P(t)} \geq -(\mu_P - c)P(t), \forall t \in [0,T]. \tag{4}$$

By direct integration of (4) we obtain

$$P(t) \geq P(0)e^{-(\mu_P - c)t} \geq 0, \tag{5}$$

as $t \in [0,T]$ and as long as $\mu_P - c < +\infty$. For variable $I(t)$, from model system (1) equation three, we have

$$\dot{I(t)} \geq -(\mu_H + \delta + \gamma_2)I(t). \tag{6}$$

This gives,

$$I(t) \geq I(0)e^{-(\mu_H + \delta + \gamma_2)t} \geq 0, \tag{7}$$

also for variable $E(t)$, from model system (1), we obtain

$$\dot{E(t)} \geq -(\mu_H + \phi + \gamma_1)E(t), \tag{8}$$

and integrating (8) gives,

$$E(t) \geq E(0)e^{-(\mu_H+\phi+\gamma_1)t} \geq 0. \tag{9}$$

Thus, the non-negativity of $S(t)$, $P(t)$ implies that of $E(t)$ and $I(t)$ are positive if $t \geq 0$. This shows that for initial conditions (2) the corresponding solution of (1) is such that $\min\{S(t), E(t), I(t), P(t)\} \geq 0$ in its interval of existence. □

2.2. Existence of Solutions

Theorem 2. *A solution of model system (1) is feasible.*

Proof. It is necessary to show that system (1) is dissipative, that is, all feasible solutions are uniformly bounded in $\Omega \subset \mathbb{R}^4$. Let $\left\{(S(t), E(t), I(t), P(t)) \in \mathbb{R}^4\right\}$ be any solution of system (1) with non-negative initial conditions. Since

$$\dot{S(t)} \leq \eta\Big(1 - \frac{S(t)}{K}\Big)S(t) - \mu_H S(t), \tag{10}$$

then, $\underbrace{\limsup S(t)}_{t\longrightarrow\infty} \leq M$, where $M = \max(S_0, K)$. Let $W(t) = S(t)+E(t)+I(t)+P(t)$, then

$$\begin{aligned}
\dot{W(t)} &= \eta\Big(1 - \frac{S(t)}{K}\Big)S(t) + \gamma_1 E(t) + \gamma_2 I(t) - \frac{aP(t)S(t)}{H + \epsilon P(t)} - \mu_H S(t) + pa\frac{P(t)S(t)}{H + \epsilon P(t)} \\
&\quad -(\mu_H + \phi + \gamma_1)E(t) + a(1-p)\frac{P(t)S(t)}{H + \epsilon P(t)} + \phi E(t) \\
&\quad -(\mu_H + \delta + \gamma_2)I(t) + cP(t) + \sigma_1 S(t) + \sigma_2 I(t) + \sigma_3 E(t) - \mu_P P(t), \\
&= \Big(\eta\Big(1 - \frac{S(t)}{K}\Big) + \sigma_1 - \mu_H\Big)S(t) + (\sigma_3 - \mu_H)E(t) + (\sigma_2 - \delta - \mu_H)I(t) + (c - \mu_P)P(t), \\
&\leq (\eta + \sigma_1 - \mu_H + 1)S(t) - S(t) - (\mu_H - \sigma_3)E(t) - (\mu_H + \delta - \sigma_2)I(t) - (\mu_P - c)P(t), \\
&\leq (\eta + \sigma_1 - \mu_H + 1)M - mW(t),
\end{aligned} \tag{11}$$

where $m = \min\{(\mu_H - \sigma_3, \mu_H + \delta - \sigma_2, \mu_P - c, 1)\}$. Thus,

$$\dot{W(t)} + mW(t) \leq (\eta + \sigma_1 - \mu_H + 1)M. \tag{12}$$

Equation (12) is a first order linear differential inequality [5], with the solution given by

$$0 < W(S, E, I, P) \leq \frac{(\eta + \sigma_1 - \mu_H + 1)M}{m} + W(S_0, E_0, I_0, P_0)e^{-mt} \tag{13}$$

as t$\longrightarrow \infty$, we have

$$0 < W(S, E, I, P) \leq \frac{(\eta + \sigma_1 - \mu_H + 1)M}{m}. \tag{14}$$

Therefore, all solutions of the system (1) enter the feasible region,

$$\Omega = \Big\{(S(t), E(t), I(t), P(t)) \in \mathbb{R}^4_+ : W \leq \frac{(\eta + \sigma_1 - \mu_H + 1)M}{m} + \varsigma, \forall \varsigma > 0\Big\}. \tag{15}$$

This completes the proof of the theorem. □

We illustrate the phase plane portraits of model system (1) in Figures 2 (a) and 2 (b). Figures 2 (a) and 2 (b) illustrate that solutions of model system (1) starting in Ω will stay in Ω and are positively invariant and are unique thus are mathematically and epidemiologically well posed.

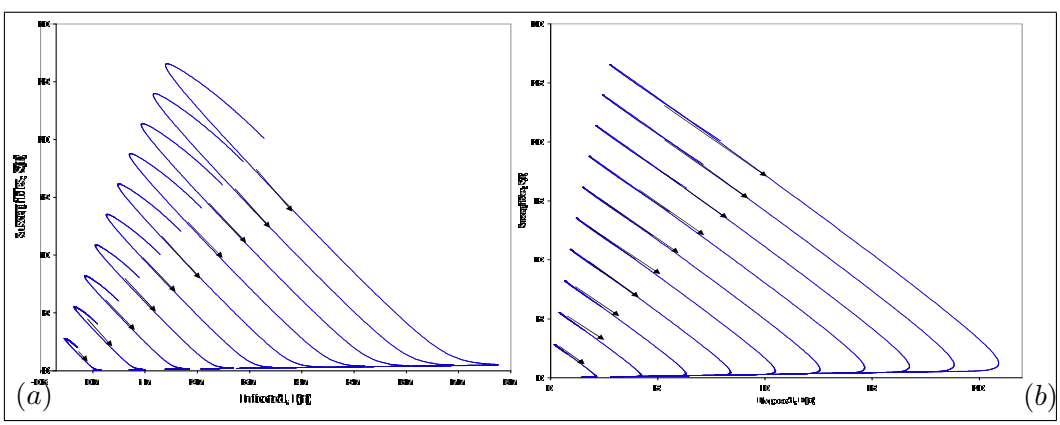

Figure 2. (a) A typical phase plane portrait for the cholera model in the SI phase plane, (b) A typical phase plane portrait for the cholera model in the SE phase plane, for $\eta = 0.0001, K = 12878000, \gamma_1 = 0.1, \gamma_2 = 0.05, a = 0.2143, H = 10^9, \epsilon = 0.5, \mu_H = 0.0000675, p = 0.8, \phi = 0.005, \delta = 0.015, c = 0.73, \sigma_1 = 10, \sigma_2 = 100, \sigma_3 = 200, \mu_P = 0.33$ with varying initial conditions. We considered general cases for illustration.

2.3. Equilibrium States and Stability

Model system (1) admits three steady states, that are

(a) the trivial equilibrium

$$\mathcal{E}_0 = (S^0, E^0, I^0, P^0) = (0, 0, 0, 0), \tag{16}$$

(b) the disease-free equilibrium

$$\mathcal{E}_1 = (S^1, E^1, I^1, P^1) = \Big(\Big(1 - \frac{\mu_H}{\eta}\Big)K, 0, 0, 0\Big), \text{ and} \tag{17}$$

this equilibrium exists when $\eta > \mu_H$ suggesting that the intrinsic human population growth rate should be greater than the human population death rate.

(c) the endemic equilibrium

$$\mathcal{E}_2 = (S^e, E^e, I^e, P^e), \tag{18}$$

where,

$$\begin{aligned} S^e &= \frac{K(\eta-\mu_H)+\sqrt{K^2(\eta-\mu_H)^2-\frac{4aK\eta\lambda_P^e(\delta\phi+(1-p)\gamma_1(\delta+\mu_H)+\mu_H(\delta+\phi+p\gamma_2+\mu_H))}{(\phi+\gamma_1+\mu_H)(\delta+\gamma_2+\mu_H)}}}{2\eta}, \\ E^e &= \frac{ap\lambda_p^e}{\phi+\gamma_1+\mu_H}, \\ I^e &= \frac{a\lambda_p^e(\phi+(1-p)\gamma_1+(1-p)\mu_H)}{(\phi+\gamma_1+\mu_H)(\delta+\gamma_2+\mu_H)} \text{ and}, \\ P^e &= \frac{1}{c-\mu_P}\Big[\sigma_3 E^e+\sigma_2 I^e-\sigma_1 S^e\Big], \end{aligned} \tag{19}$$

with $\lambda_P^e = \dfrac{P^e S^e}{H+\epsilon P^e}$. This equilibrium exists when $c > \mu_P$ suggesting that the intrinsic *V.cholerae* growth rate should be greater than the death rate.

It is important to note that the cholera model (1) is of varying population sizes (human and pathogen populations) and consequently, the trivial (or extinction) equilibrium in general is not feasible. Even though this equilibrium is not biologically relevant, we shall analyse its stability whenever it exists. The asymptotic dynamics of the steady states is determined by the following Jacobian matrix of model system (1),

$$\mathcal{J} = \begin{pmatrix} \eta(1-\frac{2S(t)}{K})-\frac{aP(t)}{H+\epsilon P(t)}-\mu_H & \gamma_1 & \gamma_2 & \frac{-aHS(t)}{(H+\epsilon P(t))^2} \\ \frac{apP(t)}{H+\epsilon P(t)} & -(\mu_H+\phi+\gamma_1) & 0 & \frac{apHS(t)}{(H+\epsilon P(t))^2} \\ \frac{a(1-p)P(t)}{H+\epsilon P(t)} & \phi & -(\mu_H+\delta+\gamma_2) & \frac{a(1-p)HS(t)}{(H+\epsilon P(t))^2} \\ \sigma_1 & \sigma_3 & \sigma_2 & c-\mu_P \end{pmatrix}. \tag{20}$$

2.3.1. Trivial Equilibrium and Stability

Theorem 3. *The trivial equilibrium $\mathcal{E}_0$ if it exists is a saddle point.*

Proof. Evaluating the Jacobian matrix (20) at the trivial equilibrium point $\mathcal{E}_0$ gives,

$$\mathcal{J}_{\mathcal{E}_0} = \begin{pmatrix} \eta-\mu_H & \gamma_1 & \gamma_2 & 0 \\ 0 & -(\mu_H+\phi+\gamma_1) & 0 & 0 \\ 0 & \phi & -(\mu_H+\delta+\gamma_2) & 0 \\ \sigma_1 & \sigma_3 & \sigma_2 & c-\mu_P \end{pmatrix}. \tag{21}$$

The resulting characteristic equation from (21) is,

$$((\eta-\mu_H)-\lambda)(-(\mu_H+\phi+\gamma_1)-\lambda)(-(\mu_H+\delta+\gamma_2)-\lambda)((c-\mu_P)-\lambda)=0. \tag{22}$$

The eigenvalues are $\lambda_1 = c - \mu_P, \lambda_2 = -(\mu_H + \delta + \gamma_2), \lambda_3 = -(\mu_H + \phi + \gamma_1)$ and $\lambda_4 = \eta - \mu_H$. Two of them are positive, while the other two are negative, thus $\mathcal{E}_0$ is a saddle point. Consequently, the determinant $\triangle$, say, of the matrix in (21) is negative [25]. This can be shown by a little re-arrangement as follows:

$$\triangle = (\mu_H + \phi + \gamma_1)(\mu_H + \delta + \gamma_2)\{\eta c - (\eta\mu_P + c\mu_H + \sigma\gamma_2)\}. \tag{23}$$

Obviously, $\{\eta c - (\eta\mu_P + c\mu_H + \sigma\gamma_2)\} < 0$ and $\mathcal{E}_0$ will be stable iff the intrinsic growth rates c and η are both negative. □

2.3.2. Disease-Free Equilibrium and Stability

The most important equilibrium state from the biomedical point of view is the disease-free equilibrium, $\mathcal{E}_1$. The linear stability of the disease-free equilibrium $\mathcal{E}_1$ is governed by the basic reproductive number $\mathcal{R}_0$ (see [2, 6, 8, 14]). Mathematically, $\mathcal{R}_0$ is defined as the spectral radius [10, 32] and it is the threshold quantity for disease control which defines the number of new infectives generated by a single infected individual in a completely susceptible population [2]. The basic reproductive number $\mathcal{R}_0$ measures the power of a disease to invade a population under conditions that facilitate maximal growth. The stability of this equilibrium will be investigated using the *next generation operator* [10, 32]. Using the notation in [32] on model system (1), the matrices $\mathcal{F}$ and $\mathcal{V}$, for the new infection terms and the remaining transfer terms are respectively given by,

$$\mathcal{F} = \begin{pmatrix} 0 & 0 & 0 & 0 \\ 0 & 0 & 0 & \frac{apK(1-\frac{\mu_H}{\eta})}{H} \\ 0 & 0 & 0 & \frac{a(1-p)K(1-\frac{\mu_H}{\eta})}{H} \\ 0 & 0 & 0 & 0 \end{pmatrix}, \text{ and} \tag{24}$$

$$\mathcal{V} = \begin{pmatrix} -\eta(1-\frac{\mu_H}{\eta}) & \gamma_1 & \gamma_2 & -\frac{aK(1-\frac{\mu_H}{\eta})}{H} \\ 0 & -(\mu_H + \phi + \gamma_1) & 0 & 0 \\ 0 & \phi & -(\mu_H + \delta + \gamma_2) & 0 \\ \sigma_1 & \sigma_3 & \sigma_2 & c - \mu_P \end{pmatrix}. \tag{25}$$

It follows that the *basic reproduction number* denoted by $\mathcal{R}_0$ is,

$$\begin{aligned} \mathcal{R}_0 &= \rho(\mathcal{F}\mathcal{V}^{-1}) \\ &= \frac{(aK(\gamma_1((\gamma_2+p(\delta+\mu_H))\sigma_1+(1-p)(\eta-\mu_H)\sigma_2)+\gamma_2((\phi+(1-p)\mu_H)\sigma_1+p(\eta-\mu_H)\sigma_3)+(\eta-\mu_H)((\phi+(1-p)\mu_H)\sigma_2+p(\delta+\mu_H)\sigma_3)))}{((\phi+\gamma_1+\mu_H)(\delta+\gamma_2+\mu_H)(-cH\eta+H\eta\mu_P+aK\sigma_1))}. \end{aligned} \tag{26}$$

Using Theorem 2 in [32], the following result is established.

Lemma 1. *The disease-free equilibrium of model system (1) is locally-asymptotically stable if* $\mathcal{R}_0 < 1$ *and unstable if* $\mathcal{R}_0 > 1$.

Thus, Lemma 1 implies that cholera can be eliminated from the community (when $\mathcal{R}_0 < 1$) if the initial sizes of the sub-populations of the model are in the basin of attraction of the disease-free equilibrium $\mathcal{E}_1$.

2.4. Effects of Cholera Carriers

The partial derivative of the basic reproduction number with respect to the proportion of carriers p is

$$\frac{\partial \mathcal{R}_0}{\partial p} = \frac{(aK(\gamma_1((\delta+\mu_H))\sigma_1+(-\eta+\mu_H)\sigma_2)+(\eta-\mu_H)(-\mu_h\sigma_2+(\delta+\mu_H)\sigma_3)+\gamma_2(\eta\sigma_3-\mu_H(\sigma_1+\sigma_3)))}{((\phi+\gamma_1+\mu_H)(\delta+\gamma_2+\mu_H)(-cH\eta+H\eta\mu_P+aK\sigma_1))} > 0. \tag{27}$$

From equation (27) we have $\frac{\partial \mathcal{R}_0}{\partial p} > 0$ suggesting that increase in the number of cholera carriers speeds up the spread of the disease. If there are no carriers ($p = \sigma_3 = E(t) = 0$), the reproductive number becomes,

$$\mathcal{R}_0^* = \frac{aK(\gamma_2\sigma_1+\sigma_2(\eta-\mu_H))}{(\delta+\gamma_2+\mu_H)(H\eta(\mu_P-c)+aK\sigma_1)}. \tag{28}$$

Expression (26) for $\mathcal{R}_0$ can be written as

$$\mathcal{R}_0 = \frac{aK\Big[\gamma_1((\gamma_2+p(\sigma+\mu_H))\sigma_1+(1-p)(\eta-\mu_H)\sigma_2)+p\sigma_3(\eta-\mu_H)(1+\sigma+\mu_H)\Big]}{(\phi+\gamma_1+\mu_H)(\sigma+\gamma_2+\mu_H)(\eta H(\mu_P-c)+aK\sigma_1)} \tag{29}$$

$$+ \frac{(\phi+(1-p)\mu_H)}{(\phi+\gamma_1+\mu_H)}\mathcal{R}_0^* \tag{30}$$

which can be written as

$$\mathcal{R}_0 = G_1 + G_2\mathcal{R}_0^*. \tag{31}$$

Here,

$$G_1 = \frac{aK\Big[\gamma_1((\gamma_2+p(\sigma+\mu_H))\sigma_1+(1-p)(\eta-\mu_H)\sigma_2)+p\sigma_3(\eta-\mu_H)(1+\sigma+\mu_H)\Big]}{(\phi+\gamma_1+\mu_H)(\sigma+\gamma_2+\mu_H)(\eta H(\mu_P-c)+aK\sigma_1)}$$

$$G_2 = \frac{(\phi+(1-p)\mu_H)}{(\phi+\gamma_1+\mu_H)}. \tag{32}$$

Equation (31) gives $\mathcal{R}_0^* = \frac{\mathcal{R}_0-G_1}{G_2}$ which implies that $\mathcal{R}_0^* < \mathcal{R}_0 \ \forall \ (G_1, G_2) > 0$. Figure 3 illustrates the relationship and behaviour of $\mathcal{R}_0$ and $\mathcal{R}_0^*$ for increasing σ_2 (number of bacteria shed into the environment by one cholera sufferer per day) using parameter values in Table 1. Figure 3 suggest that the presence of carriers in a community increases the number of cholera secondary infections.

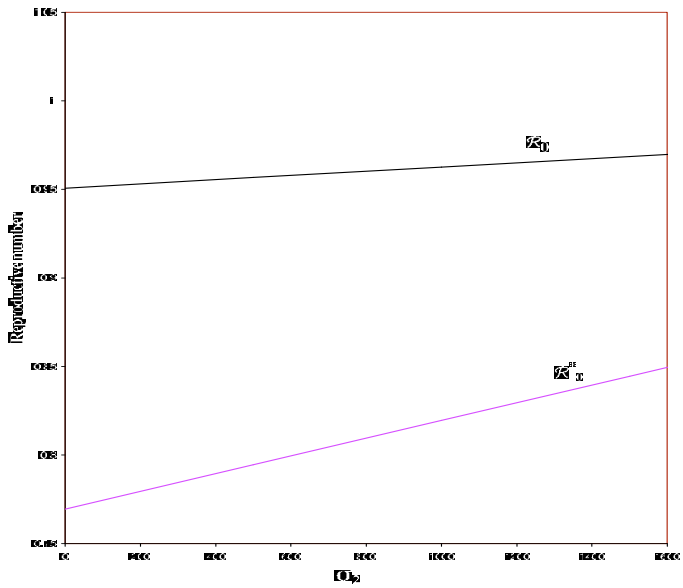

Figure 3. Trend $\mathcal{R}_0$ and $\mathcal{R}_0^*$ of the reproductive numbers for increasing σ_2 with other parameter values as given in Table 1.

Setting the reproductive number $\mathcal{R}_0 = 1$ and solving for p gives the critical threshold of the proportion of individuals becoming carriers below which cholera can be eradicated,

$$p^c = \frac{(\phi+\gamma_1+\mu_H)[(\delta+\gamma_2+\mu_H)(-cH\eta+H\eta\mu_P+aK\sigma_1)-aK(\gamma_2\sigma_1+(\eta-\mu_H)\sigma_2)]}{aK[(\gamma_1(\delta+\mu_H)-\gamma_2\mu_H)\sigma_1-(\eta-\mu_H)(\gamma_1+\mu_H)\sigma_2+(\eta-\mu_H)(\delta+\gamma_2+\mu_H)\sigma_3]}. \tag{33}$$

Theorem 4. *The disease-free equilibrium $\mathcal{E}_1$ of model system (1) is globally asymptotically stable if it is feasible.*

Proof. Let $S - S^1 > 0$, $E = E^1 = 0$, $I = I^1 = 0$, $P = P^1 = 0$. Consider an average Lyapunov function of the form,

$$L(S,E,I,P) = S^{\nu_1}E^{\nu_2}I^{\nu_3}P^{\nu_4}. \tag{34}$$

with $\nu_i > 0$, $i = 1,2,3,4$.

$$
\begin{aligned}
\tfrac{L'}{L} &= \Psi(S,E,I,P),\\
&= \frac{\nu_1 S^{\nu_1-1}E^{\nu_2}I^{\nu_3}P^{\nu_4}S' + \nu_2 E^{\nu_2-1}S^{\nu_1}I^{\nu_3}P^{\nu_4}E' + \nu_3 I^{\nu_3-1}S^{\nu_1}E^{\nu_2}P^{\nu_4}I' + \nu_4 P^{\nu_4-1}S^{\nu_1}E^{\nu_2}I^{\nu_3}P'}{S^{\nu_1}E^{\nu_2}I^{\nu_3}P^{\nu_4}},\\
&= \nu_1\frac{S'}{S} + \nu_2\frac{E'}{E} + \nu_3\frac{I'}{I} + \nu_4\frac{P'}{P},\\
&= \nu_1\left[\eta(1-\frac{S}{K}) + \gamma_1\frac{E}{S} + \gamma_2\frac{I}{S} - \frac{aP}{H+\epsilon P} - \mu_H\right] + \nu_2\left[pa\frac{PS}{E(H+\epsilon P)} - (\mu_H+\phi+\gamma_1)\right]\\
&+\nu_3\left[a(1-p)\frac{PS}{I(H+\epsilon P)} + \phi\frac{E}{I} - (\mu_H+\delta+\gamma_2)\right] + \nu_4\left[c + \sigma_1\frac{S}{P} + \sigma_2\frac{I}{P} + \sigma_3\frac{E}{P} - \mu_P\right],\\
&\leq -\nu_1\left[\eta\left(\frac{S}{K}-1\right) + \mu_H\right] - \nu_2[(\mu_H+\phi+\gamma_1)] - \nu_3[(\mu_H+\delta+\gamma_2)] - \nu_4[\mu_P - c].
\end{aligned}
\tag{35}
$$

The expression $-\nu_1[\eta(\frac{S}{K}-1)+\mu_H]$ in equation (35) is negative only if $S > K(1-\frac{\mu_H}{\eta})$, $S - S^1 > 0$ and $E - E^1 = I - I^1 = P - P^1 = 0$. Since all model parameters are nonnegative from equation (35), $L' \leq 0$ for $S - S^1 > 0$, with inequality holding only at $\mathcal{E}_1 = ((1-\frac{\mu_H}{\eta})K, 0, 0, 0)$. In this case the lyapunov function satisfies $L' \leq 0$ and hence the disease-free state is globally asymptotically stable for $S - S^1 > 0$. If S> 0, then $(S,E,I,P) \longrightarrow (S_\infty, 0, 0, 0)$ for $E = I = P = 0$. □

From the epidemiological point of view, this implies that the disease can be eradicated from the population (when $\mathcal{R}_0 < 1$) if the initial sizes of the subpopulations are in the basin of attraction of $\mathcal{E}_1$.

2.4.1. Endemic Equilibrium and Stability

Expressing the endemic equilibrium for model system (1) in terms of the reproductive number $\mathcal{R}_0$ gives

$$
\begin{aligned}
S^e &= \frac{K(\eta-\mu_H) + \frac{(\mathcal{R}_0-1)A_2}{aKA_1-(\phi+\gamma_1+\mu_H)(\delta+\gamma_2+\mu_H)A_2}\sqrt{A_3}}{2\eta},\\
E^e &= \frac{ap\lambda_P(\mathcal{R}_0-1)(\delta+\gamma_2+\mu_H)A_2}{aKA_1-(\phi+\gamma_1+\mu_H)(\delta+\gamma_2+\mu_H)A_2},\\
I^e &= \frac{a\lambda_P(\phi+(1-p)\gamma_1+(1-p)\mu_H)(\mathcal{R}_0-1)A_2}{aKA_1-(\phi+\gamma_1+\mu_H)(\delta+\gamma_2+\mu_H)A_2} \text{ and,}\\
P^e &= \tfrac{1}{c-\mu_P}[\sigma_3E^e + \sigma_2I^e - \sigma_1S^e] \text{ for } c > \mu_P,
\end{aligned}
\tag{36}
$$

here,

$$\begin{aligned}
A_1 &= \gamma_1((\gamma_2 + p(\delta+\mu_H))\sigma_1 + (1-p)(\eta-\mu_H)\sigma_2) + \gamma_2((\phi+(1-p)\mu_H)\sigma_1 \\
&\quad + p(\eta-\mu_H)\sigma_3 + (\eta-\mu_H)((\phi+(1-p)\mu_H)\sigma_2 + p(\delta+\mu_H)\sigma_3)), \\
A_2 &= (-cH\eta + H\eta\mu_P + aK\sigma_1), \text{ and} \\
A_3 &= K(\phi+\gamma_1+\mu_H)(\delta+\gamma_2+\mu_H)[K(\eta-\mu_H)^2 - 4a\eta\lambda_P(\delta\phi + (1-p)\gamma_1(\delta+\mu_H) \\
&\quad + \mu_H(\delta+\phi+p\gamma_2+\mu_H))].
\end{aligned} \tag{37}$$

We note that S^e, E^e and I^e are always positive if $A_1 > 0$, $A_2 > 0$ and the denominator,

$$aKA_1 - (\phi+\gamma_1+\mu_H)(\delta+\gamma_2+\mu_H)A_2 > 0, \tag{38}$$

which can be written as

$$aKA_1 > (\phi+\gamma_1+\mu_H)(\delta+\gamma_2+\mu_H)A_2 \tag{39}$$

$$\frac{aKA_1}{(\phi+\gamma_1+\mu_H)(\delta+\gamma_2+\mu_H)A_2} > 1, \tag{40}$$

which results in the expression $\mathcal{R}_0 > 1$. Therefore from the expressions for S^e, E^e and I^e the endemic equilibrium point is positive if and only if $\mathcal{R}_0 > 1$. We summarise the result in Lemma 2.

Lemma 2. *The endemic equilibrium $\mathcal{E}_2$ exists and is positive if and only if $\mathcal{R}_0 > 1$.*

Theorem 5. *The endemic equilibrium $\mathcal{E}_2$ of model system (1) is unstable if it is feasible.*

Proof. The proof follows Lyapunov's second method. Let $S - S^e > 0$, $E - E^e > 0$ $I - I^e > 0$, $P - P^e > 0$. Defining a suitable positive Lyapunov function $V(S,E,I,P)$ (see [21]) such that $V(S^e,E^e,I^e,P^e) = 0$ by,

$$\begin{aligned}
V(S,E,I,P) &= c_1\Big(S - S^e - S^e\ln\frac{S}{S^e}\Big) + c_2\Big(E - E^e - E^e\ln\frac{E}{E^e}\Big) \\
&\quad + c_3\Big(I - I^e - I^e\ln\frac{I}{I^e}\Big) + c_4\Big(P - P^e - P^e\ln\frac{P}{P^e}\Big),
\end{aligned} \tag{41}$$

where $c_{i's}$, $i = 1,2,3,4$ are non-negative constants to be determined. V is a positive definite function in the set Ω, except at $\mathcal{E}_2$ where it is zero. The rate of change of V along the solution of system (1) is given by

$$\begin{aligned}\dot{V} &= c_1(S-S^e)\frac{\dot{S}}{S}+c_2(E-E^e)\frac{\dot{E}}{E}+c_3(I-I^e)\frac{\dot{I}}{I}+c_4(P-P^e)\frac{\dot{P}}{P},\\ &= -c_1(S-S^e)\Big[\eta\frac{S}{K}+\frac{aP}{H+\epsilon P}+\mu_H\Big]-c_2(E-E^e)[\mu_H+\phi+\gamma_1]\\ &-c_3(I-I^e)[\mu_H+\delta+\gamma_2]-c_4(P-P^e)\mu_P \qquad (42)\\ &+c_1(S-S^e)\Big[\eta+\frac{\gamma_1 E}{S}+\frac{\gamma_2 I}{S}\Big]+apc_2(E-E^e)\frac{PS}{E(H+\epsilon P)}\\ &+c_3(I-I^e)\Big[\frac{a(1-p)PS}{I(H+\epsilon P)}+\phi\frac{E}{I}\Big]+c_4(P-P^e)\Big[c+\frac{\sigma_1 S}{P}+\frac{\sigma_2 I}{P}+\frac{\sigma_3 E}{P}\Big].\end{aligned}$$

Then $\dot{V}<0$ iff,

$$\begin{aligned}&c_1(S-S^e)\Big[\eta+\tfrac{\gamma_1 E}{S}+\tfrac{\gamma_2 I}{S}\Big]+apc_2(E-E^e)\tfrac{PS}{E(H+\epsilon P)}\\ &+c_3(I-I^e)\Big[\tfrac{a(1-p)PS}{I(H+\epsilon P)}+\phi\tfrac{E}{I}\Big]+c_4(P-P^e)\Big[c+\tfrac{\sigma_1 S}{P}+\tfrac{\sigma_2 I}{P}+\tfrac{\sigma_3 E}{P}\Big]=0.\end{aligned} \qquad (43)$$

For simplicity, assume $c_3<0$ and $c_4<0$, then $\dot{V}<0$ iff,

$$\frac{\eta c_1}{apc_2}=-\frac{E-E^e}{S-S^e}\Big[\frac{PS}{E(H+\epsilon P)}\Big(1+\frac{\gamma_1 E}{\eta S}+\frac{\gamma_2 I}{\eta S}\Big)\Big]. \qquad (44)$$

But $ap,\eta>0$ and consequently, one of c_1 or c_2 must be negative. This has the effect of changing the sign of one of the expressions in $\dot{V}$. Therefore, constants $c_1>0$, $c_2>0$, $c_3<0$ and $c_4<0$ cannot be found such that $\dot{V}<0$. In poor communities $\mathcal{E}_2$ is certainly unstable and is probably a saddle. □

2.5. Permanence of the System

System (1) is said to be permanent if the boundary (including infinity) is a repellor, i.e. if there exists a compact set Q$\in\overset{\circ}{\Omega}$, the interior of Ω, such that whenever initially $x\in\overset{\circ}{\Omega}$, then $x(t)\in Q$ for t sufficiently large. After a transient phase, all densities are uniformly bounded away from 0 (see [7]). This notion captures a basic idea in ecology of viewing an ecosystem as stable even if it exhibits violent oscillations, as long as its species remain safe from extinction. If $S_0=0$, then, $(S(t),\,E(t),\,I(t),\,P(t))\longrightarrow(0,0,0,P_\infty)$ irrespective of the initial values of $E(t)$, $I(t)$, $P(t)\geq 0$, but will not stay there. If $S(t)>0$, then, $((S(t),E(t),I(t),P(t))\longrightarrow(S_\infty,0,0,0)$ for $E(t)=I(t)=P(t)=0$, while $((S(t),E(t),I(t),P(t))\longrightarrow(S^e,E^e,I^e,P^e)$ enters Ω and stays there otherwise.

2.6. Persistence

Lemma 3. *Cholera will persist as long as the pathogen, V.cholerae is present.*

Proof. Assuming that outbreaks occur whenever the level of the pathogen reaches its initial level. Re-arranging the fourth equation in system (1) gives

$$\dot{P(t)} - (c - \mu_P)P(t) = \sigma_1 S(t) + \sigma_2 I(t) + \sigma_3 E(t), \tag{45}$$

integration yields,

$$P(t) = P(0) + e^{(c-\mu_P)t} \int_0^t e^{-(c-\mu_P)\tau} \Big[\sigma_1 S(\tau) + \sigma_2 I(\tau) + \sigma_3 E(\tau)\Big] d\tau. \tag{46}$$

Cholera will emerge whenever $P(t) = P(0)$. Which means that,

$$e^{(c-\mu_P)t} \int_0^t e^{-(c-\mu_P)\tau} \Big[\sigma_1 S(\tau) + \sigma_2 I(\tau) + \sigma_3 E(\tau)\Big] d\tau = 0, \tag{47}$$

which implies that $e^{-(c-\mu_P)t} = 0$, this implies, $t = \infty$. This means that cholera will emerge infinitely many times, except when adequate measures are taken. This is biologically a challenging problem because as long as humans continue to contaminate the environment it is difficult to eradicate the pathogen. A *V.cholerae*-free environment is feasible only if local communities are educated on the need for safe disposal of waste products and proper hygiene methods are practiced. □

We illustrate the intrinsic dynamic of the cholera model for the human and the pathogen populations in Figure 4 (a) and 4 (b). Numerical simulations of the model systems (1) were carried out using a set of reasonable parameter values given in Table (1).

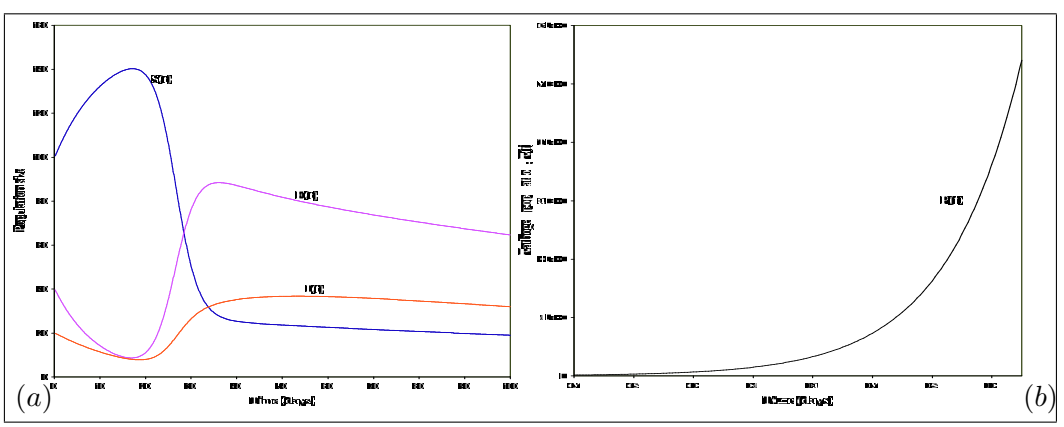

Figure 4. (a) Simulation results showing the dynamics of the human population; (b) Simulation results showing the dynamics of the pathogen population with time for model system (1). We assume initial condition: $S(0) = 100,\ E(0) = 39,\ I(0) = 20,\ P(0) = 215$ using parameter values in Table 1.

In Figure 4 (a) graph $S(t)$ denotes the susceptible population which is increasing in a period between 0-18 days and begin to fall from the period between 18-35 days attaining an equilibrium state. The graph $E(t)$ in Figure 4 (a) denotes the exposed population which begins by falling in a period between 0-18 days and starts to increase to a maximum point

in the period between 18-30 days and eventually falls to an equilibrium state. The graph $I(t)$ in Figure 4 (a) denotes the population of sufferers which begins by falling in the period between 0-20 days and increases to a maximum in the period between 20-45 days and falls slowly attaining an equilibrium state. Figure 4 (b) shows the graph of the pathogen population $P(t)$ which is showing exponential growth.

3. Cholera Model with Treatment

In this section, model system (1) is extended to incorporate treatment of cholera sufferers $(I(t))$ at a rate α into a new class $T(t)$ of treated individuals. It is assumed that treated individuals do not die from the disease and they recover at a rate w into the class, $S(t)$ of susceptible individuals. When cholera occurs in an unprepared community, case-fatality rates may be as high as 50 % usually because there are no facilities for treatment or because treatment is given too late. However, cholera is simple to treat and only the rapid and adequate replacement of fluids, electrolytes and base is required. The mortality rate for appropriately treated disease is usually less than 1 %. Most cases of diarrhoea caused by *V.cholerae* can be treated using oral rehydration solutions such as that recommended by the WHO/UNICEF [26, 31, 33]. During an epidemic, most (80-90 %) of patients can be treated using oral rehydration therapy alone, but severely dehydrated patients need the administration of intravenous fluids such as half-strength Darrows solution or Ringers Lactate. Patients with mild or moderate dehydration who can drink should be rehydrated with an oral rehydration solution about $75ml/kg$ body weight in 4 hours. The composition of the WHO/UNICEF [26, 31, 33] oral rehydration solution (made up to one litre with clean water) is shown in the following table.

Sodium chloride	$3.5g$
Trisodium citrate	$2.9g$
Potassium chloride	$1.5g$
Glucose	$20g$

The solution is safe, even for infants, if its intake is alternated with the consumption of sodium-free fluids or breast milk. If this solution is not immediately available, home-made sugar and salt solutions may be used to maintain hydration and prevent further dehydration while taking the patient to the nearest clinic for medical attention. Home-made sugar and salt solutions may also be prepared and the mixture is made up 1 level teaspoon of table salt added to 8 level tea-spoons of sugar. The mixture is dissolved in 1 litre of boiled and cooled water. Commercial oral rehydration solutions may also be used and are convenient and easy to make-up using boiled and cooled water. Note that antidiarrhoeal medicines such as those containing loperamide are not recommended.

The model structure for the cholera model with treatment is shown in Figure 5. In Figure 5, the dashed arrows indicate the indirect contribution of the human population in the growth of the pathogen.

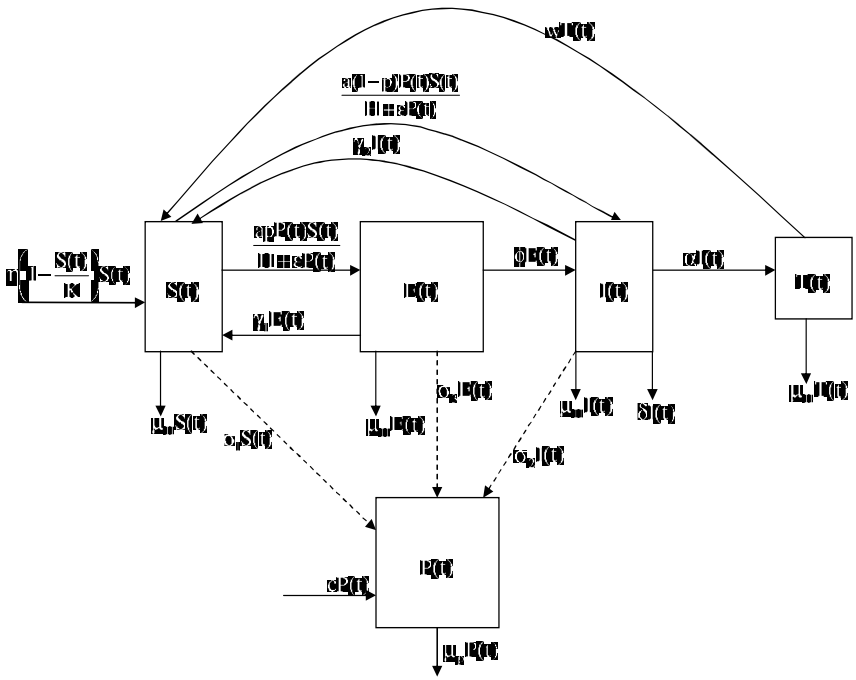

Figure 5. Flow diagram of the cholera model with treatment.

The flow diagram in Figure (5) depicts the model, which is described by the following system of differential equations,

$$\begin{aligned}
\dot{S(t)} &= \eta(1-\tfrac{S(t)}{K})S(t) + \gamma_1 E(t) + \gamma_2 I(t) + wT(t) - \tfrac{aP(t)S(t)}{H+\epsilon P(t)} - \mu_H S(t),\\
\dot{E(t)} &= ap\tfrac{P(t)S(t)}{H+\epsilon P(t)} - (\mu_H + \phi + \gamma_1)E(t),\\
\dot{I(t)} &= a(1-p)\tfrac{P(t)S(t)}{H+\epsilon P(t)} + \phi E(t) - (\mu_H + \delta + \gamma_2 + \alpha)I(t),\\
\dot{T(t)} &= \alpha I(t) - (w+\mu_H)T(t),\\
\dot{P(t)} &= (c-\mu_P)P(t) + \sigma_1 S(t) + \sigma_2 I(t) + \sigma_3 E(t).
\end{aligned} \tag{48}$$

The initial condition for model system (48) is given by,

$$\begin{cases}
S(\theta) = \varphi_1(\theta), E(\theta) = \varphi_2(\theta),\\
I(\theta) = \varphi_3(\theta), T(\theta) = \varphi_4(\theta),\\
P(\theta) = \varphi_5(\theta), \varphi_i(\theta) \geq 0,\\
\varphi_i(0) > 0, i = 1,2,3,4,5.
\end{cases} \tag{49}$$

We define,

$$\Omega_T = \Big\{(S, E, I, T, P) \in \mathbb{R}^5 | S \geq 0, E \geq 0, I \geq 0, T \geq 0, P \geq 0\Big\}, \tag{50}$$

to be the epidemiologically and mathematically feasible region.

3.1. Existence of Solutions

Theorem 6. *A solution of model system (48) is feasible.*

Proof. Let $\Big\{(S(t), E(t), I(t), T(t), P(t)) \in \mathbb{R}^5\Big\}$ be any solution of system (48) with non-negative initial conditions. Since

$$\dot{S(t)} \leq \eta\Big(1 - \frac{S(t)}{K}\Big)S(t) - \mu_H S(t), \tag{51}$$

then, $\underbrace{\limsup S(t)}_{t \longrightarrow \infty} \leq M$, where $M = \max(S_0, K)$. Let $Z(t) = S(t) + E(t) + I(t) + T(t) + P(t)$, then

$$\begin{aligned}
\dot{Z(t)} &= \eta(1 - \frac{S(t)}{K})S(t) + \gamma_1 E(t) + \gamma_2 I(t) + wT(t) - \frac{aP(t)S(t)}{H + \epsilon P(t)} - \mu_H S(t) + pa\frac{P(t)S(t)}{H + \epsilon P(t)} \\
&-(\mu_H + \phi + \gamma_1)E(t) + a(1-p)\frac{P(t)S(t)}{H + \epsilon P(t)} + \phi E(t) - (\mu_H + \delta + \gamma_2 + \alpha)I(t) \\
&+\alpha I(t) - (w + \mu_H)T(t) + cP(t) + \sigma_1 S(t) + \sigma_2 I(t) + \sigma_3 E(t) - \mu_P P(t), \\
&= (\eta(1 - \frac{S(t)}{K}) + \sigma_1 - \mu_H)S(t) + (\sigma_3 - \mu_H)E(t) + (\sigma_2 - \delta - \mu_H)I(t) + (c - \mu_P)P(t) \\
&\leq (\eta + \sigma_1 - \mu_H + 1)S(t) - S(t) - (\mu_H - \sigma_3)E(t) - (\mu_H + \delta - \sigma_2)I(t) \\
&-\mu_H T(t) - (\mu_P - c)P(t), \\
&\leq (\eta + \sigma_1 - \mu_H + 1)M - mW(t),
\end{aligned} \tag{52}$$

where $m = \min\{(\mu_H - \sigma_3, \mu_H + \delta - \sigma_2, \mu_H, \mu_P - c, 1)\}$. Thus,

$$\dot{Z(t)} + mZ(t) \leq (\eta + \sigma_1 - \mu_H + 1)M. \tag{53}$$

Equation (53) is a first order linear differential inequality [5], with the solution given by,

$$0 < Z(S, E, I, T, P) \leq \frac{(\eta + \sigma_1 - \mu_H + 1)M}{m} + Z(S_0, E_0, I_0, T_0, P_0)e^{-mt} \tag{54}$$

as $t \longrightarrow \infty$, we have

$$0 < Z(S, E, I, T, P) \leq \frac{(\eta + \sigma_1 - \mu_H + 1)M}{m}. \tag{55}$$

Therefore, all solutions of model system (2) enter the feasible region,

$$\Omega_T = \Big\{(S(t), E(t), I(t), T(t), P(t)) \in \mathbb{R}^5_+ : Z \leq \frac{(\eta + \sigma_1 - \mu_H + 1)M}{m} + \varsigma, \forall \varsigma > 0\Big\}. \tag{56}$$

This completes the proof of the theorem. □

3.2. Positivity of Solutions

Theorem 7. *Let the initial data be* $S(t) \geq 0, E(t) \geq 0, I(t) \geq 0, T(t) \geq 0, P(t) \geq 0$. *Then, solutions of* $S(t)$, $E(t)$, $I(t)$, $T(t)$, $P(t)$ *of system (48) are positive for all* $t \geq 0$.

Proof. The plane $S = 0$ of $\mathbb{R}^5$ is invariant for model system (48). Considering the variable $T(t)$ in $[0, T]$, then for $t \in [0, T]$ the fourth of equations (48) can be written as,

$$\dot{T(t)} \geq -(w + \mu_H)T(t), \forall\, t \in [0, T]. \tag{57}$$

By direct integration, we obtain

$$T(t) \geq T(0)e^{-(w+\mu_H)t} \geq 0, \tag{58}$$

as $t \in [0, T]$ and as long as $w + \mu_H < +\infty$. □

We illustrate the phase plane portrait of model system (48) in Figures 6 (a) and 6 (b). Figures 6 (a) and 6 (b) illustrate that solutions of model system (48) starting in Ω_T will stay in Ω_T and are positively invariant and are unique thus are mathematically and epidemiologically well posed.

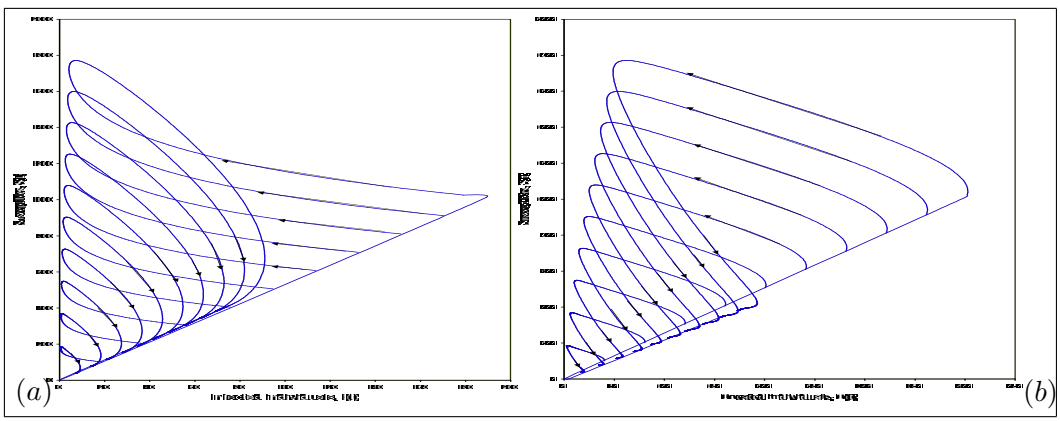

Figure 6. (a) A typical phase plane portrait for the cholera model with treatment in the SI phase plane, (b) A typical phase plane portrait for the cholera model with treatment in the ST phase plane, for $\eta = 0.0001, K = 12878000, \gamma_1 = 0.1, \gamma_2 = 0.05, a = 0.2143, H = 10^9, \epsilon = 0.5, \mu_H = 0.0000675, p = 0.8, \phi = 0.005, \delta = 0.015, c = 0.73, \sigma_1 = 10, \sigma_2 = 100, \sigma_3 = 200, \alpha = 0.5, w = 0.2, \mu_P = 0.33$ with varying initial conditions. We considered general cases for illustration.

3.3. Equilibrium States

Model system (48) has a disease-free equilibrium given by,

$$\mathcal{E}_1 = (S^1, E^1, I^1, T^1, P^1) = \Big(K\Big(1 - \frac{\mu_H}{\eta}\Big), 0, 0, 0, 0\Big). \tag{59}$$

and an endemic equilibrium given by,

$$\mathcal{E}_2 = (S^e, E^e, I^e, T^e, P^e), \tag{60}$$

where,

$$\begin{aligned}
S^e &= \frac{K(\eta - \mu_H) + \sqrt{K^2(\eta - \mu_H)^2 - \frac{4aK\eta\lambda_P^e c_2}{(w+\mu_H)(\phi+\gamma_1+\mu_H)(\delta+\gamma_2+\mu_H)}}}{2\eta},\\
E^e &= \frac{ap\lambda_p^e}{\phi + \gamma_1 + \mu_H},\\
I^e &= \frac{a\lambda_p^e(\phi + (1-p)\gamma_1 + (1-p)\mu_H)}{(\phi + \gamma_1 + \mu_H)(\delta + \gamma_2 + \mu_H + \alpha)},\\
T^e &= \frac{a\alpha\lambda_p^e(\phi + (1-p)\gamma_1 + (1-p)\mu_H)}{(w + \mu_H)(\phi + \gamma_1 + \mu_H)(\delta + \gamma_2 + \mu_H + \alpha)} \text{ and},\\
P^e &= \tfrac{1}{c-\mu_P}\Big[\sigma_3 E^e + \sigma_2 I^e - \sigma_1 S^e\Big] \text{ for } c > \mu_P,
\end{aligned} \tag{61}$$

with,

$$\begin{aligned}
c_2 &= (w\delta\phi + (1-p)\gamma_1(w\delta + \mu_H(w + \alpha + \delta + \mu_H)) + \mu_H(w(p\alpha + \delta\\
&\quad +(w + \alpha + \delta)\phi + p\gamma_2(w + \mu_H) + \mu_H(w + \alpha + \delta + \phi + \mu_H)), \text{ and}\\
\lambda_P^e &= \frac{P^e S^e}{H + \epsilon P^e}.
\end{aligned} \tag{62}$$

3.4. Stability and Reproductive Numbers

The Jacobian matrix of model (48) is given by,

$$\mathcal{J} = \begin{pmatrix}
\eta(1 - \frac{2S(t)}{K}) - \frac{aP(t)}{H+\epsilon P(t)} - \mu_H & \gamma_1 & \gamma_2 & w & \frac{-aHS(t)}{(H+\epsilon P(t))^2}\\
\frac{apP(t)}{H+\epsilon P(t)} & -(\mu_H + \phi + \gamma_1) & 0 & 0 & \frac{apHS(t)}{(H+\epsilon P(t))^2}\\
\frac{a(1-p)P(t)}{H+\epsilon P(t)} & \phi & -(\mu_H + \delta + \gamma_2 + \alpha) & 0 & \frac{a(1-p)HS(t)}{(H+\epsilon P(t))^2}\\
0 & 0 & 0 & -(w + \mu_H) & 0\\
\sigma_1 & \sigma_3 & \sigma_2 & 0 & c - \mu_P
\end{pmatrix}. \tag{63}$$

Evaluating the Jacobian matrix (63) at the disease-free equilibrium gives,

$$\mathcal{J} = \begin{pmatrix} -\eta + \mu_H & \gamma_1 & \gamma_2 & w & \frac{-aK(1-\frac{\mu_H}{\eta})}{H} \\ 0 & -(\mu_H + \phi + \gamma_1) & 0 & 0 & \frac{aKp(1-\frac{\mu_H}{\eta})}{H} \\ 0 & \phi & -(\mu_H + \delta + \gamma_2 + \alpha) & 0 & \frac{aK(1-p)(1-\frac{\mu_H}{\eta})}{H} \\ 0 & 0 & 0 & -(w + \mu_H) & 0 \\ \sigma_1 & \sigma_3 & \sigma_2 & 0 & c - \mu_P \end{pmatrix}. \quad (64)$$

Using the method of van den Driessche and Watmough [32] to compute the basic reproductive number for model system (48) gives,

$$\mathcal{F} = \begin{pmatrix} 0 & 0 & 0 & 0 & 0 \\ 0 & 0 & 0 & 0 & \frac{apK(1-\frac{\mu_H}{\eta})}{H} \\ 0 & 0 & 0 & 0 & \frac{a(1-p)K(1-\frac{\mu_H}{\eta})}{H} \\ 0 & 0 & 0 & 0 & 0 \\ 0 & 0 & 0 & 0 & 0 \end{pmatrix}, \text{ and} \quad (65)$$

$$\mathcal{V} = \begin{pmatrix} -\eta(1-\frac{\mu_H}{\eta}) & \gamma_1 & \gamma_2 & w & -\frac{aK(1-\frac{\mu_H}{\eta})}{H} \\ 0 & -(\mu_H + \phi + \gamma_1) & 0 & 0 & 0 \\ 0 & \phi & -(\mu_H + \delta + \gamma_2 + \alpha) & 0 & 0 \\ 0 & 0 & 0 & -(w + \mu_H) & 0 \\ \sigma_1 & \sigma_3 & \sigma_2 & 0 & c - \mu_P \end{pmatrix}. \quad (66)$$

It follows that the *treatment-induced* reproductive number is given by

$$\mathcal{R}_T = \frac{(aK(\gamma_1((\gamma_2+p(\alpha+\delta+\mu_H))\sigma_1+(1-p)(\eta-\mu_H)\sigma_2)+\gamma_2((\phi+(1-p)\mu_H)\sigma_1+p(\eta-\mu_H)\sigma_3)+(\eta-\mu_H)((\phi+(1-p)\mu_H)\sigma_2+p(\alpha+\delta+\mu_H)\sigma_3)))}{((\phi+\gamma_1+\mu_H)(\alpha+\delta+\gamma_2+\mu_H)(-cH\eta+H\eta\mu_P+aK\sigma_1))}. \quad (67)$$

The following result follows from van den Driessche and Watmough [32] (using Theorem 2).

Lemma 4. *The disease-free equilibrium of model system (1) is locally-asymptotically stable if* $\mathcal{R}_T < 1$ *and unstable if* $\mathcal{R}_T > 1$.

Thus, Lemma 4 implies that cholera can be eliminated from the community with treatment (when $\mathcal{R}_T < 1$) if the initial sizes of the sub-populations of the model are in the basin of attraction of the disease-free equilibrium $\mathcal{E}_1$.

The reproductive number with treatment can be written as,

$$\mathcal{R}_T = \mathcal{R}_0 \frac{(\delta + \gamma_2 + \mu_H)}{(\delta + \gamma_2 + \mu_H + \alpha)}[1 - N_1] \quad (68)$$

where,

$$N_1 = \frac{ap\alpha K((\mu_H - \eta)\sigma_3 - \gamma_1\sigma_1)}{(\phi + \gamma_1 + \mu_H)(\delta + \gamma_2 + \mu_H)(-cH\eta + H\eta\mu_P + aK\sigma_1)\mathcal{R}_0}, \quad (69)$$

$\forall\ \alpha > 0$. Equation (68) reduces to $\mathcal{R}_0$, the productive number in the absence of treatment in the community when $\alpha = 0$. Equation (68) can be written as,

$$\frac{\mathcal{R}_T}{\mathcal{R}_0} = \frac{(\delta + \gamma_2 + \mu_H)}{(\delta + \gamma_2 + \mu_H + \alpha)}[1 - N_1], \tag{70}$$

since the right hand side of equation (70) is always less than unit, thus

$$\frac{\mathcal{R}_T}{\mathcal{R}_0} < 1 \tag{71}$$

which gives,

$$\mathcal{R}_T < \mathcal{R}_0. \tag{72}$$

Figure 7 illustrates the relationship and behaviour of $\mathcal{R}_0$ and $\mathcal{R}_T$ for increasing σ_2 (number of bacteria shed into the environment by one cholera sufferer per day) using parameter values in Table 1.

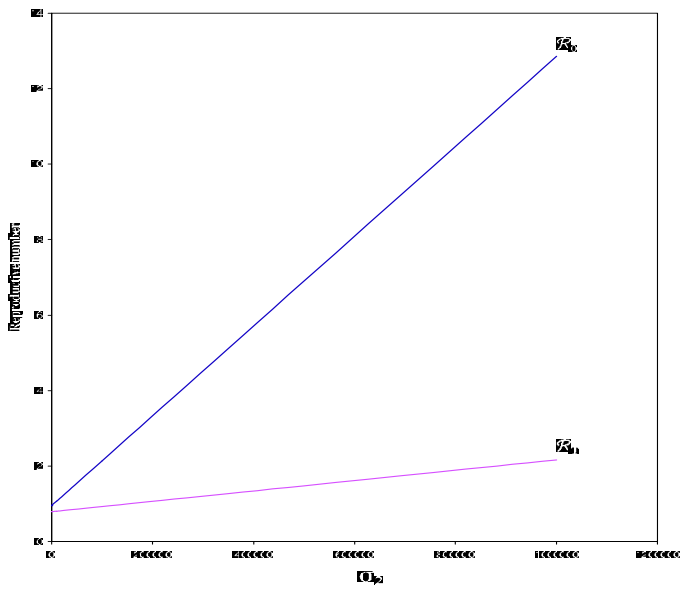

Figure 7. Trend $\mathcal{R}_0$ and $\mathcal{R}_T$ of the reproductive numbers for increasing σ_2 with other parameter values as given in Table 1.

The spectral radius $\mathcal{R}_T$ defines the number of secondary infections in the presence of treatment and is the reproductive number with treatment of model system (48). Setting the reproductive number $\mathcal{R}_T = 1$ and solving for p and α gives the critical threshold at which cholera can be eradicated,

$$\begin{aligned} p^{Tc} &= \frac{(\phi+\gamma_1+\mu_H)[(\delta+\gamma_2+\mu_H+\alpha)(-cH\eta+H\eta\mu_P+aK\sigma_1)-aK(\gamma_2\sigma_1+(\eta-\mu_H)\sigma_2)]}{aK[(\gamma_1(\delta+\mu_H+\alpha)-\gamma_2\mu_H)\sigma_1-(\eta-\mu_H)(\gamma_1+\mu_H)\sigma_2+(\eta-\mu_H)(\delta+\gamma_2+\mu_H+\alpha)\sigma_3]} > 0, \\ \alpha_c &= \frac{(\phi+\gamma_1+\mu_H)(\delta+\gamma_2+\mu_H)(-cH\eta+H\eta\mu_P+aK\sigma_1)}{(\phi+\gamma_1+\mu_H)(-cH\eta+H\eta\mu_P+aK\sigma_1)+aKp(\gamma_1\sigma_1+(\eta-\mu_H)\sigma_3)}[\mathcal{R}_0 - 1] > 0. \end{aligned} \tag{73}$$

The threshold p^{Tc} exists when

$$(\delta + \gamma_2 + \mu_H + \alpha)(-cH\eta + H\eta\mu_P + aK\sigma_1) > aK(\gamma_2\sigma_1 + (\eta - \mu_H)\sigma_2), \tag{74}$$

and

$$\gamma_1(\delta+\mu_H+\alpha)-\gamma_2\mu_H)\sigma_1-(\eta-\mu_H)(\gamma_1+\mu_H)\sigma_2+(\eta-\mu_H)(\delta+\gamma_2+\mu_H+\alpha)\sigma_3>0. \quad (75)$$

The threshold α_c exists when $\mathcal{R}_0>1$ and $(-cH\eta+H\eta\mu_P+aK\sigma_1)>0$.

If $\mathcal{R}_0<1$, cholera cannot develop into an epidemic. For $\mathcal{R}_0>1$ it is necessary to determine the necessary condition for slowing down the spread of cholera. Following Hsu Schmitz [15],

$$\begin{aligned}\Delta_v: &= \mathcal{R}_0-\mathcal{R}_T,\\ &= \mathcal{R}_0-\frac{\mathcal{R}_0(\delta+\gamma_2+\mu_H)}{(\delta+\gamma_2+\mu_H+\alpha)}[1-N_1], \quad (76)\\ &= \mathcal{R}_0[1-N_2(1-N_1)],\end{aligned}$$

for which $\Delta_v>0$ is expected for slowing down the spread of cholera at population level. Note that

$$N_2=\frac{(\delta+\gamma_2+\mu_H)}{(\delta+\gamma_2+\mu_H+\alpha)}<1. \quad (77)$$

Differentiating $\mathcal{R}_T$ in equation (67) partially with respect to α gives,

$$\frac{\partial\mathcal{R}_T}{\partial\alpha}=-\Big[\frac{aK(\phi+(1-p)\gamma_1+(1-p)\mu_H)(\gamma_2\sigma_1+(\eta-\mu_H)\gamma_2)}{(\phi+\gamma_1+\mu_H)(\alpha+\delta+\gamma_2+\mu_H)^2(-cH\eta+H\eta\mu_P+aK\sigma_1)}\Big]<0, \quad (78)$$

where the expression in square brackets (78) is always positive for $\eta>\mu_H$ and $\eta H(\mu_P-c)+a\sigma_1K>0$. From equations (78) it can be seen that treatment slows down the spread of cholera. If $\mu_P>c$ and $\eta>\mu_H$ are not satisfied, then cholera will remain endemic in the population.

Theorem 8. *The disease-free equilibrium $\mathcal{E}_1$ of model system (48) is globally stable if it is feasible.*

Proof. Let $S-S^1>0$, $E=E^1=0$, $I=I^1=0$, $T=T^1=0$,$P=P^1=0$, Considering an average Lyapunov function of the form,

$$L(S,E,I,T,P)=S^{\nu_1}E^{\nu_2}I^{\nu_3}T^{\nu_4}P^{\nu_5}, \quad (79)$$

with $\nu_i>0$, $i=1,2,3,4,5$.

$$
\begin{aligned}
\tfrac{L'}{L} &= \Psi(S,E,I,T,P)\\
&= \frac{1}{S^{\nu_1}E^{\nu_2}I^{\nu_3}T^{\nu_4}P^{\nu_5}}\Big[\nu_1 S^{\nu_1-1}E^{\nu_2}I^{\nu_3}T^{\nu_4}P^{\nu_5}S' + \nu_2 E^{\nu_2-1}S^{\nu_1}I^{\nu_3}T^{\nu_4}P^{\nu_5}E'\\
&+\nu_3 I^{\nu_3-1}S^{\nu_1}E^{\nu_2}T^{\nu_4}P^{\nu_5}I' + \nu_4 T^{\nu_4-1}S^{\nu_1}E^{\nu_2}I^{\nu_3}P^{\nu_5}T' + \nu_5 P^{\nu_5-1}S^{\nu_1}E^{\nu_2}I^{\nu_3}T^{\nu_4}P'\Big],\\
&= \nu_1\frac{S'}{S} + \nu_2\frac{E'}{E} + \nu_3\frac{I'}{I} + \nu_4\frac{T'}{T} + \nu_5\frac{P'}{P},\\
&= \nu_1\Big[\eta\Big(1-\frac{S}{K}\Big)+\gamma_1\frac{E}{S} + \gamma_2\frac{I}{S} + w\frac{I}{S} - \frac{aP}{H+\epsilon P} - \mu_H\Big] + \nu_2\Big[pa\frac{PS}{E(H+\epsilon P)} - (\mu_H+\phi+\gamma_1)\Big]\\
&+\nu_3\Big[a(1-p)\frac{PS}{I(H+\epsilon P)} + \phi\frac{E}{I} - (\mu_H+\delta+\gamma_2+\alpha)\Big] + \nu_4\Big[\alpha\frac{I}{T} - (w+\mu_H)\Big]\\
&+\nu_5\Big[c + \sigma_1\frac{S}{P} + \sigma_2\frac{I}{P} + \sigma_3\frac{E}{P} - \mu_P\Big],\\
&\leq -\nu_1\Big[\eta(\frac{S}{K}-1) + \mu_H\Big] - \nu_2[(\mu_H+\phi+\gamma_1)] - \nu_3[(\mu_H+\delta+\gamma_2)+\alpha] - \nu_4[w+\mu_H]\\
&-\nu_5[\mu_P - c].
\end{aligned}
\tag{80}
$$

The expression $-\nu_1\Big[\eta(\frac{S}{K}-1)+\mu_H\Big]$ in equation (80) is negative only if $S > K(1-\frac{\mu_H}{\eta})$, $S > S^1$ and $E-E^1 = I-I^1 = T-T^1 = P-P^1 = 0$. Since all model parameters are nonnegative from equation (80), $L' \leq 0$ for $S - S^1 > 0$, with inequality holding only at $\mathcal{E}_1 = ((1-\frac{\mu_H}{\eta})K, 0, 0, 0, 0)$. In this case the Lyapunov function satisfies $L' \leq 0$ and hence the disease-free state is globally asymptotically stable for $S - S^1 > 0$. If S> 0, then, $(S, E, I, T, P) \longrightarrow (S_\infty, 0, 0, 0, 0)$ for $E = I = T = P = 0$. □

Theorem 9. *The endemic equilibrium $\mathcal{E}_2$ of model system (48) is unstable if it is feasible.*

Proof. The proof follows Lyapunov's second method. Let $S - S^e > 0$, $E - E^e > 0$ $I - I^e > 0$, $T - T^e > 0$, $P - P^e > 0$. Defining a suitable positive Lyapunov function $V(S, E, I, T, P)$ such that $V(S^e, E^e, I^e, T^e, P^e) = 0$ by,

$$
\begin{aligned}
V(S,E,I,T,P) &= c_1\Big(S - S^e - S^e\ln\frac{S}{S^e}\Big) + c_2\Big(E - E^e - E^e\ln\frac{E}{E^e}\Big)\\
&+c_3\Big(I - I^e - I^e\ln\frac{I}{I^e}\Big) + c_4\Big(T - T^e - T^e\ln\frac{T}{T^e}\Big)\\
&+c_5\Big(P - P^e - P^e\ln\frac{P}{P^e}\Big),
\end{aligned}
\tag{81}
$$

where $c_{i's}$, $i = 1, 2, 3, 4, 5$ are constants to be determined. V is a positive definite function in the set Ω_T, except at $\mathcal{E}_2$ where it is zero. The rate of change of V along the solution of

system (48) is given by,

$$\begin{aligned}\dot{V} &= c_1(S-S^e)\frac{\dot{S}}{S}+c_2(E-E^e)\frac{\dot{E}}{E}+c_3(I-I^e)\frac{\dot{I}}{I}+c_4(T-T^e)\frac{\dot{T}}{T}+c_5(P-P^e)\frac{\dot{P}}{P}\\ &= -c_1(S-S^e)\Big[\eta\frac{S}{K}+\frac{aP}{H+\epsilon P}+\mu_H\Big]-c_2(E-E^e)[\mu_H+\phi+\gamma_1]\\ &-c_3(I-I^e)[\mu_H+\delta+\gamma_2+\alpha]-c_4(T-T^e)[w+\mu_H]\\ &-c_5(P-P^e)\mu_P+c_1(S-S^e)\Big[\eta+\frac{\gamma_1 E}{S}+\frac{\gamma_2 I}{S}+\frac{wT}{S}\Big]\\ &+apc_2(E-E^e)\frac{PS}{E(H+\epsilon P)}+c_3(I-I^e)\Big[\frac{aPS}{I(H+\epsilon P)}+\phi\frac{E}{I}\Big]\\ &+c_4(T-T^e)\Big[\frac{\alpha I}{T}\Big]+c_5(P-P^e)\Big[c+\frac{\sigma_1 S}{P}+\frac{\sigma_2 I}{P}+\frac{\sigma_3 E}{P}\Big].\end{aligned} \tag{82}$$

Then, $\dot{V}<0$ iff

$$\begin{aligned}&c_1(S-S^e)\Big[\eta+\tfrac{\gamma_1 E}{S}+\tfrac{\gamma_2 I}{S}+\tfrac{wT}{S}\Big]+apc_2(E-E^e)\tfrac{PS}{E(H+\epsilon P)}\\ &+c_3(I-I^e)\Big[\tfrac{aPS}{I(H+\epsilon P)}+\phi\tfrac{E}{I}\Big]+c_4(T-T^e)\Big[\tfrac{\alpha I}{T}\Big]+c_5(P-P^e)\Big[c+\tfrac{\sigma_1 S}{P}+\tfrac{\sigma_2 I}{P}+\tfrac{\sigma_3 E}{P}\Big]=0.\end{aligned} \tag{83}$$

For simplicity, assume $c_3<0$, and $c_5<0$, then $\dot{V}<0$ iff

$$\eta c_1(S-S^e)\Big[1+\tfrac{\gamma_1 E}{\eta S}+\tfrac{\gamma_2 I}{\eta S}+\tfrac{wT}{\eta S}\Big]+apc_2(E-E^e)\tfrac{PS}{E(H+\epsilon P)}+\alpha c_4(T-T^e)\Big[\tfrac{I}{T}\Big]=0, \tag{84}$$

and can be written as,

$$\frac{\eta c_1}{\alpha c_4}\Big(\frac{B_1}{B_3}\Big)+\frac{apc_2}{\alpha c_4}\Big(\frac{B_2}{B_3}\Big)=-1 \tag{85}$$

here,

$$\begin{aligned}B_1 &= (S-S^e)\Big(1+\tfrac{\gamma_1 E}{\eta S}+\tfrac{\gamma_2 I}{\eta S}+\tfrac{wT}{\eta S}\Big)>0,\\ B_2 &= (E-E^e)\Big(\tfrac{PS}{E(H+\epsilon P)}\Big)>0,\\ B_3 &= (T-T^e)\Big(\tfrac{I}{T}\Big)>0,\end{aligned} \tag{86}$$

and $\eta>0$, $ap>0$, $\alpha>0$. Therefore, $c_1>0$, $c_2>0$, $c_4>0$, $c_3<0$, $c_5<0$, cannot be found such that $\dot{V}<0$. The endemic equilibrium is globally asymptotically unstable. □

We illustrate the dynamic of the cholera model for the human and the pathogen populations in Figure 8 (a) and 8 (b). Numerical simulations of the model systems (48) were carried out using a set of reasonable parameter values given in Table (1)

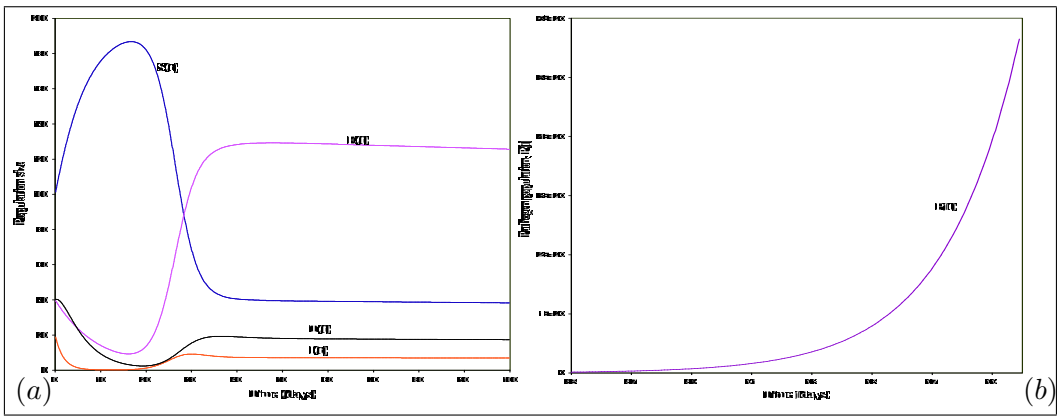

Figure 8. (a) Simulations trends showing the dynamics of human population; (b) Simulation results showing the dynamics of the pathogen population with time for model system (48). We assume initial condition:$S(0) = 101,\ E(0) = 39,\ I(t) = 19,\ T(t) = 40,\ P(t) = 526$ using parameter values in Table 1.

In Figure 8 (a) graph $S(t)$ denotes the trend for the susceptible population which is increasing in a period of between 0-20 days and begins to fall from the period between 20-38 days attaining an equilibrium state. The graph $E(t)$ in Figure 8 (a) denotes the exposed population which begins by falling in a period between 0-20 days and starts to increase to a maximum point in the period between 20-38 days attaining an equilibrium state. The graph $T(t)$ in Figure 8 (a) denotes the class of treated individuals which begins by falling in the period between 0-35 days attaining an equilibrium state. The graph $I(t)$ in Figure 8 (a) denotes the population of sufferers which begins by falling to a nearly constant value in the period between 0-20 days and increases to a maximum point in the period between 20-35 days attaining an equilibrium state. Figure 8 (b) shows the graph of the pathogen population $P(t)$ which is showing exponential growth.

4. Numerical Simulations

Numerical simulations of the model systems (1) and (48) are carried out to investigate the effects of treating cholera cases in a community using parameter values given in Table 1. The parameter values in Table 1 are obtained from published data and others are reasonable estimates. We use a fourth order Runge-Kutta numerical scheme coded in C^{++} programming language for the numerical simulations. The obtained results from the numerical simulation of model system (1) and (48) for the susceptibles, exposed, infectives and pathogen are illustrated in Figures 9 (a), 9 (b), 9 (c) and 9 (d) respectively. In Figures 9 (a), 9 (b), 9 (c) and 9 (d), each figure consists of two graphs, one for the basic cholera model (1) and the other for the cholera model (48) with treatment. The subsript N and T in these figures denotes the graphs for a case with no treatment (for the basic model (1)) and for a case with treatment (model system (48)).

Table 1. Model parameters and their interpretations

η	human intrinsic growth rate	0.0001/day	Estimate
K	environmental carrying capacity of humans	12.878M	[33]
γ_1	recovery rate of carriers	0.1/day	Estimate
γ_2	recovery rate of cholera sufferers who do not receive treatment	0.05/day	Estimate
w	recovery rate of cholera sufferers who receive treatment	0.2/day	Estimate
H	*V.cholerae* biomass level at which half of the contacts with contaminated water produce infection	10^9 cells/L	[9]
a	maximal rate of exposure	0.2143/day	[13]
ϵ	limitation of the growth velocity of *V.cholerae*	0.5	Estimate
μ_H	natural human mortality rate	0.0000675/day	[24]
p	proportion of carriers	0.8/day	Estimate
ϕ	per capita rate at which carriers eventually become infected	0.005/day	Estimate
δ	per capita mortality rate from cholera infection	0.015/day	[29]
c	per capita growth rate of *V.cholerae* bacteria	0.73/day	Estimate
σ_1	number of bacteria shed into the environment by one susceptible individual per day	10 cells/L-pers-day	Estimate
σ_2	number of bacteria shed into the environment by one cholera sufferer per day	100 cells/L-pers-day	[17]
σ_3	number of bacteria shed into the environment by one carrier per day	200 cells/L-pers-day	Estimate
μ_P	mortality rate for bacteria	0.33/day	[9]
α	treatment rate of cholera sufferers	0.5 /day	Estimate

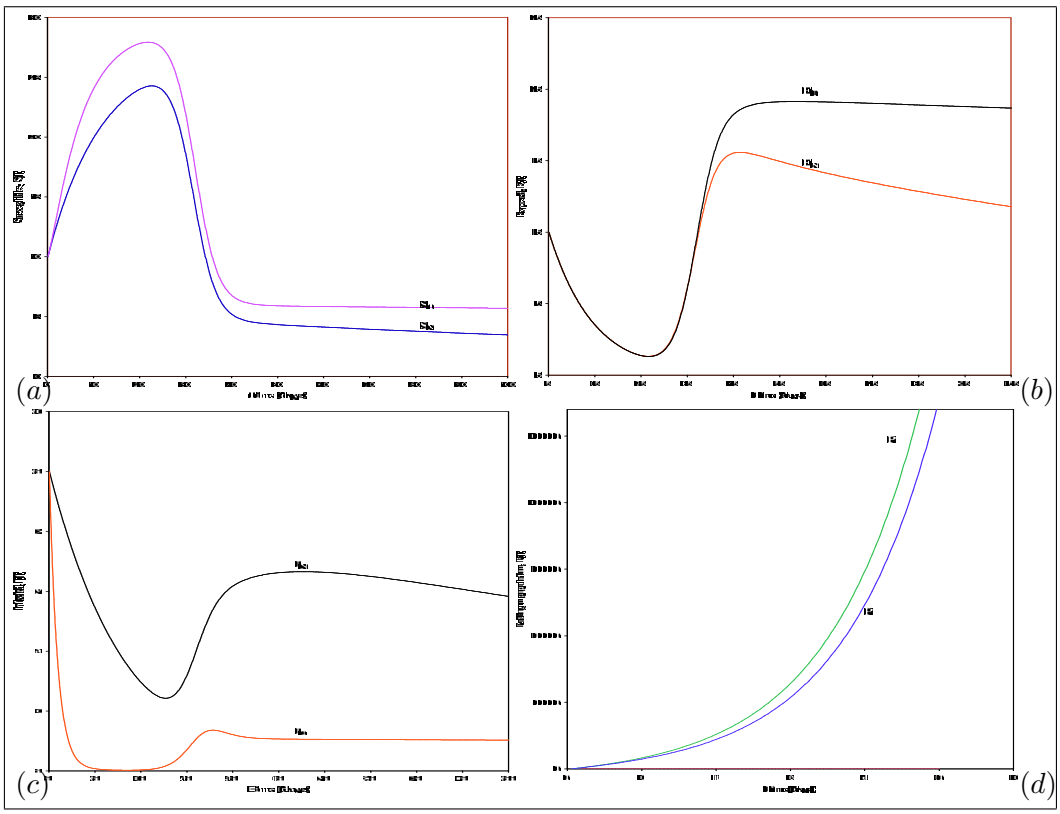

Figure 9. Simulation results showing the effect of treatment on: (a) Susceptible population, (b) Exposed population, (c) Infected population, (d) Pathogen population. Where: S_T is the susceptible population where there is treatment, S_N is the susceptible population where there is no treatment, E_T is the exposed population where there is treatment, E_N is the exposed population where there is no treatment, I_T is the infected population where there is treatment, I_N is the infected population where there is no treatment, P_T is the pathogen population where there is treatment, P_N is the pathogen population where there is no treatment. The initial conditions used in the simulations are : $S_N(0) = S_T(0) = 10$, $E_N(0) = E_T(0) = 10$, $I_N(0) = I_T(0) = 10$, $T(0) = 0$, $P_N(0) = P_T(0) = 10$.

In Figure 9 (a), the results obtained illustrate that treatment of cholera infected individuals results in an increase in the susceptible population (graph for S_T always greater than graph for S_N). The results in Figure 9 (b) show that treatment of cholera sufferers $(I(t))$ result in an increase of the number of carriers $(E(t))$ with time. In Figure 9 (c), the obtained results illustrate that, treatment of cholera sufferers reduces the number of individuals suffering from cholera, thus treatment of cholera sufferers in the community reduces the burden of the disease. We also note from the results in Figure 9 (d) that treatment of cholera sufferers in a community reduces the growth of the pathogen population since the gradient of graph P_N is always greater than that of graph P_T for all time. We note from the numerical analysis that, treatment of cholera sufferers in the community reduces the number of infected individuals but does not reduce the number of carriers. Thus, the existence of carriers may remain a challenge in the control of the epidemic in settings with treatment targeted to cholera

sufferers only since carriers can not be identified.

5. Conclusion

We formulated and analyzed a cholera-pathogen model with and without treatment, and evaluated the impact of treatment. The model is analyzed qualitatively to determine criteria for control of a cholera epidemic and is used to compute the threshold treatment rate necessary for community-wide control of cholera. The mathematical features such as the epidemic threshold, equilibria and stabilities were determined. We used a Lyapunov functional approach to show the global stability of the disease-free and endemic equilibrium. Positivity and boundedness of solutions were presented. The epidemic threshold, which depends solely on parameters associated with the model, is used to assess the effectiveness of treatment in controlling cholera in a community.

In the absence of treatment, the origin (or trivial equilibrium) is a saddle, while the two biologically meaningful equilibria, namely the disease-free is globally asymptotically stable provided certain conditions are met (the public health implication of this is that cholera can be eradicated, but not without adopting strict and proper sanitation rules), and the endemic steady state is only locally stable. This is important as it shows that persistence is temporal or seasonal and from the public health point of view, in between two outbreaks, adequate measures could be put in place to combat the resurgence of the epidemic. The periodic nature of the epidemic outbreaks may dictate the reason why global stability is not achieved, and consequently, this suggests a natural extension of the model to include seasonal effects. This will be introduced elsewhere as well as vaccination and quarantine, with the hope that our simulation results will show that the dynamic of the disease depends on the amplitude of the seasonally varying contact rate. Migration of infectives even though most of the patients are too sick too travel will also be given prominence, because in some rural settings, especially in Sub-Saharan Africa where health care facilities are not available or inadequate, infected individuals are often moved to communities where such services are provided. One other way to extend this study is to further investigate the stability of the endemic equilibrium for the phenomenon of backward bifurcation, where it may co-exist with the disease-free steady state.

It is shown from the study that treatment slows down the spread of the epidemic. As long as the pathogen is present in the environment, it will be difficult to eradicate cholera in poor settings where clean water is not available. Numerical simulations qualitatively show the benefits of treatment and we note from the simulation analysis that, treatment of cholera sufferers in the community reduces the number of infected individuals but does not reduce the number of carriers. Thus, the existence of carriers may remain a challenge in the control of the epidemic in settings with treatment targeted to cholera sufferers only since they can not be identified. An important question to address for cholera is sanitation related (non-pharmaceutical measure) and the cost effectiveness of vaccine. Despite the availability of preventive vaccines, cholera still inflicts substantial morbidity, mortality, and socio-economic costs and remains a major public health problem in the developing world. Here we ask: Can a strategic use of effective vaccines controls the

spread of cholera? We shall address this question elsewhere by constructing a deterministic mathematical model to study the transmission dynamics of cholera and the combined effects of vaccination and treatment.

Acknowledgements

S. D. Hove-Musekwa acknowledges with thanks financial support given to her by the African Millennium Mathematical Sciences Initiative (AMMSI).

References

[1] Alberts B., Johnson A., Lewis J., Raff M., Roberts K. and Walter P., *Molecular biology of the cell*, Garland Science, New York, pp856-1437, (2002).

[2] Anderson R. M. and May R.M. *Infectious diseases of humans,* Oxford University Press, London/New York, (1991).

[3] Anderson R.M. and May R.M. *Infectious diseases of humans: dynamics and control,* Oxford: Oxford University Press, (1992).

[4] Bailey N. T. J., *The mathematical theory of infectious diseases and its applications*, Griffin, London, (1975).

[5] Birkhoff G. and Rota G.C. *Ordinary differential equations,* Ginn (1982).

[6] Brauer F. and Castillo-Chavez C. Mathematical models in population biology and epidemiology, In: *Texts in Applied Mathematics Series*, **40**, Springer-Verlag, New York (2001).

[7] Butler G.J. and Waltman P. Persistence in dynamical systems, *Proc. Amer. math. Soc.*, **96**, 425-430, (1986).

[8] Castillo-Chavez C., Feng Z. and Huang W. *On the computation of $\mathcal{R}_0$ and its role on global stability,* (2002) (math.la.asu.edu/chavez/2002/JB276.pdf).

[9] Codeco, C.T., Endemic and epidemic dynamics of cholera: the role of the aquatic reservoir, *BMC Inf. Dis.* **1(1)**, (2001) (http://www.biomedcentral.com/1471-2334/1/1).

[10] Diekmann O., Heesterbeek J.A.P. and Metz J.A.P., On the definition and computation of the basic reproductive ratio $\mathcal{R}_0$ in models for infectious diseases in heterogeneous populations, *J. Math. Biol.*, **365-382**, (1990).

[11] Finkelstein, R.A. Cholera, vibrio cholerae $O1$ and $O139$, and other pathogenic vibrios, in: *Medical Microbiology,* 4^{th} edition, Baron S. (ed), Univ. of Texas, (1996).

[12] Grais R.F., Ellis J.H., Kress A. and and Glass G.E., Modeling the Spread of Annual Influenza Epidemics in the U.S.: The Potential Role of Air Travel, *Health Care Management Science* **7**(2), 127-134, (2004).

[13] Hartley D.M., Morris J.G. and Smith D.L., Hyperinfectivity: A critical element in the ability of V. cholerae to cause epidemics? . *PLoS Med.3*:**e7** (2006).

[14] Hethcote H.W. The mathematics of infectious diseases, *SIAM Rev.* **42**(4), 599-653, (2000).

[15] Hsu Schmitz S.F. Effects of treatment or/and vaccination on HIV transmission in homosexuals with genetic heterogeneity, *Math. Biosci.*, **167**, 1-18, (2000).

[16] Huang Ji-cai and Xiao Dong-mei, Analyses of Bifurcations and Stability in a Predator-prey System with Holling Type-IV Functional Response, *Acta Math. Appl. Sinica (English Series)*, **20**(1), 167-178 (2004).

[17] Jensen M.A, Faruque S.M., Mekalanos J.J. and Levin B.R., Modeling the role of bacteriophage in the control of cholera outbreaks, *PNAS* **103**(12), 4652-4657 (2006).

[18] Kermack W. O. and McKendrick A. G., A Contribution to the Mathematical Theory of Epidemics, *Proc. Roy. Soc. Lon. Ser. A* **115**: 700-721 (1927).

[19] Kermack W. O. and McKendrick A. G., Contributions to the Mathematical Theory of Epidemics. II. The Problem of Endemicity, *Proc. Royal Soc. London. Series A*, Vol. 138, 55-83 (1932).

[20] Kermack W. O. and McKendrick A. G., Contributions to the Mathematical Theory of Epidemics. III. Further Studies of the Problem of Endemicity, *Proc. Royal Soc. London Series A,* Vol. 141, 94-122 (1933).

[21] Korobeinikov A., Lyapunov functions and global stability for SIR and SIRS epidemiological models with non-linear transmission, *Bull. Math. Biol*. **30**, 615-626 (2006).

[22] Liang W., Wang S., Yu F., Zhang L., Qi G., Liu Y., Gao S., and Kan B., Construction and Evaluation of a Safe, Live, Oral *Vibrio cholerae* Vaccine Candidate, IEM108, *Infection and Immunity*, Vol.71(10), 5498-5504, (2003), DOI: 10.1128/IAI.71.10.5498-5504.2003

[23] McKendrick A.G., Applications of mathematics to medical problems *Proc. Edinburgh Math. Soc.* **44**, 1-34 (1925-6).

[24] MSF - $www.doctorswithouthborders.org/pr/2006/04-07-2006.cfm$, (Retrieved, 2007)

[25] Perko L. Differential equations and dynamical systems, *Text in Applied Mathematics*, **7**, Springer: Berlin, (2000).

[26] Professional nursing today, Medpharm publications, (2005), $http://www.cholera.html$ (*Retrieved, 2007*)

[27] Qu M., Xu J., Ding Y., Wang R., Liu P., Kan B., Qi G., Liu Y, and Gao S., Molecular Epidemiology of Vibrio cholerae O139 in China: Polymorphism of Ribotypes and CTX Elements, *J. Clin. Microbiol,* Vol. 41(6), 2306-2310, (2003). doi: 10.1128/JCM.41.6.2306-2310.2003.

[28] Ross R., *The Prevention of Malaria,* London, John Murray, (1911).

[29] Sepulveda J, Gomez-Dantes H. and Bronfman M., Cholera in the Americas: an overview. *Infection*. **20**(5):243-248 (1992).

[30] Stryer L., *Biochemistry*, W.H. Freeman and Company, New York pp 982, (1988).

[31] UNICEF: $http://www.unicef.org/infobycountry/media_3$3913$.html$ (Retrieved, 2007).

[32] van den Driessche P. and Watmough J., reproductive numbers and sub-threshold endemic equilibria for compartmental models of disease transmission, *Math. Biosci.,* **29-48**, (2002).

[33] WHO, www.who.int/topics/cholera (*Retrieved, 2007*).

[34] Wikipedia (2007), http://en.wikipedia.org/wiki/Cholera.

In: Mathematical Biology Research Trends
Editor: Lachlan B. Wilson, pp. 147-173
ISBN 978-1-60456-141-8

Chapter 5

MATHEMATICAL MODELS AND PARAMETER ESTIMATION FOR HETEROGENEOUS CELL POPULATION DYNAMICS

***Gennady Bocharov*[a], *Tatyana Luzyanina*[b], *Dirk Roose*[c], *Hagit Alon*[d], *Martin Meier-Schellersheim*[e] *and Zvi Grossman*[d,e]**
[a] Institute of Numerical Mathematics, RAS, Moscow, Russia,
[b] Institute of Mathematical Problems in Biology,
RAS, Pushchino, Russia,
[c] Department of Computer Science, Katholieke Universiteit Leuven, Belgium,
[d] Tel Aviv University School of Medicine, Tel Aviv, Israel,
[e] National Institute of Allergy and Infectious Diseases, NIH, Bethesda, USA

Abstract

The functioning of the immune system involves tightly regulated proliferation, differentiation and death processes of heterogeneous cell populations, including T lymphocytes, B lymphocytes, antigen presenting cells, etc. To quantify the turnover kinetics of specific subsets of immune cells under normal conditions and during infections, labeling techniques (e.g., with fluorescent markers CFSE or BrdU) in conjunction with flow cytometry analysis (FACS) are used in experimental and clinical immunology. To obtain information about the kinetic structure of the cellular responses of heterogenous cell populations from data that in addition to experimental fluctuations (noise) exhibit considerable variation between different study animals, careful computational analysis is needed. The primary objectives of this chapter are: (i) to introduce mathematical models in the form of hyperbolic partial differential equations (PDEs) which allow direct reference to single or double label histograms of cell distributions, (ii) to illustrate the potential of our modeling and parameter identification technology by representative examples from CFSE and BrdU labeled T cell proliferation studies, and (iii) to compare the proposed PDE models with alternative modeling approaches which are based upon the use of ordinary differential equations.

1. Introduction

The heterogeneity of the turn-over kinetics of cell populations in living systems can be described in terms of a wide range of characteristics, such as the number of divisions since the administration of a label, the position in the cell cycle, the cellular mass, expression of cellular antigens, or the doubling time and death rate. To quantify this heterogeneity of cell labeling techniques in conjunction with the flow cytometry are widely used in today's experimental and clinical immunology. Flow cytometry is a technique based on the use of fluorescence activated cell sorter (FACS) for a quantitative single-cell analysis of suspensions of cells labeled with fluorescent substance(s). There exists a wide range of labeling techniques for the analysis of cell proliferation in response to stimuli inducing cell division:

- *in vitro* cytoplasmic labeling with carboxy-fluorescein diacetate succinimidyl ester (CFSE). After labeling, cells can be re-transferred into study animals for analysis of *in vivo* behavior. Labeled cells distribute their CFSE contents approximately equally onto their two daughter cells. CFSE can thus be used in combination with flow cytometry to trace cell populations over time and count the number of divisions they undergo, see Fig. 1.

- bromodeoxyuridine (BrdU) can - in animal studies - be administered through the food or intravenously and is incorporated into the newly synthesized DNA strands of all dividing cells in the organism. After the labeling phase (in the absence of BrdU) dividing cells dilute their BrdU contents by a factor of 2 during each division. BrdU contents can be analyzed by FACS.

- deuterated glucose (^2H-glucose) is non-toxic and can therefore be used in human subjects. Like BrdU, it is incorporated into the newly synthesized DNA strands of dividing cells but evaluating the ^2H-glucose contents of labeled cell populations requires mass-spectroscopic measurement on the DNA of many cells and does therefore not allow single-cell analysis.

- $[^3H]$ thymidine incorporation by dividing cells.

- fluorescent antibody labeling of the nuclear Ki-67 antigen that is expressed by cycling cells in late G_1, the S, G_2 and M phases of the cell cycle. Ki67 is detectable by flow cytometry for a few days after the last division. It is commonly used to assess the fraction of cells that have divided during the last 3-5 days, the so-called growth fraction of a given cell population.

FACS allows researchers to analyze up to a dozen parameters per cell at rates of up to 10^5 cells per second [1, 33]. The high throughput FACS technology provides a researcher with large amounts of data on the evolution of labeled cell distributions with time. But to make reliable inferences about the kinetic structure of the cellular responses of heterogenous cell populations from data that in addition to their inherent complexity exhibit experimental fluctuations (noise) and considerable variation between different study animals, specific computational analysis is needed. The existing mathematical approaches to model

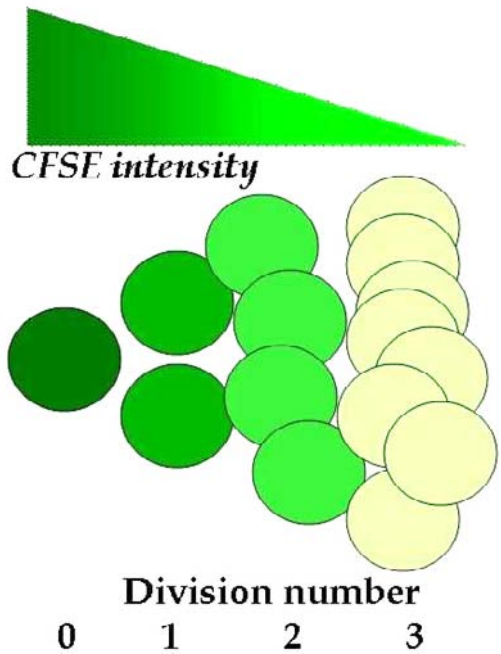

Figure 1. The proliferation associated dilution of CFSE label.

and analyze flow cytometry data take into account two aspects of the heterogeneity of proliferating cells: the number (j) of divisions the cells have undergone since the adminstration of the label and the age (s) of the cell (progression through the division cycle). The mathematical models were developed to describe the dynamics of cell populations labeled with CFSE. The corresponding models consist of systems of either ordinary- (ODE), or delay- (DDE), or (age-structured) partial differential (PDE) equations [2, 9, 11, 12, 14, 15, 21].
(i) *An ODE model.* The general linear compartmental model considered in [21] describes the rates of change in the numbers of cells $N_j(t)$ having undergone j divisions and in the number of dead but yet not disintegrated cells, $D(t)$, at time t. The scheme of the model is shown in Fig. 2.

The model assumes that the rates of cell proliferation and death, α_j and β_j, respectively, are division number dependent. In generic form, the model equations are as follows:

$$\begin{aligned} \frac{dN_0}{dt}(t) &= -(\alpha_0+\beta_0)N_0(t), \\ \frac{dN_j}{dt}(t) &= 2\alpha_{j-1}N_{j-1}(t) - (\alpha_j+\beta_j)N_j(t),\ j=1,\ldots,J, \\ \frac{dD}{dt}(t) &= \sum_{k=0}^{J}\beta_k N_k(t) - \delta D(t). \end{aligned} \tag{1.1}$$

In the original application, the birth-, death- and disintegration (δ) rate parameters were estimated using *in vitro* data on the growth of CFSE labeled T lymphocytes.
(ii) *A model based on DDEs.* A well-known biological model for cell cycle data analysis is

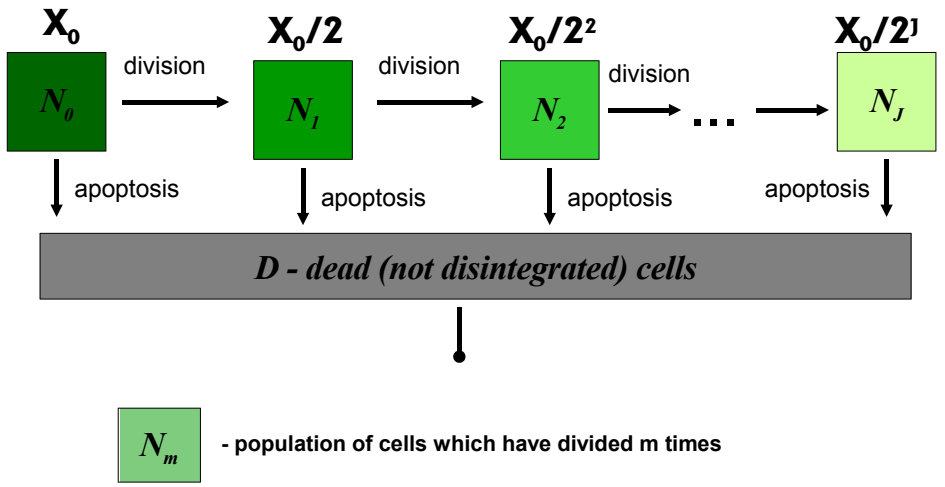

Figure 2. The compartmental model of labeled cell proliferation assay. X_0 stands for the initial label intensity per cell at t_0.

the Smith-Martin model, which lumps the different phases of the cell cycle into two states. The first state (called A) corresponds to the G_1 phase of cycle, and the second one (state B) represents the $S - G_2 - M$ phases of the cell cycle [32]. The progression through the cell cycle is assumed to have a stochastic component (the recruitment of cells from state A into B) and a deterministic component (a progression with a fixed time-lag through the B state). In a recent study [12] a DDE-type model was proposed which describes the rate of change of the population of T lymphocytes in the A and B states that have undergone j divisions:

$$\begin{aligned}
\frac{dA_0}{dt}(t) &= -(\alpha_0+\beta_0)A_0(t),\\
\frac{dA_1}{dt}(t) &= 2\alpha_0 A_0(t-\tau_0)\exp^{-\beta_B\tau_0} -(\alpha_1+\beta_A)A_1(t),\\
\frac{dA_j}{dt}(t) &= 2\alpha_1 A_{j-1}(t-\tau)\exp^{-\beta_B\tau} -(\alpha_1+\beta_A)A_j(t), \quad j=1,\ldots,\infty, \qquad (1.2)\\
B_0(t) &= \alpha_0\int_0^{\tau_0} A_0(t-s)\exp^{-\beta_B s}\,ds,\\
B_j(t) &= \alpha_1\int_0^{\tau} A_j(t-s)\exp^{-\beta_B s}\,ds, j=1,\ldots,\infty.
\end{aligned}$$

The parameters of the model characterize separately the division rates and the time lags of transit through the B state of naive and divided cells as well as the death rates of cells in the A and B states. In [12] the model variables $A_j(t_i)+B_j(t_i)$ were fitted to *in vivo* data (extracted from the CFSE histograms) on T-lymphocyte distributions with respect to the division number.

(iii) *PDE model.* A model describing explicitly the progression through the B state of the cell cycle as an age-structured process ($s \in [0,\tau]$ being the age variable) was analyzed in [15]. For data fitting, the authors considered the population of cells that have undergone

j divisions in the A state and in the B state, the latter being defined using the time distribution of cells at time t in the B state $b_j(t,s)$: $B_j(t) = \int_0^\tau b_j(t,s)ds$. The corresponding equations read

$$\begin{aligned} \frac{dA_j}{dt}(t) &= 2b_{j-1}(t,\tau) - (\alpha+\beta_A)A_j(t), \\ \frac{\partial b_j}{\partial t}(t,s) &+ \frac{\partial b_j}{\partial s}(t,s) = -\beta_B b_j(t,s), \quad j = 1,\dots,\infty. \end{aligned} \tag{1.3}$$

To estimate the parameters of the PDE version of the Smith-Martin model, three different parameter estimation approaches (direct fitting, indirect fitting and rescaling method) were examined [15]. The model proved to be consistent with the *in vivo* data characterizing the CFSE profile of transgenic T-lymphocyte adoptively transferred into irradiated mice.

A more general age-structured PDE model considering the age-distribution of the resting ($n_j(t,s)$) and proliferating ($p_j(t,s)$) cells which have undergone j divisions was examined in [9]. The equations of the model are

$$\begin{aligned} \frac{\partial p_j}{\partial t}(t,s) &+ \frac{\partial p_j}{\partial s}(t,s) = -\gamma p_j(t,s), \\ \frac{\partial n_j}{\partial t}(t,s) &+ \frac{\partial n_j}{\partial s}(t,s) = -(\mu+\beta)n_j(t,s), \\ p_j(t,0) &= \beta\int_0^\infty n_j(t,s)ds,\ n_j(t,0) = 2p_j(t,\tau),\ \ j = 1,\dots,J. \end{aligned} \tag{1.4}$$

Extending the deterministic treatment, a number of recently proposed models take into account that the cell division time is a random variable and is distributed in the cell population [17, 20, 34]. All the above modeling approaches focus on the generation structure of proliferating cell populations and were developed for the analysis of the CFSE cell systems in vitro and in vivo. Although other labeling techniques (BrdU and ^2H-glucose) are extensively used to quantify lymphocyte turnover in vivo, the mathematical models proposed for such data analysis are (i) based exclusively on systems of ODEs and (ii) reduce the heterogeneity of the labeled cell populations to two subsets, i.e. labeled (above some threshold) and unlabeled cells, see e.g. [18, 25, 27].

None of the above approaches considered the label intensity as a structure variable. Therefore, they require preprocessing of the raw data by assigning a division number to cells in a CFSE profile. This interpretation can be subject to significant errors. The present study introduces mathematical models which allow a direct reference to data on distributions of fluorescence label intensities. First, we formulate a basic hyperbolic PDE model for a single label structured population and apply it to numerically approach the inverse problem using original data coming from CFSE proliferation in vitro. The model performance is compared to that of the ODE model (1.1). As many of the in vivo lymphocyte turnover experiments employ two and more labels, we then extend the basic model to the double-labeled cell populations (e.g. CFSE/BrdU). Finally, we propose a generalization of a simple ODE model of T lymphocyte homeostasis that is formulated as a large-scale system of ODEs. This model is used for the parameter estimation of lymphocyte division and death in the analysis of BrdU/Ki-67 labeling experiments in SIV infected monkeys.

2. Single Label-Structured Cell Population Model

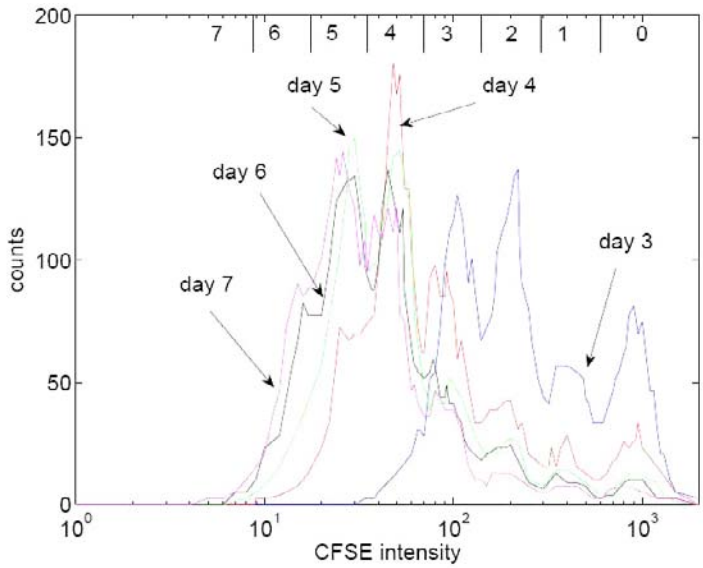

Figure 3. The original CFSE histograms giving the counts (number of fluorescence events of various intensities) obtained by FACS at days 3-7. The vertical lines at the top of the figure indicate the intervals of CFSE intensity which correspond to distinct cell generations (Data provided by S. Ehl).

CFSE histograms (see Fig. 3) give information about the distribution of cells $n(t,x)$ at a given time t with respect to the fluorescence intensity x. In a standard approach, the CFSE histograms are used to evaluate the fractions of cells that have completed certain numbers of divisions using various deconvolution techniques implemented in commercial software such as ModFit (Verify Software), CFSE Modeler (ScienceSpeak), CellQuest (Becton Dickinson) and others. The corresponding lumped CFSE distribution data, characterizing cell populations in terms of the mean fluorescence intensity per generation, can be subject to significant errors if the peaks corresponding to cells of different generations have large overlap. We formulate a mathematical model using a first order hyperbolic PDE which allows us to quantitatively describe and interpret the dynamics of CFSE labeled cell populations.

We consider a population of cells that are distinguishable from each other in terms of their fluorescence intensity with the distribution function $n(t,x)$, characterizing the number of cells at time t which have a label intensity between x and $x+dx$. The total number of cells in a system is then given by $N(t) = \int_0^{x_{max}} n(t,x)dx$. We assume that (i) at the beginning of the experiment, the cells are labeled with a distribution function $n(0,x)$ and (ii) some proliferation inducing stimuli are provided starting at time $t_0 = 0$. We assume that the level of stimulation remains uniform during the experiment. Under the above assumptions, the cell population dynamics can be modeled by the following population balance hyperbolic

PDE:

$$\frac{\partial n}{\partial t}(t,x) - v(x)\frac{\partial n}{\partial x}(t,x) = -(\alpha(x)+\beta(x))n(t,x) + 2\gamma\alpha(\gamma x)n(t,\gamma x), \quad t > t_0, \quad (2.1)$$

where

$$\alpha(\gamma x) = \begin{cases} \alpha(\gamma x), & x_{\min} \le x \le x_{\max}/\gamma \\ 0, & x_{\max}/\gamma \le x \le x_{\max}. \end{cases}$$

The advection term on the left-hand side, $v(x)\frac{\partial n(t,x)}{\partial x}$, describes the natural decay of the CFSE fluorescence intensity of the labeled cells with the rate $v(x)$ (UI/day). The composite term on the right-hand side, $-(\alpha(x)+\beta(x))n(t,x)$, describes the local disappearance of cells with the CFSE intensity x due to the division associated CFSE dilution and the death with the functions $\alpha(x) \ge 0$ and $\beta(x) \ge 0$ characterizing the proliferation and death rates, respectively $(1/hour)$. The last term $2\gamma\alpha(\gamma x)n(t,\gamma x)$ represents the birth of two cells due to division of the mother cell with the label intensity γx. The factor 2 accounts for the doubling of numbers and the coefficient γ accounts for the difference in the size of the CFSE intervals to which daughter and mother cells belong. Indeed, those cells who originate from division of cells with CFSE in the range $(\gamma x, \gamma(x+dx))$ enter into the range $(x, x+dx)$. Notice that under the assumption of equal partition of the label between the two daughter cells and no death during the division one expects that $\gamma = 2$. This would ensure conservation of CFSE label, similar to the conservation of volume/size in well known size-structured models, see [8, 13, 31]. However, we allow the label partitioning parameter γ to take values smaller than 2 so that $x < \gamma x \le 2x$, in order to check the consistency of the assumptions with experimental data. The above consideration applies to cells with levels of CFSE below the maximal initial staining $x_{\max}/\gamma$. The population dynamics of the cells with $x_{\max}/\gamma < x \le x_{\max}$ is governed by the equation without the source term. The cell division, death and label loss rates, $\alpha(x)$, $\beta(x)$ and $v(x)$, of the heterogeneous cell population are assumed to be functions of the CFSE intensity[1]. The precise dependence on x is not known a priori and is estimated from the CFSE FACS data.

The initial-boundary conditions for model (2.1) are specified as follows

- $n(t_0,x) = n_0(x), \quad x \in [x_{\min}, x_{\max}]$, which describes the distribution of cells at time t_0. This can be either the cell distribution at the start of the experiment, $t_0 = 0$, or at some later time, $t_0 > 0$.
- $n(t, x_{\max}) = 0, \quad t > t_0$, reflecting the fact that there is some maximum CFSE staining per cell, $x_{\max}$, for all $t > t_0$.

3. Computational Approach to the Direct and Inverse Problems

The model of CFSE labeled cell proliferation (2.1) allows one to predict the outcome of CFSE experiments if (i) the initial-boundary conditions are specified and (ii) the birth-, death- and advection rate functions are known. This type of prediction based on a mathematical model is known as the direct problem. When the data on the time evolution of the CFSE distribution are measured, the model can be used to identify the turnover rates

[1]Notice that given a non-homogeneous initial labeling this may be problematic

of the cells, giving rise to the inverse problem. In general, the treatment of the direct and inverse problems for the models (2.1) relies on the use of computational techniques. We implemented our computational approach in MATLAB [24].

3.1. Numerical Treatment of the Direct Problem

For the numerical solution of the cell population balance model (2.1) with specified initial-boundary conditions we used the MATLAB routine `hpde` developed by Shampine [30]. The routine is designed for first order hyperbolic PDEs in one space variable. It implements the second order Richtmeyer's two-step variant of the Lax-Wendroff scheme. The method can be fully vectorized, which allows to speed up computations in MATLAB significantly. This is important feature for data fitting problems in which the initial-boundary value problem has to be solved repeatedly to minimize the least-squares function.

The CFSE histograms obtained by flow cytometry use the base 10 logarithm of the marker expression level. Therefore, for computational analysis we reformulate model (2.1) using the $z = \log_{10}(x)$ coordinate:

$$\begin{aligned} \frac{\partial n}{\partial t}(t,z) &- \nu(z)\frac{\partial n}{\partial z}(t,z) = -(\alpha(z)+\beta(z))n(t,z) \\ &+ 2\gamma\alpha(z+\log_{10}(\gamma))n(t,z+\log_{10}(\gamma)), \quad t > t_0, \end{aligned} \tag{3.1}$$

where $\nu(z) = v(10^z)/\ln(10)10^z$.

To compute the solution of (3.1), a uniform discretization mesh $Z := [z_0, z_1, \ldots, z_N]$ was used with $\Delta_z := z_j - z_{j-1},\ j = 1, \ldots, N$. The Courant-Friedrichs-Lewy condition with safety factor 0.9 was employed to compute the time step in the PDE discretization:

$$\Delta_t = 0.9\Delta_z / \max_{z\in Z} \nu(z). \tag{3.2}$$

The solution of the transformed equation (3.1) with the shifted argument $(z + \log_{10}\gamma)$ was evaluated between the discretization mesh points using a third order interpolation polynomial so that the second order accuracy of the Lax-Wendroff scheme was preserved. The initial data $n_0(z_j)$, specified on some mesh $\mathcal{Z}_0$, which is in general unrelated to the PDE discretization, was recomputed on the mesh Z using the MATLAB code `interp1` implementing a shape-preserving piecewise monotone cubic interpolation.

3.2. Numerical Treatment of the Inverse Problem

3.2.1. Parametrization of the Unknown Rate Functions

The population balance model (3.1) depends on the unknown rate functions of cell division $\alpha(z)$, death $\beta(z)$ and the label loss $\nu(z)$, so that $n(t,z) \equiv n(t,z;\alpha(z),\beta(z),v(z),\gamma)$. To identify these functions from the observed CFSE histograms, we parameterize them following a general approach to the numerical treatment of the function estimation problem in distributed parameter systems [4–7, 10, 29]. The cell turnover rate functions are approximated using finite expansions with cubic interpolation polynomials $\phi_j(z)$ as basis functions

$$\alpha_{L_1}(z) = \sum_{j=1}^{L_1} a_j \phi_j^{(1)}(z), \quad \beta_{L_2}(z) = \sum_{j=1}^{L_2} b_j \phi_j^{(2)}(z), \quad z \in [z_{\min}, z_{\max}]. \tag{3.3}$$

The basis functions are constructed using sets of the knot sequences $(\tilde{z}_{k_1}, a_{k_1})$ and $(\tilde{z}_{k_2}, b_{k_2})$, respectively, where $\tilde{z}_{k_1}, \tilde{z}_{k_2} \in [z_{\min}, z_{\max}]$, $k_1 = 1, \ldots, L_1$, $k_2 = 1, \ldots, L_2$, $\tilde{z}_{L_1} = \tilde{z}_{L_2} = z_{\max}$, so that $\alpha_{L_1}(\tilde{z}_{k_1}) = a_{k_1}$, $k_1 = 1, \ldots, L_1$, $\beta_{L_2}(\tilde{z}_{k_2}) = b_{k_2}$, $k_2 = 1, \ldots, L_2$.

It is important that different meshes z_k and $\tilde{z}_k$ are used for the numerical solution of PDE model (3.1) and the parametrization of the unknown functions. This approach allows one to estimate

- the expansion coefficients, i.e. the elements of the unknown parameter vectors $\mathbf{a} = \{a_{k_1}\}_1^{L_1}$, $\mathbf{b} = \{b_{k_2}\}_1^{L_2}$. This is the case when the parametrization mesh $\tilde{z}_{k_1}, \tilde{z}_{k_2}$ is fixed ad hoc;

- both the expansion coefficients and the knots of the parametrization mesh, $\mathbf{a} = \{a_{k_1}\}_1^{L_1}$, $\tilde{\mathbf{z}}^{(1)} = \{\tilde{z}_{k_1}^{(1)}\}_1^{L_1-1}$, $\mathbf{b} = \{b_{k_2}\}_1^{L_2}$, $\tilde{\mathbf{z}}^{(2)} = \{\tilde{z}_{k_2}^{(2)}\}_1^{L_2-1}$.

For the advection rate function we consider two choices:

$$\nu(z) \equiv c \quad \text{or} \quad v(x) \equiv c, \quad c \in \mathbb{R}^+. \tag{3.4}$$

The first case assumes that the rate of label decay is directly proportional to the amount of label expressed in the cell: $v(x) = cx \log 10$, while the second option implies that the CFSE loss does not depend on its level in the cells.

The above parametrization reduces the original infinite dimensional function identification problem to a finite dimensional parameter estimation problem for the following vector of parameters,

$$\mathbf{p} = [\mathbf{a},\ \mathbf{b},\ \gamma,\ c] \in \mathbb{R}^{Q_1} \quad or \quad \mathbf{p} = [\mathbf{a},\ \tilde{\mathbf{z}}^{(1)},\ \mathbf{b},\ \tilde{\mathbf{z}}^{(2)},\ \gamma,\ c] \in \mathbb{R}^{Q_2}, \tag{3.5}$$

with $Q_1 = L_1 + L_2 + 2$ or $Q_2 = 2L_1 + 2L_2$, respectively.

3.2.2. Maximum Likelihood Parameter Estimation

Our objective is to find the parameter values $\mathbf{p}^\star$ such that the corresponding model solution $n(t, z; \mathbf{p})$ is qualitatively consistent with the available data on the evolution of CFSE histograms of cell distributions, i.e. with the time series $\mathbf{n}_i \equiv \{n_{i,j}\}_{j=1}^{M_i}$. Here the subscripts i, j specify the observation times t_i and the particular CFSE intensity bin which can range from 1 to some M_i, corresponding to the CFSE fluorescence z_j.

For optimal estimation of parameter values, we seek to maximize the likelihood that the data arose from the model [3, 16]. To apply the maximum likelihood approach, we further assume that (i) the observational errors, i.e., the residuals defined as a difference between observed and model-predicted values, are normally distributed; (ii) the errors in observations at successive times are independent; (iii) the errors in cell counts for consecutive label bins are independent; (iv) the variance of observation errors (σ^2) is the same for all the state variables, observation times and label expression level. Note that $(ii) - (iii)$ imply that the errors in the components of the state vector are independent. Then the corresponding likelihood function is

$$\mathcal{L}(\mathbf{p}) = \prod_{i=1}^{M} \frac{1}{\sqrt{(2\pi\sigma^2)^{M_i}}} \exp\{-\frac{1}{2}[n(t_i, \mathbf{z}_i; \mathbf{p}) - \mathbf{n}_i]^T \sigma^{-2} [n(t_i, \mathbf{z}_i; \mathbf{p}) - \mathbf{n}_i]\}. \tag{3.6}$$

The maximization of the log-likelihood function

$$\ln(\mathcal{L}(\mathbf{p};\sigma)) = -0.5\Big(n_d \ln(2\pi) + n_d \ln(\sigma^2) + \sigma^{-2}\Phi(\mathbf{p})\Big) \tag{3.7}$$

is equivalent to the minimization of the ordinary least-squares function $\Phi(\mathbf{p})$:

$$\Phi(\mathbf{p}) = \sum_{i=1}^{4}\sum_{j=1}^{M_i}(n_{i,j} - n(t_i, z_{i,j}; \mathbf{p}))^2, \tag{3.8}$$

provided that σ^2 is assigned the value $\sigma^{*^2} = \Phi(\mathbf{p}^*)/n_d$, where $\mathbf{p}^*$ is the vector which gives a minimum to $\Phi(\mathbf{p})$ and $n_d := \sum_{i=1}^{M} M_i$ is the total number of scalar measurements. To find numerically the minimum of the objective function, we used the MATLAB code `fminsearch` implementing the Nelder-Mead direct search simplex method.

3.3. Application to CFSE Proliferation Assay

The original data on CFSE labeled cell growth kinetics in vitro were provided by S. Ehl [21]. The experiment is briefly summarized below. Peripheral blood mononuclear cells were labeled with CFSE. The mitogen stimulator phytohenmagglutinin (PHA) was added to the PBMC sample in vitro to induce proliferation of T cells present in the sample. At regular times after stimulation the cells are harvested, stained with antibodies to CD4 and CD8 and analyzed by flow cytometry. The absolute number of live cells per well was determined by microscopy. Overall, the data characterize the kinetics of PHA-induced T cell proliferation.

3.3.1. Preprocessing of CFSE Data

The set of CFSE histograms in Fig. 3 represents the distribution of the CD3+ T lymphocytes (both CD4 and CD8 subsets) with respect to the CFSE expression level at days 3 to 7. When the initial cell labeling is fairly homogeneous, each CFSE peak represents a cohort of cells that proceed synchronously through the division rounds. As cells proliferate, the whole distribution moves from right to left reflecting sequential dilution of CFSE fluorescence with time.

Each of the histograms of CFSE-labeled cell counts at times $t_i,\ i = 0, 1, \ldots, M$, is a two-dimensional array consisting of vectors $\mathbf{z}_i := [z_{i,1}, \ldots, z_{i,M_i}]$, $\mathbf{c}_i := [c_{i,1}, \ldots, c_{i,M_i}] \in \mathbb{R}^{M_i}$, which correspond to the $\log_{10}$ of the measured marker expression level, and the corresponding count numbers. Here M_i stands for the number of mesh points at which the CFSE histogram at time t_i is specified. To translate the flow cytometry counts data to cell numbers considered in the model, the following transformation is used,

$$n_{i,j} = \frac{c_{i,j}N_i}{F_i}, \quad F_i = \int_{z_{\min}}^{z_{\max}} \tilde{c}_i(z)dz, \quad i = 0, 1, \ldots, M, \quad j = 1, \ldots, M_i, \tag{3.9}$$

where N_i is the total number of cells at time t_i and $\tilde{c}_i$ is a continuous approximation of the vector $\mathbf{c}_i$ defined on the histogram mesh $\mathbf{z}_i$. F_i is the total number of cell counts at time t_i. Figure 4 shows the resulting set of histograms of CFSE cell distributions.

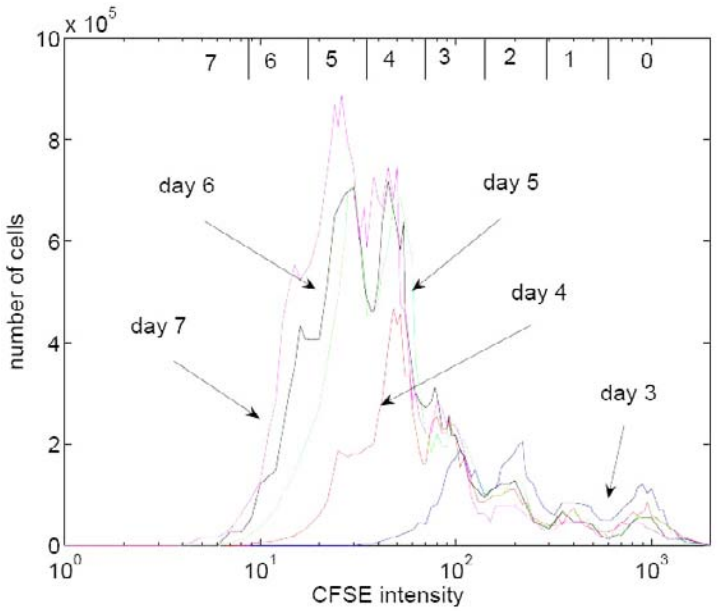

Figure 4. The CFSE-labeled cell distribution histograms at days 3-7. The vertical lines at the top of the figure indicate intervals of the CFSE intensity corresponding to the sequential generations of cells which have undergone $0, 1, \ldots, 7$ divisions.

3.3.2. Results of Parameter Estimation for the PDE Model

The best-fit solution of the distributed parameter model (3.1) and the underlying data set are presented in Fig. 5. Both the CFSE-labeled cell distributions at 96, 120, 144 and 168 hours, and the overall pattern of cell population surface are consistently reproduced by the model. The computed best-fit value of the objective function is $\Phi \approx 6.84 \times 10^{11}$ being about 2.4% of the squared l_2-norm of the original data values array $\mathbf{n}$, $\|\mathbf{n}\|_2^2 = \sum_{i=1}^{4} \sum_{j=1}^{M_i} (n_{i,j})^2$.

The best-fit continuous approximation to the birth rate function $\alpha(z)$ is presented in Fig. 6. It appears to be bell-shaped. To translate the identified function $\alpha(z)$ into biologically meaningful division rate estimates, which may depend on the generation number j, with each generation specified by the CFSE range $[s_j, s_{j+1}]$, see Fig. 6, we used the following "averaging" procedure,

$$\tilde{\alpha}_j = \frac{1}{s_j - s_{j+1}} \int_{s_j}^{s_{j+1}} \alpha(z) \mathrm{d}z, \quad j = 0, 1, \ldots, 7, \quad s_8 = 0. \tag{3.10}$$

The birth rate function $\alpha(z)$ was parameterized with four terms in the expansion (3.3) ($L_1 = 4$) and both the expansion coefficients $\mathbf{a}$ and the knots $\tilde{\mathbf{z}}^{(1)}$ were estimated. Notice that for the considered CFSE data there exists some z^* such that there are no dividing cells with the marker intensity $z < z^*$ for the time range 3 to 7 days of the proliferation assay. To take into account this feature in our computations, we set $\alpha_{L_1}(z) = 0$ for $z < z^*$. Therefore, for defining the basis functions in parametrization (3.3), the following range of the log-transformed marker intensity $[z^*, z_{\max}]$ with $z^* = 1.15$ was considered.

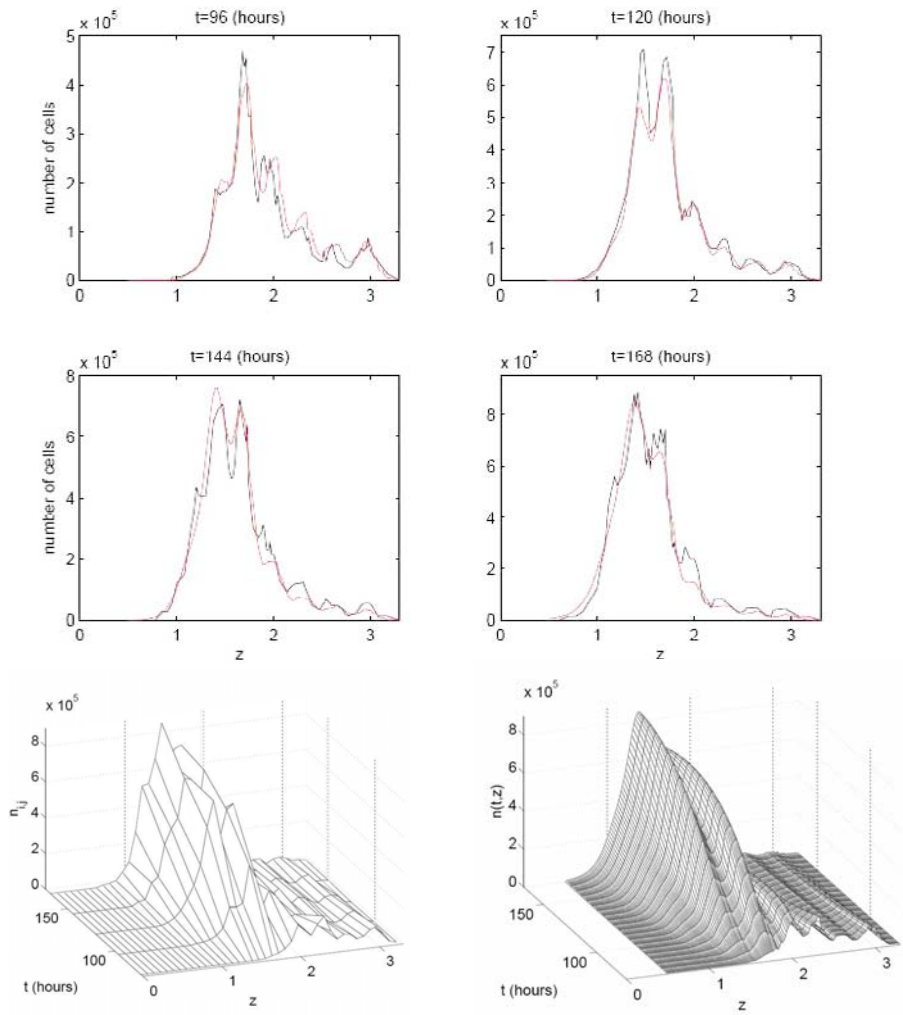

Figure 5. The experimental data set (cf. histograms in fig. 4) and the model solution corresponding to the best-fit parameter estimates. Two first rows: Experimental data (black curves) and the best-fit solution of model (3.1) (red curves). The last row presents the cell population surface: experimental data (left) and the model solution (right) as functions of time and the $\log_{10}$-transform of the marker expression level.

Figure 6 shows the 95% confidence intervals (CIs) for the best-fit parameters $a_k,\ k = 1, \ldots, 4$, computed by the profile-likelihood approach (see [21] for comparison with other approaches). The uncertainty in the parameter estimates is larger for larger values of z, but decreases as z decreases. Indeed, the CIs for a_1 and a_2, determining the left part of $\alpha(z)$ are relatively small. A large CI for the expansion parameter a_4 (determining the right tail of $\alpha(z)$) is likely to be due to the fact that the number of naive cells and of cells that have undergone few divisions (1 or 2) by days 4 to 7 is rather small as compared to the size of the population. Thus it might be subject to a large observation error. Therefore, the PDE

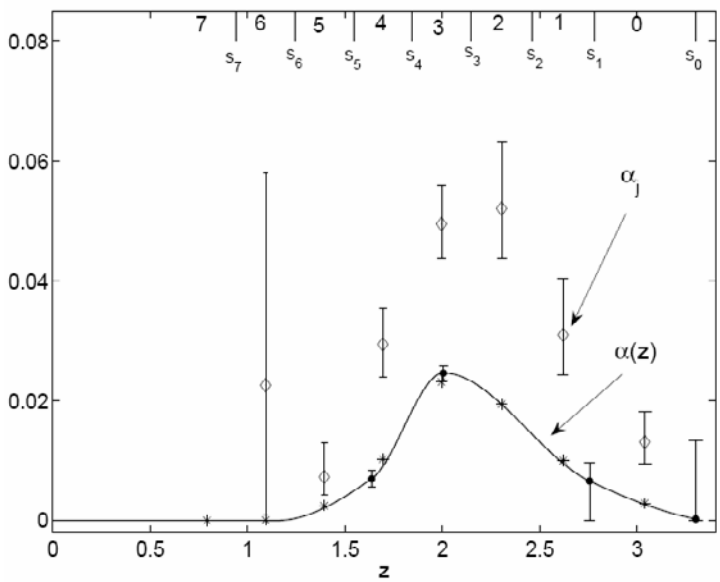

Figure 6. The estimated birth rate function $\alpha(z)$ of the PDE model (3.1) (solid curve) and the estimated birth rate parameters $\alpha_j,\ j = 0, 1, \ldots, 6$, of the ODE model (3.11) (diamonds). The best-fit estimates $a_k,\ k = 1, \ldots, L = 4$, defining the function $\alpha(z)$, are indicated by bullets. Stars denote $\tilde{\alpha}_j$, computed by (3.10). The values α_j and $\tilde{\alpha}_j$ are placed in the middle of the CFSE intervals (the boundaries of which are denoted by $s_j,\ j = 0, 1, \ldots, 7$) corresponding to subsequent division numbers starting from 0. Vertical lines indicate approximations to 95% confidence intervals for the estimated parameters $\alpha_j,\ j = 0, 1, \ldots, 6$, and $a_k,\ k = 1, \ldots, 4$.

model allows to identify reliably the rate function $\alpha(z)$ for small values of z, corresponding to a large number of cell divisions.

Following the proposed parametrization of the rate functions, the best-fit approximation to the death rate function $\beta(z)$ appears to be independent of z, see Fig. 7 (left).

For the CFSE decay rate $\nu(z)$, the second version of the parametrization (3.4) provides a better fit to the data by the model, with the best-fit estimate of the rate parameter $c \approx 0.15$. Finally, the best estimate for the CFSE dilution parameter associated with cell division γ appeared to be smaller than 2, $\gamma \approx 1.91$. The difference suggests that the CFSE molecules bonded to protein upon release from cells dying in the process of division can be taken up actively by, or adhere to the live cells.

The kinetics of the total cell growth observed experimentally and predicted by the model (the integral of the distribution density over the observed label intensity range, $\int_0^{z_{max}} n(t, z)dz$) are shown in Fig. 7 (right). The heterogeneous PDE model consistently reproduces the kinetics of T cell population growth.

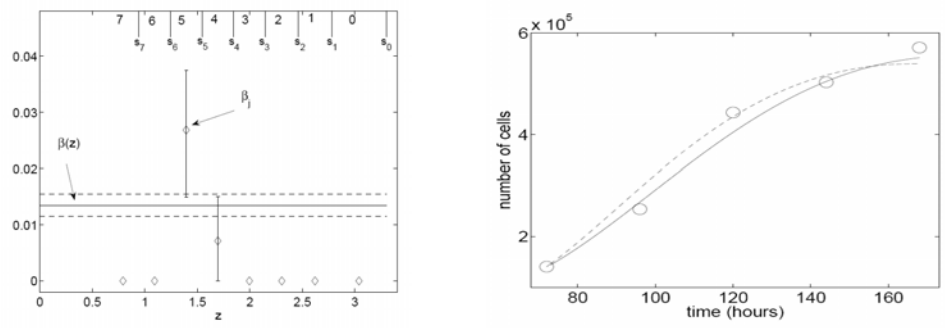

Figure 7. Left: The estimated death rate function $\beta(z)$ of the PDE model (3.1) (solid curve) and the death rate parameters $\beta_j,\ j = 0, 1, \ldots, 7$, of the ODE model (3.11) (diamonds). The values β_j are placed in the middle of the CFSE intervals (the boundaries of which are denoted by $s_j,\ j = 0, 1, \ldots, 7$) corresponding to subsequent division numbers starting from 0. Vertical lines indicate the 95% confidence interval for the estimated parameters $\beta_j,\ j = 4, 5$. The dashed lines indicate the 95% confidence interval for the estimated $\beta(z)$. Right: The kinetics of the total number of live lymphocytes for the CFSE data set (circles) predicted by the ODE and PDE models (dashed and solid curves, respectively).

3.3.3. Compartmental ODE Model

Usually, the CFSE fluorescence histograms are used to quantify the fractions of cells that have completed a certain number of divisions [17, 23]. This type of 'mean fluorescence intensity' data can be obtained either manually or by using various deconvolution techniques. The number of divisions which can be followed is limited by the autofluorescence of unlabeled cells. For the data that we consider, the division peaks resolution is not possible after about 7 division cycles. Using a uniform spacing between the consecutive cell generations, as shown in Fig. 4, the CFSE histogram data suggest for the kinetics of the division number structured cell distributions presented in table 1. This table specifies the total number of live cells, $N(t_i)$, and the number of cells divided that j times, $N_j(t_i),\ j = 0, 1, \ldots, 7$, at the indicated time $t_i,\ i = 0, 1, \ldots, 4$.

These data on the generation structure of proliferating cells can be used to estimate the division and death rate parameters using simpler ODE models of cell proliferation. We consider the following compartmental model of cell population growth of a Kendall type [21]. The rate of change of the population of live lymphocytes having undergone j divisions (which define the j-th compartment), $N_j(t)$, is modeled by the following system of ODEs,

$$\begin{aligned} &\frac{dN_0}{dt}(t) = -(\alpha_0 + \beta_0)N_0(t), \quad t > t_0, \\ &\frac{dN_j}{dt}(t) = 2\alpha_{j-1}N_{j-1}(t) - (\alpha_j + \beta_j)N_j(t), \quad j = 1, \ldots, J, \quad t > t_0. \end{aligned} \tag{3.11}$$

The model assumes that the per capita proliferation and death rates of T lymphocytes, α_j and β_j, depend on the number of divisions the lymphocytes performed. The term $2\alpha_{j-1}N_{j-1}(t)$ for $j \geq 1$ represents the cell birth (influx from the previous compartment

Table 1. The total number of live lymphocytes, N_i, and the distribution of lymphocytes with respect to the number of divisions they have undergone, N_i^J, at the indicated times t_i.

Time (days) t_i	Total number of live cells $N(t_i)$	Numbers of cells w.r.t. the number of divisions (j) they underwent $N_j(t_i)$							
		0	1	2	3	4	5	6	7
3	1.4×10^5	29358	22876	43372	39970	5208	98	14	0
4	2.5×10^5	16050	12600	22650	57025	96350	46950	2500	25
5	4.4×10^5	14476	14784	25344	58652	141460	156290	32076	440
6	5.0×10^5	13500	12150	24150	55000	137850	188950	69450	2150
7	5.7×10^5	13509	12198	21603	51927	140560	232160	96102	3420

because of division), whereas the $(\alpha_j + \beta_j)N_j(t)$ represents cell loss (outflux from the compartment) due to division and death. The population size at time t_0 is specified by initial data $N_j(t_0)$ with $t_0 = 72$ hours (i.e., data at day 3, cf. table 1). Model (3.11) allows an analytical solution which was used in the parameter estimation procedure.

The best-fit solution of the model (3.11) and the data set are shown in Fig. 8. The kinetics of cells which have undergone more than two divisions is consistently reproduced by the ODE model. The observed discrepancy between the model and data for undivided cells and cells with one or two divisions can be due to a large experimental and modeling error. In terms of the total population size the model perfectly matches the observed kinetics, see Fig. 7 (right). The computed best-fit value of the objective function is $\Phi \approx 1.27 \times 10^9$ which is about 0.59% of the squared l_2-norm of the data $\sum_{i=1}^{4}\sum_{j=0}^{7}(N_j^i)^2$. The best-fit estimates and their 95% CIs for the birth rates α_j are presented in Fig. 6. The model predicts that the division rate depends on the division age of the cells so that the discrete function $(\alpha_j,\ j = 0, 1, \ldots, 5)$ is bell-shaped. The estimated death rates β_j are shown in Fig. 7 (left). Our results suggest that a reliable estimation of the compartmental model parameters (α_j and β_j) is limited to those cell generations with the division age being two divisions less than the maximum number quantified in the CFSE assay. For example, the parameters α_6 and α_7 characterizing the division rate of cells that have undergone 6 and 7 divisions cannot be identified reliably from the finite series of data covering the division range from 0 to 7: the obtained best-fit estimates $\alpha_6 = 0.0226,\ \alpha_7 = 1.37$ are characterized by extremely large uncertainty intervals (a_7 is not shown in Fig. 6).

Two major conclusions can be drawn from the comparison of the PDE and ODE based CFSE data analysis: (i) the label-structured cell population balance model allows one a direct analysis of the raw CFSE histograms, and (ii) the accuracy of the parameter estimates (CIs) is much higher for the distributed PDE model.

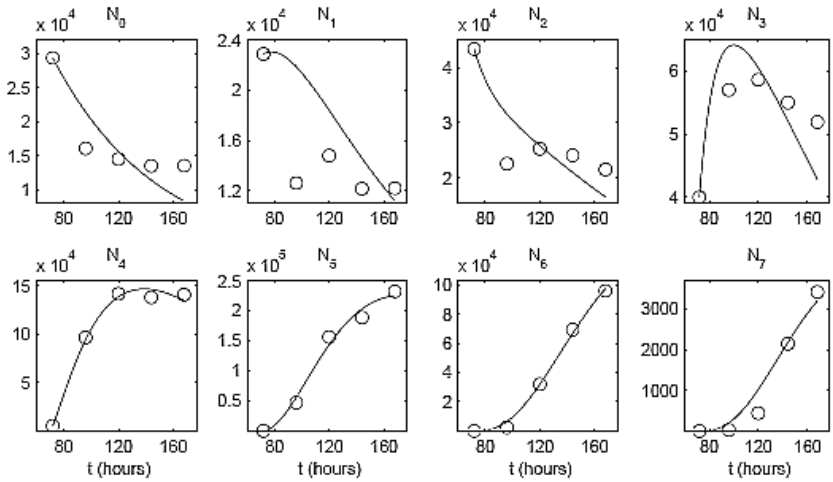

Figure 8. Experimental data set (cf. table 1) and the best-fit solution of the compartmental ODE model (3.11) for the generation structure of the dividing population. Experimental data are denoted by circles, the best-fit solution is denoted by solid lines. N_j is the number of cells that divided j times.

4. Modeling Cell Populations Structured by Two Fluorescence Markers

In order to understand the homeostatic turnover of cells in the immune system under normal conditions and during chronic infections, in vivo DNA labeling combined with multiparameter flow cytometry are used to follow the kinetics of activated cells in various tissues. An extensively documented example is provided by the non-human primate/SIV infection model [19, 28]. To quantify the short- and long-term in vivo dynamics of T-lymphocytes in SIV infection, two complementary labeling approaches are used in tandem:

- In vivo pulsing with the thymidine analogue BrdU, followed by quantification of $BrdU^+$ lymphocytes. BrdU incorporation allows precise determination of the fraction of cells in S-phase during the labeling period and their division rate. Tracing the numbers of labeled cells over time provides information on the survival and post-labeling proliferation and migration of the cells. The cycling cells can then be distinguished from non-cycling cells due to the successive loss of BrdU fluorescence with each cell division. Labeled cells are also characterized phenotypically by tagging them with antibodies that bind various cell surface molecules and counting cells with different markers using FACS analysis;

- Quantification of T cells expressing the cell-cycle associated nuclear antigen Ki-67. The expression of Ki-67 is more diffuse than that of BrdU, and gradually disappears after the last division cycle.

The kinetics of labeled cell subsets in blood and other tissues was monitored during labeling and post-labeling (data provided by L. Picker). Two-dimensional dot-plots of labeled

T lymphocytes in SIV infected monkeys at various days following a 1.5 day BrdU infusion are shown in Fig. 9 using a scaled colormapping, with red colors reflecting larger cell numbers. The plots characterize the BrdU/Ki-67 distribution of cells assessed by a combination of a short term BrdU labeling and the use of antibodies against BrdU and Ki-67 antigen for differential FACS counting.

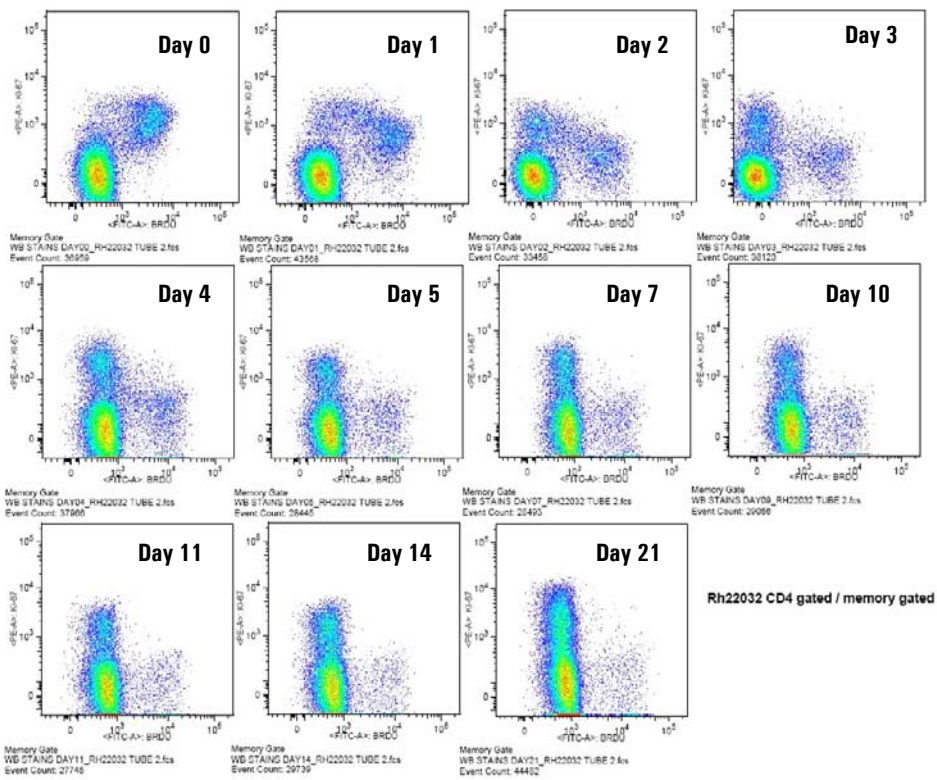

Figure 9. The evolution of BrdU/Ki-67 distributions of T-lymphocytes in blood of SIV infected monkey generated by flow cytometry analysis. The dot-plots of BrdU-labeled cells stained with antibodies against Ki-67 protein following 1.5 days BrdU labeling in vivo characterize the topography of cell distributions. (Data provided by L. Picker)

The simultaneous measurement of BrdU and Ki-67 allows one to discriminate the contributions of proliferative dilution versus cell death. The interpretation of such cell population data in mechanistic terms requires mathematical modeling and multi-parameter estimation. So far, the mathematical models developed for the parameter estimation of BrdU labeled cell populations were based upon a simple discrete classification of labeled or unlabeled cells, see for a review of such models for labeled and unlabeled cell population dynamics [18, 27].

To characterize the true heterogeneity of T-lymphocyte populations with respect to the expression of BrdU and Ki-67 for the in vivo labeling experiments, a finer resolution models are needed. To set up such a model, two approaches can be implemented: (i) a large set of ODEs, each describing the dynamics of a single subset of labeled cells characterized by

the same mean intensity of the marker, and (ii) hyperbolic PDEs of the type presented in the previous sections. In the next section we extend the basic single label-structured PDE model to two-fluorescence markers.

4.1. PDE Model for Double Labeled Cell Population

Let the vector $\mathbf{x} = [x_1, x_2]$ denote the fluorescence intensity of BrdU and Ki-67, and let the state function $n(t, \mathbf{x}) = n(t, x_1, x_2)$ represent the cell number distribution at time t with the expression level of BrdU and Ki-67 labels between $\mathbf{x}$ and $\mathbf{x} + \mathrm{d}\mathbf{x}$. The total number of cells is defined by the integral $N(t) = \int_0^{x_{1,\max}} \int_0^{x_{2,\max}} n(t, x_1, x_2) \mathrm{d}x_2 \mathrm{d}x_1$. The dynamics of the state distribution function of the initially BrdU-labeled population can be described with the following model (with $\overline{\gamma}\mathbf{x} \equiv [\gamma_1 x_1, \gamma_2 x_2]$)

$$\begin{aligned} &\frac{\partial n}{\partial t}(t, \mathbf{x}) - v_1(\mathbf{x}) \frac{\partial n}{\partial x_1}(t, \mathbf{x}) + v_2(\mathbf{x}) \frac{\partial n}{\partial x_2}(t, \mathbf{x}) = \\ &\qquad - (\alpha(\mathbf{x}) + \beta(\mathbf{x})) n(t, \mathbf{x}) + 2\alpha(\overline{\gamma}\mathbf{x}) \gamma_1 \gamma_2 n(t, \overline{\gamma}\mathbf{x}), \\ &\alpha(\overline{\gamma}\mathbf{x}) = \begin{cases} \alpha(\overline{\gamma}\mathbf{x}), & 0 \le x_1 \le x_{1,\max}/\gamma_1 \\ 0, & x_{1,\max}/\gamma_1 \le x \le x_{1,\max}. \end{cases} \end{aligned} \tag{4.1}$$

The structure of the model, which is a scalar hyperbolic PDE with two "space" variables, is similar to that we have already described, i.e. (2.1). The loss and accumulation of the labels is characterized by the rate functions $v_1(\cdot)$ and $v_2(\cdot)$. γ_1 and γ_2 are the parameters defining the relative decrease and increase in the level of expression of the BrdU and Ki-67 labels, respectively, on the daughter cells compared to the mother cells after one division. The fundamental assumption is that Ki-67 expression is amplified during division *multiplicatively* by some factor γ_2. The biology further suggests that the advection rate functions and the dilution coefficients have the following properties $v_i(\mathbf{x}) \ge 0, \quad x_i \in (0, x_{i,\max}], \quad v_i(\mathbf{0}) = 0, \quad i = 1, 2$, and $1 < \gamma_1 \le 2, \quad 0 < \gamma_2 < 1$.

4.2. The (Forward) Prediction Problem

To use the above model of BrdU dilution for predictions, the initial-boundary conditions have to be provided. We illustrate how they can be plausibly constructed.

- The initial condition at time $t = 0$ has to be specified in the domain

  $$[0,\ x_{1,\max}] \times [0,\ x_{2,\max}].$$

  If we assume that at the beginning of the experiment cells express only the first label, x_1, and no label x_2, then the corresponding initial condition reads

  $$n(0, x_1, 0) \ne 0, \quad n(0, x_1, x_2) = 0, \quad x_2 > 0.$$

- Two boundary conditions have to be given. For the *first boundary condition* we refer to the time dependence of cells, which do not express Ki-67 antigen but are BrdU labeled

  $$n(t, x_1, 0) = N_0 f(x_1) \mathrm{e}^{-a_s t}, \quad t > 0. \tag{4.2}$$

Here $N_0 \in \mathbb{R}^+$ is the total number of cells at $t = 0$. It is assumed to decline exponentially at some rate a_s, related to the kinetics of entering the S phase in which the label x_2 (Ki-67) is expressed. The function $f(x_1)$ characterizes the distribution of BrdU labeled cells starting the division, e.g. it could be described as a bell-shaped function around some value x_1 close to $x_{1,\max}$, see Fig. 10.

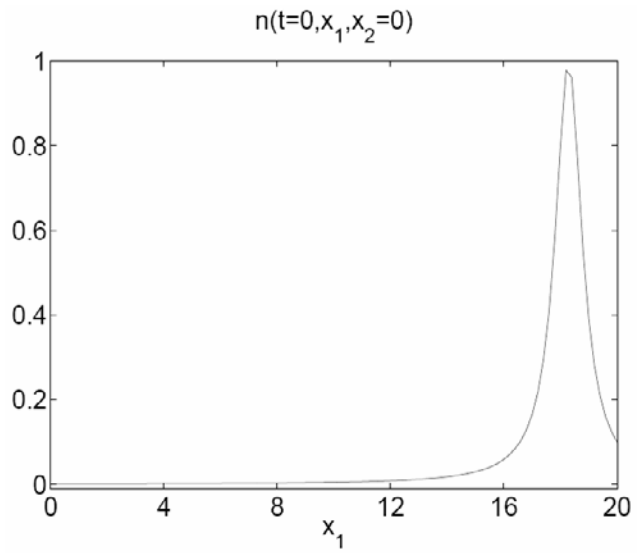

Figure 10. The localized initial condition $n(0, x_1, 0)$ for model 4.1

For the *second boundary condition* we consider the following one,

$$n(t, x_{1,\max}, x_2) = 0, \quad t > 0. \tag{4.3}$$

It says that for all $t > 0$ there are no cells expressing more than $x_{1,\max}$ units of BrdU molecules, irrespectively of x_2.

For the numerical solution of the initial-boundary value problem for the model (4.1), an extension of the Lax-Wendroff scheme to 2D hyperbolic PDEs can be used. It was implemented following the approach described in [26]. The CFL stability condition in this case reads

$$\left(\frac{v_1\Delta_t}{\Delta_{x_1}}\right)^2 + \left(\frac{v_2\Delta_t}{\Delta_{x_2}}\right)^2 \leq 1. \tag{4.4}$$

To illustrate the performance of the model, we present here the simulated evolution of the two labels-structured cell population using the following parameter values:

$$v_1 = 0.1,\ v_2 = 1, \quad \alpha = 0.1,\ \beta = 0.01,\ \gamma_1 = 2,\ \gamma_2 = 0.5, \quad x_{1,\max} = 20, x_{2,\max} = 10.$$

The initial condition was taken as

$$n(0, x_1, 0) = \frac{1}{1+y^2}, \quad y = \frac{35x_1}{x_{1,\max}} - 32, \quad n(0, x_1, x_2 > 0) = 0.$$

The boundary conditions for $t > 0$ were

$$n(t, x_1, 0) = \frac{\mathrm{e}^{-0.1t}}{1 + y^2}, \quad y = \frac{35x_1}{x_{1,\max}} - 32,$$
$$n(t, x_{1,\max}, x_2) = 0.$$

The model solutions computed for $t = 5,\ 10,\ 20,\ 30$ are shown as two-dimensional cell distribution functions in Fig. 11. We observe the cohort-type behavior of cells that is characterized by the acquisition of the second label (Ki-67) going in parallel with the dilution of the first label (BrdU).

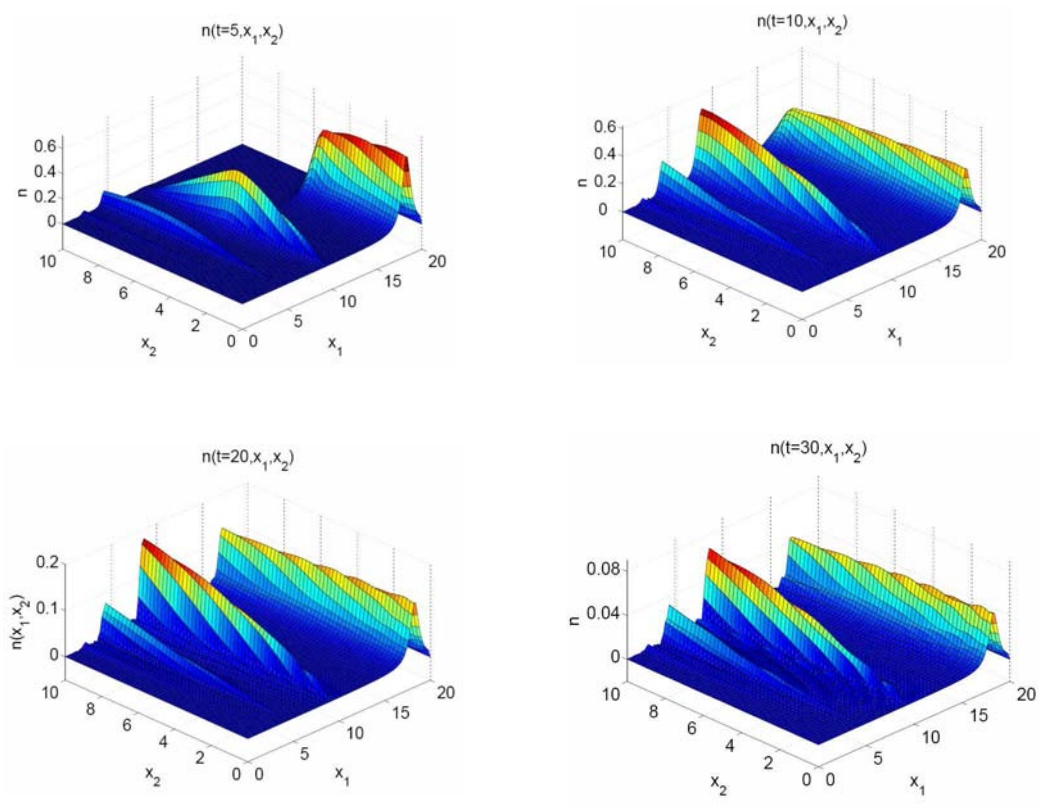

Figure 11. Solutions of model (4.1) at times $t = 5,\ 10,\ 20,\ 30$ computed using the uniform 2D mesh $[0 : 0.2 : 20] \times [0 : 0.2 : 10]$. The corresponding parameter values and the initial-boundary conditions are described in the text.

4.3. Large-Scale ODE Model for the Microdynamics of Double-Labeled Cell Populations

Here we give an example of a simple compartmental model that investigates the dynamics of cells that had been labeled in vivo with BrdU and then were traced, with high resolution

in terms of their BrdU content and level of Ki67 expression. The immunology underlying the burst-type model has been recently discussed in [19]. The biological model considers the population dynamics of the resting $R(t)$, activated $A(t)$, and differentiated effector cells $E1(t),\ E2(t),\ E3(t)$, differing in the degree of their differentiation. The set of ODEs describing the steady-state kinetics of these cell subsets is

$$\begin{aligned}
\frac{dR}{dt} &= rE_3 - aR \\
\frac{dA}{dt} &= aR + pA - (e_1 + e_2 + e_3)A \\
\frac{dE1}{dt} &= e_1 A - d_1 E1 \\
\frac{dE2}{dt} &= e_2 A - d_2 E2 \\
\frac{dE3}{dt} &= e_3 A - (d_3 + r)E3.
\end{aligned} \tag{4.5}$$

Close examination of the flow cytometry data for each functionally defined cell compartment shows that in every cell population, not only the cell numbers but also the distributions of intensities of incorporated BrdU and expressed Ki-67 are changing with time and their dynamics provides information regarding rates of division and of elimination of these cells. The heterogeneity of intensities is modeled by a subdivision into a number of subcompartments, each corresponding to a different narrow interval of BrdU and Ki-67 levels. The typical range of BrdU expression observed in SIV infected monkeys after short term labeling allows subdivision into 8 bins, corresponding to 7 two-fold dilution steps (7 division cycles), and Ki-67 intensities are divided into 7 bins. Therefore, the dot-plot data on cell distributions can be approximated by a set of 8x7 cell compartments differing in the fluorescence intensities, see Fig. 12.

The corresponding fine resolution model is thus formulated by splitting the cell populations $\mathbf{Y} \equiv [R, A, E1, E2, E3]$ into 56 subsets, each parameterized by the BrdU and Ki-67 bin identifiers $b = 0, 1, \ldots, 7, \quad k = 0, 1, \ldots, 6$ as $R_{b,k}, A_{b,k}, E1_{b,k}, E2_{b,k}, E3_{b,k}$. The set of equations (4.5) thus expands into a system of 280 ODEs describing the microdynamics of the labeled cell compartments. This high-dimensional system of equations describes the BrdU labeling and Ki-67 antigen expression of turning over T-lymphocytes and takes into account the differences in the fluorescence intensities of these cells.

Let t_1 be the duration of labeling and let ϵ be the sum of the rates at which activated cells become effectors: $\epsilon := e_1 + e_2 + e_3$. Furthermore, we define as L_j the probability for a cell to become labeled with sufficient BrdU to be in BrdU bin j upon division during the labeling phase ($t < t_1$). $C_j = \sum_{k=0}^{j-1} L_k$, $j = 0, 1, ..., 7$ is the probability of obtaining less BrdU than required for bin j. Finally, let d be the rate at which cells that stopped dividing go from one Ki-67 bin to the next lower one (that is, d is the discretized Ki-67 decay rate).

The large-scale ODE system then reads as

$$
\begin{aligned}
&R'_{i,0} = -aR_{i,0} + dR_{i,1} + rE3_{i,0}, \quad i = 0, 1, \dots 7,\\
&R'_{i,j} = -(a+d)R_{i,j} + dR_{i,j+1} + rE3_{i,j}, \quad i = 0, 1, \dots 7, \quad j = 1, \dots 5,\\
&R'_{i,6} = -(a+d)R_{i,6} + rE3_{i,6}, \quad i = 0, 1, \dots 7,
\end{aligned}
$$

$$
\begin{aligned}
&A'_{i,0} = -(\epsilon+p)A_{i,0} + dA_{i,1} + aR_{i,0}, \quad i = 0, 1, \dots 7,\\
&A'_{i,j} = -(\epsilon+p+d)A_{i,j} + dA_{i,j+1} + aR_{i,j}, \quad i = 0, 1, \dots 7, \quad j = 1, \dots 5,\\
&A'_{0,6} = -(\epsilon+p+d)A_{0,6} + aR_{0,6} + 2p\Big(L_0 \sum_{k=0}^{6} A_{0,k} + C_1 \sum_{k=0}^{6} A_{1,k}\Big), \quad \text{if} \quad t \le t_1,\\
&A'_{0,6} = -(\epsilon-p+d)A_{0,6} + aR_{0,6} + 2p\Big(\sum_{k=0}^{5} A_{0,k} + \sum_{k=0}^{6} A_{1,k}\Big), \quad \text{otherwise},\\
&A'_{i,6} = -(\epsilon+p+d)A_{i,6} + aR_{i,6} + 2p\sum_{k=0}^{6}\Big(L_i \sum_{j=0}^{i} A_{j,k} + C_{i+1}A_{i+1,k}\Big),\ i = 1, \dots, 6, \quad \text{if } t \le t_1,\\
&A'_{i,6} = -(\epsilon-p+d)A_{i,6} + aR_{i,6} + 2p\sum_{k=0}^{6} A_{i+1,k}, \quad i = 1, \dots, 6, \quad \text{otherwise},\\
&A'_{7,6} = -(\epsilon+p+d)A_{7,6} + aR_{7,6} + 2pL_7 \sum_{i=0}^{7}\sum_{k=0}^{6} A_{i,k}, \quad \text{if} \quad t \le t_1,\\
&A'_{7,6} = -(\epsilon-p+d)A_{7,6} + aR_{7,6}, \quad \text{otherwise},
\end{aligned}
$$

$$
\begin{aligned}
&E1'_{i,0} = -d_1E1_{i,0} + dE1_{i,1} + e_1A_{i,0}, \quad i = 0, 1, \dots 7,\\
&E1'_{i,j} = -(d_1+d)E1_{i,j} + dE1_{i,j+1} + e_1A_{i,j}, \quad i = 0, 1, \dots 7, \quad j = 1, \dots 5,\\
&E1'_{i,6} = -(d_1+d)E1_{i,6} + e_1A_{i,6}, \quad i = 0, 1, \dots 7,
\end{aligned}
$$

$$
\begin{aligned}
&E2'_{i,0} = -d_2E2_{i,0} + dE2_{i,1} + e_2A_{i,0}, \quad i = 0, 1, \dots 7,\\
&E2'_{i,j} = -(d_2+d)E2_{i,j} + dE2_{i,j+1} + e_2A_{i,j}, \quad i = 0, 1, \dots 7, \quad j = 1, \dots 5,\\
&E2'_{i,6} = -(d_2+d)E2_{i,6} + e_2A_{i,6}, \quad i = 0, 1, \dots 7,
\end{aligned}
$$

$$
\begin{aligned}
&E3'_{i,0} = -(d_3+r)E3_{i,0} + dE3_{i,1} + e_3A_{i,0}, \quad i = 0, 1, \dots 7,\\
&E3'_{i,j} = -(d_3+r+d)E3_{i,j} + dE3_{i,j+1} + e_3A_{i,j}, \quad i = 0, 1, \dots 7, \quad j = 1, \dots 5,\\
&E3'_{i,6} = -(d_2+r+d)E3_{i,6} + e_3A_{i,6}, \quad i = 0, 1, \dots 7.
\end{aligned}
\tag{4.6}
$$

Here the sign $'$ denotes the derivative. The steady state assumption on the populations imposes the following constraint on the parameter values:

$$p = \epsilon - \frac{re_3}{d_3 + r}. \tag{4.7}$$

The complete vector of estimated parameters of the large scale model includes a number of additional parameters, which represent the transition probabilities between the subcompartments after single division.

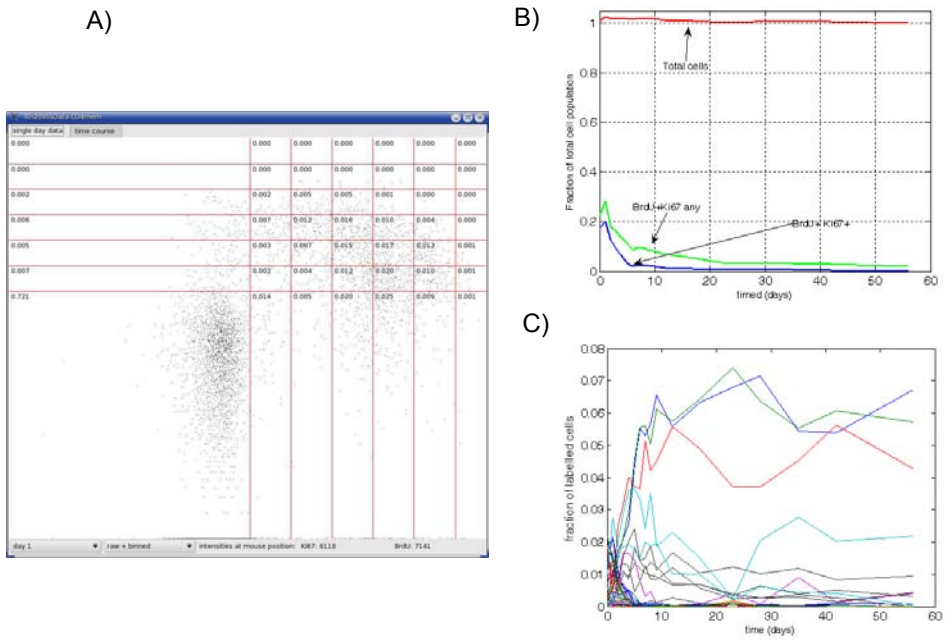

Figure 12. Example of cell compartments associated with different levels of BrdU and Ki-67 fluorescence intensities in blood of SIV infected monkey. A) Each dot represents a single cell with a specific intensity of Ki67 and BrdU staining B) Microdynamics of individual cell compartments. C) Macrodynamics of the lumped cell compartments

Figure 13 shows the flow cytometry data and the model prediction of the short-term labeling kinetics for some roughly estimated set of parameter values: $r = 0.94$, $a = 0.041$, $d = 2.67$, $e_1 = 1.44$, $e_2 = 0.074$, $e_3 = 0.43$, $d_1 = 0.24$, $d_2 = 0.034$, $d_3 = 0.13$, $L_j = 0.125, \quad j = 0, ..., 7$. The homeostatic proliferation rate p takes the value ~ 1.56. The labeling data represent the sum of the functionally distinct cell compartments with the same fluorescence intensity b, k.

5. Conclusion

The major objective of our study, inspired by the development and broad application of the labeling and flow cytometry experimental tools, was to advance PDE based mathematical modeling of the kinetics of heterogeneous cell populations and to facilitate the estimation of cell turnover parameters. Using an original CFSE data set, we demonstrated the biological consistency of the proposed single label-structured model and compared its predictions to the predictions of the ODE compartmental model (see for further details [21, 22]). The (single- and double-) label structured models offer the following potential advantages with respect to existing compartmental models: (i) they allow to estimate the kinetic parameters of cell proliferation and death as functions of the label or marker expression level (and hence of the number of cell divisions) directly from the distributions of labeled cells followed

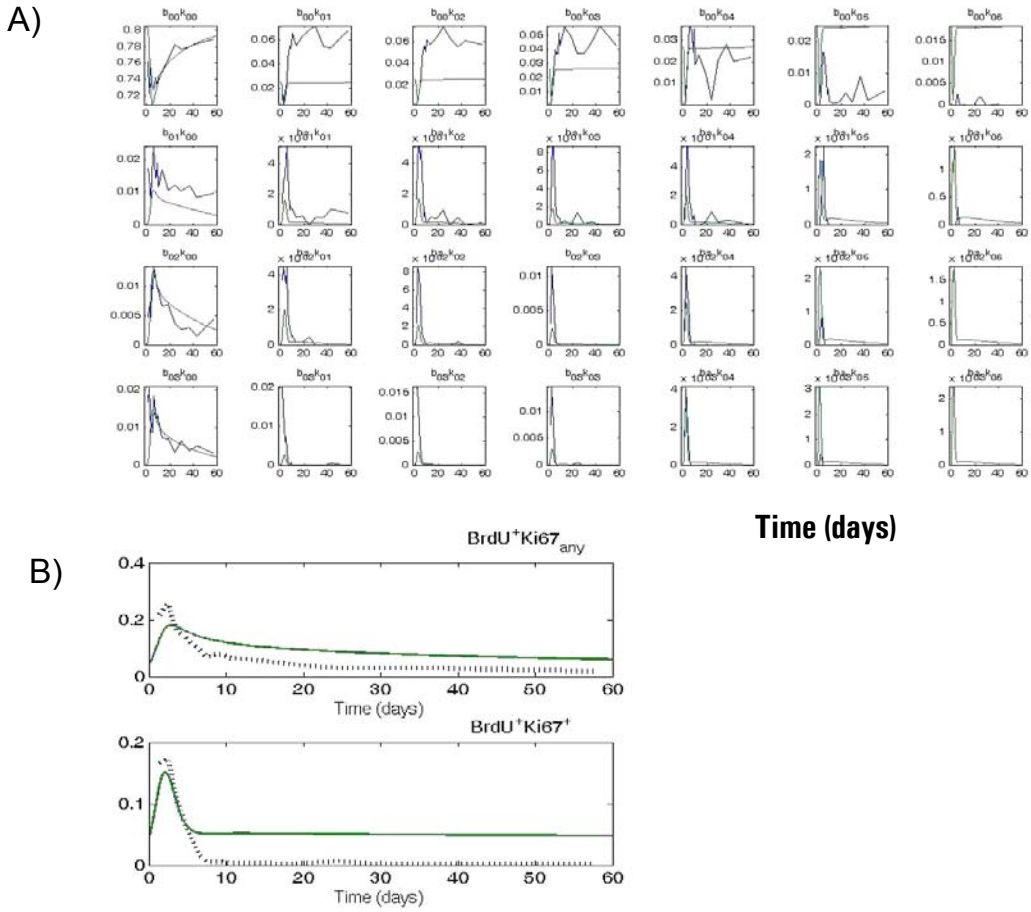

Figure 13. Flow cytometry data and the prediction by the large-scale model (smooth curves) of the (A) microdynamics and (B) macrodynamics of T-lymphocytes heterogeneous with respect to BrdU and Ki-67 label intensity in SIV infected monkeys.

over time by flow cytometry; (ii) they do not require ad hoc estimates of the relationship between the label expression level and the number of divisions that cells have undergone. Note that this is an important advantage for a long-term follow-up of labeled populations as the correspondence between the marker intensity range and the division generation becomes increasingly blurred by the overall loss of the label over time and by the initial heterogeneity of the labeled cell population.

Modeling with hyperbolic PDEs, in the context of data-driven parameter identification, presents a significant computational challenge due to the hyperbolic nature of the equations and to the large size of the discretized problem. To our knowledge, no publicly available software packages exist which deal with optimization of hyperbolic PDE models. We formulated a computational methodology for modeling and parameter estimation of single-label structured cell populations. The numerical treatment of both the direct and inverse problems for heterogeneous cell populations, structured by two labels, is computationally

more challenging. The time required to solve the initial-boundary value problem with an extension of the Lax-Wendroff scheme for a hyperbolic PDE with two space dimensions is few orders of magnitude larger than for a single label hyperbolic PDE model. Therefore further research is necessary to develop a more efficient solver for the two-dimensional PDE models to be used in real-life parameter estimation problems.

Acknowledgements

The authors thankfully acknowledge financial support provided by the U.S. Civilian Research and Development Foundation (Award RUX1-2710-MO-06), the Russian Foundation of Basic Research (RFBR) and the Ministry of Flanders Programme "Bilateral scientific cooperation" (RFBR-MF-05-01-02853-MF-a), and the RFBR Grant RFBR-05-01-00732.

References

[1] N R Abu-Absi, A Zamamiri, J Kacmar, S J Balogh, and F Srienc. Automated flow cytometry for acquisition of time-dependent population data. *Cytom Part A*, **51**:87–96, 2003.

[2] B Asquith, C Debacq, A Florins, N Gillet, T Sanchez-Alcaraz, A Mosley, and L Willems. Quantifying lymphocyte kinetics in vivo using carboxyfluorescein diacetate succinimidyl ester (CFSE). *Proc R Soc B*, **273**:1165–1171, 2006.

[3] C T H Baker, G A Bocharov, C A H Paul, and F A Rihan. Computational modelling with functional differential equations: identification, selection and sensitivity. *Appl Numer Math*, **53**:107–129, 2005.

[4] H T Banks. Some remarks on estimation techniques for size-structured population models. In *Lect. Notes Biomath.*, volume 100. Springer, Berlin, 1994.

[5] H T Banks and B G Fitzpatrick. Statistical methods for model comparizon in parameter estimation problems for distributed systems. *J Math Biol*, **28**:501–527, 1990.

[6] H T Banks and B G Fitzpatrick. Estimation of growth rate distributions in size structured population models. *Q Appl Math*, **XLIX**(2):215–235, 1991.

[7] H T Banks, S Reich, and I G Rosen. An approximation theory for the identification of nonlinear distributed parameter systems. *SIAM J Control Optim*, **28**:552–569, 1990.

[8] G I Bell and E C Anderson. Cell growth and division I. A mathematical model with application to cell volume distributions in mammalian suspension cultures. *Biophys J*, **7**:330–351, 1967.

[9] S Bernard, L Pujo-Menjouet, and M C Mackey. Analysis of cell kinetics using a cell division marker: mathematical modelling of experimental data. *Biophys J*, **84**:3414–3424, 2003.

[10] A Bertuzzi, A Gandolfi, and R Vitelli. Influence of cell loss in the analysis of proliferating populations by flow cytometry. *Math Biosc*, **82**:257–260, 1986.

[11] R J De Boer, V V Ganusov, D Milutinovic, P D Hodgkin, and A S Perelson. Estimating lymphocyte division and death rates from CFSE data. *Bul Math Biology*, **68**(5):1011–1031, 2006.

[12] R J De Boer and A S Perelson. Estimating division and death rates from CFSE data. *J Comput Appl Math*, **184**(1):140–164, 2005.

[13] O Diekmann, H J M Heijmans, and H R Thieme. On the stability of the cell size distribution. *J Math Biol*, **19**:227–248, 1984.

[14] V V Ganusov, D Milutinovic, and R J De Boer. Il-2 regulates expansion of $CD4^+$ T cell populations by affecting cell death: insights from modelling CFSE data. *J Immunol*, **179**:950–957, 2007.

[15] V V Ganusov, S S Pilyugin, R J De Boer, K Murali-Krishna, R Ahmed, and R Antia. Quantifying cell turnover using CFSE data. *J Immunol Methods*, **298**:183–200, 2005.

[16] N Gershenfeld. *The Nature of Mathematical Modelling*. Cambridge University Press, 2002.

[17] A V Gett and P D Hodgkin. A cellular calculus for signal integration by T cells. *Nat Immunol*, **1**:239–244, 2000.

[18] Z Grossman, R B Herberman, and D S Dimitrov. T cell turnover in SIV infection. *Science*, **284**:555a–555d, 1999.

[19] Z Grossman, M Meier-Schellersheim, W E Paul, and L J Picker. Pathogenesis of HIV infection: what virus spares is as important as what it destroys. *Nature Medicine*, **12**(3):289–295, 2006.

[20] K Leon, J Faro, and J Carneiro. A general mathematical framework to model generation structure in a population of asynchronously dividing cells. *J Theor Biol*, **229**:455–476, 2004.

[21] T Luzyanina, S Mrusek, J T Edwards, D Roose, S Ehl, and G Bocharov. Computational analysis of CFSE proliferation assay. *J Math Biol*, **54**(1):57–89, 2007.

[22] T Luzyanina, D Roose, T Schenkel, M Sester, S Ehl, A Meyerhans, and G Bocharov. Numerical modelling of label-structured cell population growth using CFSE distribution data. *Theor Biol Math Mod*, **4**:26, 2007.

[23] A B Lyons. Divided we stand: tracking cell proliferation with carboxyfluorescein diacetate ester. *Immunol Cell Biol*, **77**:509–515, 1999.

[24] Matlab. http://www.mathworks.com/.

[25] R Mehr, G Shahaf, A Sah, and M Cancro. Asynchronous differentiation models explain bone marrow labelling kinetics and predict reflux between the pre- and immature B cell pools. *Int Immunol*, **15**(3):301–312, 2003.

[26] K W Morton and D D Mayers. *Numerical solution of partial differential equations*. Cambridge University Press, Cambridge, 1994.

[27] A S Perelson. Modelling viral and immune system dynamics. *Nature Rev Immunol*, **2**(1):28–36, 2002.

[28] L J Picker, S I Hagen, R Lum, E F Reed-Inderbitzin, L M Daly, A W Sywester, J M Walker, D C Siess, M Jr Piatak, C Wang, D B Allison, V C Maino, J D Lifson, T Kodama, and M K Axthelm. Insufficient production and tissue delivery of $CD4^+$ memory T cells in rapidly progressive simian immunodeficiency virus infection. *J Exp Med*, **200**(10):1299–1314, 2004.

[29] K Schittkowski. *Numerical Data Fitting in Dynamical Systems*. Kluwer Academic Publishers, Dordrecht, 2002.

[30] L Shampine. Solving hyperbolic PDEs in MATLAB. *Appl Numer Analysis and Comput Math*, **2**(3):346–358, 2005.

[31] J W Sinko and W Streifer. A model for populations reproducing by fission. *Ecology*, **52**:330–335, 1971.

[32] J A Smith and L Martin. Do cell cycle? *Proc Nat Acad Sci USA*, **70**(4):1263–1267, 1973.

[33] F Srienc. Cytometric data as the basis for rigorous models of cell population dynamics. *J Biotechnol*, **71**:233–238, 1999.

[34] A Yates, C Chan, J Strid, S Moon, R Callard, A J George, and J Stark. Reconstruction of cell population dynamics using CFSE. *BMC Bioinformatics*, **8**:196, 2007.

In: Mathematical Biology Research Trends
Editor: Lachlan B. Wilson, pp. 175-192
ISBN 978-1-60456-141-8

Chapter 6

IMMUNO-EPIDEMIOLOGY AND HIV/AIDS: A MODELING PERSPECTIVE

***Swati DebRoy**[*] **and Maia Martcheva**[†]*
Department of Mathematics, University of Florida, 358 Little Hall,
PO Box 118105, Gainesville, FL 32611–8105

Abstract

In this article we review a number of immunological models of HIV as well as the contribution of mathematical immune modeling of HIV to understanding of HIV. We also review a number of epidemiological models, particularly those of HIV. The focus of this review is the development of novel immuno-epidemiological models which link immunological and epidemiological models. We first review a simple immuno-epidemiological model of transient disease (a disease where infected individuals necessarily recover), and then we introduce an immuno-epidemiological model of HIV. We discuss the drawbacks of this simple immuno-epidemiological model as well as methods to address them. We introduce and discuss several other models and their advantages and disadvantages. In the discussion we focus on the types of questions that can be addressed with immuno-epidemiological models and how those can contribute for the development of mathematical biology.

Keywords: HIV, AIDS, immunology, epidemiology, immuno-epidemiology, nested models.

AMS Subject Classification: 92D30

1. Introduction

Mathematical modeling of within-host dynamics (Immunology) and between-host dynamics (Epidemiology) was treated separately for a long time. Within-host models explore the natural selection within a single host where pathogens compete for uninfected host cells

[*]E-mail address: swati@math.ufl.edu. (author for correspondence)
[†]E-mail address: maia@math.ufl.edu

whereas the epidemiological models explore the competition between pathogens for uninfected hosts. But the most successful pathogens are those that are able to balance trade-offs between intra-host virulence and inter-host transmission [9]. Successful invasion and colonization of a single host by a parasite does not necessarily imply that it can optimally spread in the uninfected host population. Thus both immunological and epidemiological models are limited in terms of biological realism. To incorporate further biological realism and also to allow for proper mathematical analysis, researchers developed the nested models structured by the age-since-infection. This approach strings together both these interdependent scales of host-parasite co-evolution. Immunological and epidemiological aspects of *micro-parasitic* infections were first considered together by Anderson in [13]. But Gilchrist and Sasaki [4] introduced the nested model approach where the epidemiological model is an SIR model structured according to the age-since-infection and the immunological model is a simple prey-predator model. Early immuno-epidemiological models were developed to study *macro-parasitic* diseases. For instance, R. J. Quinnell's paper studies human hookworm infection. These studies, structured by host age, represent community-based surveillance of immune responses, mounting of protective immunity, and re-infections. In this context immuno-epidemiology is the study of the distribution of immune responses and infection in populations, and of the factors influencing this distribution. In other words, immuno-epidemiology represents taking an epidemiological approach to immunology [14]. In this paper we consider immunological, epidemiological and immuno-epidemiological models addressing the advantages and disadvantages of each as discussed in the review articles of Bonhoeffer, Coffin and Nowak [1], Hethcote [5] and others. We discuss the suitability of the classical within-host and between-host models when applied to HIV/AIDS and the possibility to include further details of this disease. We study the characteristics of a simple nested model as in the paper of Gilchrist and Sasaki [4], and propose possible modifications to suit HIV.

2. Typical "Building Blocks": Immunological and Epidemiological Models

Most generally within-host immunological models include state variables such as virus load, uninfected cells, infected cells and also differentiated elements of the immune response, i.e. T-cells, B-cells, antibodies etc. These models deal with a single infection where the initial pathogenic load and immune status is arbitrarily assigned. The difference between an innate immune response and an adaptive immune memory response developed through prior exposure to the pathogen is often ignored. These models typically assume density dependent transmission and homogeneous mixing of host cells, which is necessary to allow proper analysis. More importantly they ignore the different amounts of virus that is transmitted during infection, superinfections and coinfections. Consider a simple example of a within-host model for HIV [1] including state variables, x for density of infectible (susceptible) cells (this variable describes the number of activated CD4 cells), y for density of virus producing cells. Furthermore, the parameters for the various rates are: rate of creation of infectible cells - λ, rate of infection of uninfected cells - β, natural death rate of susceptible cells - d, and death rate of infected cells - a. The model takes the form:

$$\begin{aligned} x' &= \lambda - dx - \beta xy \\ y' &= \beta xy - ay - pyz \\ z' &= ky - bz \end{aligned} \tag{2.1}$$

where p is the killing rate of virus producing cells by Cytotoxic T Lymphocytes (CTL), z is the density of the CTL response against the virus infected cells, k is the rate of stimulation of CTL, and b is death rate of CTL. Analysis of this model under definite conditions reveal that individuals with a weak CTL response have a less reduction of virus load compared to the ones with high CTL response under a certain drug therapy [1]. Mathematical modeling of the in-vivo dynamics of HIV/AIDS has influenced our understanding of the HIV pathogenesis [8]. Before modeling was applied, AIDS was thought to be a slow progressing disease in which delayed treatment was not a major problem. Hence patients were monitored only once every six months. But application of quite trivial mathematics created a revolution about the perception of HIV. Calculations in [8] have concluded that at least 10^{10} virus particles are produced and released into bodily fluids in a single day within an average HIV infected person. Considering the calculated virus generation time of about 1.8 days, HIV can go through 200 replication cycles per year inside a single host with a possibility of mutation at each replication. This easily explains the rapid evolution of HIV. This result showed that a single drug intended for a few mutations was not going to be sufficient ever, and hence the present concept of a combination of antiretroviral drugs was applied to the treatment of HIV. Also the necessity of initiating treatment at the earliest after diagnosis was established. Hugely increased interest in this topic and extensive study soon exposed the limitations of these models. From [10] we know that coinfection is an important aspect in HIV and [11] indicates possibility of superinfection in HIV. The epidemiological aspects of these two mechanisms cannot be incorporated within immunological models. When considering application of medicine to HIV patients, Perelson and Nelson [8] have not included the spatial and compartmental aspects of the body and have implicitly assumed that the drug is available everywhere at a constant effectiveness. Parts of the body like the brain, where the immune system has limited access and the testes, where drug penetration is poor, can act like sanctuaries for the virus. Inclusion of these aspects would complicate the model to a great extent.

The population level *epidemiological* models are mostly used to study population immunity and various vaccination-related results obtained from these are important to public health projects. These models include a susceptible class and may include several recovered classes such as immune class, vaccinated class etc. according to the need of the disease being modeled [5]. Some models incorporate the differences in the immune status of the hosts by dividing the host population into classes according to different levels of parasite-specific immunity and cross immunity. This, however, leads to models which are not analyzable to a great extent. Now we consider a basic epidemic model consisting of the number of individuals in the susceptible class- S, the number of individuals in the infectious class I,

and the number of individuals in recovered class R. The model is given by

$$\begin{aligned} S' &= -\beta \frac{SI}{N} \\ I' &= -\beta \frac{SI}{N} - \gamma I \\ R' &= \gamma I \end{aligned} \tag{2.2}$$

together with the following initial conditions: $S(0) = S_0$, $I(0) = I_0$, $R(0) = R_0$. The total population number N is given by $N(t) = S(t) + I(t) + R(t)$. In addition, β is the rate of infection and γ is the rate of recovery [5]. Here we do not consider the passively immune infants and the exposed class as separate classes. Similar population level models have been extensively studied for HIV. May and Anderson have considered age-structured models for HIV and have calculated the basic reproduction ratio $\mathcal{R}_0$ for simple HIV transmission models [6]. They have also studied the demographic effects of AIDS in African countries [7]. HIV models often unrealistically assume that the population is uniform and there is homogeneous interaction. Transmissible interaction in the population, however, depends on age. HIV being a sexually transmitted disease, horizontal (host-to-host) transmission only takes place among adults, and children are usually vertically (mother-to-child) infected. There is also a greater chance of infection among people who share needles for taking drugs. Moreover, different geographic and socio-economic groups have different contact rates, which is especially true for HIV.

In general, the epidemiological models are used in calculating the reproduction number which in turn could provide an estimate of the herd immunity for a certain disease. This and other information derived from the epidemiological level models have proved crucial for application of vaccines in public health projects for several infectious diseases. In the case of HIV though, the within-host parasite situation is intertwined with the transmission between hosts; hence finding accurate vaccine related results from epidemiological HIV models is difficult. Epidemiological HIV models can be structured by the time-since-infection as the infectivity of an individual is dependent on how long that person has been infected. In case of HIV, an individual is most infective during the period it shows symptoms, which is usually 2 to 6 weeks after getting infected. In models of other diseases, the time-since-recovery is sometimes used as the structure to account for the loss of immunity with time. This is immaterial for HIV since immunity for HIV is apparently present only in a negligible fraction of the world population, and recovery is not known, hence can be ignored. However, epidemiological HIV models are unable to incorporate the virus load and the dependence of transmissibility of HIV on this virus load. Besides, the dynamic nature of host-parasite co-evolution that influences the genetic variability of the parasite population and its transmissibility is not accounted for.

3. One Scale vs Multi-Scale Models

Immunological and epidemiological models give dynamical description of the living world on two different scales: the within-host scale where the participants are cells and virus

particles, and the epidemiological scale where participants are complex multicellular organisms. Because of the complexity of structure and function on each level, this concentration of modeling to one scale is very typical. The investigations are restricted to the given scale and different scales are often studied by different biological disciplines. Mathematical modeling has strongly paralleled that. Ordinary and partial differential equations have contributed enormously to the understanding of biological systems, particularly at a given scale. The body of literature applying such models to understanding the immunology, and epidemiology, each at their own scale, is immense.

Many biological processes, however, involve several levels of organization. Phenomena on each level have impact on phenomena on other levels. In infectious diseases, pathogens change their genetic and antigenic characteristics (mutate) during replication within a cell. This causes an individual's immune system to shift from experienced to naive. The pathogen strain that dominates on a population level depends on which of the mutants has had the ability to evade the particular host's immune system and has transmitted better. Biological processes, whose outcome depends on multiple cross-scale mechanisms, have to be investigated through mathematical models that involve linking multiple scales with different dynamical variabilities. Such multi-scale dynamic models are seldom developed, particularly so in regard to infectious diseases. The main approach used most often in multi-scale modeling is computational. Simple dynamic models that link several scales, e.g. immunological and epidemiological, can lead to simple principles just as early simple models lead to the concept of the reproduction number [15].

4. Immuno-Epidemiology

Immuno-epidemiology bridges the gap between immunology and epidemiology in the empirical studies and mathematical and theoretical approaches. It investigates the influence of population immunity on epidemiological patterns. Immuno-epidemiology seeks to translate individual characteristics like immune status and virus load to population level and traces their epidemiological significance [2]. It can also help to understand the dynamics of recurrent diseases and the dynamic variability of the immunity acquired due to previous exposure to the disease within the host population. Gilchrist and Coombs [9] try to understand the conditions where the within-host and between-host selection are not in conflict. Their results show that the usual assumption that both virulence and transmission increase with increase in parasite load does not always cause conflict in the selection priorities in the between-host and within-host levels.

Generally a nested immuno-epidemiological model consists of a simple ODE model of the within host immune response with compartments for the parasite load, immune response (T or B cells) and/or immune memory cell load as considered before in Section 2. Consider a simple example from [4]. Let τ be the time since infection, $P(\tau)$ - the within host size of parasite population, $B(\tau)$ - the immune response cells which recognize the parasite (T or B cells). The immunological model is then given by:

$$\begin{aligned} P' &= (r - eB)P \\ B' &= aBP \end{aligned} \tag{4.3}$$

Parameters are: r- per capita parasite within-host replication rate, a - immune response activation rate, e - parasite mortality rate caused by immune response cells.

A simple PDE system structured by the time-since-infection τ is considered for the epidemiological model. The disease under consideration leads to recovery which is modeled typically by a model of the SIR type. Denoting by S the susceptible individuals, by $I(\tau, t)$ the density of infected individuals structured by the time-since-infection τ, by R - the recovered individuals, and by N - the total population size, we have the following epidemiological model:

$$\begin{aligned} \frac{dS}{dt} &= bN - S\int_0^T \beta(\tau)I(\tau,t)d\tau - dS \\ \frac{\partial I}{\partial t} + \frac{\partial I}{\partial \tau} &= -(\alpha(\tau) + \iota(\tau) + d)I \\ I(0,t) &= S\int_0^T \beta(\tau)I(\tau,t)d\tau \\ \frac{dR}{dt} &= I(T,t) - dR \end{aligned} \tag{4.4}$$

The parameters are: b - per capita population level birth rate, d -per capita population level natural death rate and T - maximal infection-age, that is the time of recovery. The immunological and epidemiological scales are linked through the age-since-infection. We note that here S and R are functions of time, but the infectious class $I(\tau, t)$ is a function of both time t and the age since infection τ. We consider an infectious host recovered when the age of infection τ is equal to T, that is the present model is a discrete lag model. For the epidemiological model it is assumed that the time scale of the infection is very small compared to the lifespan of the host. Infection of the host by multiple strains of the same parasite is not possible. Finally, it is assumed that recovery induces permanent immunity.

The variables and parameters of the immunological and the epidemiological models are linked in the following way. The transmission coefficient of parasitic infection $\beta(\tau)$, is proportional to the parasite load at a given age-since-infection τ,

$$\beta(\tau) = cP(\tau),$$

where c is the transmission rate. Again the disease virulence depends on the parasite load and immune system resource use. Hence we have,

$$\alpha(\tau) = \delta r P(\tau)$$

where, $\alpha(\tau)$ gives the additional host mortality due to the parasite and δ is the parasite cost coefficient which is equal to the increase in host mortality rate caused by a single unit of parasite reproducing at rate $r = 1$. Also the additional host mortality due to immune response $\iota(\tau)$, is proportional to the immune response cell proliferation rate. Thus,

$$\iota(\tau) = \mu\frac{dB}{d\tau}$$

where μ is the immune response coefficient. From equation (4.3) we can derive that,

$$\iota(\tau) = \mu\frac{dB}{d\tau} = \mu a P B.$$

From this set of equations we can analyze the optimal host immune response rate and the optimal parasite replication rate to predict a co-evolutionary behavior of the system. The nested model approach requires assumptions regarding the nature of host immune system activation and the process of transmission of the disease between hosts. Thus, we can modify it to suit the specific requirements of a disease. For example, in the case of HIV we can easily incorporate the fact that it is a sexually transmitted disease by altering the assumptions about the underlying within-host model. Again, since the relation between the transmission rate and the additional host mortality is calculated from the within host model, this approach is much more biologically realistic than the single scale disease modeling. In the immuno-epidemiological model above the rate of change of B is always positive but for other models it could be negative or of changing sign, in which case $\iota(\tau)$ would have to be defined differently. The epidemiological reproduction number of the infection $\mathcal{R}_0$ can be expressed in terms of the parasite load or immune response cells.

Among other advantages of the age-since-infection model is the fact that it allows for increase in complexity of the immunological model to a great extent, without this increase in complexity leading to mathematical difficulties with the epidemiological model. It is also easy to incorporate parasite genetic diversity with a competitive exclusion outcome of the competition of the genetically distant variants of the parasite. From [12] we see that by using a detailed model of virus dynamics in conjunction with a simple SI between host model, it can be established that a strong competitor strain could be competitively excluded by a weaker within host strain which was more efficient in transmitting at the early stages of infection. Using nested immuno-epidemiological models it is also possible to study coinfection and superinfection. Nested models are used extensively to study host-parasite co-evolution in [4]. More complex models than the one here can incorporate a lot of experimental and clinical details and produce more accurate results regarding a specific disease. Another advantage of the nested immuno-epidemiological models, coupled through the age-since-infection, is that the age-since-infection model has been well studied over the years and many things about its dynamics are already known.

There are also certain drawbacks of the age-since-infection approach. Due to the inclusion of minute details about the disease in question, a unique model has to be created for every disease. For instance, the model above is not adequate to model diseases with great variability in the time till recovery such as Tuberculosis, or diseases without recovery, such as HIV. For diseases with recovery, the main disadvantage of this immuno-epidemiological model is that the host immune status upon recovery is not retained, i.e. each new infection has to start with the same immune status. Ideally, for diseases that allow repeated infections we would like to retain the immune status, so that upon reinfection the immune system can mount a more efficient response and clear the pathogen faster. Upon primary infection the virus load should lead to full-blown infection, modeled by a peak of the virus load. On the other hand, upon secondary infections the virus should be cleared from the body without causing infection, modeled by a steady decline in the virus load. These two possible scenarios for the virus load are described in Figure 1.

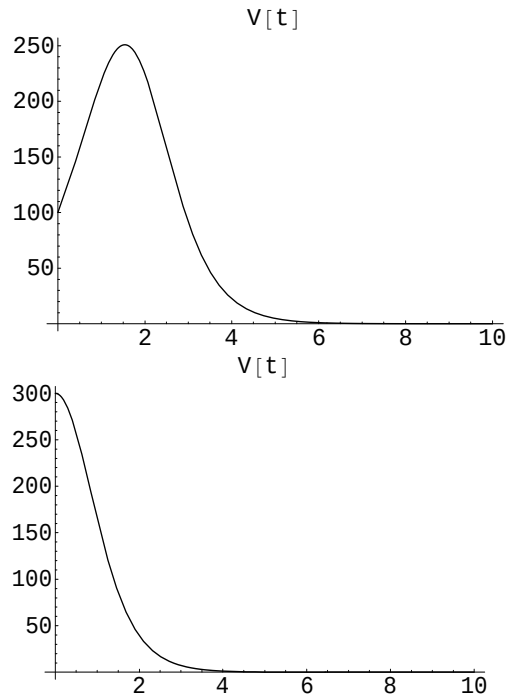

Figure 1. The top figure illustrates that upon a primary infection the virus load first increases and then decreases signifying a viable infection with the pathogen. The bottom figure illustrates that upon a secondary infection the virus load decreases signifying that the pathogen is cleared before causing infection.

5. Immuno-Epidemiological Models for HIV

The models in the above section are not adequate to model HIV. There is usually no acquired immunity from HIV and at each new infection with HIV the immune system is weakened and the overall immunity of the body declines. In addition, model (4.3-4.4) assumes a fixed duration of infection T which is relatively short. This is also a hindrance for HIV models, since the infection can take as long as 10 years before it progresses to AIDS. To allow proper analysis of the model (4.3-4.4) the natural death rate d is taken to be zero [4]. This is also unrealistic in the case of HIV, since in the span of a decade of chronic infection, there is a high chance that the patient dies by accident, old age or other unrelated reason.

We build an immuno-epidemiological model of HIV by linking immunological model of HIV and a simple epidemiological model of SI type. In this immuno-epidemiological model of HIV we incorporate an important characteristic of the HIV pathogen, i.e., shedding. There are some pathogens which multiply in an infected host continuously, using up all the resources available till the host dies, which results in the immediate death of all the pathogens living in that host. This situation is not a desirable one from the evolutionary aspect of a pathogen, considering the fact that all its new and evolved generation is killed all at once. HIV, being a more 'advanced' pathogen, takes recourse to shedding. In this case, the pathogen is emitted from the infected host throughout the period of infection. This may contribute to the host's survival as an infected/infective for a really long time,

even to becoming a sanctuary for the pathogen, but not dying. It is this amount of shedding from an infected host which determines the infectivity. The possibility that an infected host will infect a susceptible individual upon intimate contact is directly related to the amount of virus present in the host at that very moment. Thus when creating a model for HIV, we have to consider this shedding of virus particles as a negative factor in the dynamics of the virus load, which is distinctively different from the other factors. It is also particularly important to consider it as a separate factor since these shed pathogens are the elements causing infection at the epidemiological level. To build a nested age-since-infection model for HIV/AIDS infection, let x be the number of susceptible cells which are being produced at a fixed rate r and they die at the rate μ. The amount of virus in the blood is given by $V(\tau)$. Healthy cells are infected by the virus V at the rate β and become infected cells y. The infected cells die at a rate d and produce ν viruses at bursting. The virus dies at the rate δ and is shed at the rate s. The within-host model takes the form [17]:

$$\begin{aligned}\frac{dx}{d\tau} &= r - \beta V x - \mu x \\ \frac{dy}{d\tau} &= \beta V x - dy \\ \frac{dV}{d\tau} &= \nu dy - (\delta + s)V - \beta V x.\end{aligned} \tag{5.5}$$

We write the differential equations with respect to τ, the time-since-infection. Simple mathematical computation gives the within host reproduction number as

$$\Re = \frac{\nu\beta\frac{r}{\mu}}{\delta + s + \beta\frac{r}{\mu}}.$$

The infection persists in the host to become chronic only if $\Re > 1$. Since HIV is a persistent infection it is natural to assume $\Re > 1$. In the epidemiological model the population is structured into a susceptible class $S(t)$, where t is the chronological time. The infected individuals in the infected class are structured by the time-since-infection τ of the within host dynamics and t, described by the density function $i(\tau, t)$. The transmission of the disease from the infected individuals to the susceptible individuals occurs at a rate which is proportional to the virus load of the infected person. We assume that s denotes the shedding at the cellular level. Thus, $sV(\tau)$ is the rate at which the shedding occurs. If c is the fraction of those pathogens shedded which succeed in infecting another host then csV is the transmission rate [16]. Thus the dynamics of the susceptible hosts is given by,

$$\frac{dS}{dt} = \Lambda - \frac{S}{N}\int_0^\infty csV(\tau)i(\tau, t)d\tau - m_0 S.$$

Here, Λ is the total recruitment rate and $m_0 = m(0)$ is the natural death rate of susceptible hosts at zero virus load. Here we assume that all susceptible individuals have approximately the same equilibrium level of healthy cells. Also the infected hosts die at a variable rate dependent on their virus load $m(V(\tau))$. This gives the dynamics of the infected class as

$$\frac{\partial}{\partial t}i(\tau, t) + \frac{\partial}{\partial \tau}i(\tau, t) = -m(V(\tau))i(\tau, t).$$

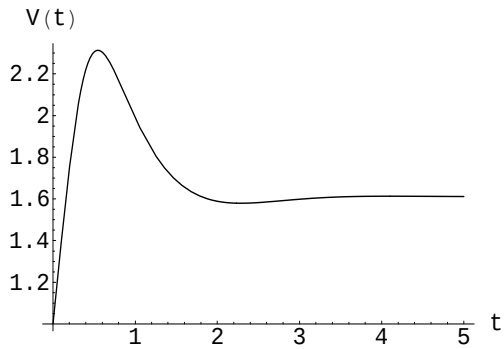

Figure 2. Characteristic behavior of the virus load obtained as a solution of (2.1).

Therefore the probability that a host survives from the time of initial infection, time 0 to time-since-infection τ can be given by

$$e^{-\int_0^\tau m[V(\sigma)]d\sigma}.$$

Also under the given assumptions we impose the following initial condition:

$$i(0,t) = \frac{S}{N}\int_0^\infty csV(\tau)i(\tau,t)d\tau.$$

The total population N is given by

$$N(t) = S(t) + \int_0^\infty i(\tau,t)d\tau.$$

An SI model captures to a large extent HIV infections since recovered class does not exist. The epidemiological reproduction number $\Re_0$ for this system, which depends on the immunological characteristics through the virus load, is given by

$$\Re_0 = \int_0^\infty csV(\tau)e^{-\int_0^\tau m[V(\sigma)]d\sigma}d\tau.$$

The immunological model has been analyzed in [18], which suggests that the solutions approach an equilibrium, or a periodic orbit. There are certain aspects of this model that could lead to a critique of the model and should be addressed and rectified. The first observation is that when the solutions giving the virus load of the immunological model are graphed they do not produce the sudden increase in virus load depicting progression to AIDS after the initial stabilizing. A typical solution of the model (4.3) looks like the graph in Figure 2. For a long time it was thought that immunological models of HIV cannot produce the the characteristic spike in the virus load at the time of progression to AIDS.

M. A. Nowak and R. M. May [25, 27] have been successful in creating immunological mathematical model which under certain conditions can produce the graph with the sudden rise of virus load depicting progression to AIDS. The authors are able to incorporate the fact that any one strain can be suppressed by its strain specific immune response and cross-reactive immune response, but for the virus as a whole cross-reactive immunity is not

enough. The virus over course of time changes its surface proteins (mutates) and is thus able to invade the host immune system better. This results in antigenic variation which does not allow strain specific immune response to make difference anymore. With time the antigenic variation is so high that immune response is totally ineffective and virus load increases without bound causing the rise in the graph and the progression to AIDS. If the immunological models of this type are included into the immuno-epidemiological model then the progression to AIDS can be accounted for while an individual is still in the infectious class. Another approach is to introduce a separate AIDS class into the epidemiological model [26].

6. Multigroup Immuno-Epidemiological Models

Another drawback in the model (4.3-4.4) is that it assumes that all individuals in the population have the same immune response. It has been observed in case of antiretroviral therapy that patients with a stronger immune system respond better to treatment [1]. In addition, the optimum virus load at which the pathogen starts shedding may well vary according to the strength of the CTL response of an individual host. The immune response of an individual and the resulting virus loads are unique to each patient. But, for the purpose of modeling, we can divide the population into n groups according to their immunological characteristics and their virus load. The within-host dynamics of the pathogen of each group $\jmath$ of infecteds is described by the following within-host model:

$$\frac{dx_\jmath}{d\tau} = r - \beta_\jmath V_\jmath x_\jmath - \mu x_\jmath$$

$$\frac{dy_\jmath}{d\tau} = \beta_\jmath V_\jmath x_\jmath - d_\jmath y_\jmath$$

$$\frac{dV_\jmath}{d\tau} = \nu_\jmath d_\jmath y_\jmath - (\delta_\jmath + s_\jmath)V_\jmath - \beta_\jmath V_\jmath x_\jmath$$

where the number of healthy cells is $x_\jmath$ and they are produced at a constant rate r and die at a rate μ. Healthy cells are infected by the virus $V_\jmath$ in the $\jmath^{\text{th}}$ group of individuals at a rate $\beta_\jmath$ and become infected cell $y_\jmath$. Infected cells die at a rate $d_\jmath$ and produce $\nu_\jmath$ virions at bursting. The virus dies at a rate $\delta_\jmath$ and is shed at the rate $s_\jmath$. Hence the within host reproduction number of the infection in the $\jmath^{\text{th}}$ group is

$$\Re_\jmath = \frac{\nu_\jmath \beta_\jmath \frac{r}{\mu}}{\delta_\jmath + s_\jmath + \beta_\jmath \frac{r}{\mu}}.$$

Epidemiologically the population will be structured into a susceptible class $S(t)$ and n immunologically heterogeneous groups of infected classes. Infected individuals in each infected class are structured by the time-since-infection of the within-host dynamics τ, chronological time t and described by density function $\imath_\jmath(\tau, t)$. The transmission of infection to susceptibles occurs at a rate proportional to the virus load of the infected individuals in the $\jmath^{\text{th}}$ group: $c_\jmath s_\jmath V_\jmath(\tau)$ and may occur from an individual with any of the immunological groups. Thus the dynamics of the susceptibles is described by

$$\frac{dS}{dt} = \Lambda - \frac{S}{N}\Sigma_\jmath \int_0^\infty c_\jmath s_\jmath V_\jmath(\tau) i_\jmath(\tau, t) d\tau - m_0 S.$$

Here also, Λ is the total recruitment rate and $m_0 = m(0)$ is the natural death rate of susceptible hosts. We assume that all the susceptible individuals have approximately the same equilibrium level of healthy cells. The infected hosts die at a variable rate dependent on the virus load of the $\jmath^{\text{th}}$ class, given by $m(V_\jmath(\tau))$. Thus the dynamics is given by

$$\frac{\partial}{\partial t} i_\jmath(\tau, t) + \frac{\partial}{\partial \tau} i_\jmath(\tau, t) = -m(V_\jmath(\tau)) i_\jmath(\tau, t), \qquad \jmath = 1, 2, \ldots, n$$

Susceptible individuals who may become infected by an infectious individual in any of the immunological groups moves to the $\jmath^{\text{th}}$ immunological class with probability $p_\jmath$:

$$i_\jmath(0, t) = p_\jmath \frac{S}{N} \sum_k \int_0^\infty c_k s_k V_k(\tau) i_k(\tau, t) d\tau.$$

Here, $p_\jmath$ is the probability that a susceptible individual who becomes infected has immunological dynamics of type $\jmath$. Since all newly infected individuals enter an infectious class with a certain immunological dynamics, we must have $\sum_\jmath p_\jmath = 1$. The total population N is the sum of all the classes given by

$$N(t) = S(t) + \sum_k \int_0^\infty i_k(\tau, t) d\tau.$$

7. Multi-Strain Immuno-Epidemiological Models

HIV has a very inaccurate reverse transcription process during which recombination takes place. In a single infected individual many replicated virus particles are produced from a single cell. Moreover, the virus tends to adapt itself to the specific immune response of the individual, and to suite itself to the different cells the HIV is capable of infecting [19, 20, 25]. Due to this constant supply of varied stranded versions of the virus, superinfection and coinfection with multiple variants of the virus is inevitable.

Biologically superinfection is often defined as the following: suppose an individual is infected by a certain strain of the virus, say x, and has established an immune response against it. Then if this person gets infected by another strain of the same virus, say y, while still being infected by x, then the individual is said to be superinfected by two strains. The term superinfection does not necessarily imply that y is a stronger strain than x [11]. Similarly, in the biological sense coinfection is defined to be the state when an individual gets infected by strain x and by strain y simultaneously or before any immune response against x has been initiated by the body, irrespective of their relative virulence [11]. In our case, however, we define these two modes of reinfection somewhat differently but along the lines they have been defined in [21, 22]. That is, superinfection will be the case when strain y is more virulent than strain x and strain y actually overtakes strain x after infecting, as in [21]. And coinfection will signify coexistence of strains x and y in the same host without excluding each other, as in [22]. Hence we basically study the two 'opposite extremes' in situations where hosts experience multiple infection with different strains [22]. Nowak and May [21]

find that superinfection causes an overall rise in the virulence level of the parasite HIV. In fact this rise could be way above the optimum desirable limit for maximum reproduction. It is generally observed that parasites try to increase their virulence to reach an equilibrium level of reproduction, which is disturbed to a great extent by superinfection. It is reasoned in [21] that the cause for this is the development of intra-host competition between strains leading to high virulence and decrease in overall transmission rates. Superinfection can actually sustain strains with a very high virulence level. A strain with virulence level which is too high cannot exist in an uninfected host population for long as it ends up killing the first hosts it infects without getting enough time to transmit to a large number of other hosts, resulting in its own destruction. However, the conditions produced by superinfection make it possible for high-virulence strains to persist in the population. Thus, superinfection is one of the key factors which make formulation of an effective vaccine that much more difficult. To analyze this scenario mathematically, we reformulate the previously presented model as a *two-strain superinfection model*.

The following model assumes that the immune response against HIV is capable of controlling the progression of the disease at least in the initial stages of the infection. It also assumes that HIV continuously mutates as long as it is in an infected individual and some of the strains are capable of escaping the immune response. The most significant assumption regarding HIV, which is the root of all problems for finding a successful treatment, is that it can harm the immune system of an individual. That is, it can actually kill CD4+ T helper cells which initiate the immune response of the body against any foreign attack. To introduce the model, let $V_1(\tau)$ and $V_2(\tau)$ be the virus load of the first and second strain of HIV virus with $i^1(\tau,t)$ and $i^2(\tau,t)$ being the density of infected individuals by the respective strain viruses. In addition, let s_1 and s_2 denote the shedding of the two strains. We assume that strain 1 can superinfect and replace strain 2. Then the infectivity of all individuals infected with strain 1 is measured by

$$\int_0^\infty cs_1V_1(\tau)i^1(\tau,t)d\tau.$$

The susceptibility of those infected with strain 2 is assumed constant with respect to time-since-infection and rescaled to unity. Then the equations for the first infected class are as follows

$$\frac{\partial}{\partial t}i^1(\tau,t)+\frac{\partial}{\partial \tau}i^1(\tau,t)=-m(V_1(\tau))i^1(\tau,t)+i^2(\tau,t)\int_0^\infty cs_1V_1(\tau)i^1(\tau,t)d\tau.$$

The boundary condition becomes

$$i^1(0,t)=(N-I_1-I_2)\int_0^\infty cs_1V_1(\tau)i^1(\tau,t)d\tau.$$

where $(N-I_1-I_2)$ is the total susceptible population and the total number of infected individuals with strain i, $i=1,2$, is given by

$$I_i(t)=\int_0^\infty i^i(\tau,t)d\tau.$$

For the second strain the dynamics of the infected class can be represented by the following equation.

$$\frac{\partial}{\partial t}i^2(\tau,t)+\frac{\partial}{\partial \tau}i^2(\tau,t)=-m(V_2(\tau))i^2(\tau,t)-i^2(\tau,t)\int_0^\infty cs_1V_1(\tau)i^1(\tau,t)d\tau.$$

In this case the boundary condition is

$$i^2(0,t)=(N-I_1-I_2)\int_0^\infty cs_2V_2(\tau)i^2(\tau,t)d\tau.$$

The basic reproduction number for a strain gives the expected number of secondary infections an infectious individual can produce in its entire lifetime as an infectious individual when introduced in a completely susceptible population. It has been observed [23] that the strain with the largest reproduction number will dominate in the population in the case when there is no coexistence of strains and only one of the strains will survive excluding all the others. However, articles [22] and [3] suggest that if we consider the case where coexistence is possible, the strain with the highest reproduction number might not be able to persist at all. The possibility of a strain dominating in a population cannot be understood completely by studying the initial dynamics of a pathogen when introduced in a completely susceptible host population as determined by the basic reproduction number. The ability of a strain to invade a host population in which a different strain is already existing at an equilibrium is measured by a quantity called the *invasion reproduction number*, $\Re_x^y$. The invasion reproduction number $\Re_x^y$ gives the expected number of secondary infections produced by one infectious individual infected by strain x introduced in a population already at equilibrium with strain y [24]. For the system with two strains and superinfection we can calculate the invasion reproduction numbers for the two strains. The invasion reproduction number of the second strain when the first strain is at equilibrium is calculated to be

$$\Re_2^1=(N-I_1^*)\int_0^\infty cs_2V_2(\tau)\pi_2(\tau)e^{-v_1^*\tau}d\tau$$

where

$$v_1^*=\int_0^\infty cs_1V_1i_1^*(\tau)d\tau,$$

$i_1^*(\tau)$ is the equilibrium value of strain 1, and I_1^* is the integral of that equilibrium distribution. The invasion reproduction number of the first strain when the second strain is at equilibrium is calculated as

$$\Re_1^2=(N-I_2^*)\int_0^\infty cs_1V_1(\tau)\pi_1(\tau)d\tau+i_2^*(0)\int_0^\infty cs_1V_1(\tau)\int_0^\tau e^{-\int_\sigma^\tau m(V_1(\eta))d\eta}\pi_2(\sigma)d\sigma d\tau$$

where,

$$\pi_i(\tau)=e^{-\int_0^\tau m(V_i(\tau))d\tau},\qquad i=1,2$$

and $i_2^*(0)$ is the equilibrium value of strain 2 when time-since-infection τ is zero. These results give for the first time epidemiological invasion criteria that depend on the immunological dynamics through the virus load of each strain.

Typically, the conditions $\Re_2^1 < 1$ and $\Re_1^2 > 1$ imply that strain 2 cannot invade the equilibrium of strain 1 which leads to competitive exclusion of strain 2 by strain 1. Similarly $\Re_1^2 < 1$ and $\Re_2^1 > 1$ mean that strain 1 cannot invade the equilibrium of strain 2. Thus, under these conditions strain 2 will competitively exclude strain 1. When $\Re_2^1 < 1$ and $\Re_1^2 < 1$ neither of the strains can overcome the other one. The resulting domination will depend on the initial conditions. Finally, $\Re_2^1 > 1$ and $\Re_1^2 > 1$ describes the situation when both the strains can invade the other strain's equilibrium, resulting in coexistence [24].

8. Conclusion

Immuno-epidemiology is a fairly new concept in modeling compared to the immunological or epidemiological modeling. A good amount of important information was obtained from the single scale models which was path-breaking at the beginning of bio-mathematical modeling. The single scale immunological and epidemiological models form the basis for the development of the nested models. However, the within-host evolution of a parasite and the between-host evolution of the disease were never independent phenomena for any disease. Although the initial motivation for the development of the age-since-infection structured immuno-epidemiological model was to understand the host-parasite co-evolution, the model could also be adapted for HIV/AIDS case-study.

A different approach to multi-scale immuno-epidemiological modeling which will lead to more realistic models are the individual based models. These are the models which study the immunological dynamics of each infected individual separately instead of considering classes as in the immuno-epidemiological models considered here. At the population level individual-based network models trace the possible contacts between any pair of individuals in the population and therefore formulate the most accurate map of the disease progression. Although this approach is closer to reality than any other model, individual based models are mostly simulational. In fact, they seldom have closed mathematical form which makes drawing general conclusions about the global scenarios difficult. Moreover, getting accurate data for parameter estimation for a general slice of the population may be impossible. The immuno-epidemiological models we build here by embedding an ODE immunological model into a PDE epidemiological model can give more insight into the general principles of disease dynamics and transmission in the global sense. The parameters can be estimated from various statistical Public Health data concerning HIV/AIDS epidemiology while the immunological parameters can be estimated from direct measurements or the research literature.

One question of interest to be addressed with nested immuno-epidemiological models is how the transient immunological dynamics affects the epidemiology of the disease. The transient immunological dynamics is linked to the epidemiology of the disease through the transmission rate which depends on the age-since-infection via its dependence on the virus load. It is well known about age-since-infection dependent epidemiological models that considering infection-age-dependent infectivity structure leads to destabilization of the endemic equilibrium and sustained oscillations in the dynamics of the infected individuals [26]. However, in the nested immuno-epidemiological models we consider, the time-since-infection dependent transmission rate is not arbitrary as is the case with age-since-infection dependent epidemiological models. In the nested immuno-epidemiological

models the transmission rate has predetermined shape which is dependent on the immunological parameters. It is interesting to investigate whether and when the transient immunological dynamics can destabilize the epidemiological disease-dynamics.

In general, we expect that the immuno-epidemiological models will help us understand the mutual interdependence between the immunology and epidemiology of an infectious disease. In particular, these models will advance our knowledge on how the epidemiology of a disease impacts the within-host dynamics. Conversely, immuno-epidemiological models will advance our knowledge on the impact of immunology on the disease and its distribution on the population level. We would also like to investigate the evolution of virulence depending on the ability of a virus to use host immune defense resources keeping in mind the trade-off theory. Another interesting direction of study is the evolution of host resistance on immunological level and lifting it to the epidemiological level. The correlation between the virulence and epidemiological transmission of HIV is also a question of interest. The overall aim would be to identify the host (human)-pathogen (HIV) co-evolution. It is important to acknowledge that previous modeling attempts have provided useful information for development of treatment strategies for AIDS. However, we are still far from being able to eradicate HIV from an infected individual. Further analysis of the proposed models and modifications should throw light into these questions. Understanding the progression of HIV to AIDS and possible directions of advancement of treatment could also be approached with immuno-epidemiological mathematical models.

References

[1] S. Bonhoeffer, J. M. Coffin and M. A. Nowak (1997), Human Immunodeficiency Virus drug therapy and virus load, *J. Virol.* **71**, No. 4, p. 3275-3278.

[2] B. Hellriegel (2001), Immunoepidemiology – bridging the gap between immunology and epidemiology, *TRENDS Paras.* **17**, p. 102-106.

[3] M. Martcheva and S.S. Pilyugin (2006), An epidemic model structureed by host immunity, *J. Biol. Syst.* **14**, No.2, p. 185-203.

[4] M.A. Gilchrist, A. Sasaki (2002), Modeling host-parasite coevolution: A nested approach based on mechanistic models, *J. Theor. Biol.* **218**, p. 289-308.

[5] H.W. Hethcote (2000), The mathematics of infectious diseases, *SIAM Review* **42**, No.4, p.599-653.

[6] R. M. May and R. M. Anderson (1987), Transmission dynamics of HIV infection, *Nature* **326**, p. 137 - 142.

[7] R. M. May, R. M. Anderson and A. R. McLean (1988), Possible demographic consequences of HIV/AIDS, *Math. Biosci.* **90**, p. 455-501.

[8] A.S. Perelson and P.W. Nelson (1999), Mathematical analysis of HIV-1 dynamics in vivo, *SIAM Review* **41**, No. 1, p. 3-44 .

[9] M.A. Gilchrist and D. Coombs (2006), Evolution of virulence: Interdependence, constraints, and selection using nested models, *Theoretical Population Biology* **69**, p. 145-153.

[10] T. Zhu, N. Wang, A. Carr, S. Wolinsky and D.D. Ho (1995), Evidence for coinfection by multiple strains of Human Immunodeficiency Virus type 1 subtype B in an acute seroconverter, *J. of Virol.* **69**, No. 2, p. 1324-1327.

[11] D.M. Smith, D.D. Richman and S. J. Little (2005), HIV superinfection, *J. Infect. Dis.* **192** (3), p. 438-444.

[12] D. Coombs, M.A. Gilchrist and C.L. Ball (2007), Evaluating the importance of within- and between-host selection pressures on the evolution of chronic pathogens *Theoretical Population Biology*, **72**, No. 4, p576-591.

[13] R.M. Anderson (1998), Complex dynamic behaviors in the interaction between parasite populations and the host immune system, *Int. J. Paras.* **28**, p. 551-566.

[14] R. J. Quinnell (2004), The Immunoepidemiology of human hookworm infection, *Parasite Immunology* **26**, No. 11-12, p. 443-454.

[15] N. T. J. Bailey , *The Biomathematics of Malaria*, Charles Griffin and Co., London,(1982).

[16] R. D. Holt and M. Barfield (2006), Within-host pathogen dynamics: Some ecology and evolutionary consequences of transients, dispersal mode, and within-host spatial heterogenity. Disease Evolution: Models, Concepts, and Data Analysis (Z. Feng, U. Dieckmann, S. Levin, eds.), *DIMACS Series in Discrete Mathematics and Theoretical Computer science*, Vol 71, p. 45-66.

[17] J. K. Kelly (2006), Evolutionary and dynamic models of infection with internal host structure. Disease Evolution: Models, Concepts, and Data Analysis (Z. Feng, U. Dieckmann, S. Levin, eds.), *DIMACS Series in Discrete Mathematics and Theoretical Computer science*, Vol 71, p. 67-86.

[18] P. De Leenheer and H. L. Smith (2003), Virus dynamics: A global analysis, *SIAM J. Appl. Math.* **63**, No. 4, p.1313-1327.

[19] M. Peeters (2000), Recombiant HIV sequences: their role in the global epidemic. (Kuiken CL, Foley B, Hahn B, et al, eds.) HIV Sequence Compendium 2000, The Theoretical Biology and Biophysics Group, Los Alamos National Laboratory, p. 39-54.

[20] J.T. Blackard, D. E. Cohen and K.H. Mayer (2002), Human Immunodeficiency Virus superinfection and recombination: current state of knowledge and potential clinical consequences. *Clin Infect Dis* **34**, p. 1108-1114.

[21] M. A. Nowak and R. M. May (1994), Superinfection and the evolution of the parasite virulence, *Proceedings, Biological Sciences* **255**, No. 1342. p.81-89.

[22] M. A. Nowak and R. M. May (1994), Coinfection and the evolution of the parasite virulence, *Proceedings, Biological Sciences* **261**, No. 1361, p.209-215.

[23] H.J. Bremermann and H. R. Thieme (1989), Competetive exclusion principle for pathogen virulence, *J. Math. Biol.* **27**, p. 179-190.

[24] M. Martcheva, B. M. Bolker and R. D. Holt (2008), Vaccine-induced pathogen strain replacement: what are the mechanisms?, *J. R. Soc. Inferface* **5**, p. 3-13

[25] M. A. Nowak and R. M. May, *Virus Dynamics, Mathematical Principles of Immunology and Virology*, First Edition, New York, Oxford University Press, 2000.

[26] H. R. Thieme and C. Castillo-Chavez (1993), How may infection-age-dependant infectivity affect the dynamics of HIV/AIDS?, *SIAM J. Appl. Math.* **53**, No.5., p.1947-1479.

[27] M. A. Nowak, *Evolutionary Dynamics, Exploring the Equations of Life*, Chapter10, First Edition, The Belknap Press of Harvard University Press, Cambridge, MA, 2006.

In: Mathematical Biology Research Trends
Editor: Lachlan B. Wilson, pp. 193-215
ISBN: 978-1-60456-141-8

Chapter 7

MATHEMATICAL MODELS OF PARTICLE DEPOSITION AND BRONCHIAL CLEARANCE IN THE HUMAN RESPIRATORY TRACT – A REVIEW

Robert Sturm
University of Salzburg, Department of Materials Engineering and Physics,
Hellbrunnerstrasse 34, A-5020 Salzburg, Austria

Abstract

The development of physical and mathematical models dealing with the deposition and bronchial clearance of aerosol particles in the human respiratory tract has its origin in the 1970s. Theoretical approaches of this time were usually based on an airway geometry being either approximated by a sequence of straight cylindrical tubes or by a single, variable cross-section channel resembling a trumpet shape. The branching network of lung airways was initially described by a fully symmetrical tree structure (e.g. Weibel's lung model A), within which tubes of the same airway generation were characterized by identical geometric parameters (i.e. diameters, lengths, branching and gravity angles). As a further consequence of this symmetry pathways leading from the trachea to the closing alveolar sacs consisted of the same number of tubes, representing a remarkable simplification for the simulation of deposition and clearance scenarios.

In reality, the human tracheobronchial tree is marked by a significant asymmetry due to the variation of airway geometry within a given generation. Since the end of the 1970s and the early 1980s increased attention was paid to this important fact by the construction of a five-lobe lung model, where intrasubject variation of bronchial geometry was still limited to the first three or four bifurcations. A better approach of the variability of airway properties took place by the formulation of a stochastic model of the human respiratory tract in the middle of the 1980s. With this model both asymmetry and randomness could be well approximated on the basis of available morphometric data. In addition, computation of deposition and bronchial clearance was improved due to a variation in the number of bifurcations leading from the proximal to the distal end of the bronchial pathway.

Currently, stochastic lung models represent the state of the art in simulating deposition and clearance of inhaled particles. In recent years, computation of particle deposition was successively refined by numerical approaches, enabling the determination of exact particle trajectories within single, double, and triple bifurcations. Bronchial clearance was improved by generation-specific variations of mucus thickness and mucus production, causing a

remarkable variability of mucus velocity. Additionally, slow bronchial clearance mechanisms were defined, with the help of which particle residence times > 24 hours could be explained.

Introduction

During the past three decades mathematical models have increasingly come into vogue in various fields of biological and medical science. While in molecular biology theoretical approaches to the structures of highly complex macromolecules have made a stir in professional circles, in ecology diverse population models have remarkably helped to increase our knowledge on the function of ecosystems controlled by a wide net of environmental factors. In the meantime the importance of biological modelling has found its expression in numerous scientific articles and monographs giving a review on various aspects which are essential for the preparation of reliable mathematical approaches to biological processes [1-4].

Concerning medical science first modelling attempts date back to the 1960s, whereby the scientific branch of pneumology has adopted a leading role in this context [5]. Based on the circumstance that exposure to various airborne particles, either being attached by radioactive elements or not, could cause serious lung diseases ranging from chronic bronchitis over different kinds of fibrosis to lung cancer, enhanced efforts were invested to elucidate the intricate morphology of the human respiratory system and the behaviour of inhaled particulate matter. In the following decades three main fields of activity for mathematical modelling were established. The first group of models mainly focused on an appropriate description of the lung structure, whose geometry was successively decoded by the production and precise measuring of lung casts [6]. Although being advised of the asymmetric structure of the human lung, preliminary approaches of the geometry were based on deterministic airway paths and thus contained high uncertainties. One of the milestones in lung modelling was the substitution of this symmetrical lung model by a stochastic approach describing the multiple-path geometry of the human respiratory tract in a more satisfactory way [7-9]. Mathematical approaches to the lung structure formed the basis for any further modelling purposes introduced in the following.

The second group of mathematical models concentrated on the simulation of particle deposition in the human lungs and thereby mainly tried to follow the questions, at which sites of the respiratory tract and to which extent deposition of inhaled particles takes place [5]. In the case of radioactive aerosols the approaches should additionally help to estimate the radioactive dose, to which specific lung regions (e. g. the bronchi and the alveoli) are exposed. The microdosimetric aspects standing behind the theoretical description of particle deposition in single respiratory compartments have forfeit nothing of their significance until today [10,11] and represent a main driving force in present and future model development.

At the same time, when first attempts of deposition modelling were made, pneumologists and biophysicists also started to decode and simulate those mechanisms which stand behind the clearance of particles from the human respiratory tract [5,12]. Hence clearance models became the third field of modelling activity that has lost nothing of its former attraction due to many questions being unsolved hitherto. Similar to the deposition models also the theoretical approaches to lung clearance have continuously increased in complexity during the past decades, whereby actual efforts are dedicated to the clearance in diseased lungs and in children [13-16].

In this chapter, main principles of particle deposition and bronchial clearance modelling that have been developed during the past decades will be subject to a brief description, and future aspects of theoretical models in lung medicine will be discussed. For the sake of completeness, however, the overview is preceded by a section including basic properties of aerosols as well as principles standing behind the inhalation, deposition, and clearance of particles in the human respiratory tract. This should help the non-expert to find a fast entrance into the topic.

Aerosol Particle Deposition and Clearance in the Human Respiratory Tract – Basic Considerations

General Characteristics of Aerosols

In general, aerosols are defined as solid particles or liquid drops suspended in a gaseous system. In the atmosphere, numerous kinds of aerosols can be detected, ranging from haze particles that are formed over vegetation, mineral dusts, and volcanic ashes to the important group of bioaerosols [17-19]. Biological aerosols are characterized by high variability in size, including viruses (~20 – 100 nm), bacteria (0.5 – 1 μm), spores, and pollen of coniferous trees and angiosperms (– 100 μm). Besides the natural aerosols listed above, also numerous aerosols of anthropogenic origin are distributed in the atmosphere. These include artificial dusts, i.e. solids formed by disintegration processes such as crushing, grinding, blasting, and drilling, fumes, which are produced by physiochemical reactions such as combustion, sublimation, and distillation (e.g. metallurgical fumes of PbO, ZnO, or Fe_2O_3), as well as smoke, defining a cloud of particles produced by the burning of coal, oil, wood, or other carbonaceous fuels [17].

Since a specific aerosol in the atmosphere always occurs as a collection of particles, an important feature of risk assessment is to indicate, whether the particles are all alike or are dissimilar. For an appropriate solution of this question, the definitions of monodisperse, polydisperse, and homogeneous aerosols have been introduced into the scientific literature [17]. While a monodisperse aerosol contains only particles of exactly the same size, a condition which is very rare in nature, a polydisperse aerosol contains particles of more than one size. Homogeneous aerosols consist of particles which are marked by identical chemical compositions. For investigating the deposition of aerosols in the human respiratory system, basic knowledge of their morphological and physical properties is indispensable.

Besides the size of particles or liquid drops, which is usually described by the median aerodynamic diameter (e.g. AMAD = activity median aerodynamic diameter, MMAD = mass median aerodynamic diameter), the shape of aerosol particles plays an important role concerning their respirability and deposition in the lung. As a major simplification in recent lung models, aerosol particles are usually defined as spheres. However, with the exception of liquid droplets, which are always spherical, many particle shapes have been described in the literature due to extensive microscopic investigations. Generally, these shapes can be subdivided into the following three classes: 1) Isometric particles are characterized by a similarity (polyhedral particles) or even equality of the three dimensions (spherical particles). Most knowledge regarding aerosol behaviour in the environment and the human body

pertains mainly to isometric particles. 2) Platelets are defined as particles that have two long dimensions and a small third dimension. Aerodynamic properties of these specific particles are not well understood until now, because applying knowledge derived from studying isometric particles to platelets is not possible without further ado. Classical examples for platelets are graphite particles as well as small dust particles produced by mechanical friction. 3) Fibres are particles marked by great length in one dimension and much smaller lengths in the other two dimensions. Contrary to platelets, much information on the behaviour of fibres in the air has been collected during the last decades [20-22]. This increased scientific interest was mainly prompted by the fact that inhalation of asbestos fibres, the most important particle species of this class, has been recognized as a considerable health hazard, being responsible for numerous lung diseases (e.g. asbestosis, lung cancer). Further particle properties, which are of interest for scientific studies, are the specific weight (g cm^{-3}), surface characteristics, which is important concerning chemical reactions, possible electric charges, hygroscopic growth, radioactivity as well as the light scattering and absorption behaviour.

The uptake of specific aerosols by inhalation can bear considerable health risks. Besides the above described asbestos fibres, the deposition of numerous other particle types (e.g. tobacco smoke, mineral dusts, radioactive particles, bioaerosols) in the respiratory tract can be responsible for short-term or long-term (i.e. chronic) lung diseases. In the last decades, the main interest of aerosol science has been focused on the investigation of radioactive particles in the atmosphere, their inhalation and deposition in the human lung as well as possible transport routes (e.g. blood, lymph system) in the human body. The studies were chiefly initiated by well documented observations on uranium mine workers in the middle of the last century, who showed a significantly increased rate of lung cancer with respect to the remaining population. For an appropriate assessment of health risks due to the inhalation of radioactive aerosols (e.g. radon progeny), several models calculating their deposition distribution in the human lung have been developed in the meantime [5].

In medical science, aerosols have found a wide application concerning the inhalation therapy of specific lung diseases (e.g. asthma, bronchitis, pneumonia, cystic fibrosis), but also concerning the medical treatment of several metabolic insufficiencies (e.g. diabetes) [23,24]. For both cases, the effectiveness of inhalation therapy has to be optimized by producing a maximum deposition of medical aerosols in the respective target region of the human respiratory tract (e.g. bronchial region for asthma or bronchitis, alveolar region for diabetes).

The Human Respiratory System

The organization of the human respiratory tract is illustrated in Fig. 1. Generally, the respiratory system can be subdivided into an extrathoracic part including the nose, mouth cavity, oropharynx, nasopharynx, and larynx as well as a thoracic part consisting of the tracheobronchial tree and the alveolar compartment. In the naso- and oropharynx, both very small (nm-size) and very large particles (> 10 μm) are already filtered with high efficiency and therefore penetrate into the deeper lung only in small amounts. Besides its high importance as a particle filter, the nasopharynx also adapts the temperature of the inhaled air to body temperature. Within the thoracic part of the respiratory tract, the tracheobronchial tree (i.e. conducting zone) can be defined as a sequence of airway bifurcations and consists of three main units: a) the trachea, b) the bronchi, and c) the bronchioli [5,25,26].

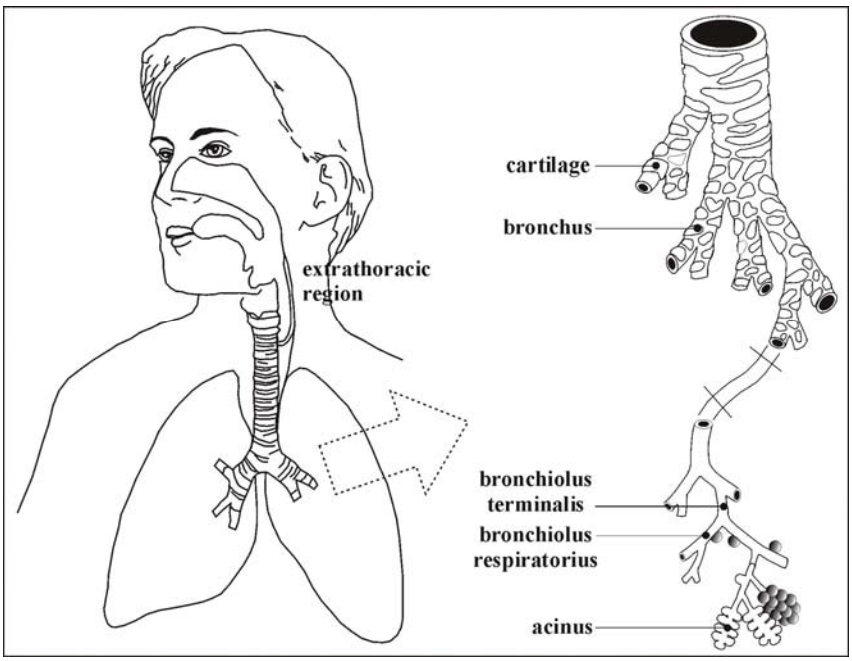

Figure 1. Illustration of the respiratory system with its extrathoracic part containing oro-, nasopharynx, and larynx as well as its thoracic part including the tracheobronchial tree and the alveolar system.

The trachea (airway generation 0) represents the connecting link between the extrathorcic system and the lungs. In adults, it has a length between 10 and 12 cm and a diameter of about 2 cm. A specific property of the trachea is the development of horseshoe-like hyaline cartilage, guaranteeing an increased stability of this airway. The bronchi are usually defined as airway generations 1 to 8. Similar to the trachea, these airways are stabilized by platelets and sponges of hyaline cartilage. At the hili, the two main bronchi (primary bronchi) enter the lungs (Fig. 1) and subsequently divide into five lobar bronchi (secondary bronchi), two in the left lung and three in the right lung. The bronchioli represent the airway generations 9 to 16 and are, contrary to the trachea and the bronchi, characterized by the absence of any hyaline cartilage. The diameters of these airways typically range from about 0.5 to 1.5 mm. By definition, the bronchiolus terminalis is the last non-alveolated airway within a pre-defined bronchial path, while the bronchiolus respiratorius already contains some alveoli and thus defines the transitional zone of the lung. Finally, the respiratory bronchiolus divides into the alveolar ducts, where gas exchange takes place (respiratory zone).

The main histology of the bronchial tubes is very similar among the different airway generations and is schematically illustrated in Fig. 2. In general, the bronchial airway wall can be subdivided into several histological units, including the airway epithelium, fibroelastic connective tissue (lamina propria) with nerves, capillaries, and lymph vessels, subepithelial gland tissue as well as smooth muscle tissue [5,25,26]. As already mentioned above, in airway generations 0 to 8 this basic histology is extended by a stabilizing cartilage tissue. The airway epithelium is usually covered by a liquid film (mucus layer), containing a low-viscous sol layer and a high-viscous gel phase. The mucus layer plays an important role concerning the defense against bacterial infections and the fast removal of deposited particles out of the tracheobronchial tree. The airway epithelium itself consists of several cell types which are

e.g. responsible for mucus movement (ciliated cells), mucus production (globlet cells) and the release of transmitters (endocrine cells). The organization is completed by brush cells with apical microvilli and the basal cells, from which all other epithelial cell types are generated. The thickness of single tissue types decreases significantly from the trachea to the terminal bronchioli [5,27].

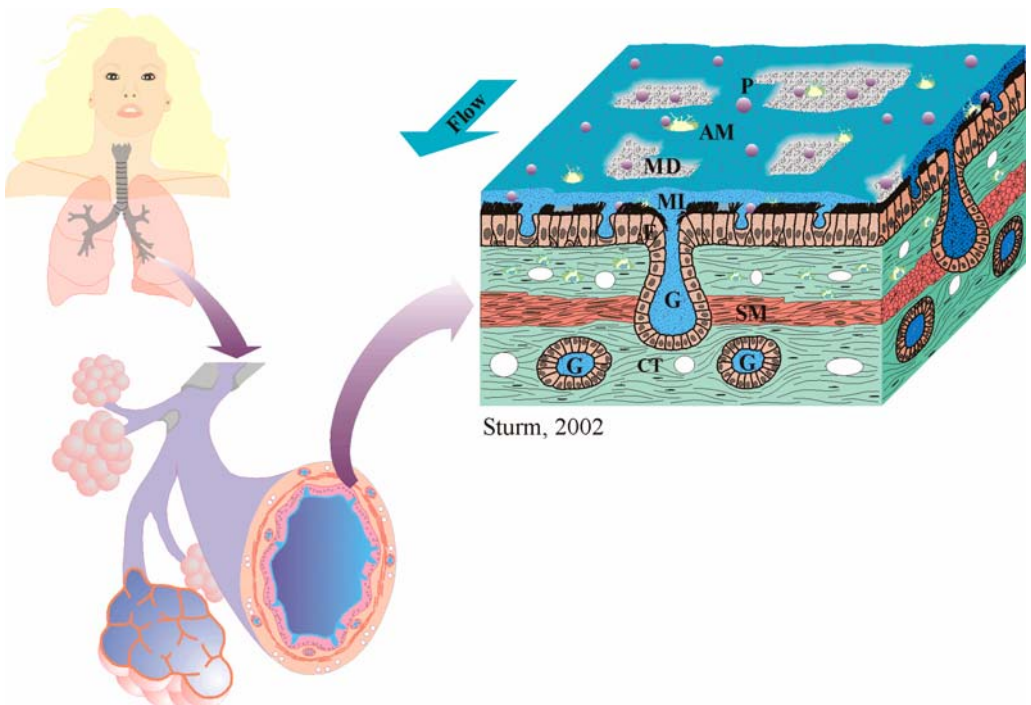

Figure 2. Sketch illustrating the general morphology of the bronchial airway wall. As shown in the upper right picture, each bronchus consists of the airway epithelium (E), which is covered by the mucus layer (ML), connective tissue (CT), and a smooth muscle layer (SM). Depending on the airway generation, the bronchus is additionally stabilized by pieces of elastic cartilage. The mucus layer is characterized by specific discontinuities (MD), whose number is thought to increase significantly from proximal to terminal airways. Further abbreviations: P...deposited particle, G...subepithelial gland, AM...airway macrophage. The arrow indicates the flow direction of the mucus.

In the alveoli, O_2 is transferred from the inhaled air to the blood and CO_2 from the blood to the expired air. The basic histology of the alveolar system contains an epithelial layer, whose thickness is reduced to 0.5 – 1 µm, and an interstitium (fibroelastic tissue) including lots of capillaries. Diffusion of gases takes place along the following path: 1) epithelial cytoplasm, 2) epithelial basal membrane, 3) basal membrane of the associated capillary, 4) capillary endothelium, and 5) erythrocyte membrane (blood-air barrier). The alveolar epithelium consists of thin platelet cells (type-I pneumocytes) as well as granular cells (type-II pneumocytes) which are able to differentiate to type-I cells and additionally produce the surfactant covering the alveolar wall and reducing the surface tension for a faster uptake of O_2 molecules. Clearance within the alveoli is mainly guaranteed by alveolar macrophages that phagocytize any deposited material. After losing their ability of particle uptake, the cells are transported out of the lung via the tracheobronchial tree or the interstitium [27,28-30].

Inhalation and Deposition of Aerosol Particles

A basic requirement for the inhalability of aerosol particles is their size. Therefore, particles with diameters >100 µm are not able to enter the respiratory tract due to their increased mass causing an immediate drop out of the inhaled air stream. For particle sizes between 10 µm and 100 µm, the respirability (i.e. the probability to enter the lungs) decreases considerably with increasing diameter because of an enhanced deposition in extrathoracic compartments (e.g. oropharynx or nasopharynx) [5,8,31].

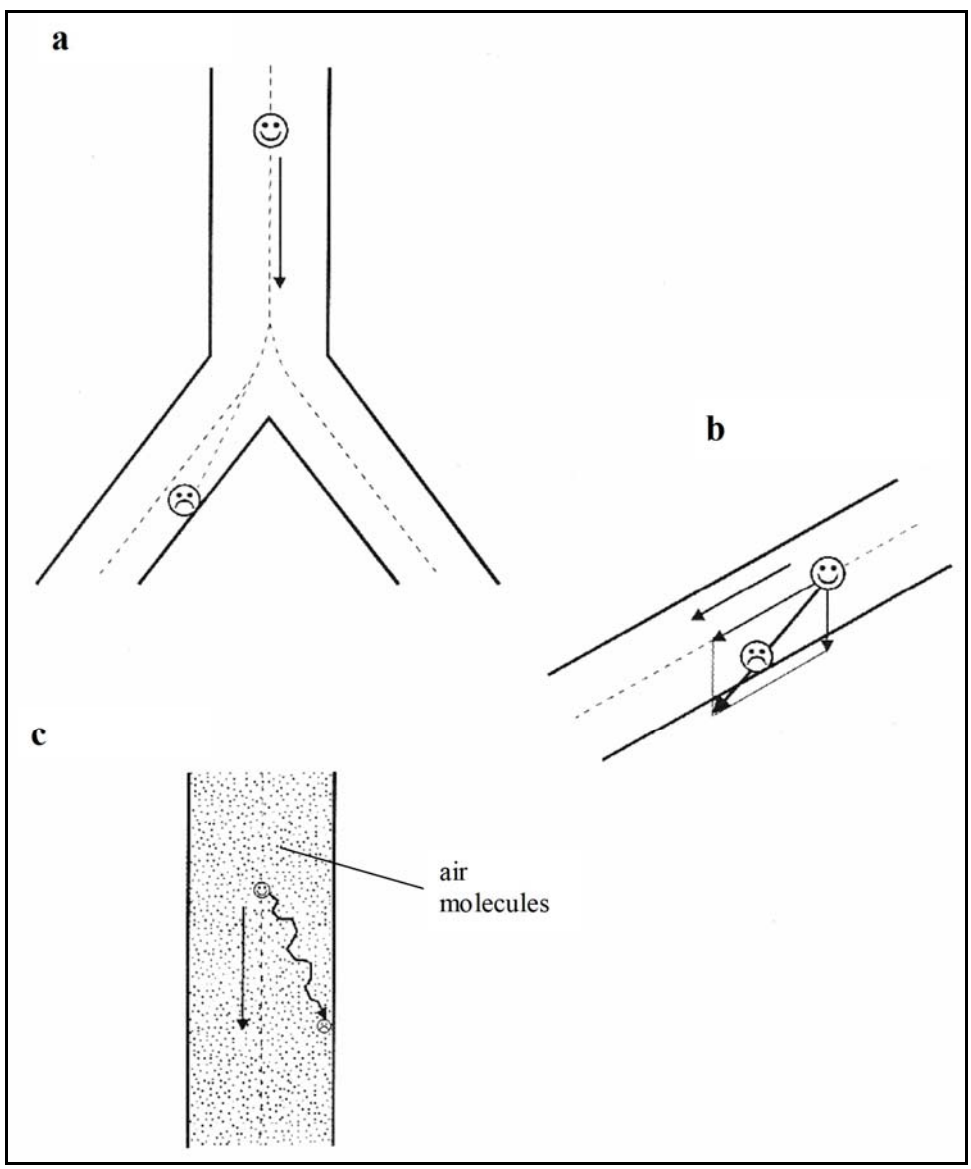

Figure 3. The three main deposition mechanisms in airways of the tracheobronchial tree. **a)** Inertial impaction, **b)** Sedimentation, **c)** Brownian diffusion.

Assuming a laminar air stream in the tracheobronchial tree, deposition of aerosol particles is caused by three main mechanisms (Fig. 3): a) Brownian diffusion, b) inertial impaction, and c) sedimentation [5,31-33]. Important deposition forces can be also generated by the occurrence of secondary air flows at the carinal sites of airway bifurcations. At the moment, this additional mechanism can be only simulated for single airway generations. Brownian diffusion is regarded as the main deposition mechanism of small and ultrafine particles (< 0.5 µm). By a permanent collision with surrounding air molecules, such particles are transferred along stochastic trajectories that are mainly oriented perpendicular to the direction of the airflow. Where the trajectories hit the airway wall, particles are deposited. Concerning molecule-sized particles (~ 1 nm), interaction with surrounding gas molecules reaches a minimum (Knudson number >> 1) and deposition occurs very immediately (i.e. in the first airway generations). Impaction expresses the inertial behaviour of particles in the air stream and is most important for particle diameters > 3 µm. Such large particles show a high probability to leave their trajectories after a rapid change of the airflow direction (e.g. at carinal sites of airway bifurcations) and tend to continue along their original paths, causing a deposition in pre-defined discrete areas ('hot spots') [34].

Deposition efficiency by inertial impaction can mainly be recognized in the proximal airway generations, where flow velocities of the inhaled air are rather high. For large aerosol particles, which are transported in a slow air stream, deposition by sedimentation is of high importance. Contrary to inertial impaction, deposition efficiency due to this specific mechanism mainly occurs in small peripheral airways, where flow velocities reach a minimum and thus particles have enough time to settle down by gravitation.

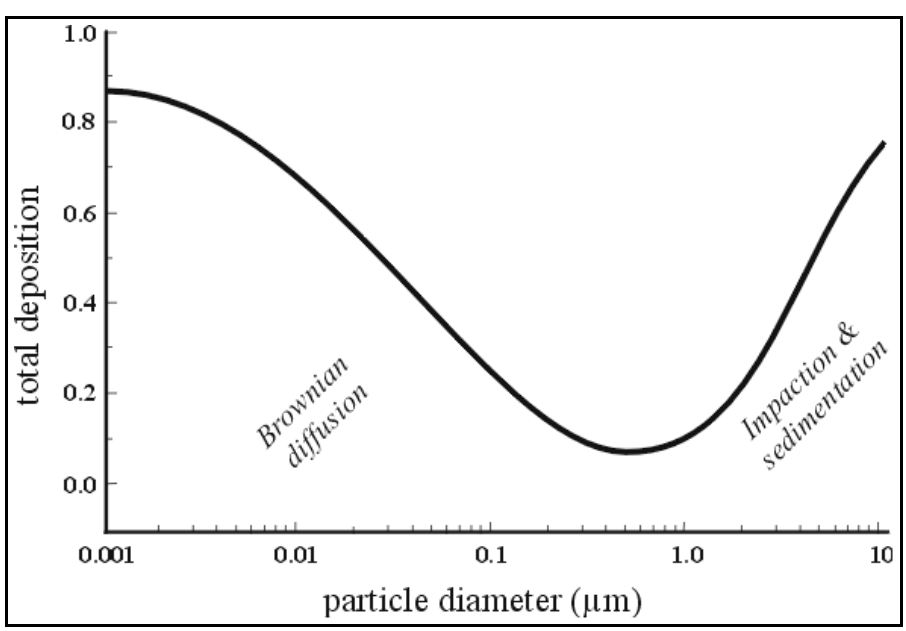

Figure 4. Total deposition in the human respiratory tract (extrathoracic and thoracic compartment) as a function of particle size (see e.g. [9]). While deposition of small and ultrafine particles (<0.5 µm) is mainly caused by Brownian diffusion, deposition of µm-sized particles is chiefly controlled by impaction and sedimentation. Particle sizes around 0.5 µm show a deposition minimum due to the absence of a favourite deposition mechanism.

In Fig. 4, total deposition (i.e. extrathoracic and thoracic deposition) is illustrated as a function of particle size. The graph shows a minimum for particle sizes around 0.5 µm. Such particles are too big for an efficient deposition by Brownian diffusion and, on the other hand, too small for deposition by inertial impaction or sedimentation and are therefore marked by low deposition probabilities in the respiratory tract.

Clearance of Deposited Particles

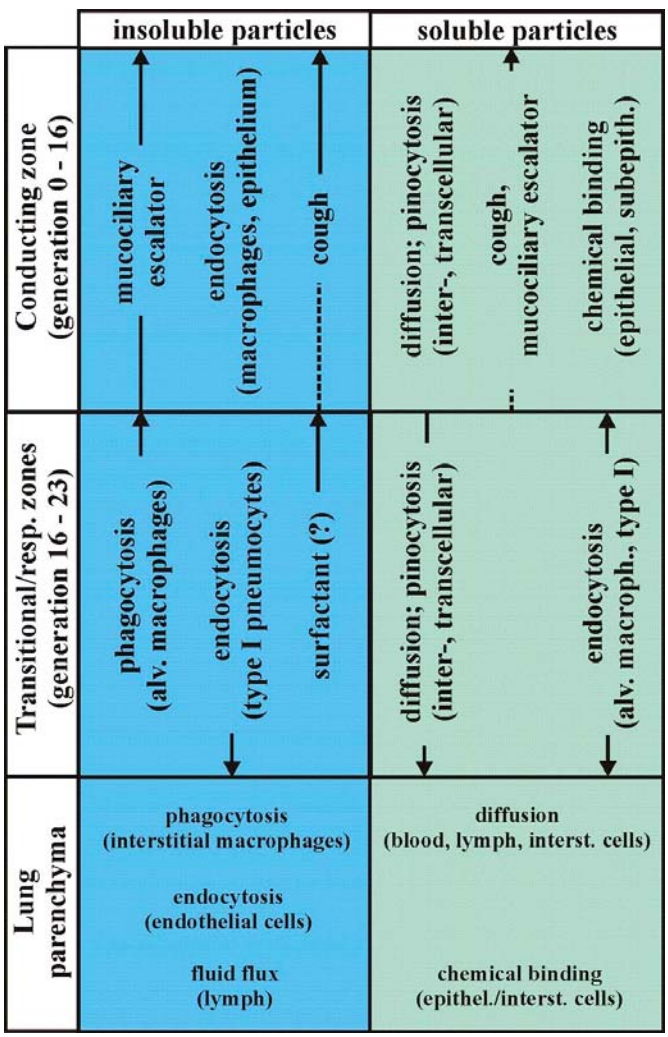

Figure 5. Scheme representing possible clearance mechanisms of inhaled particles deposited in the lung (from [35], modified). Insoluble particles are persistent to biological dissolution processes, e.g. intracellular lysis, whereas soluble particles are metabolized within a rather short period of time.

During evolution, the human lung has developed several clearance mechanisms for an efficient evacuation of deposited aerosol particles out of the lungs. In general, the conducting zone (i.e. tracheobronchial tree) and respiratory zone (i.e. alveolar region) are characterized by different clearance mechanisms, which are summarized in Fig. 5 [35]. For a

comprehensive overview, specific clearance types of both insoluble and soluble particles are illustrated. At the moment, the modelling of clearance scenarios is chiefly limited to insoluble particles which are not or only insignificantly affected by lytic reactions or other cellular decomposition processes.

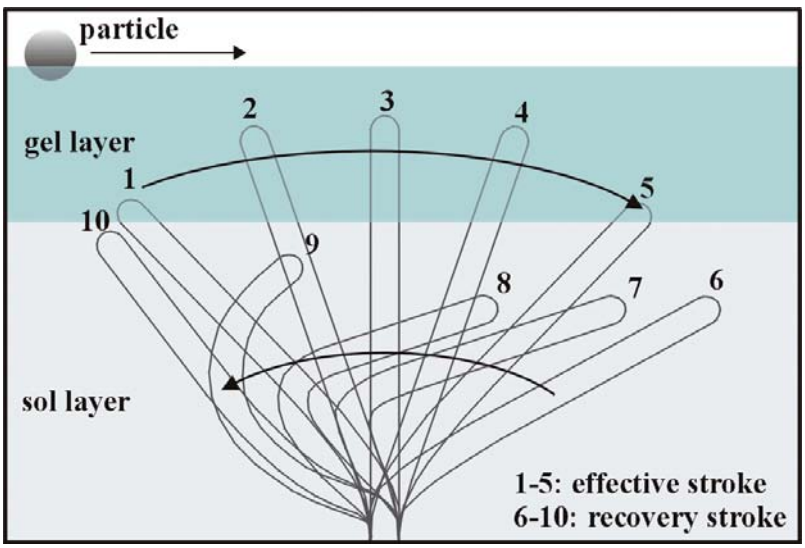

Figure 6. Schematic illustration of a cilia beating cycle. During the effective stroke (1 – 5), the cilium dips into the gel layer. Due to its viscoelastic behaviour, this phase is subsequently driven towards the trachea. During the recovery stroke (6 – 10), the cilium moves only in the sol layer and therefore avoids any movement of the gel layer in the opposite direction.

Concerning the tracheobronchial tree, deposited particles are mainly cleared by the so-called mucociliary escalator, where a mucus layer covering the airway walls is transported towards the larynx due to the permanent beating of epithelial cilia ($\nu \sim 20$ Hz) [5,36]. For optimizing this beating activity, the mucus layer is subdivided into a low-viscous periciliary sol phase and a superposed high-viscous gel phase, on which deposited material is transported (Fig. 6). According to the classical hypothesis, dipping of single cilia into the gel layer causes a local increase of its viscosity (viscoelastic liquid) and, as a consequence, its movement along the epithelial surface. To avoid an ineffective movement of the mucus in both directions, each beating cycle of a single cilium consists of an effective stroke and a recovery stroke (Fig. 6). Based on numerous experimental data [37-40], mucociliary clearance is assumed to take place within the first 24 hours after dust exposure. This is underlined by mucus velocity measurements in the trachea which range from 3 mm min^{-1} to about 20 mm min^{-1}. Besides the fast mucus clearance, also several slower clearance mechanisms play an important role in the bronchial airways. As a basic requirement for the occurrence of slow bronchial clearance, particles have to reach the sol phase either by penetrating the gel layer [36,41] or by passing through a mucus discontinuity. Possible slow clearance mechanisms are illustrated in Fig. 7 and include 1) the re-transfer of particles onto the gel layer due to the beating activity of adjacent cilia, 2) the phagocytosis of particles by airway macrophages, and 3) the transepithelial transfer (transcellular or intercellular) of particulate matter and subsequent uptake in blood or lymph vessels [5]. Each of these mechanism depends on the

size of the deposited material and is characterized by specific half-times, ranging from several days to a few months.

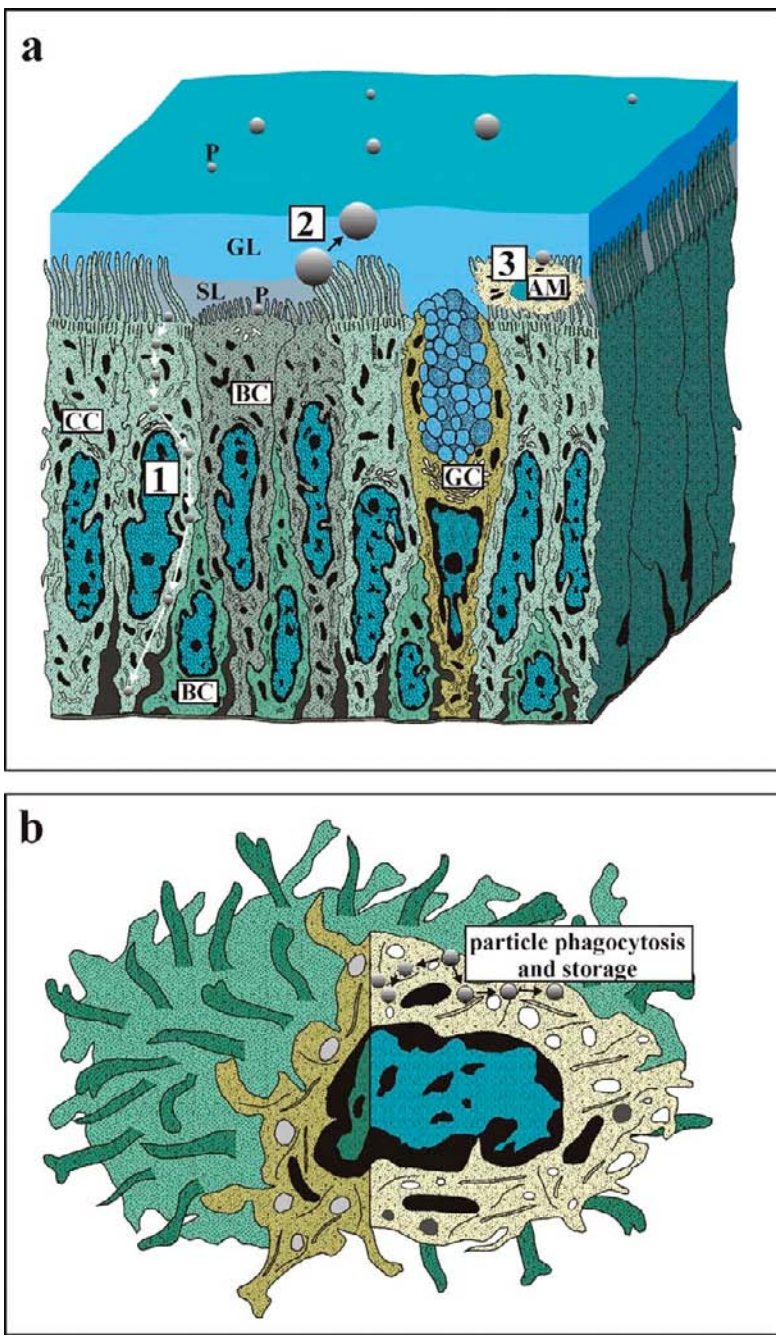

Figure 7. **a)** Illustration of the bronchial epithelium with its diverse cell types, including ciliated cells (CC), globlet cells (GC), basal cells (BC), and brush cells (BC). The three main mechanisms of slow bronchial clearance are also shown: 1) transepithelial transfer, 2) re-transfer onto the gel layer, and 3) uptake by airway macrophages (AM). Abbreviations: P…particle, GL…gel layer, SL…sol layer. **b)** Schematic illustration of an airway macrophage with its numerous pseudopodia.

Within the alveolar region, clearance of deposited particles mainly takes place by alveolar macrophages which penetrate through the epithelium, after their differentiation in the interstitium has been finished [12]. Orientation and mobility of single macrophages is controlled by chemotaxis (i.e. movement along a concentration gradient). Each macrophage has a certain particle loading capacity, determining its motility and lifetime [42]. After their phagocytotic activity in the alveoli, macrophages either emigrate into the bronchial compartment, where they are transported on the mucus layer towards the larynx, or penetrate back into the alveolar interstitium. As suggested in Fig. 7, smaller particle fractions may also be endocytized by epithelial cells and evacuated via the lymph system. The role of the surfactant as a possible alveolar clearance mechanism is not fully understood until now [43].

Models of Particle Deposition in the Human Lungs

Development of Deterministic and Probabilistic Deposition Models

Basic requirements for the calculation of particle deposition in the lungs are, besides the creation of an appropriate structure of the lungs, the simulation of aerosol transport in the compartments of the respiratory tract, and the estimation of specific deposition mechanisms with mathematical equations. These formulae are either empirically derived from related experimental data or obtained from theoretical considerations. Airway geometry is usually approximated either by a sequence of straight cylindrical tubes [6,31,44], by a channel with exponentially increasing cross section resembling a trumpet shape [45], or by a sequence of Y-shaped bifurcations with geometric correlation between parental and daughter airways [7,8]. While the second approximation was limited to a rather short period of usage, the remaining two geometries are frequently applied in modern mathematical approaches. In early models of the lung structure, airway dimensions including length, diameter, number of airways per generation, and branching and gravity angles were not treated statistically. These among other resulted in a fully symmetric structure of the branching network of the tracheobronchial tree (Fig. 8) [6].

Symmetric or deterministic lung models and mathematical equations describing particle behaviour in straight and bent tubes (Fig. 9) were used in theoretical approaches to aerosol deposition until the middle of the 1990s. As a main drawback standing behind the assumption of a symmetric lung architecture all tubes of the same airway generation were characterized by identical geometric parameters. Furthermore, each pathway leading to the closing sacs consisted of the same number of tubes. As a consequence of this simulation of particle deposition provided constant values which could be only varied by a change of breathing and particle parameters. Intrasubject variability describing the partly significant variation of airway geometry within a given lung generation was not considered at this stage of model development.

To overcome the deficit of an inaccurate simulation of the lung structure in a first step the human lungs were subdivided into five compartments representing the five lung lobes [31]. Each lobe was marked by a specific geometry of the first three or four bronchial generations, resulting in an intrasubject variation of the proximal part of the tracheobronchial tree. The following airway generations were again defined according to the deterministic construction principle. Hence, variation of particle deposition showed a progress with respect to earlier

models but was still subject to remarkable limits. In another approach the constant length of airway paths, representing another problem of symmetric lung structures, was tried to be solved by the assumption that airways may branch into daughter tubes belonging to different generations. Geometric parameters within a generation were still kept constant [44].

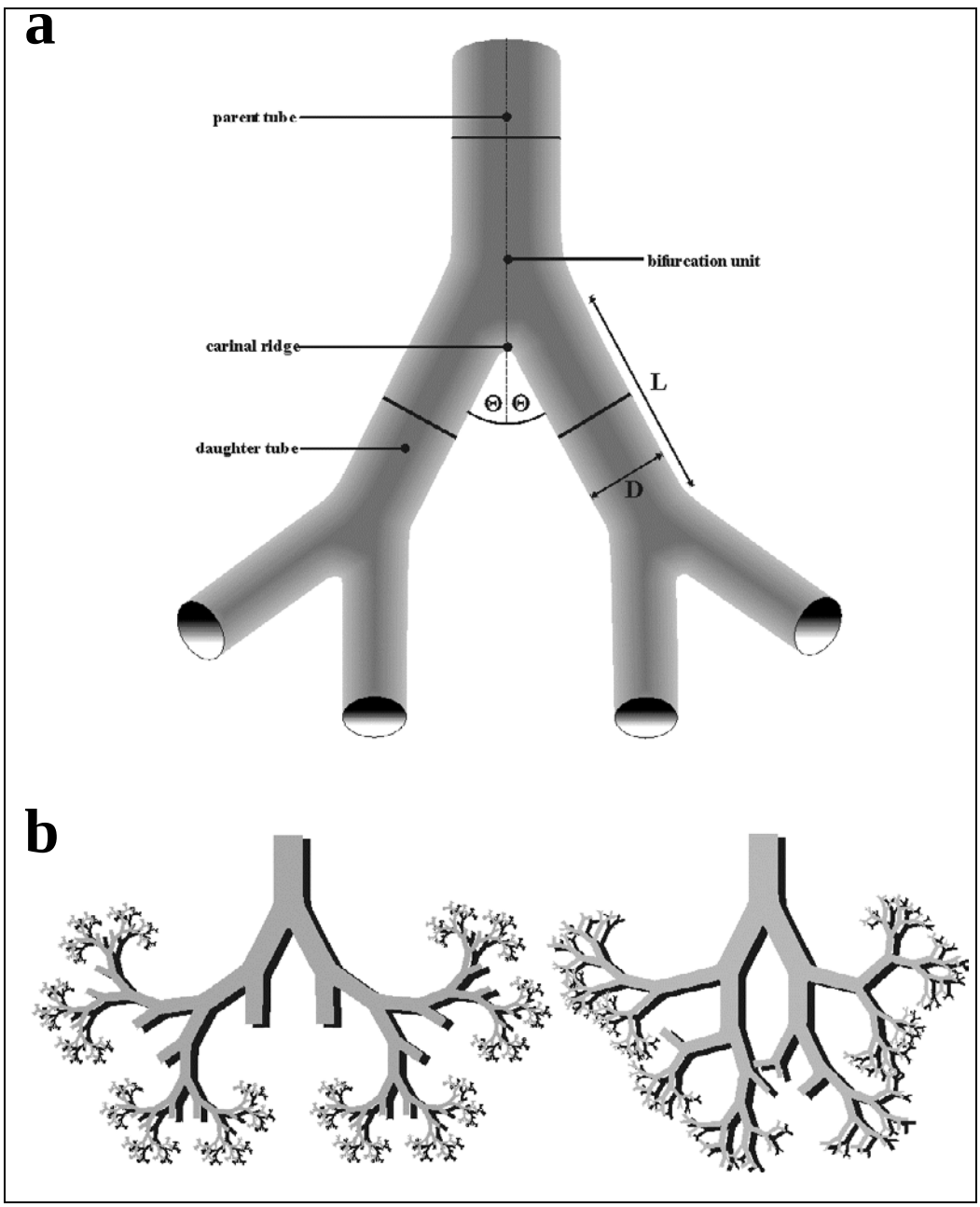

Figure 8. **a)** Model of the tracheobronchial tree as numerous sequences of airway bifurca-tions, including half of the parent tube and half of the daughters (D...diameter, L...airway length, Θ...branching angle). **b)** Symmetric (left) and asymmetric (right) lung geometry.

A) Deposition probability by Brownian diffusion p_d

$$p_d = 1 - \sum_{i=1}^{3} a_i \cdot e^{-b_i \cdot x} - a_4 \cdot e^{-b_4 \cdot x^{\frac{2}{3}}}$$

$$x = \frac{L \cdot D}{2 \cdot R^2 \cdot v}$$

D…diffusion coefficient

R…radius of the tube

L…length of the tube

v…mean flow velocity

a_i, b_i…empirical coefficients

B) Deposition probability by sedimentation p_s

$$p_s = 1 - e^{\left(\frac{4 \cdot g \cdot C \cdot \rho \cdot r^2 \cdot L \cdot \cos \Phi}{9 \cdot \pi \cdot \mu \cdot R \cdot v}\right)}$$

g…acceleration of gravity

Φ…angle relative to gravity

ρ…density of the particle

C…Cunningham slip correction factor

r…radius of the particle

μ…viscosity of the fluid

C) Deposition probability by impaction p_i

$$p_i = 1 - \frac{2}{\pi} \cdot \cos^{-1}(\theta \cdot St) + \frac{1}{\pi} \cdot \sin[2 \cdot \cos^{-1}(\theta \cdot St)], \text{ for } \theta\, St < 1,$$

$$p_i = 1, \text{ for } \theta\, St > 1$$

θ…branching angle

St…Stokes number

Figure 9. Deposition formulae for cylindrical tubes [31] which are used in the stochastic deposition model of Koblinger and Hofmann [7].

A more promising approximation to the realistic lung structure and its application to particle deposition succeeded in the 1980s with the extensive statistical treatment of morphometric lung data [46-48]. Preliminary approaches were still based on Weibel's lung model [6]. Although they could provide geometric variations for each bronchial airway

generation and in a following step also for the acinar region, the concept of symmetric branching, where a parent tube branches into two geometrically identical daughter tubes, was still preserved. A complete break with the deterministic lung model was reached for the first time in the middle of the 1980s and should results in a revolutionary progress concerning the simulation of particle deposition [6,7,49,50]. A stochastic model was defined which expressed the randomness of the bronchial and acinar airway system by means of probability density functions of all relevant geometric parameters. Within a given lung generation size and orientation of a single airway was determined by the random selection of parameters from the related distributions. The distributions were derived from detailed morphometric measurements of the bronchial tree [51] and the acinar region [52].

Although intrasubject variablity was considered in an appropriate way in the first stochastic lung and deposition models, prediction were only valid for a standard subject but not for a population, where aerosol deposition may be characterized by high differences between two individuals. This circumstance is commonly termed intersubject variability and is routinely expressed by a large number of scaling factors which are implemented into the model. First approximations to this problem date back to the early 1980s [53,54]. In more recent times intersubject variability could be simulated with more success due to a continuous increase of available morphometric data [5].

Open Questions in Recent Deposition Modelling

Currently, deposition modelling concentrates upon three main questions: First, the exact behaviour of particles in single, double and triple airway bifurcations is tried to be decoded with the help of numerical simulations [55-57]. Any findings derived from these models are implemented into the deposition models of the entire lung and therefore increase the accuracy and reliability of deposition predictions. Numeric simulation of the whole tracheobronchial tree recently fails due to the lack of computer power but will be a main topic in future. The second question in deposition modelling concerns the behaviour of particles in diseased lungs. Here models among other help to increase the deposition efficiency of therapeutic aerosols by the adjustment of particle parameters and to develop breathing techniques, with the help of which the aerosol is more effectively transported to the target site of the lung [58-60]. The third question concerns the deposition of nonspherical particles in the human lungs. A continuous increase of our knowledge concerning this problem is important, since most inhalable aerosols do not have spherical but fibrous, platelet-like or irregular shape. Modelling studies show that nonspherical particles behave in a different way compared to spheres and partly represent important occupational hazards [22,61-63].

Currently Used Deposition Models – Two Examples

At present, both deterministic and stochastic particle deposition models are used, whereby the preference of a model strongly depends on which kind of statement is made. For giving coarse predictions the deterministic model is preferably applied due to a limited parameter input, whereas for more precise predictions application of the stochastic model is

insurmountable. In the following, the two most frequently used mathematical approaches, namely LUDEP© and IDEAL, are subject to a brief description.

The computer model LUDEP© was primarily developed to estimate regional (i. e. extrathoracic, bronchial, and alveolar) deposition for a wide range of particle sizes. Further, fractions of radioactivity in breathing air which are deposited in the anatomical lung regions of exposed individuals should be estimated [5]. From a mathematical point of view the approach represents a multicompartment model including compartments for the extrathoracic airways (ET_1, ET_2) and the thoracic airways (BB, bb, AI). Deposition in the extrathoracic airways is simulated according to an empirical method based on experimental data [64,65], whereby deposition efficiencies are subsequently scaled by anatomical dimensions to obtain reliable results for women and children [73]. Modelling of thoracic deposition and gas transport is realized by the implementation of theoretical results of the 1970s and 1980s [66-68] dealing with gas transport and particle deposition in the single lung regions and their dependence on a subject's lung size and breathing rate [5]. Also a mixing of tidal with residual air in the alveoli is considered, and aerosol deposition is calculated from the combined effects of inertial impaction, sedimentation, and Brownian diffusion. In general, computation of deposition takes place on the basis of a semiempirical approach using rather simple algebraic formulae that can be looked up in the related publication of the ICRP [5].

In the stochastic deposition model IDEAL (Inhalation, Deposition, and Exhalation of Aerosols in the Lung) outlined by Koblinger and Hofmann [7], the path of an inhaled particle is selected randomly ('random walk'). By application of a Monte Carlo method, the pathways of a large number of particles are simulated, selecting a new transport trajectory for each particle. For improving the statistics of the Monte Carlo calculations, the statistical weight method is used, where a unit weight is assigned to particles entering the trachea. This initial value is subsequently multiplied by $(1 - p)$ at each bifurcation with p denoting the bifurcation-specific deposition probability. The contribution to the deposition fraction is finally given by the product of the actual weight and the respective deposition probability. Generation-specific probabilities of deposition are usually computed by deterministic formulae. Within bronchial airways, Brownian motion, inertial impaction, and sedimentation are considered as the primary deposition mechanisms. Inertial impaction is calculated for a bent tube, where the bend angle equals the branching angle and the flow velocity is an average value of all velocities in a bifurcation unit [31]. For an appropriate calculation of particle deposition in the alveoli, these structures are approximated by spheres or parts of spheres with identical diameters. Deposition in alveoli strongly depends on whether total air mixing is assumed in the respective spheres or not. However, relevant deposition mechanisms are sedimentation and Brownian diffusion. Deposition calculation is based on the input of numerous parameters regarding lung volumes, breathing, and particle properties. The model allows a prediction of particle deposition for each airway generation [9,69].

Mathematical Approaches to Bronchial Clearance of Insoluble Particles from the Lungs

Development of Clearance Models Based on Symmetric and Asymmetric Lung Structures

Similar to deposition modelling, numerous mathematical approximations of tracheobronchial particle clearance have been published during the last three decades. In the 1970s and 1980s, main interest was focused on the development of appropriate models describing only mucociliary clearance in the bronchial airway generations and using mainly deterministic lung geometry ('typical-path models'). Estimations of bronchial mucus velocities, which are necessary for the description of a continuous particle transport from the site of deposition to the larynx, were uniformly based on 1) velocity measurements in the trachea and 2) geometrical considerations like cross section ratios between parent and daughter airways in a selected bifurcation [70]. Computed velocity data based on these assumptions were published by a great number of scientific groups [71-73]. At the end of the 1980s physicists succeeded in the generation of a retention curve for the tracheobronchial region and the calculation of clearance time of deposited particles in each airway generation [74] which meant a considerable break-through on this field.

Results produced by the deterministic clearance models stated above were adopted by national and international committees for a more reliable risk assessment of hazardous particles. The ICRP [5] for instance used selected models [72-74] for the computation of mucus velocities in the first 9 airway generations and assumed a constant clearance rate of 2 day^{-2} for the remaining generations. The NCRP [75], on the other hand, developed an approach similar to that of Cuddihy & Yeh [74] and was able to generate mucus velocities for the entire lung.

Approximation of mucus clearance in a stochastic lung structure was attempted for the first time by Yeh & Schum [31] who divided the lung into five lobes with symmetric geometry ('lobar-specific typical-path model'). This improvement caused a significant derivation of particle clearance taking place along an average pathway which was a main drawback of earlier models. A better consideration of the complex lung structure was finally realized in various stochastic clearance models based on the assumption of a steady-state steady-flow of mucus in the tracheobronchial tree [70] or, in a more simplified approach, the circumstance of an exponential velocity decrease from proximal to terminal airways [76].

The consideration of slow bronchial clearance, being of high importance for small particles (100 nm – 1 μm), was necessary, after numerous inhalation experiments confirmed the existence of clearance mechanisms requiring much more time than few hours [35,36,41]. A respective slow bronchial clearance fraction was implemented into the multicompartment model outlined by the ICRP in the middle of the 1990s [5] and into more current models [76], whereas a more detailed theoretical formulation of slow bronchial clearance was carried out with the compartment model introduced by Sturm & Hofmann [77].

The Multicompartment Clearance Model of the ICRP

In general, the model of the of the ICRP [5] assumes that particulate matter deposited in the respiratory tract is cleared by three main routes, i. e. into cardiovascular system by absorption, in the gastrointestinal tract (GIT) via the pharynx, and to regional lymph nodes (LN) via lymphatic channels. Clearance by these routes takes place from four regions, namely the extrathoracic compartment (ET), the bronchi (BB), the bronchioli (bb), and the alveoli (AI). Clearance kinetics are expressed in terms of transfer rates (in d^{-1}) between specific compartments which are independent of any particle properties and take values between 0.00002 and 100 d^{-1} [5].

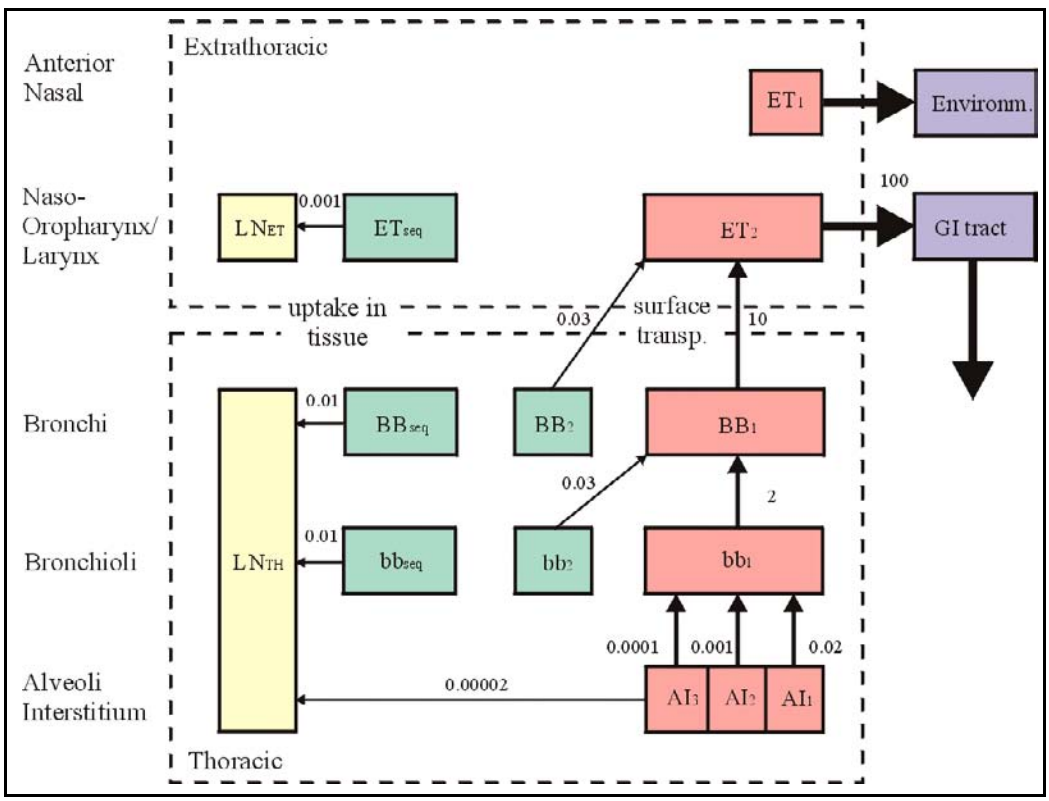

Figure 10. Multicompartmental clearance model proposed by the ICRP [5]. The model already considers a slow bronchial clearance phase represented by the compartments BB_2, BB_{seq}, bb_2, and bb_{seq}. Transfer rates between two compartments are given in $days^{-1}$.

Based on numerous experimental data, a slow bronchial clearance fraction, f_s, is defined representing the fraction of deposited particles which are exclusively cleared by slow mechanisms (epithelial/macrophage uptake etc.). The respective slow bronchial clearance phase is implemented into the multicompartmental clearance model. For the bronchial (generations 1 – 8) and bronchiolar (generations 9 – 16) regions, this phase is expressed by the compartments BB_2, BB_{seq}, bb_2, and bb_{seq}. A scheme of the ICRP model with its single compartments and related transfer rates (in d^{-1}) is presented in Fig. 10. In the multicompartment approach a dependence of f_s on the aerodynamic diameter, d_{ae}, of particles

deposited in the tracheobronchial tree is assumed. For spherical particles with $d_{ae} < 2.5$ µm f_s is believed to amount to a constant value of 0.5, i. e. 50 % of the particulate matter deposited on the airway walls is subject to slow clearance mechanisms, while for spheres with $d_{ae} > 2.5$ µm an exponential decrease of f_s with particle size is taken into account. In addition, the deposition fraction as a function of d_{ae} is different in the bronchial and bronchiolar lung region, resulting in different slow clearance fractions in these specific compartments [5]. There can be no doubt that the model provided by the ICRP represented an important milestone concerning the theoretical treatment of particle clearance in the middle of the 1990s. Meanwhile certain processes attributing to slow bronchial clearance have been decoded more in detail, so that a refinement of the model seems to be justified.

Conclusion

In this chapter main developments concerning the theoretical simulation of particle deposition and clearance in the human respiratory tract have been illustrated. As could be exhibited in detail, the complexity of such models has continuously increased during the past decades, so that currently used approaches mostly provide precise and highly realistic predictions. A significant part of this progress is indeed based on the rapid development of the computer technology which represented a main limiting factor in the 1970s and 1980s but enables highly intricate numeric calculations at present. Future improvements of lung models will mainly concern the extrathoracic architecture as well as the geometric variability of the alveoli during the breathing cycle. Also structural changes of the lung due to specific diseases such as chronic bronchitis, asthma or cystic fibrosis will find increased attention. Regarding particle deposition, influences of asymmetric and asynchronous filling of the lung with air will be an important topic in future, because these phenomena play a significant role in the diseased lung and therefore need a reliable mathematical description. Finally, the application of therapeutic aerosol will attract main attention of biophysicists and mathematicians, because theoretical deposition models act as excellent tools for the maximization of deposition efficiencies hitherto. This very positive co-operation between physics and medical/pharmaceutical science will be further strengthened in the following years. Concerning particle clearance out of the human respiratory tract, slow clearance mechanisms still representing some kind of enigma will be successively decoded by experiments. This will finally result in a more complete and realistic approach describing the evacuation of particulate matter from the lungs. Additionally, clearance modelling will follow the same questions as deposition modelling and thus will increasingly concentrate on the insufficient lung.

References

[1] Rose, M. R. (1987). *Quantitative ecological theory: An introduction to basic models*. Baltimore, Md.: The John Hopkins University Press.

[2] Atkins, G. L. (1969). *Multicompartment models for biological systems*. London, UK: Methuen.

[3] Smitalova, K. & Sujan, S. (1991). *A mathematical treatment of dynamical models in biological science*. New York, NY: Horwood.

[4] Meinhardt, H. (1982). *Models of biological pattern formation*. London, UK: Academic Press.

[5] International Commission on Radiation Protection (ICRP) (1994). *Human respiratory tract model for radiological protection: Publication* **66.** *Ann. ICRP*. Oxford, UK: Pergamon Press.

[6] Weibel, E. R. (1963). *Morphometry of the Human Lung*. Berlin, Germany: Springer Verlag.

[7] Koblinger, L. & Hofmann, W. (1985). Measurement of human lung morphometric data for stochastic aerosol deposition calculations. *Phys. Med. Biol.* **30**, 541-556.

[8] Koblinger, L. & Hofmann, W. (1990). Monte Carlo modeling of aerosol deposition in human lungs. Part I: Simulation of particle transport in a stochastic lung structure. *J. Aerosol Sci.* **21**, 661-674.

[9] Hofmann, W. & Bergmann, R. (1998). Predictions of particle deposition patterns in human and rat airways. *Inhal. Toxicol.* **10**, 557-583.

[10] Hofmann, W., Martonen, T. & Menaché, M. (1990). A dosimetric model for localised radon progeny accumulations at tracheobronchial bifurcations. *Rad. Prot. Dosim.* **30**, 245-259.

[11] Attix, F. H. (1986). *Introduction to radiological physics and radiation dosimetry*. New York, NY: Wiley.

[12] Kreyling, W. G. & Scheuch G. (2000). Clearance of Particles Deposited in the Lungs. In P. Gehr & J. Heyder (eds.), *Particle-Lung Interactions* (pp. 323-376). New York, Basel, Marcel Dekker, Inc.

[13] Boucher, R. C. (2002). An overview of the pathogenesis of cystic fibrosis lung disease. *Adv. Drug Del. Rev.* **54**, 1359-1371.

[14] Marks, J. H. (2007). Airway clearance devices in cystic fibrosis. *Paed. Resp. Rev.* **8**, 17-23.

[15] Rogers, D. F. (2005). Mucociliary dysfunction in COPD: effect of current pharmacotherapeutic options. *Pul. Pharm. Therap.* **18**, 1-8.

[16] Stanley, P. J., Wilson, R., Greenstone, M. A., Mackay, I. S. & Cole, P. J. (1985). Abnormal nasal mucociliary clearance in patients with rhinitis and its relationship to concomitant chest disease. *Brit. J. Dis. Chest* **79**, 77-82.

[17] Hinds, W. C. (1999). *Aerosol technology: properties, behaviour, and measurement of airborne particles* (2nd ed.). New York, NY: Wiley.

[18] Colbeck, I. (1998). *Physical and chemical properties of aerosols*. London, UK: Blackie Acad. & Professional.

[19] Finlay, W. H., ed. (2001). *The mechanics of inhaled pharmaceutical aerosols: an introduction*. San Diego, CA: Academic Press.

[20] Yu, C. P., Zang, L., Oberdörster, G., Mast, R. W., Glass, L. R. & Utell, M. J. (2004). Deposition modeling of refractory ceramic fibers in the rat lung. *J. Aerosol Sci.* **25**, 407-417.

[21] Hesterberg, T. W. & Hart, G. A. (2001). Synthetic Vitreous Fibers: A Review of Toxicology Research and ist Impact on Hazard Classification. *Crit. Rev. Toxicol.* **31**, 1-53.

[22] Su, W. C. & Cheng, Y. S. (2006). Deposition of fiber in a human airway replica. *J. Aerosol Sci.* **37**, 1429-1441.
[23] Hansel, T. T., ed. (2001). *New drugs for asthma, allergy and COPD*. Basel, Switzerland: Karger.
[24] Kaliner, M. A., ed. (1991). *Asthma: its pathology and treatment*. New York, NY: Dekker.
[25] Crystal, R. G. & West J. B. (1991). *The Lung*. New York, NY: Raven Press.
[26] Bonsignore, G., ed. (1982). *The lung in its environment*. New York, NY: Plenum Press.
[27] Mercer, R. R., Russell, M. L., Roggli, V. L. & Crapo, J. D. (1994). Cell number and distribution in human and rat airways. *Am. J. Respir. Cell Mol. Biol.* **10**, 613-624.
[28] Hlastala, M. P., ed. (1998). *Complexity in structure and function of the lung*. New York, NY: Dekker.
[29] Ross, M. H. (1995). *Histology: a text and atlas* (3rd ed.). Baltimore, Md.: Williams & Wilkins.
[30] Telford, I. R. (1995). *Introduction to functional histology* (2nd ed.). London, UK: Harper Collins.
[31] Yeh, H. C. & Schum, G. M. (1980). Models of human lung airways and their application to inhaled particle deposition. *Bull. Math. Biol.* **42**, 461-480.
[32] Taulbee, D. B. (1978). Simultaneous diffusion and sedimentation of aerosol particles from Poiseuille flow in a circular tube. *J. Aerosol Sci.* **9,** 17-23.
[33] Lippmann, M., Yeates, D. B. & Albert R. E. (1980). Deposition, retention, and clearance of inhaled particles. *Brit. J. Ind. Med.* **37**, 337-362.
[34] Balásházy, I. & Hofmann, W. (1993). Particle deposition in airway bifurcations - I. Inspiratory flow. *J. Aerosol Sci.* **24**, 745-772.
[35] Oberdörster, G. (1988). Lung clearance of inhaled insoluble and soluble particles. *J. Aerosol Med.* **1**, 289-330.
[36] Gehr, P. & Im Hof, V. (1991). The fate of particles deposited in the airways. *J. Aerosol Med.* **4**, 6-15.
[37] Albert, R. E. & Arnett, L. C. (1955). Clearance of radioactive dust from the human lung. *AMA Arch. Ind. Health* **12**, 99-106.
[38] Albert, R. E., Lippmann, M. & Briscoe, W. (1969). The characteristics of bronchial clearance in humans and the effects of cigarette smoking. *Arch. Env. Health* **18**, 738-755.
[39] Albert, R. E., Lippmann, M., Peterson Jr., H. T., Berger, J., Sanborn, K. & Bohning D. (1973). Bronchial deposition and clearance of aerosols. *Arch. Int. Med.* **131**, 115-127.
[40] Brain, J. D., Proctor, D. F. & Reid, L. M. (1977). *Respiratory defense mechanisms*. New York, NY: Marcel Dekker Inc.
[41] Geiser, M., Im Hof, V., Gehr, P. & Cruz-Orive, L. M. (1990). Histological and stereological analysis of particle retention in the conducting airways of hamster lungs. *J. Aerosol Med.* **3**, 131-145.
[42] Gradon, L. & Podgorski, A. (1992). Mathematical model of dust retention in the human respiratory system. *J. Aerosol Med.* **5**, 229-234.
[43] Gehr, P., Schürch, S., Berthiaume, Y., Im Hof, V. & Geiser, M. (1990). Particle retention in airways by surfactant. *J. Aerosol Med.* **3**: 27-43.
[44] Horsefield, K., Dart, G., Olson, D. E., Finley, G. F. & Cumming, G. (1971). Models of the human bronchial tree. *J. Appl. Physiol*. **31**, 207-217.

[45] Taulbee, D. B. & Yu, C. P. (1975). A theory of aerosol deposition in the human respiratory tract. *J. Appl. Physiol.* **38**, 77-85.

[46] Soong, T. T., Nicolaides, P., Yu, C. P. & Soong, S. C. (1979). A statistical description of the human tracheobronchial tree geometry. *Respir. Physiol.* **37**, 161-172.

[47] Yu, C. P., Nicolaides, P. & Soong, T. T. (1979). Effect of random airway sizes on aerosol deposition. *Ann. Ind. Hyg. Assoc. J.* **40**, 999-1005.

[48] Hofmann, W. & Daschil, F. (1986). Biological variability influencing lung dosimetry for inhaled ^{222}Rn and ^{220}Rn. *Health Phys.* **50**, 345-367.

[49] Koblinger, L. & Hofmann, W. (1986). Aerosol deposition calculations with a stochastic lung model. *Acta Phys. Hung.* **59**, 31-34.

[50] Koblinger, L. & Hofmann, W. (1988). Monte Carlo model for aerosol deposition in human lungs. In J. Dodgson, R. I. McCallum, M. R. Bailey & D. R. Fisher (eds.), Inhaled Particles IV (pp. 65-70). Oxford, UK : Pergamon Press.

[51] Raabe, O. G., Yeh, H. C., Schum, G. M. & Phalen, R. F. (1976). *Tracheobronchial geometry: Human, Dog, Rat, Hamster,* **LF-53**. Albuquerque, NM: lovelace Foundation Report.

[52] Haefeli-Bleuer, B. & Weibel, E. R. (1988). Morphometry of the human pulmonary acinus. *Anat. Rec.* **220**, 401-414.

[53] Yu, C. P. & Diu, C. K. (1982). A comparative study of aerosol deposition in different lung models. *Ann. Ind. Hyg. Assoc. J.* **43**, 54-65.

[54]Yu, C. P. & Diu, C. K. (1982). A probabilistic model for intersubject deposition variability of inhaled particles. *Aerosol Sci. Technol.* **1**, 335-362.

[55] Zhang, Z., Kleinstreuer, C. & Kim, C. S. (2001). Effects of curved inlet tubes on air flow and particle deposition in bifurcating lung models. *J. Biomech.* **34,** 659-669.

[56] Zhang, Z., Kleinstreuer, C. & Kim, C. S. (2002). Cyclic micron-size particle inhalation and deposition in a triple bifurcation lung airway model. *J. Aerosol Sci.* **33**, 257-281.

[57] Heistracher, T., & Hofmann, W. (1997). Flow and deposition patterns in successive airway bifurcations. *Ann. Occup. Hyg.* **41**, 537–542.

[58] Swift, D. L. (1992). Apparatus and method for measuring regional distribution of therapeutic aerosols and comparing delivery systems. *J. Aerosol Sci.* **23/S1**, 495-498.

[59] Everard, M. L. (2003). Inhalation therapy for infants. *Adv. Drug Del. Rev.* **55**, 869-878.

[60] Sturm, R. & Hofmann, W. (2004). Stochastic Simulation of Alveolar Particle Deposition in Lungs Affected by Different Types of Emphysema. *J. Aerosol Med.* **17**: 357-372.

[61] Lippmann, M. (1990). Effects of fiber characteristics on lung deposition, retention, and disease. *Env. Health Persp.* **88**, 311-317.

[62] Dai, Y. T. & Yu, C. P. (1998). Alveolar deposition of fibers in rodents and humans. *J. Aerosol Med.* **11**, 247-258.

[63] Stöber, W. (1972). Dynamic shape factors of nonspherical aerosol particles. In T. Mercer et al. (eds.) *Assessment of airborne particles* (pp. 249-289). Springfield: Thomas.

[64] Stahlhofen, W., Rudolf, G., and James, A. C. (1989). Intercomparison of Experimental Regional Aerosol Deposition Data. *J. Aerosol Med*. **2**, 285-308.

[65] Rudolf, G., Gebhart, J., Heyder, J., Schiller, C. F. & Stahlhofen, W. (1986). An empirical formula describing aerosol deposition in man for any particle size. *J. Aerosol Sci.* **17**, 350-355.

[66] Heyder, J. & Rudolf, G. (1984). Mathematical models of particle deposition in the human respiratory tract. *J. Aerosol Sci.* **15**, 517-532.

[67] Scherer, P. W., Shendalman, L. H., Greene, N. M. & Bouhuys, A. (1975). Measurement of axial diffusivities in a model of the bronchial airways. *J. Appl. Physiol.* **38**, 719-723.

[68] Egan, M. J. & Nixon, W. (1985). A model for aerosol deposition in the lung for use in inhalation dose assessments. *Radiat. Prot. Dosim.* **11**, 5-17.

[69] Hofmann, W., Asgharian, B. & Winkler-Heil, R. (2002). Modelling intersubject variability of particle deposition in human lungs. *J. Aerosol Sci.* **33**, 219-235.

[70] Asgharian, B., Hofmann, W. & Miller, F. J. (2001). Mucociliary clearance of insoluble particles from the tracheobronchial airways of the human lung. *J. Aerosol Sci.* **32**, 817-832.

[71] Lee, P. S., Gerrity, T. R., Hass, F. J. & Lourenco, R. V. (1979). A model for tracheobronchial clerance of inhaled particles in man and a comparison with data. *IEEE Trans. Biomed. Eng.* **26**, 624-630.

[72] Yeates, D. B., Gerrity, T. R. & Garrard, C. S. (1982). Characteristics of tracheobronchial deposition and clearance in man. *Ann. Occup. Hyg.* **26**, 245-257.

[73] Yu, C. P., Hu, J. P., Yen, B. M., Spektor, D. M. & Lippmann, M. (1986). Models of mucociliary particle clearance in lung airways. In S. D. Lee, T. Schneider, L. D. Grant & P. J. Verkerk (eds.), *Aerosols: Research, risk assessment and control strategies* (pp. 569-578). Chelsea, MI: Lewis.

[74] Cuddihy, R. G. & Yeh, H. C. (1988). Respiratory tract clearance of particles and substances dissociated from particles. In U. Mohr (ed.), Inhalation toxicology: The design and interpretation of inhalation studies and their use in risk assessment (pp. 169-193). Berlin, GER: Springer.

[75] National Council on Radiation Protection & Measurement (NCRP) (1997). *Deposition, retention and dosimetry of inhaled radioactive substances*. Report No. 125.

[76] Hofmann, W. & Sturm, R. (2004). Stochastic Model of Particle Clearance in Human Bronchial Airways. *J. Aerosol Med.* **17**, 73-89.

[77] Sturm, R. & Hofmann, W. (2006). A multicompartment model for bronchial clearance of insoluble particles in the human lung. *Radiat. Prot. Dosim.* **118**, 384-394.

In: Mathematical Biology Research Trends
Editor: Lachlan B. Wilson, pp. 217-235
ISBN 978-1-60456-141-8

Chapter 8

SYSTEMS BIOLOGY OF THE TRYPTOPHAN OPERON

***M. Santillán*[1,2]*, *Eduardo S. Zeron*[3†] *and M.C. Mackey*[2,4‡]**
[1] Centro de Investigación y Estudios Avanzados del IPN, Unidad Monterrey,
Parque de Investigación e Innovación Tecnológica,
Autopista Monterrey-Aeropuerto Km 10,
Apodaca NL 66600, MÉXICO,
[2]Centre for Nonlinear Dynamics in Physiology and Medicine,
McGill University, 3655 Promenade Sir William Osler,
Montreal, QC H3G 1Y6, CANADA
[3]Departamento de Matemáticas, CINVESTAV-IPN,
Apartado Postal 14-740, México DF 07000, MÉXICO
[4]Departments of Physiology, Physics, and Mathematics,
McGill University, Montreal, QC, CANADA

Abstract

We start by introducing a brief review of the history of interdisciplinary research in biology, as well as some of basic concepts from molecular biology. Then, we present a survey of the philosophy and goals of a new area of interdisciplinary research: systems biology. Finally, we review our efforts of the past few years to understand, via mathematical modeling, the dynamic behavior of one of the most studied gene regulatory networks in bacteria: the tryptophan operon, and offer new results.

1. Introduction

The knowledge of the complete genome of a given species is just a small piece of the information thought to be useful in the understanding of one of the most complicated and

*E-mail address: moises.santillan@mac.com,
URL: `http://homepage.mac.com/moises.santillan/`.
†E-mail address: eszeron@math.cinvestav.mx
‡E-mail address: michael.mackey@mcgill.ca

important puzzles in science: “How does a biological system work?”. To fully understand the behavior of an organism, an organ, or even a single cell, we need to understand the underlying gene regulatory dynamics. Given the complexity of even a single cell, answering this questions is impossible at the moment and will remain so for the foreseeable future. However, by analyzing the simplest genetic regulatory systems we may be able to develop the mathematical techniques and procedures required to tackle ever more complex genetic networks in the future.

In this paper, we review our efforts of the past few years to understand, via mathematical modeling, the dynamic behavior of one of the most studied gene regulatory networks in bacteria: the tryptophan operon. As we shall see, it is possible to obtain valuable information with relatively simple models, despite all of the assumptions underlying them.

2. A Brief Historical Review

During the Enlightenment, in the latter part of the 18th and early part of the 19th Centuries, scientific disciplines started to be hierarchically classified. This classification into the so called *exact sciences* (physics and mathematics) and those of the *life sciences* (biology and medicine) has led to the notion that these two broad divisions have evolved following distinct, separate, and sometimes even contradictory or conflicting pathways. The truth, however, is far different. Since the origins of modern science, there have been people making important contributions to both the exact and life sciences as well as the very interface between them. William Harvey discovered blood circulation with the aid of a mathematical model. Electrodynamics started with the work of Galvani and Volta (both physicians) on animal electricity. Later, Helmholtz (also a physician, but better known for his contributions to physics) invented the myograph and the ophthalmoscope, recorded for the first time the velocity of a nervous impulse, discovered the first law of thermodynamics (based on metabolic considerations), and helped to settle the foundations of all modern theories of resonance with his studies on auditory physiology.

During the 20th century, electrophysiology (the science that studies the interactions between biological tissues and electromagnetic fields) advanced enormously. Archibald V. Hill, Bernard Katz, Max Planck, Walter Nernst, Kenneth S. Cole, Alan L. Hodgkin, Andrew, F. Huxley, Erwin Neher, and Haldan K. Hartline, among others, made important contributions to its progress. Some remarkable events in the history of electrophysiology were: the explanation for the origin of the action potential, elucidated by Hodgkin and Huxley with the aid of highly sophisticated mathematical models; the Huxley cross-bridge model for muscle contraction; and the invention of the patch clamp technique by Neher.

Charles Darwin published his theory of evolution through natural selection in 1859. From the beginning, it was clear that this theory lacked proper statistical foundations, and this was its main weakness. Indeed, an apparent contradiction between Darwinism and Mendel’s laws of inheritance arose immediately after the Mendelian laws were rediscovered in 1900. This gap was closed through the work of many mathematicians who, between 1860 and 1940, developed the necessary statistical tools to fuse genetics and Darwinism. The result is what we know today as population genetics or neo-Darwinism. Some of the most important contributors to this success were: Fleeming Jenkin, Francis Galton, Karl Pearson, Raphael Weldon, Godfrey H. Hardy, Ronald A. Fisher, Sewall Wright, and

Theodosius Dobzhansky. Interestingly, Godfrey H. Hardy and Ronald A. Fisher are well known in the mathematical community for their contributions to real analysis and number theory [Hardy], and probability and statistics [Fisher].

Molecular biology consolidated between 1940 and 1960, and until 1970 two different schools were recognized: the structural and the informatics schools. The physicists W. H. Bragg and W. L. Bragg (father and son) founded the structural school in Cambridge. They invented X-ray crystallography in 1912, and the structural analysis of biological molecules soon started in their lab. Some of the best known structuralists were W. T. Astbury , John D. Bernal, Max Perutz, and John C. Kendrew (all of them from Cambridge), as well as Linus Pauling from Caltech. The structuralists were convinced that no new physical laws were required to explain vital phenomena. They endeavored to explain the function of biomolecules (and so of tissues and organs) from their inner structure. The secondary proteinic structure known as the alpha helix, and the structures of hemoglobin and myoglobin are some of the most important discoveries from this school.

Inspired on the uncertainty principle of quantum mechanics, Niels Bohr proposed that new principles from physics may be necessary to understand life. With this assertion, Bohr founded the informatics school of molecular biology. Max Delbrück and Erwin Schrödinger (both physicists) were two of the most important spokesmen for this school. When the Nazis took power in Germany, Delbrück moved to the USA were he started a very successful collaboration with Salvador Luria on bacteriophage research. This collaboration greatly advanced our knowledge of the molecular basis of genetics. On the other hand, Schrödinger had to move to Dublin after the Nazis invaded Austria, and there he published a little book entitled *What is life?*, which was tremendously influential on the development of molecular biology.

Some of those recruited by Schrödinger's book were James Watson and Francis Crick (who later discovered the structure of DNA in 1953), Maurice Wilkins (who provided essential physical data to Watson and Crick), Seymour Benzer (who sequenced the first gene), and François Jacob (who discovered mRNA and, together with Jacques Monod, the regulatory mechanisms of the *lac* operon.

During the second half of the 20th Century, biomathematics, also known as mathematical biology, developed as a branch of applied mathematics. Biomathematics is an active field of research and interest in it is accelerating as is the number of individuals working on it. It is essentially dedicated to mathematical modeling biological phenomena. Biomathematicians have made important contributions to ecology (through population dynamics), epidemiology, pattern formation (through the study of reaction diffusion equations), molecular biology, integrative physiology, and medicine. Some of the most best known biomathematicians are B. van der Pol, A. J. Lotka, V. Volterra, A. Turing, J. M. Smith, A. T. Winfree, etc. Readers interested in learning more about the common history of biology, mathematics, and physics are recommended to read References [1, 2, 3, 4, 5, 6].

3. Systems Biology

A new designation for an area of interdisciplinary research in biology, currently termed *systems biology*, emerged a few year ago; it continues with the long tradition described in the previous section, and especially with the long tradition of an integrative approach in

physiology. The closest ancestors to what is called systems biology are systems theory and cybernetics. Since systems biology inherits part of the philosophy and the goals of both, it is interesting to briefly review these latter two.

Systems theory is an interdisciplinary field which studies relationships between systems as a whole. It was founded in the 1950s and focuses on organization and interdependence of relationships. Systems dynamics is a central part of systems theory; it provides methods for understanding the dynamic behavior of complex systems. Such methods rely on the recognition that the structure of any system—the multi-circular, interlocking, sometimes time-delayed relationships among its components—is often just as important in determining its behavior as the individual components themselves. Indeed, in many cases, it is impossible to explain the behavior of the whole system in terms of the behavior of its separated parts only. Examples are chaos theory and social dynamics.

Cybernetics is the study of communication and control, typically involving regulatory feedback, in living organisms, in machines, and in combinations of the two. It is an earlier but still-used generic term for many of the subject areas that are subsumed under the headings of adaptive systems, artificial intelligence, complex systems, complexity theory, control theory, decision support systems, dynamical systems, information theory, learning organizations, mathematical systems theory, operations research, simulation, and systems engineering.

Contemporary cybernetics began in the 1940s as an interdisciplinary study connecting the fields of control theory, electrical network theory, logic modeling, neuroscience, and human physiology. The emphasis of cybernetics is on the functional relations that hold between the different parts of a system; rather than the parts themselves. These relations include the transfer of information, and circular relations (feedback) that result in emergent phenomena such as self-organization. The name cybernetics was coined by its intellectual father, Norbert Wiener, to denote the study of "teleological mechanisms" (i.e. machines with corrective feedback) and was popularized through his book *Cybernetics, or Control and Communication in the Animal and Machine* (1948). Wiener was, incidently, one of the most influential and original mathematicians of the first half of the 20th century.

Systems biology is an academic field that seeks to integrate different levels of information, and so to understand how biological systems work. By studying the relationships and interactions between various parts of a biological system (e.g., gene and protein networks involved in cell signalling, metabolic pathways, organelles, cells, physiological systems, organisms, etc.) it is hoped that eventually a comprehensive model of the whole system can be developed. As the intellectual grandchild of what was originally called human physiology it endeavors to expand physiology to include biochemistry as well as molecular biology.

In contrast to much of molecular biology, systems biology does not seek to break down a system into all of its parts and to study each part of the process at a time with the hope of being able to reassemble all the parts into a whole again. Systems biology begins with the study of genes and proteins in an organism using high-throughput techniques to quantify changes in the genome and proteome in response to a given perturbation. These techniques include microarrays to measure the changes in mRNAs and mass spectrometry, which is used to identify proteins, detect protein modifications, and quantify protein levels. However, systems biology is much more since it balances these molecular details against whole system performance and behavior. Using this integrated knowledge, the system biologist

can formulate hypotheses that explain a system's behavior. Importantly, these hypotheses can be used to mathematically model the system. Models are then used to predict how different changes in the environment affect the system itself, and so they can be iteratively tested for their validity.

Recent analysis has revealed that cell signals do not necessarily propagate linearly. Instead, cellular signalling networks can be used to regulate multiple functions in a context dependent fashion. Because of the magnitude and complexity of the interactions inside the cell, it is often impossible to understand intuitively the *systems behavior* of these networks. Rather, it has become necessary to develop mathematical models and analyze the behavior of these models, both to develop a systems-level understanding and to obtain experimentally testable predictions.

New approaches to these problems are constantly being developed by quantitative scientists, such as computational biologists, statisticians, mathematicians, computer scientists, engineers, and physicists, to improve our ability to create, refine, and retest the models until the predicted behavior accurately reflects the seen phenotype.

The reader interested in reading more about the definition and philosophy of systems biology may find References [7, 8, 4, 9, 5, 10, 11, 12] appealing.

4. The Central Dogma of Molecular Biology

The central dogma of molecular biology deals with the information flow between DNA, RNA, and proteins. The standard information-flow pathway can be summarized in a very short and oversimplified manner as follows: DNA $\rightarrow$ RNA $\rightarrow$ proteins. Proteins in turn facilitate the previous two steps, as well as the replication of DNA. This whole is therefore broken down into three steps: transcription, translation, and replication. Nevertheless, information can flow backwards in some steps; see Figure 1. Below, two of the processes accounted for by the central dogma (transcription and translation) are briefly reviewed.

Transcription

Transcription is the process through which a DNA amino acid sequence is copied by an enzyme known as RNA polymerase to produce a complementary RNA. In other words, it is the transfer of genetic information from DNA into RNA. In the case of protein-encoding DNA, transcription is the beginning of the process that ultimately leads to the translation of the genetic code (via the mRNA intermediate) into a functional peptide or protein.

In prokaryotic cells, like bacteria, transcription initiation takes place through the following steps:

- RNA polymerase (RNAP) recognizes and specifically binds to a DNA segment known as the promoter. At this stage, the DNA is double-stranded and (*closed*). This RNAP/wound-DNA structure is referred to as the closed complex.
- The DNA is unwound and becomes single-stranded (*open*) in the vicinity of the initiation site. This RNAP/unwound-DNA structure is called the open complex.
- The RNA polymerase transcribes DNA into RNA.

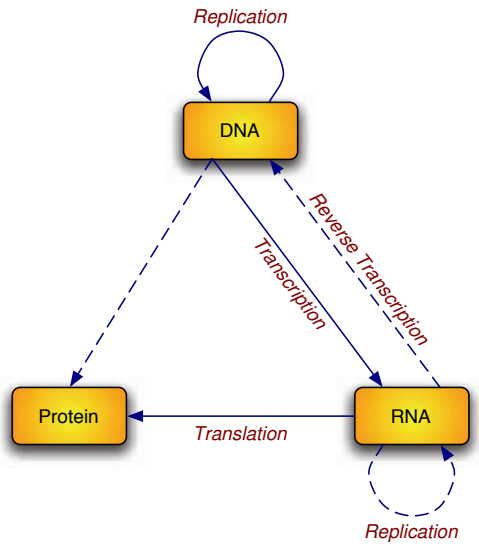

Figure 1. The 1970 version of the Central Dogma. The arrows represent the flow of information. Solid arrows represent *probable* information flow, while dotted arrows represent *possible* information flow. Note that information flow from proteins to RNA or DNA is regarded as impossible

Promoters can differ in *strength*; that is, how actively they promote transcription of their adjacent DNA sequence. Promoter strength is in many (but not all) cases, a matter of how tightly RNA polymerase and its associated accessory proteins bind to their respective DNA sequences. The more similar the sequences are to a consensus sequence, the stronger the binding is.

Translation

In prokaryotic cells, a nascent messenger RNA (mRNA) molecule is bound by a ribosome, where it is translated. The mRNA is read by the ribosome as triplet nucleotide sequences (codons). Complexes of initiation factors and elongation factors bring aminoacylated transfer RNAs (tRNAs) into the ribosome-mRNA complex, matching the codon in the mRNA to the anti-codon in the transfer RNA (tRNA), thereby adding the correct amino acid in the sequence encoding the gene. As the amino acids are linked into the growing peptide chain, they begin folding into the correct conformation. This folding continues until the nascent polypeptide chains are released from the ribosome as a mature protein.

5. The Tryptophan Operon

An operon is a DNA segment that includes an operator, a common promoter, and one or more structural genes. All of these structural genes are controlled as a single unit to produce messenger RNA (mRNA). Operons occur primarily in very simple organisms as prokaryotes and nematodes. The operon concept was introduced by François Jacob and Jacques

Monod in 1961, though their studies on what is now known as the lactose operon.

A promoter is a short DNA sequence that provides a site for RNA polymerase to bind and initiate transcription; thus, it is located before the structural genes. Close to the promoter, and usually beside it, lies an operator sequence. An operator is a segment of DNA that regulates the activity of the operon promoter by interacting with a specific protein. This protein can act either as a repressor or as an activator. The operon may also contain regulatory genes, such as a repressor gene, which codes for a protein that binds to the operator and inhibits transcription.

Tryptophan (Trp) is one of the 20 main amino-acids in the genetic code (codon UGG). It is an essential amino acid because it cannot be synthesized by mammals, and therefore must be part of our day-to-day diet. Among other important substances, tryptophan is a precursor for serotonin (a neurotransmitter) and melatonin (a neurohormone).

Tryptophan can be synthesized by bacteria like *E. coli* through a series of catalysed reactions. The catalyzing enzymes in *E. coli* are made up of the polypeptides encoded by the tryptophan operon genes: *(trpE*, *trpD*, *trpC*, *trpB*, and *trpA*). These genes are transcribed from *trpE* to *trpA*. Finally, transcription is initiated at promoter *trpP*, which is indeed located just before the gene *trpE*.

The *trp* operon is regulated by three different negative-feedback mechanisms: repression, transcription attenuation, and enzyme inhibition. Below, these regulatory mechanisms are briefly reviewed. It is convenient for this to refer to Figure 2.

The *trp* operon is a repressible operon. This happens because there is an operator *trpO* overlapping with the operon promoter, *trpP*. When an active repressor is bound to *trpO* it blocks the binding of a mRNA to *trpP* and prevents transcription initiation. The *trp* repressor normally exists as a dimeric protein (called the *trp* aporepressor) and may or may not be complexed with tryptophan (Trp). Each portion of the *trp* aporepressor has a binding site for tryptophan.

When not complexed with tryptophan, the *trp* aporepressor cannot bind tightly to the operator *trpO*. However, if two tryptophan molecules bind to their respective binding sites, the *trp* aporepressor is converted into the functional repressor. The resulting functional repressor complex can bind tightly to the *trp* operator, and so the synthesis of tryptophan catalyzing enzymes is prevented. This fact completes the repression negative-feedback mechanism: An increase in the concentration of tryptophan induces an increase in the concentration of the functional repressor complexes, thus preventing the synthesis of tryptophan.

Transcription attenuation works by promoting an early termination of mRNA transcription, see Figure 3. The transcription starting site in the *trp* operon is separated from *trpE* by a leader region responsible for attenuation control. The transcript of this leader region consists of four segments which can form three stable hairpin structures between consecutive segments. The first segment contains two tryptophan codons in tandem. If there is an abundance of tryptophan, and thus of loaded $tRNA^{Trp}$, the ribosome rapidly finishes translation of the first two segments, and so it promotes the formation of a stable hairpin structure between the last two segments. mRNA polymerase molecules recognize this hairpin structure as a termination signal, and transcription is prematurely terminated. However, if the ribosome stalls in the first segment due to lack of tryptophan, hairpin development between Segments 2 and 3 (the antiterminator) is facilitated, and transcription proceeds until the end.

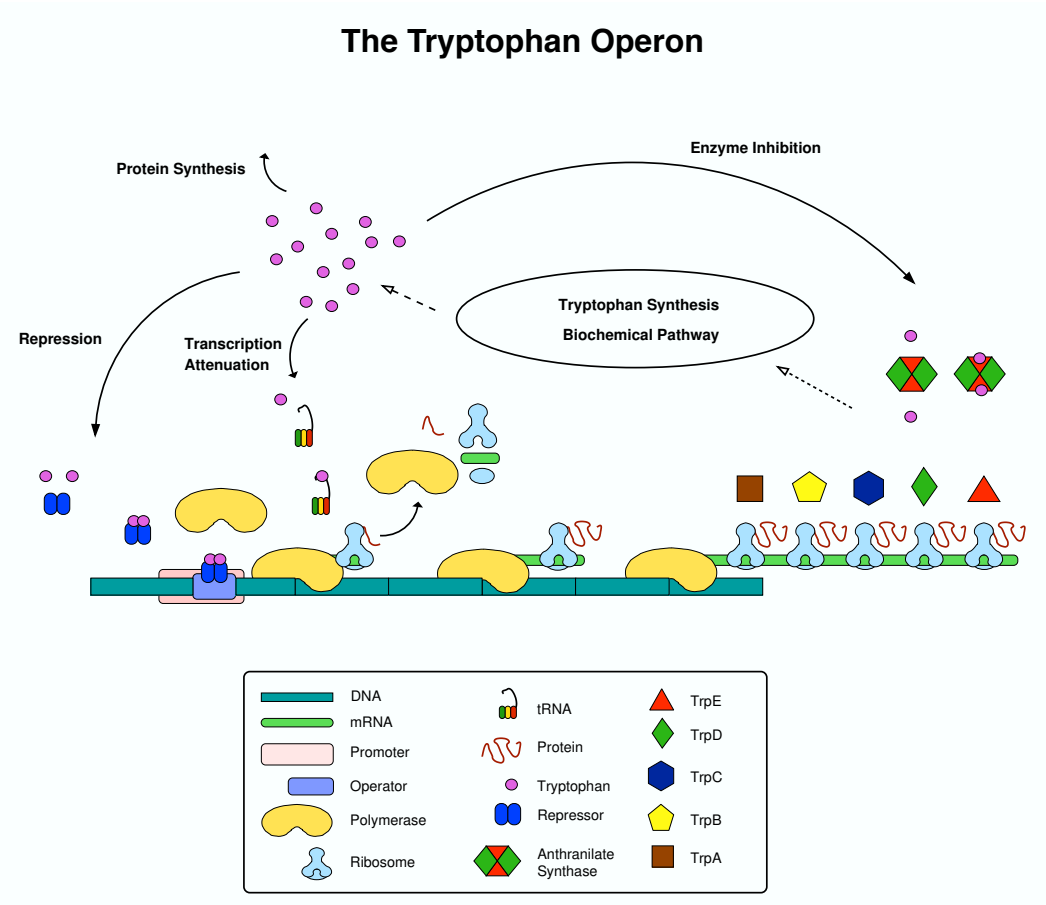

Figure 2. Schematic representation of the *trp* operon regulatory mechanisms.

Finally, anthranilate synthase is the first enzyme to catalyze a reaction in the catalytic pathway that leads to the synthesis of tryptophan from chorismate. This enzyme is a heterotetramer consisting of two TrpE and two TrpD polypeptides. Anthranilate synthase is inhibited by tryptophan by negative-feedback. This feedback inhibition is achieved when the TrpE subunits in anthranilate synthase are individually bound by a tryptophan molecule. Therefore, an excess of intracellular tryptophan inactivates most of the anthranilate synthase protein, avoiding the production of more tryptophan.

We recommend References [13, 14, 15] for those interested in reading more about the regulatory mechanisms in the *trp* operon.

6. Mathematical Modelling

The tryptophan operon has been the object of intensive studies for more than fifty years. The detailed knowledge we have today regarding the regulatory mechanisms in this operon is impressive. We mainly owe this knowledge to the research carried out at Charles Yanofsky's

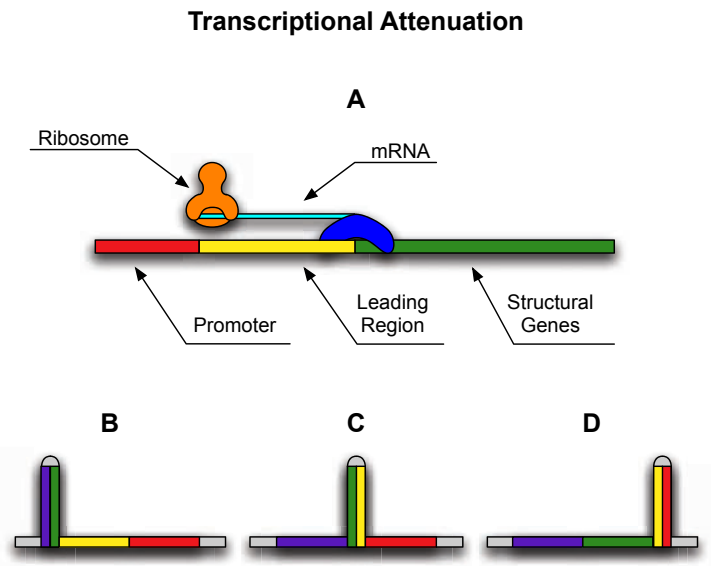

Figure 3. A) In the tryptophan operon there is a leading region between the promoter and the structural genes. The transcript (cyan) of the *trp* leading region comprises four equally large segments, which can fold to form three different hairpin structures. B) After Segments 1 (purple) and two (green) have been transcribed, they form a hairpin (the Hairpin 1:2) and it causes the polymerase to stop. A ribosome may then bind to the nascent mRNA and starts translation; transcription is resumed when the ribosome disrupts Hairpin 1:2. C) Segment 1 contains two Trp codons in tandem. Hence, under conditions of low tryptophan, there is a reduced number of loaded $tRNA^{Trp}$, and so the ribosome gets stacked in Segment 1. Transcription continues anyway, so that Segment 2 forms a hairpin with Segment 3 (yellow) when the latter is transcribed. Hairpin 2:3 is recognized as an antiterminator by the polymerase, and so transcription proceeds until the end of the structural genes. D) Conversely, if there is an abundance of tryptophan, the ribosome rapidly starts translation of Segment 2, and precludes formation of Hairpin 2:3. Then, when Segments 3 and 4 are transcribed, they form a hairpin that is recognized as a terminator; it destabilizes the polymerase-DNA complex and prematurely aborts transcription.

lab at Stanford University. However, there are still some open questions concerning the dynamic tryptophan operon behaviour. One of this questions is why the tryptophan operon involves three, apparently redundant, negative feedback regulatory mechanisms: repression, transcriptional attenuation, and enzyme inhibition. Together with other groups, we have addressed this question from a mathematical modelling perspective to try to gain more insight. The rest of this section describes our results.

We have developed a mathematical model of the tryptophan operon regulatory pathways, which takes into account all three known regulatory mechanisms: repression, transcription attenuation, and enzyme inhibition. The model equations are presented in Table 1. These equations govern the dynamic evolution of the concentration of mRNA, M; enzyme,

Table 1. Mathematical model of the tryptophan operon. These equations govern the dynamic evolution of the concentration of mRNA, M; enzyme, E; and intracellular tryptophan, T. The positive terms on the right-hand side of the equations stand for the production rates of the corresponding variables, while the negative terms stand for loss due to dilution (due to cell growth) and degradation. The term $\rho T/(K_\rho + T)$ represents tryptophan consumption during the synthesis of all proteins. The constant k_M is the rate of transcription initiation per promoter, k_E is the rate of translation initiation per mRNA, and k_T is the rate of tryptophan production per enzyme E. The terms γ_M, γ_E and γ_T are the dilution plus degradation rates. Finally, the functions $\mathcal{R}_R(T)$, $\mathcal{R}_A(T)$, and $\mathcal{R}_I(T)$ are all nonlinear decreasing functions of T, and respectively represent the three different regulatory mechanisms present in the tryptophan operon: repression, transcription attenuation, and enzyme inhibition.

$$
\begin{aligned}
\frac{dM}{dt} &= k_M D \mathcal{R}_R(T) \mathcal{R}_A(T) - \gamma_M M, \\
\frac{dE}{dt} &= k_E M - \gamma_E E, \\
\frac{dT}{dt} &= k_T E \mathcal{R}_I(T) - \rho \frac{T}{K_\rho + T} - \gamma_T T, \\
\mathcal{R}_R(T) &= \frac{\dfrac{P}{K_P}}{1 + \dfrac{P}{K_P} + \dfrac{R}{K_R}\left(\dfrac{T}{T + K_T}\right)^2}, \\
\mathcal{R}_A(T) &= \frac{1 + 2\alpha \dfrac{T}{K_G + T}}{\left(1 + \alpha \dfrac{T}{K_G + T}\right)^2}, \\
\mathcal{R}_I(T) &= \left(\frac{K_I}{T + K_I}\right)^2 .
\end{aligned}
$$

E; and intracellular tryptophan, T. The positive right-hand-side terms at the equations stand for the production rates of the corresponding variables, while the negative terms stand for loss due to dilution (due to cell growth) and degradation. The term $\rho T/(T + K_\rho)$ represents tryptophan consumption during the synthesis of all types of proteins. The constant k_M is the rate of transcription initiation per promoter, k_E is the rate of translation initiation per mRNA, and k_T is the rate of tryptophan production per enzyme E. The terms γ_M, γ_E, and γ_T are the dilution plus degradation rates. Finally, the functions $\mathcal{R}_R(T)$, $\mathcal{R}_A(T)$, and $\mathcal{R}_I(T)$ are all nonlinear decreasing functions of T, and respectively represent the three different regulatory mechanisms present in the tryptophan operon: repression, transcription attenuation, and enzyme inhibition. To derive these functions we took into consideration all of the biochemical reactions underlying the regulatory mechanisms described above, used chemical kinetics, and made quasi-steady state assumptions for all fast processes. The

meaning of the parameters in the functions $\mathcal{R}_R(T)$, $\mathcal{R}_A(T)$, and $\mathcal{R}_I(T)$ is as follows: P represents the intracellular mRNA polymerase (mRNAP) concentration, K_P is the dissociation constant for the mRNAP-promoter complex formation reaction, K_R is the dissociation rate for the repressor-operator complex formation reaction, K_T is the dissociation constant for the reaction in which a tryptophan binds one of its corresponding binding sites in the aporepressor, α is a constant associated to the strength of transcription attenuation, K_G is the dissociation rate for the tryptophan-tRNATrp complex formation reaction, and K_I is the dissociation rate for the reaction in which a tryptophan molecule binds one of its binding sites in the anthranilate synthase enzyme.

It is important to mention that, although not introduced here, special attention was given to the estimation of all the model parameters from reported experimental data. The estimated parameter values are tabulated in Table 2. The reader interested in the derivation of the model equations, as well as in the estimation of the model parameters, may consult Reference [16].

Table 2. The model parameters as estimated in Reference [16]

μ	$\approx$	$2.3 \times 10^{-2}\,\mathrm{min}^{-1}$	P	$\approx$	$1,500\,\mathrm{mpb}$	O	$\approx$	$2\,\mathrm{mpb}$
R	$\approx$	$400\,\mathrm{mpb}$	K_T	$\approx$	$20,000\,\mathrm{mpb}$	K_R	$\approx$	$0.1\,\mathrm{mpb}$
K_P	$\approx$	$22.5\,\mathrm{mpb}$	α	$\approx$	18.5	K_G	$\approx$	$2,500\,\mathrm{mpb}$
K_I	$\approx$	$2,050\,\mathrm{mpb}$	γ_M	$\approx$	$0.69\,\mathrm{min}^{-1}$	γ_E	$\approx$	$0.01\,\mathrm{min}^{-1}$
ρ	$\approx$	$1.2 \times 10^5\,\mathrm{mpb}$	K_ρ	$\approx$	$5,000\,\mathrm{mpb}$	τ_E	$\approx$	$1\,\mathrm{min}$
k_M	$\approx$	$5.1\,\mathrm{min}^{-1}$	k_E	$\approx$	$30\,\mathrm{min}^{-1}$	k_T	$\approx$	$3.2 \times 10^4\,\mathrm{min}^{-1}$

7. Dynamic Influence of the Three Regulatory Mechanisms in the *trp* Operon

Once we had the model, the next step was to analyze the dynamic influence of the three different regulatory mechanisms. To test the effect of enzyme inhibition, the model was modified to mimic a tryptophan operon in which enzyme inhibition is the only regulatory system, as well as a trp operon lacking enzyme inhibition. Then, we simulated derepression experiments, in which a bacterial culture that has grown for a long time in a medium rich in tryptophan (to shut the trp operon off) is suddenly shifted to a tryptophan-free medium (so the operon is reactivated).

After carrying out these simulations we observed that, when enzyme inhibition regulates Trp production by its own, the enzyme activity returns to its steady state almost immediately [16]. Thus, this mechanism is quite efficient, from the viewpoint of control theory, in maintaining a steady state. Apparently, the reason for this high controlling efficiency is that when Trp concentration is high, tryptophan acts as a buffer which captures the enzymes that catalyze Trp production, and these enzymes are rapidly released when the Trp concentration decreases. On the other hand, in the simulations in which enzyme inhibition

is absent, we observed that the operon produces enzymes at high rates, and this results in an overshoot of Trp production; approximately sixty times the production in normal conditions [17]. In our interpretation, this overshot is due to the much longer characteristic times of repression and attenuation. In conclusion, it seems that enzyme inhibition increases the operon stability because, due its rapid response, it relieves the system from the necessity to synthesize large amounts of polypeptide under conditions of tryptophan starvation.

It is known that regulation by transcription attenuation is exercised over the range from mild to extreme tryptophan depletion, while repression regulates over the range from excess tryptophan to mild Trp starvation. Thus, transcription attenuation increases the trp operon sensitivity to changes that alter the need for endogenous tryptophan. To investigate whether or not this system has any other dynamic effects, an operon reactivation simulation was carried out with a *trp* operon lacking transcription attenuation. The results were then compared with those of the normal operon. Our observations indicate that transcription attenuation makes the system reactivate sooner. Thus, this mechanism accelerates the trp operon response to nutritional shifts, by increasing its sensitivity range. In conclusion, enzyme inhibition and transcription attenuation provide the trp operon with important dynamic advantages. Enzyme inhibition increases the system stability, and transcription attenuation speeds up its response to nutritional shifts.

We further investigated the stability of the tryptophan operon model by means of the second Lyapunov method to generalize the results described previously [17]. First, we proved that the unique fixed point of the system is stable for a wide range of the parameters that determine the intensity of transcription attenuation and enzyme inhibition. Afterwards, we proceeded to analyze the stability strength in the *wild-type*, *inhibition-less* and *attenuation-less* bacterial strains. From this, we concluded, in agreement with the numerical results, that both regulatory mechanisms strengthen the system stability. Nevertheless, while the lack of enzyme inhibition greatly weakens the stability of the system fixed-point, the dynamic influence of transcription attenuation is much less important, since it speeds up the operon response but only slightly. In conclusion, enzyme inhibition is very important from a dynamic viewpoint. Conversely, the main effect of transcription attenuation is increasing the trp-operon sensitivity range to nutritional shifts, whereas its effect on the system stability is much weaker.

8. Comparison with Experimental Results and Model Improvement

As we said in the previous section, our *trp* operon model allowed us to study the dynamic influence of its three different regulatory mechanisms, and analyze them from an evolutionary perspective. However, we still need to test the model feasibility, by comparing it with reported experimental dynamic results, before we can be completely confident about its predictions. In this respect, there are some experiments carried out by Yanofsky's group in which a bacterial culture that had grown for a long time in a medium rich in tryptophan —to shut the trp operon off— was suddenly shifted to a tryptophan-free medium, and the temporal evolution of the corresponding genes' expression level was measured [18]. These experiments will be referred to as derepression experiments. On the other hand, Bliss et al.

[19] carried out derepression experiments with an *E. coli* mutant strain in which enzyme inhibition is attenuated. They observed that the phase-space trajectories do not converge to the steady state but oscillate in a limit cycle.

We simulated the derepression experiments of Yanofsky and Horn [18] and compare them with the model results in Figure 4A). Notice that, according to our model, the operon activity level should recover more slowly than it actually does. Moreover, we were also unable to reproduce the oscillatory behaviour observed by Bliss et al. by modifying the parameters corresponding to the enzyme inhibition regulatory function (to mimic their mutant *E. coli* straint). At this point, we could have started to arbitrarily modify the model parameters to fit the experimental results, but instead we decided to trust our estimations and wondered whether some important aspect in the biology had been neglected.

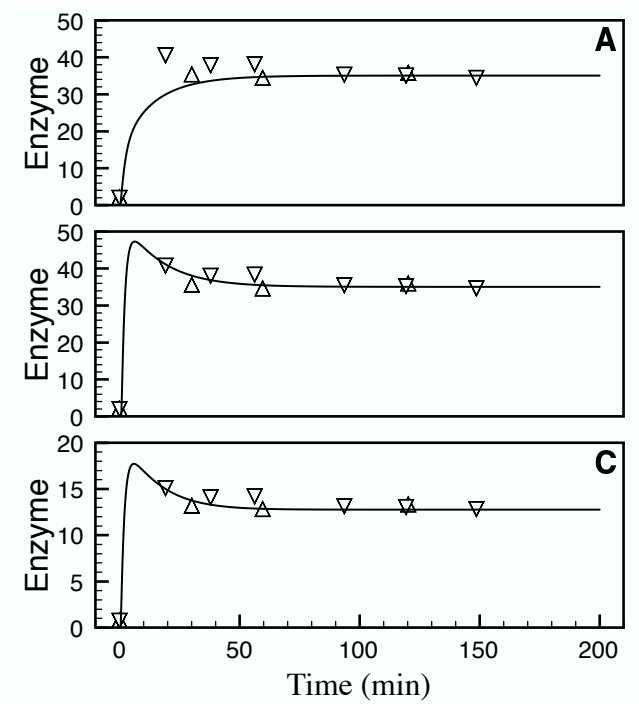

Figure 4. Plots of enzyme count *vs.* time resulting from derepression experiments simulated with the model introduced in [16] (A), with the same model but considering the time delays due to transcription and translation (B), and the modified model that considers the existence of three different operators, including the time delays (C).

Transcription and translation are not instantaneous processes. Compared with all the other biochemical processes involved in the *trp* operon regulatory pathways, they take long times to occur. In a previous work [17] we estimated the time delays associated with transcription ($\tau_M \simeq 1\,\mathrm{s}$) and translation ($\tau_E < 1\,\mathrm{min}$), but dismissed them apriori because of their shortness. Here, we take them into consideration to explicitly test their effect on the system dynamics. To do that, we have to modify the differential equations governing the

dynamics of M and E as follows:

$$\begin{aligned} \frac{dM}{dt} &= k_M D \mathcal{R}_R(T_{\tau_M}) \mathcal{R}_A(T_{\tau_M}) - \gamma_M M, \\ \frac{dE}{dt} &= k_E M_{\tau_E} - \gamma_E E, \end{aligned}$$

where the notation X_τ means that variable X is delayed a time τ, i.e. $X_\tau(t) = X(t-\tau)$. We then numerically solved these modified equations with the aid of the program `xppaut`. The results are plotted in Figure 4B, where we used $\tau_E = 12\,\text{s}$. Notice how, by simply taking into account such rather short time delays, there is a much better agreement between the model predictions and the experimental results of Yanofsky and Horn. On the other hand, despite this success, we were still unable to reproduce the oscillatory behaviour observed by Bliss et al. [19] by modifying the parameters associated to the enzyme inhibition regulatory function.

There is one further level of complexity in the *trp* operon regulatory pathway that we have not taken into account in our previous models. Namely the DNA regulatory region upstream of gene *trpE* contains three different repressor binding sites, denoted as O1, O2, and O3, and two repressors can cooperatively bind O1 and O2 [20]. This can be taken into account by modifying the function $\mathcal{R}_R(T)$ as follows (see the Appendix):

$$\mathcal{R}_R(T) = \frac{\frac{P}{K_P}}{\left(1+\frac{R_{2T}}{K_R^1}\right)\left(1+\frac{R_{2T}}{K_R^2}\right)\left(1+\frac{R_{2T}}{K_R^3}\right) + \frac{R_{2T}^2}{K_R^1 K_R^2}\left(1+\frac{R_{2T}}{K_R^3}\right)\left(k_{\text{cop}}-1\right) + \frac{P}{K_P}},$$

where

$$R_{2T} = R\left(\frac{T}{T+K_T}\right)^2$$

is the amount of active repressor, K_R^i ($i = 1, 2, 3$) is the dissociation constant for the R_{2T}-Oi complex formation reaction, and $k_{\text{cop}} > 1$ is a constant accounting for the cooperativity between Operators O1 and O2. The parameters for this new repression function are also estimated in the Appendix, and their values are as follows:

$$\begin{aligned} &K_R^1 = 0.625\,\text{mpb}, \quad K_R^2 = 7.9\,\text{mpb}, \quad K_R^3 = 100.0\,\text{mpb}, \\ &K_P = 2\,\text{mpb}, \qquad k_{\text{cop}} = 11.1125. \end{aligned}$$

All the other parameters remain set at the values estimated in Table 2.

After modifying the model to take into account the existence of three operators and the cooperativity observed between Operators O1 and O2, we simulated the derepression experiments of Yanofsky and Horn [18] with a time delay $\tau_E = 6\,\text{s}$; the results are shown in Figure 4C. Notice that, again, there is an excellent agreement between the model results and the experimental data.

As mentioned above, Bliss et al. [19] carried out derepression experiments with an *E. coli* mutant strain in which the enzyme anthranilate synthase cannot be inhibited by tryptophan, and observed an oscillatory expression of the *trp* operon genes. After modifying the model to account for the time delays due to transcription and translation and the three

repressor binding sites, we were able to reproduce the oscillations observed by Bliss et al.. For this, we reset:

$$K_I = 5 \times 10^7 \text{ mpb}.$$

The results of these new simulations are plotted in Figure 5. Although there is a good qualitative agreement between the model simulations and the model results of Bliss et al., we obtained a longer oscillation period. We conclude from this that, most probably, there are still some important aspects of repression which are not accounted for in the improved model.

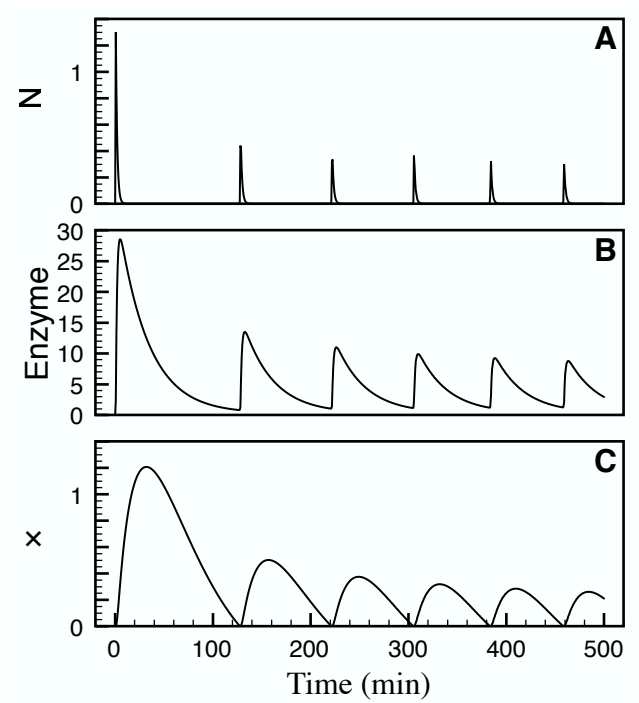

Figure 5. Plots of mRNA (A), enzyme (B), and tryptophan (C) molecule count resulting from derepression experiments simulated with the modified version of the model, which takes into account the time delays due to transcription and translation and the existence of three repressor binding sites.

9. Conclusions

We have reviewed out past efforts to understand the dynamic behaviour of the *trp* operon from a mathematical modelling approach. To develop the model we took into account the three different known mechanisms in the operon regulatory pathway. Special attention was paid to the estimation of the model parameters from reported experimental data. Among other things, the model was used to analyze the influence of the three different regulatory mechanisms (in the *trp* operon) over the system dynamic behaviour. These studies suggest

that the system has three redundant negative-feedback regulatory mechanisms to guarantee a rapid response to variation on the growing medium. On the other hand, as seen in Figure 4A, the agreement of the model simulations with the experiments of Yanofsky and Horn [18] is rather poor. Besides, it is impossible to reproduce the oscillatory behaviour observed by Bliss et al. while carrying out derepression experiments with mutant *E. coli* strain in which anthranilate synthase cannot be inhibited.

Given that our models take into account the chemical details of all the regulatory mechanisms, and that all the parameters were estimated from experimental results, we interprete the consistent disagreement observed between the model results and the experiments of Yanofsky and Horn as a deficiency in the model. Then, we looked in the literature and found that there are indeed some important aspects which we did not consider. Namely there are three repressor binding sites, two of which interact cooperatively, and the processes of transcription and translation involve non-negligible time delays. Once the model was modified accordingly, it could reproduce the experiment results of Yanofsky and Horn, as well as the oscillatory data observed by Bliss et al..

An interesting conclusion, arising from the results discussed in the previous paragraph, is that the time delays have a strong influence on the system transient behaviour, despite their rather small value. In our opinion this is important because small time delays are usually neglected by employing the argument that they do not have an important effect on the dynamic system behaviour. If we were only interested on the system stationary behaviour, we could indeed neglect short time delays because only the long ones can cause bifurcations. However, if the transients are biologically meaningful (as in this case), no time delay should be ignored, regardless its value.

Finally, these results and conclusions reveal, in our opinion, the importance of developing detailed models whenever the biological information is available. With them, it is possible to gain a deeper insight into the system dynamics than with simpler phenomenological models.

A. Modelling the Three *trp* Operators

Repression Function

Up to three active repressors, R_{2T}, and one polymerase, P, can bind to the *trp* DNA regulatory region through the following reactions:

$$R_{2T} + O \overset{K_R^1}{\rightleftharpoons} O_R^1, \qquad R_{2T} + O \overset{K_R^2}{\rightleftharpoons} O_R^2, \qquad R_{2T} + O \overset{K_R^3}{\rightleftharpoons} O_R^3,$$

$$R_{2T} + O_R^1 \overset{K_R^2/k_{\text{cop}}}{\rightleftharpoons} O_{2R}^{12}, \quad R_{2T} + O_R^1 \overset{K_R^3}{\rightleftharpoons} O_{2R}^{13}, \quad R_{2T} + O_R^2 \overset{K_R^3}{\rightleftharpoons} O_{2R}^{23},$$

$$R_{2T} + O_{2R}^{12} \overset{K_R^3}{\rightleftharpoons} O_{3R}^{123}. \qquad P + O \overset{K_P}{\rightleftharpoons} O_P,$$

These these are not all the possible chemical reactions. However, the equilibrium equa-

tions arising from them, plus the conservation equation for the *trp* DNA regulatory region, form a complete system and therefore there is no need to consider more reactions. In the above reactions, O, O_R^i, O_{2R}^{ij}, O_{3R}^{123}, and O_P respectively denote the states in which all operators are free, in which only Operator Oi is bound by an active repressor, in which Operators Oi and Oj are both bound by active operators, in which all three operators are repressor-bounded, and in which a polymerase is bound to the promoter. Furthermore, K_R^i and K_P are the dissociation constants for the Oi:R_{2T} and promoter-polymerase complex formation reactions, respectively. Finally, $k_{\text{cop}} > 1$ denotes the cooperativity between Operators O1 and O2.

The equilibrium equations for these reactions are:

$$\begin{aligned}
&R_{2T}O = K_R^1 O_R^1, && R_{2T}O = K_R^2 O_R^2, && R_{2T}O = K_R^3 O_R^3,\\
&R_{2T}O_R^1 = K_R^2 O_{2R}^{12}/k_{\text{cop}}, && R_{2T}O_R^1 = K_R^3 O_{2R}^{13}, && R_{2T}O_R^2 = K_R^3 O_{2R}^{23},\\
&R_{2T}O_{2R}^{12} = K_R^3 O_{3R}^{123}.
\end{aligned}$$

From these equations, and the conservation equation for the total concentration of the *trp* DNA regulatory region, we have:

$$O + O_R^1 + O_R^2 + O_R^3 + O_{2R}^{12} + O_{2R}^{13} + O_{2R}^{23} + O_{3R}^{123} + O_P = O_{\text{Tot}},$$

It then follows that:

$$\begin{aligned}
\mathcal{R}_R(T) &= \frac{O_P}{O_{\text{Tot}}}\\
&= \frac{\frac{P}{K_P}}{\left(1+\frac{R_{2T}}{K_R^1}\right)\left(1+\frac{R_{2T}}{K_R^2}\right)\left(1+\frac{R_{2T}}{K_R^3}\right) + \frac{R_{2T}^2}{K_R^1 K_R^2}\left(1+\frac{R_{2T}}{K_R^3}\right)\left(k_{\text{cop}}-1\right) + \frac{P}{K_P}}.
\end{aligned}$$

Parameter Estimation

According to [20], an active repressor molecule R_{2T} can bind to three different operator sites (O1, O2, and O3) all of which overlap the *trp* promoter. Additionally, two repressors bound to O1 and O2 interact in such a way that the corresponding binding energy is larger than the sum of the binding energies of single repressors separately binding to O1 and O2. Grillo et al. also report several measurements from which the following dissociation constants can be estimated:

$$\begin{aligned}
K_R^1 &\simeq 0.625\,\text{mpb},\\
K_R^2 &\simeq 7.9\,\text{mpb},\\
K_R^3 &\simeq 100\,\text{mpb}.
\end{aligned}$$

K_R^i denotes the dissociation constant for the reaction in which a repressor molecule binds the operator Oi alone. Since Grillo et al. also measured the binding energy when Operators O1 and O2 are simultaneously bound by repressor molecules, the following cooperativity constant can also be estimated from their experiments:

$$k_{\text{cop}} \simeq 11.13.$$

Finally, we used the fact that the operon activity decreases 60 times due to repression when there is abundance of tryptophan in the growing medium [13] (that is, $\mathcal{R}(0)/\mathcal{R}(T^*_{\text{max}}) \simeq 60$) to estimate parameter K_P:

$$K_P \simeq 5,000\,\text{mpb}.$$

T^*_{max} is the maximum steady-state intracellular concentration of tryptophan, and according to Bliss et al. [19] it is

$$T^*_{\text{max}} \simeq 20,000\,\text{mpb}.$$

Acknowledgments

This work was partially supported by *Consejo Nacional de Ciencia y Tecnología* (CONACyT), México, under Grant: 55228; the Natural Sciences and Engineering Research Council (NSERC) of Canada; and the Canadian NCE Mathematics of Information Technology and Complex Systems (MITACS).

References

[1] J. D. Bernal. *Science in history*. MIT Press, Cambridge, Mass., 1971.

[2] I. Asimov. *Asimov's biographical encyclopedia of science and technology*. Doubleday, Garden City, NY, 2nd/rev edition, June 1982.

[3] D. Depew. *Darwinism evolving : systems dynamics and the genealogy of natural selection*. MIT Press, Cambridge, Mass., 1995.

[4] J. E. Cohen. Mathematics if biology's next microscope, only better; biology is mathematics next physics, only better. *PLoS Biology*, **2**(12):e439–e440, December 2004.

[5] H. V. Westerhoff and B. O. Palsson. The evolution of molecular biology into systems biology. *Nat. Biotechnol.*, **22**(10):1249–1252, October 2004.

[6] M. C. Mackey and M. Santillán. Mathematics, biology, and physics: interactions and interdependence. *Notices of the AMS*, **52**(8):832–840, September 2005.

[7] T. Ideker, T. Galitski, and L. Hood. A new approach to decoding life: systems biology. *Annu. Rev. Genomics Hum. Genet.*, **2**:343–372, 2001.

[8] Y. Lazebnik. Can a biologist fix a radio?—Or,what I learned while studying apoptosis. *Cancer Cell*, **2**:179–182, 2002.

[9] A. Marshall. End of the interlude? *Nature Biotechnol.*, **22**:1191, 2004.

[10] S. Bornholdt. Less is more in modeling large genetic networks. *Science*, **310**:449–450, 2005.

[11] A. Friboulet and D. Thomas. Systems biology — an interdisciplinary approach. *Biosens. Bioelectron.*, **20**:2404–2407, 2005.

[12] M. W. Kirschner. The meaning of systems biology. *Cell*, **121**:503–504, May 2005.

[13] C. Yanofsky and I. P. Crawford. The tryptophan operon. In F. C. Neidhart, J. L. Ingraham, K. B. Low, B. Magasanik, and H. E. Umbarger, editors, *Escherichia coli and Salmonella thyphymurium: Cellular and Molecular Biology*, Vol. 2, pages 1453–1472. Am. Soc. Microbiol., Washington, DC, 1987.

[14] C. Yanofsky. Transcription attenuation, once viewed as a novel regulatory strategy. *J. Bacteriol.*, **182**:1–8, 2000.

[15] G. Xie, N. O. Keyhani, C. A. Bonner, and R. A. Jensen. Ancient origin of the tryptophan operon and the dynamics of evolutionary change. *Microbiol. Mol. Biol. Rev.*, **67**:303–342, 2003.

[16] M. Santillán and E. S. Zeron. Dynamic influence of feedback enzyme inhibition and transcription attenuation on the tryptophan operon response to nutritional shifts. *J. Theor. Biol.*, **231**:287–298, 2004.

[17] M. Santillán and E. S. Zeron. Analytical study of the multiplicity of regulatory mechanisms in the tryptophan operon. *Bull. Math. Biol.*, **68**:343–359, 2006.

[18] C. Yanofsky and V. Horn. Role of regulatory features of the trp operon of *Escherichia coli* in mediating a response to a nutritional shift. *J. Bacteriol.*, **176**:6245–6254, 1994.

[19] R. D. Bliss, P. R. Painter, and A. G. Marr. Role of feedback inhibition in stabilizing the classical operon. *J. Theor. Biol.*, **97**:177–193, 1982.

[20] A. O. Grillo, M. P. Brown, and C. A. Royer. Probing the physical basis for *trp* repressor-operator recognition. *J. Mol. Biol.*, **287**:539–554, 1999.

In: Mathematical Biology Research Trends
Editor: Lachlan B. Wilson, pp. 237-259
ISBN 978-1-60456-141-8

Chapter 9

NON-LINEAR TRANSMISSION, MORTALITY AND STABILITY OF DISCRETE-TIME INFECTIOUS DISEASE MODELS

***A. Korobeinikov*[1]*, *P.K. Maini*[2] *and *W.J. Walker*[3]**
[1]MACSI, Department of Mathematics and Statistics,
the University of Limerick, Limerick, Ireland
[2]Centre for Mathematical Biology, Mathematical Institute, University of Oxford,
24–29 St Giles', Oxford OX1 3LB, UK
[3]Department of Mathematics, University of Auckland
Private Bag 92019, Auckland, New Zealand

Abstract

In this chapter we consider the impacts of two factors, namely the form of the non-linearity of the infectious disease transmission rate the and mortality associated with a disease, on the dynamics of this infectious disease in a population. We consider a very simple discrete-step compartment epidemiological models and a very general form of the nonlinear transmission assuming that the transmission is governed by an arbitrary function constrained by a few biologically feasible conditions. We show that when the population size can be considered constant, these models exhibit asymptotically stable steady states. Precisely, we demonstrate that the concavity of the disease transmission function with respect to the number of infective individuals is a sufficient condition for this stability: in this case the models have either an unique and stable endemic equilibrium state, or no endemic equilibrium state at all; in the latter case the infection-free equilibrium state is stable.

We demonstrate that under some circumstances the mortality inflicted by the disease is able to destabilise endemic equilibrium state and can lead to a supercritical Hopf bifurcation in the system. However, it appears that for the majority of human infections the threshold for this bifurcation is too high to be realistic.

Key words: Infectious disease, discrete-time models, nonlinear transmission, endemic equilibrium state, global stability, Hopf bifurcation, Neimark-Sacker bifurcation, non-linear dynamics.

*E-mail address: andrei.korobeinikov@ul.ie; phone (353 61) 23 37 26; fax (353 61) 33 49 27

AMS Classification: 92D30 (primary), 34D20 (secondary)

Acknowledgement

AK was supported by Japan Society for the Promotion of Science, through Project 17540099, and is currently supported by the Science Foundation Ireland Mathematics Initiative through MACSI.

1. Introduction

Numerous deterministic mathematical models for the spread of infectious diseases in a population, where transmission of the infection is governed by the principle of mass action, have asymptotically stable equilibria, and consequently the level of the infected population exhibits damped oscillations toward an equilibrium level [1]. This stability of the equilibrium state is in striking contradiction with the available clinical data on a number of diseases, which demonstrate that if an infection persists in a population endemically then it maintains self-sustained oscillations in the number of infected. These oscillations are of almost constant period, and the magnitudes of the infectious level variations are generally too high to suggest that they simply reflect stochastic perturbations [1, p. 44]. Moreover, observed changes in disease incidence occur more regularly through time than can be expected on the basis of chance fluctuations alone.

A number of authors have suggested that a specifically chosen nonlinear disease transmission function (or incidence rate) can lead to a system with an unstable endemic equilibrium state. There is a variety of reasons for nonlinear transmission to be used in modelling. The first is that the principle of mass action is based on the underlying assumptions of homogeneous mixing of the population and of homogeneous environment; either of these assumptions may be invalid. In this case it is best to introduce the necessary population structure and represent heterogeneous mixing directly using a specific form of the nonlinear incidence rate function. Incidence rates that increase more gradually than linear in numbers of the infective and the susceptible individuals can also arise from saturation effects: if the number of infectives is very high, so that exposure to the disease agent is virtually certain, the incidence rate may respond more slowly than linear to increase in the number of infectives. This effect was encountered in clinical observations as well as in laboratory experiments, e.g. see [5, 7]. Furthermore, the details of transmission of infectious diseases are generally unknown, and may vary for different conditions; this observation justifies the growing interest to the models with incidence rates of more general form.

Another phenomenon which appears to be able to affect the system behaviour is mortality associated with the disease.

In this chapter we consider the impact of these two factors, namely non-linear disease transmission and mortality caused by the disease, on the disease dynamics. We show that, disregarding the reasons that can cause the non-linearity of the disease transmission and, under the assumption that the population size is constant, any nonlinear disease transmission function satisfying certain biologically reasonable conditions leads to a system with an asymptotically stable equilibrium. However, the mortality caused by the disease is generally a destabilising factor reducing the system stability by decreasing the associated Lyapunov

exponents. Under some circumstances it can even lead to a supercritical Hopf bifurcation and thus may cause self-sustained oscillations in the number of infected. However, for the majority of human infections (with perhaps such exceptions as AIDS) the threshold value of the mortality for this bifurcation is too high to be biologically feasible.

In Section 2 we describe the basic discrete-generation model we use in this work. In Section 3 we consider some examples of nonlinear transmission. In Section 4 we analyse stability of equilibrium states of a general model with nonlinear transmission. The impact of mortality associated with the disease is considered in Section 5, while in Section 6 we estimate the threshold values of mortality for some of the specific models considered earlier in Section 3. Finally, in Section 7 we make some additional observations.

2. Basic Discrete-Generation Model

To study the impacts of non-linear transmission and the mortality inflicted by the disease, we consider a very simple discrete-generation epidemiological model. This model can be viewed as a special case of discrete-time models. Discrete-time models are not new for mathematical epidemiology: difference equations have been used by Soper [23], Bartlett [4], Hoppensteadt [12, 13, 14] and others.

Following the classical assumptions of mathematical epidemiology, we assume that a population of size N is partitioned into a number of compartments. In this case we assume that the population is composed from susceptibles S, infected I, and removed (or recovered) R compartments, that is $N = S + I + R$. After infection an individual moves from the class of susceptibles into the class of infected and then into the class of removed as a result of recovery, death or isolation. Recovery implies life-long immunity, that is no return from the removed compartment into the susceptibles compartment is possible; thus we are considering a SIR model.

We will denote the number of individuals in a compartment in a generation by a capital letter with a subindex, e.g. I_n, S_{n+1} etc. Let us assume that an infected individual is introduced into an entirely susceptible population, that is in the first generation $I_1 = 1$ and $S_1 = N - 1$. This infected individual infects R_0 individuals who form the second generation of infected, $I_2 = R_0 I_1$. Here R_0 is the basic reproduction number, that is, the average number of secondary cases produced by a single infective introduced into an entirely susceptible population. These I_2 infected produce, in turn, I_3 infected in the third generation, etc.

We assume that the population size is constant, that during one generation there are bN new births all of whom come into the susceptibles compartment, and that the probability for a susceptible to die during a generation from natural causes is c. Then, if at the nth generation there are S_n susceptibles, I_n infected and R_n recovered, and if these I_n infected produce I_{n+1} infected of the $(n+1)$th generation, we have for the susceptible population the equation

$$S_{n+1} = S_n + bN - I_{n+1} - cS_n. \tag{2.1}$$

The *principle of mass action* assumes homogeneous mixing and takes into account that an infective comes into contact with and might infect R_0 individuals some of whom may be already infected or recovered and therefore clinically unaffected by the contact. Then the

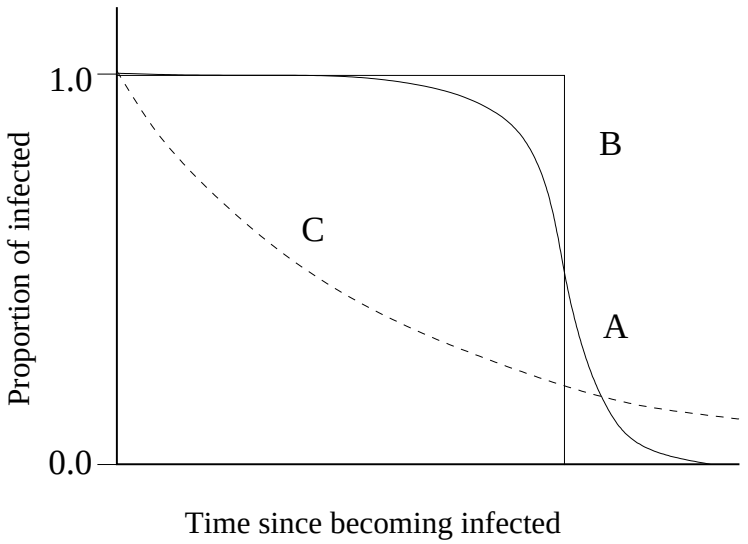

Figure 1. Schematic representation of recovery. Here the curve A is typical observed data, the curve B is for recovery of all infected after a definite period of time (a generation) and the curve C is for continuous-rate recovery.

number of infective contacts in the nth generation is

$$E_n = R_0 \frac{I_n S_n}{N}. \tag{2.2}$$

Assuming that the number of infectives in the $(n+1)$th generation is equal to the number of infective contacts, we obtain the equations

$$I_{n+1} = R_0 I_n \frac{S_n}{N} \tag{2.3}$$

for the infected population. The constant population size assumption allows us to omit the third equation which describes dynamics of the removed population R.

The main advantage of such a model compared with continuous-time models is its natural time scaling which leads to important consequences. Firstly, the model ensures that all infected recover after a definite period of time. This implies a natural approximation of the recovery process by a step function (Fig. 1, curve A, B), whereas for continuous-time models, unless we use integro-differential equations or equations with a time delay, we are to postulate that "continuous recovery" arises from the standard assumption that motion from exposed to the infectious class and then to the recovery class occurs at constant rates (Fig. 1, curve C). This last assumption, while mathematically convenient, is rarely realistic and can lead to results contradicting observations (see, for example [15]). Secondly, since in the discrete generation model we consider disease transmission not as a continuous process but in terms of secondary cases produced by an infective for a generation, we do not have any need for the time delay associated with the incubation or the latent state; neither do we have need for an exposed class (as for a $SEIR$ model) to incorporate the delay between the event of infection and the moment when the infected host becomes actually infectious into

the model. The third (but not the least important) advantage of this model is that it allows natural interpretation of all model parameters and data obtained.

An apparent drawback of the generation model is that generations may overlap in time, and the infected individuals of several generations coexist. Nevertheless, it is obvious that the model preserves the dynamic properties of discrete-time or continuous time models. The system (2.1), (2.3) may be considered as a discrete-time model with a time step equal to a generation (implying by this term the average time interval which commences when a susceptible host is exposed to an infective dose, includes the period during which the host passes infection and ends when the host is fully recovered, isolated or dead).

3. Non-linear Transmission

A model based on the principle of mass action is deficient in some aspects. The main deficiency is that according to the principle the probability for a susceptible individual to be infected during a generation (the "infection probability") is not limited and can be larger that one (Fig. 2). This feature is completely unrealistic, and it leads to the unrealistic behaviour of the system: when the numbers of infectives and susceptibles are large enough but still biologically feasible, some phase trajectories leave the positive quadrant of the SI space (that is the positive quadrant is not an invariant set of discrete-time or discrete-step models).

This unlimited growth of the infection probability occurs because by the principle of mass action for a finite time interval a susceptible may receive an infective dose from more than one infective and will be counted eventually as several infectives in the next generation. We have to stress that this is not a consequence of the length discrete time step: it is easy to see that for transmission governed by the bilinear form with any transmission rate there are such values of S and I which give the infection probability that is larger that 1. This unlimited growth of the infection probability is a specific feature of discrete-time systems exclusively, and that the bilinear incidence rate associated with the principle of mass action is adequate for continuous-time models.

Furthermore, the principle of mass action assumes homogeneous mixing of the population and homogeneous environment, which can be unrealistic in some cases. To avoid these and other problems, other forms of transmission can be suggested. We now consider a number of examples.

Example 3.1. Bartlett [4] assumed that infective contacts are distributed binomially, and, instead of the infection probability $R_0 I_n/N$, given by the principle of mass action, he used the expression

$$1 - (1 - R_0/N)^{I_n} .$$

This function reduces to the standard mass action form when $R_0 I_n/N$ is very small. This infection probability leads to the equations

$$\begin{aligned} S_{n+1} &= bN + S_n \left(1 - \frac{R_0}{N}\right)^{I_n} - cS_n, \\ I_{n+1} &= S_n - S_n \left(1 - \frac{R_0}{N}\right)^{I_n} . \end{aligned}$$

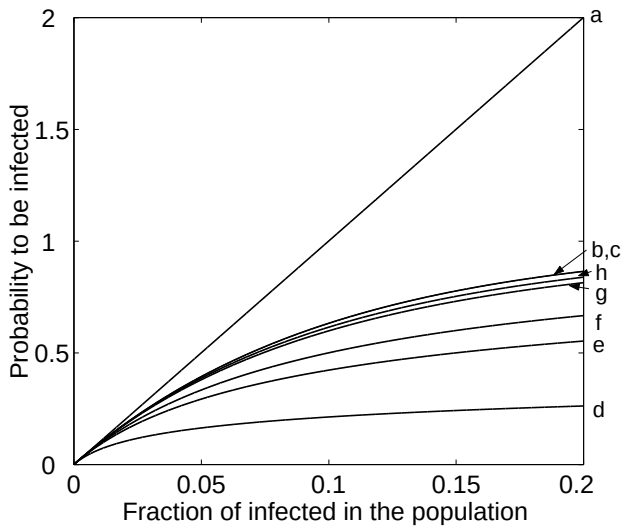

Figure 2. The probability for a susceptible to be infected during a generation for different transmission functions. Here (a) is the data for the principle of mass action; (b) and (c) are for binomial and Poisson distributions of infective contacts (these curves practically coincide); (d) to (h) are for negative binomial distribution with $m = 0.1, 0.5, 1.0, 5.0, 10.0$ respectively. All data for $N = 10^6$ and $R_0 = 10$.

Example 3.2. Infectious contacts are rare events (compared with the population size), and hence we can assume that the number of contacts is a Poisson variate. According to the principle of mass action, the average number of infective contacts per susceptible (the expectation) is

$$\mu = R_0 I_n / N.$$

If the infective contacts have a Poisson distribution, then the probability for a susceptible to escape infection is $\exp(-\mu)$, which leads us to the infection probability

$$1 - \exp(-R_0 I/N),$$

and to the disease transmission function $S - S\exp(-R_0 I/N)$. The corresponding system is

$$\begin{aligned} S_{n+1} &= bN + S_n \exp(-R_0 I_n/N) - cS_n, \\ I_{n+1} &= S_n - S_n \exp(-R_0 I_n/N). \end{aligned}$$

A transmission function of this form was used by Cullen *et al*. [8] and Hoppensteadt [12, 13] (who did not mention that this transmission function is due to the Poisson distribution of infectious contacts).

Example 3.3. To examine the impact of spatial heterogeneity due, for example, to demographic, social or geographical factors, the negative binomial distribution of infective contacts can be used. Specifically, the negative binomial distribution has been used to describe variation in the environment and diversity leading to a qualitative change in system

behaviour [22, p. 94]. The stabilisation of the Nicholson-Bailey host-parasitoid system (see Hassell [11] for details) is the classical example.

Let x be a random variable having a Poisson distribution $\mu^k e^{-\mu}/k!$ $(k = 0, 1, 2, \ldots)$ which is the probability that a susceptible has k infective contacts. Inhomogeneity, whether due to social or geographical factors, can be captured if $\mu > 0$ is itself considered as a random variable with probability density function

$$P(\mu) = \frac{\alpha^m}{\Gamma(m)} \mu^{m-1} e^{-\alpha\mu},$$

where $m,\ \alpha > 0$ are constant parameters. Then the probability that x takes the value k is

$$\begin{aligned} Q(k) &= \int_0^\infty \frac{\mu^k e^{-\mu}}{k!} P(\mu)\, d\mu \\ &= \int_0^\infty \frac{\mu^k e^{-\mu}}{k!} \frac{\alpha^m}{\Gamma(m)} \mu^{m-1} e^{-\alpha\mu}\, d\mu \\ &= \left(\frac{\alpha}{1+\alpha}\right)^m \binom{-m}{k} \frac{(-1)^k}{(1+\alpha)^k}. \end{aligned}$$

This is the negative binomial distribution with mean m/α and variance $m(1+\alpha)/\alpha^2$. The parameter α can be eliminated by assuming that the mean is the average number of infective contacts per susceptible, that is

$$\frac{m}{\alpha} = \frac{R_0 I_n}{N}.$$

Then the probability of a susceptible escaping infection is

$$Q(0) = \left(1 + \frac{1}{\alpha}\right)^{-m} = \left(1 + \frac{R_0 I_n}{mN}\right)^{-m},$$

which leads to the transmission function

$$S\left[1 - \left(1 + \frac{R_0 I}{Nm}\right)^{-m}\right],$$

and to the model equations

$$\begin{aligned} S_{n+1} &= bN + S_n \left(1 + \frac{R_0 I}{mN}\right)^{-m} - cS, \\ I_{n+1} &= S_n \left[1 - \left(1 + \frac{R_0 I}{mN}\right)^{-m}\right]. \end{aligned}$$

The transmission function of this form was used by Cullen *et al.* [9].

Example 3.4. Cullen *et al.* [8] suggested to consider the susceptibles as a collection of marbles in a bag, and each contact with an infective is equivalent to taking a marble out of the bag and then replacing it in the bag. The total number of times a marble is withdrawn

from the bag (the total number of trials) equals the total number of contacts between infectives and susceptibles during a generation and is assumed to be given by the mass action principle (2.2). The probability that a particular marble is not withdrawn on any particular trial is $(S-1)/S$. Hence the probability that a particular marble is not withdrawn on any of the trials during a generation is

$$\left(\frac{S-1}{S}\right)^{R_0\frac{IS}{N}},$$

and the number of susceptibles (marbles) that remain uninfected at the end of the generation is

$$S\left(\frac{S-1}{S}\right)^{R_0\frac{IS}{N}}.$$

This leads to the transmission function

$$S - S\left(\frac{S-1}{S}\right)^{k}, \quad \text{where } k = R_0\frac{IS}{N},$$

and to the system of difference equations

$$\begin{aligned} S_{n+1} &= bN + S_n\left(\frac{S_n-1}{S_n}\right)^{k} - cS_n, \\ I_{n+1} &= S_n - S_n\left(\frac{S_n-1}{S_n}\right)^{k}. \end{aligned}$$

Figure 2 shows the probability for a susceptible to be infected during a generation as a function of I for different transmission functions. Note that the infection probability under the principle of mass action grows linearly with I, and can be larger that one. We would like to note that the binomial and Poisson distributions of infective contacts provide practically indistinguishable infection probabilities.

4. Stability of a General Model with Nonlinear Transmission

If we assume that disease transmission is governed by an unspecified function of the general form $F(S,I,N)$, then

$$\begin{aligned} S_{n+1} &= S_n - F(S_n, I_n, N) + bN - cS_n, \\ I_{n+1} &= F(S_n, I_n, N). \end{aligned} \tag{4.4}$$

To be a disease transmission function, the function $F(S,I,N)$ must satisfy the conditions

$$F(S,I,N) > 0 \quad \text{for all} \quad S, I > 0 \tag{4.5}$$

and

$$F(S,0,N) = F(0,I,N) = 0. \tag{4.6}$$

Also for all $S, I, N > 0$ the function $F(S,I,N)$ must satisfy the conditions

$$\frac{\partial F}{\partial S} > 0, \qquad \frac{\partial F}{\partial I} > 0, \qquad \frac{\partial F}{\partial N} \le 0. \tag{4.7}$$

Since the number of infectives in the $(n+1)$th generation can not exceed the number of susceptibles in the nth generation, the function $F(S, I, N)$ must also satisfy the condition

$$I_{n+1} = F(S_n, I_n, N) < S_n. \tag{4.8}$$

Since the probability for a susceptible to be infected for a generation is less than one, we must expect that the increase of the susceptible population by one person will lead to the increase of the next generation infected population by less than one individual, that is the condition

$$\frac{\partial F(S, I, N)}{\partial S} < 1 \tag{4.9}$$

holds. Note that the condition (4.8) follows from the condition (4.9).

Furthermore, for a finite time interval a susceptible may come into infective contact a number of times and may be considered as a number of infectives in the next generation. To avoid "multiple" infection of a susceptible, a transmission function must necessarily satisfy the condition

$$\frac{\partial^2 F(S, I, N)}{\partial I^2} < 0, \qquad \text{for all} \quad S, I, N > 0. \tag{4.10}$$

Note that the mass action model (2.3) does not satisfy condition (4.10) and what is more important, conditions (4.8) and (4.9) do not hold for this model. All examples of transmission functions given in Section 3. satisfy conditions (4.5)–(4.9); condition (4.10) holds for all these functions as well.

The basic reproduction number R_0 of the system may be defined as

$$R_0(N) = \lim_{S \to N, I \to 0} \frac{\partial F(S, I, N)}{\partial I}.$$

It is easy to see that for all the above examples of transmission function this limit is equal to R_0 indeed. We also define the "effective reproduction number"

$$\rho = \lim_{S, I \to Q_0} \frac{\partial F(S, I, N)}{\partial I}.$$

It is easy to see that $\rho = R_0$ (and $S_0 = N$) when $c = b$, and that $\rho = \frac{b}{c} R_0$ when transmission depends linearly on S.

If $c \neq 0$, the system (4.4) has an infection-free equilibrium state $Q_0 = (bN/c, 0)$. Apart from this, the system can have endemic equilibrium states satisfying

$$I^* = bN - cS^*, \qquad F(S^*, I^*, N) = I^*. \tag{4.11}$$

Condition (4.8) implies that $S^* \geq bN \geq I^*$ (in fact, for most infectious diseases of humans $S^* \approx N/R_0 \gg bN$).

Lemma 4.1. *If* $\frac{\partial^2 F(S,I,N)}{\partial I^2} \leq 0$ *holds for all* $S, I, N > 0$, *then* $\frac{\partial F(S^*,I^*,N)}{\partial I} \leq 1$.

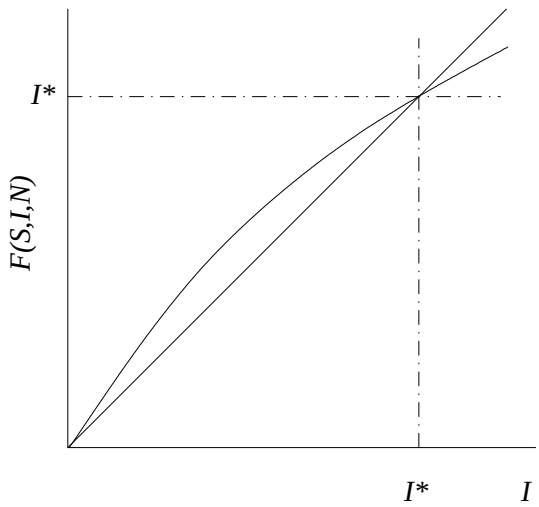

Figure 3. Transmission function $F(S, I, N)$ as a function of I (see text for details).

Proof. Assume that

$$\frac{\partial F(S^*, I^*, N)}{\partial I} > 1. \tag{4.12}$$

Then, by (4.6) and (4.11), and by the mean value theorem, there exists a point (S^*, I_1), $I_1 \in (0, I^*)$ such that

$$\frac{\partial F(S^*, I_1, N)}{\partial I} = \frac{F(S^*, I^*, N) - F(S^*, 0, N)}{I^* - 0} = 1.$$

Applying the mean value theorem to the function $g(I) = \frac{\partial F(S^*, I, N)}{\partial I}$, we get that, if (4.12) holds, then there exists a point (S^*, I_0), $I_0 \in (I_1, I^*)$ such that

$$\frac{\partial^2 F(S^*, I_0, N)}{\partial I^2} = \frac{\frac{\partial F(S^*, I^*, N)}{\partial I} - \frac{\partial F(S^*, I_1, N)}{\partial I}}{I^* - I_1} > 0.$$

This contradicts the hypothesis of this Lemma, and hence $\frac{\partial F(S^*, I^*, N)}{\partial I} \leq 1$. Furthermore, under condition (4.10) the strict equality $\frac{\partial F(S^*, I^*, N)}{\partial I} = 1$ holds only if $\frac{\partial^2 F(S^*, I, N)}{\partial I^2} = 0$ for all $I \in (0, I^*)$. Figure 3 shows a function with $\frac{\partial^2 F(S, I, N)}{\partial I^2} < 0$ and a function with $\frac{\partial^2 F(S, I, N)}{\partial I^2} = 0$. □

Conditions (4.7) and (4.10) ensure that the endemic equilibrium state is unique.

Lemma 4.2. *If*

$$\frac{\partial^2 F(S, I, N)}{\partial I^2} \leq 0$$

holds for all $S, I, N > 0$, and $\rho > 1$, then, apart from the infection-free equilibrium state Q_0, there exists an unique positive endemic equilibrium state Q^* satisfying equalities (4.11). If $\rho \leq 1$ then the infection free equilibrium state is the only non-negative equilibrium of the system.

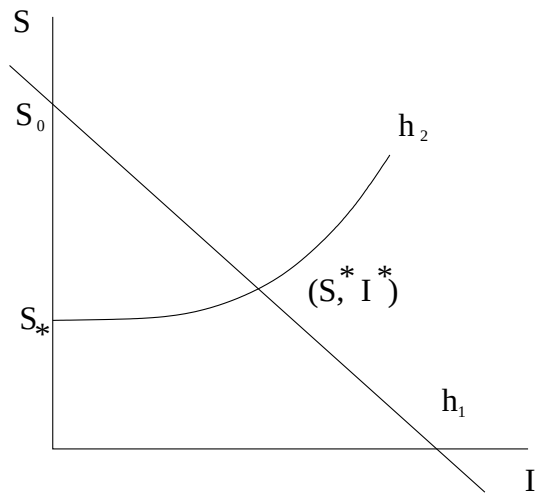

Figure 4. The curves h_1 and h_2. See text for details.

Proof. Let us consider the curves defined by the equalities (4.11) on the SI plane, denoting them by h_1 and h_2 respectively (Fig. 4).

The first equality, $I + cS = bN$, defines a negatively-sloped straight line h_1. Existence of the curve h_2, defined by the equality $F(S, I, N) - I = 0$, is ensured by the implicit function theorem and by the condition $\dfrac{\partial F(S, I)}{\partial S} > 0$. For the slope of the curve h_2 we have

$$h_2' = \frac{dS^*}{dI^*} = \frac{1 - \frac{\partial F}{\partial I}}{\frac{\partial F}{\partial S}}.$$

Lemma 4.1 holds for all S, I satisfying the equality $F(S, I, N) - I = 0$, and hence the curve h_2 is positively sloped (or at least, non-negatively sloped). Therefore, if $S_* = h_2(0) < S_0 = bN/m = h_1(0)$, then there is an unique point of intersection of the curves h_1 and h_2. Otherwise, that is if $S_* > S_0$, the curves h_1 and h_2 do not intersect.

The value $S_* = h_2(0)$ is either a minimal value of S such that $\dfrac{\partial F(S, 0)}{\partial I} = 1$ holds, or, if such a value does not exist (for example, if $\dfrac{\partial F(S, 0)}{\partial I}$ is unlimited for all $S > 0$, as in the case of an exponent), $S_* \equiv 0$. By (4.6) and (4.7), $\dfrac{\partial F(S, 0)}{\partial I}$ is a non-decreasing function of S, and hence the condition $\dfrac{\partial F(S_0, 0)}{\partial I} > 1$ is sufficient to ensure that $S_* < S_0 = bN/c$. □

The following theorem is a straightforward consequence of Lemma 4.1.

Theorem 4.3. *If* $\rho > 1$ *and*

$$\frac{\partial^2 F(S, I, N)}{\partial I^2} \leq 0$$

for all $S, I, N > 0$*, then the endemic equilibrium state* Q^* *of the system (4.4) is asymptotically stable. If* $\rho \leq 1$*, then the system has no positive equilibrium state, and the infection-free equilibrium is asymptotically stable.*

Proof. The Jacobian of the system (4.4) is

$$J = \begin{bmatrix} 1 - c - \frac{\partial F}{\partial S} & -\frac{\partial F}{\partial I} \\ \frac{\partial F}{\partial S} & \frac{\partial F}{\partial I} \end{bmatrix}.$$

The characteristic equation of the Jacobian is

$$\lambda^2 - a_1\lambda + a_2 = 0,$$

where $a_2 = \det J = (1-c)\dfrac{\partial F}{\partial I}$ and $a_1 = \mathrm{tr}J = \dfrac{\partial F}{\partial I} + 1 - c - \dfrac{\partial F}{\partial S}$. Since c is the probability for a susceptible to die during a generation, $a_2 > 0$. Depending on the sign of $a_1 = \lambda_1 + \lambda_2 > 0$, there are three possibilities:

(*i*) both roots of the characteristic equation are complex conjugate;

(*ii*) both roots of the characteristic equation are real and positive (in this case $a_1 > 0$);

(*iii*) both roots of the characteristic equation are real and negative (in this case $a_1 < 0$).

By Lemma 4.1, at the endemic equilibrium state $Q^* = (S^*, I^*)$, $a_2 < 1$. Therefore, if the roots are complex conjugate, then $|\lambda| = \sqrt{a_2} \leq 1$ (where strict equality holds only when $c = 0$ and $\frac{\partial^2 F(S^*,I)}{\partial I^2} = 0$ for all $I \in (0, I^*)$), and hence the equilibrium state is asymptotically stable in this case. If the roots are real and positive ($a_1 > 0$ holds in this case) then we note that at Q^*, by Lemma 4.1, $a_1 < 1 + a_2$, and hence

$$\lambda_1 = \frac{a_1 + \sqrt{a_1^2 - 4a_2}}{2} < \frac{1 + a_2 + \sqrt{(1+a_2)^2 - 4a_2}}{2} = 1,$$

and

$$\lambda_2 = \frac{a_1 - \sqrt{a_1^2 - 4a_2}}{2} < \lambda_1 < 1.$$

Therefore, the equilibrium state Q^* is asymptotically stable in this case. If the roots are real and negative, then $a_1 < 0$ holds, and we note that, by (4.9),

$$|a_1| = \left|\frac{\partial F}{\partial I} + 1 - c - \frac{\partial F}{\partial S}\right| < c < 1.$$

Hence,

$$|\lambda_2| = \left|\frac{a_1}{2} - \frac{\sqrt{a_1^2 - 4a_2}}{2}\right| < \left|\frac{a_1}{2}\right| + \left|\frac{\sqrt{a_1^2}}{2}\right| = |a_1| < m < 1$$

and

$$|\lambda_1| = \left|\frac{a_1}{2} + \frac{\sqrt{a_1^2 - 4a_2}}{2}\right| < |\lambda_2|.$$

Hence the equilibrium state Q^* is asymptotically stable in this case as well.

At the infection-free equilibrium Q_0, $a_2 = (1-c)\rho$ and $a_1 = \rho + 1 - c$. For this equilibrium state $a_1^2 - 4a_2 = (\rho + c - 1)^2$, and hence $\lambda_1 = \rho$ and $\lambda_2 = 1 - c < 1$. That is, the infection free equilibrium Q_0 is a stable node when $\rho < 1$, and a saddle point when $\rho > 1$.

This completes the proof. □

It is remarkable that stability of the equilibrium states is independent of how the transmission rate depends on the number of susceptibles.

All examples of disease transmission functions given in Section 3. satisfy conditions (4.5)–(4.10). Therefore, according to Theorem 4.3, all these transmission functions lead to the systems having asymptotically stable endemic equilibria states. We now proceed to analyse the impact of mortality caused by the disease on this disease dynamics.

5. Disease-Induced Mortality

The dynamics of a host-microparasite system depends on the size of the host population, and that varies in time because, firstly, the host population varies as a consequence of ordinary demographic processes (growth or decline of a population), and secondly, a disease itself may cause population size variations. For most human infections (with a very few exceptions the most notorious of which is HIV) the demographic processes are slow compared with epidemic processes. That is, in other words, the characteristic time scale of the demographic process is considerably longer than that for the epidemic process. Therefore a system combining both demographic and epidemic processes is a "slow-fast" (or "singularly perturbed") system, where the demographic process is "slow" whereas the epidemic process is "fast". A traditional approach to such a system is to consider in the first instance the so-called "frozen" system, that is a system where the slow process is neglected, and the corresponding slow-varying variables (the population size in this case) are postulated constant. For epidemic models this leads to the traditional constant population size assumption.

However, while for the demographic processes the constant population size assumption is a well posed and sound assumption, it is questionable for the population variation caused by the disease: in this case variations in the population size, however small they are, coincide in their occurrence with disease outbreak, and hence their characteristic time-scales coincide. For this reason the variation of the population caused by the disease cannot be omitted so easily as the "slow" demographic variations.

While the influence of "slow" demographic variation of the population size has been considered by a number of authors, the impact of the disease-induced variations of the population size on the disease dynamics has so far not been studied systematically. Here we attempt to investigate the impact of the mortality caused by a disease on the disease dynamics, and we come to the conclusion that under some circumstances this mortality, even if small, may affect the system by destabilising an otherwise stable endemic equilibrium state.

The direct consequence of disease-induced mortality is a reduction of the population size, which can affect behaviour of the system in two different ways. Firstly, disease-induced deaths directly decrease the birth of new susceptibles which is usually assumed to be proportional to the population size (we call this Effect A). Secondly, the probability for a susceptible to come into an infective contact and to be infected is inversely proportional to the population size, and hence decreasing the population size can effectively increase the disease transmission (we call this Effect B).

N.T.J. Bailey was probably the first scientist who made an attempt to consider the impact of disease-induced mortality on disease dynamics and come to the conclusion that it

may affect the system stability [3, p. 142]. He considered a SIR model for a disease assumed to be lethal to all those contracting it and sufficiently virulent to suppress any live births amongst circulating infectives. Thus all removals are in fact deaths, and make no further contribution to the life of the community, and all new susceptible births therefore arise solely from the susceptible group itself, i.e. reproduction of new susceptibles in this case is proportional to the number of susceptibles S only. Under these assumptions the SIR model equations are [3, p. 142]

$$\dot{S} = \gamma S - \beta SI, \qquad \dot{I} = \beta SI - \sigma I, \tag{5.13}$$

where I and S are numbers of infected and susceptibles respectively, β is incidence rate, γ is host reproduction rate and σ is rate of removals. The system (5.13) is the Lotka-Volterra prey-predator system where the "prey" are the susceptibles and the "predators" are the infected. This system is known to be neutrally stable and structurally unstable. The phase trajectories of the system (5.13) are an one-parameter family of closed curves given by its first integral

$$V(S, I) = S - S^* \ln S + I - I^* \ln I,$$

where $S^* = \sigma/\beta,\ I^* = \gamma/\beta$ are the equilibrium levels of the susceptibles and the infected respectively [10, 22].

Bailey's analysis is not complete: of the two effects mentioned above he considered only Effect A and disregarded dependence of the incidence rate on the population size. That is. However even this incomplete analysis indicates that the mortality associated with the disease may affect the system stability: for a lethal disease Effect A alone is able to put the system on the edge of stability.

It may appear at first that incorporating the disease-induced mortality into an epidemic model does not greatly affect its analysis. However, with the constant population size assumption we can reduce the system dimension by one, so if this assumption is omitted then we must consider the full system whose dimension is equal to the number of compartments. This leads to unexpected complications. Firstly, such a system may either have no non-zero equilibrium states at all, or have a continuum of these. Secondly, as we have mentioned already the natural growth or decline of the population is a slow process compared with the epidemic processes, and hence they should be considered separately.

Here we apply an approach adopted from perturbation theory. Let us assume that as a consequence of the disease a portion of infectives δ in the nth generation dies (that is $0 \leq \delta \leq 1$ is a mortality expectation). We assume that in absence of the disease the population is static or varies slowly enough to justify the constant population size assumption. Then the population size in the nth generation is

$$N_{n+1} = N_n - \delta I_n = N_0 - \delta \sum_{i=0}^{n} I_i. \tag{5.14}$$

We further assume that the magnitudes of the variations of the population size caused by the disease are small compared with the population size itself. This may be due to a comparatively low number of cases or a low value of the mortality expectation δ. Then we can assume that

$$N_n = N = \text{const}, \tag{5.15}$$

while at the same time, according to equation (5.14),

$$\frac{\partial N_n}{\partial I_n} = -\delta, \qquad \frac{\partial N_n}{\partial S_n} = 0. \tag{5.16}$$

We have to stress that the assumptions (5.15) and (5.16) are independent assumptions.

As a result of the incorporation of disease-induced mortality given by equations (5.14)–(5.16) into the system (2.3), the system behaviour can change remarkably: a supercritical Hopf bifurcation may occur in the system, the stable equilibrium can reverse its stability and a stable limit cycle can arise. The approach used here is intuitively straightforward, but it may appear to be not rigorous enough. The justification of this approach is given in the Appendix.

Remark 5.1. In discrete-time systems the appearance of a closed invariant curve surrounding a fixed point while a pair of complex multipliers crosses the unit circle is sometimes referred to as a *Neimark-Sacker bifurcation*, rather than Hopf bifurcation; the latter term is reserved for a similar bifurcation in continuous-time systems [18, ch. 4]. However, here we prefer to use the term Hopf bifurcation as it is more familiar to the majority of readers.

Theorem 5.2. *There is a critical value $\delta_{cr} \geq 0$ such that the endemic equilibrium state Q^* of the system (2.3) with disease-associated mortality defined by the equations (5.14)–(5.16) is asymptotically stable for all $0 \leq \delta < \delta_{cr}$ and unstable for all $\delta > \delta_{cr}$.*

Proof. According to (5.14), N depends on I, and hence, by (5.16),

$$\frac{dF}{dI} = \frac{\partial F}{\partial I} + \frac{\partial F}{\partial N}\frac{\partial N}{\partial I} = \frac{\partial F}{\partial I} - \delta\frac{\partial F}{\partial N}.$$

The Jacobian of the system (4.4) is now

$$J = \begin{bmatrix} 1 - c - \frac{\partial F}{\partial S} & -\delta b - \frac{\partial F}{\partial I} + \delta\frac{\partial F}{\partial N} \\ \frac{\partial F}{\partial S} & \frac{\partial F}{\partial I} - \delta\frac{\partial F}{\partial N} \end{bmatrix}. \tag{5.17}$$

Here the term $-\delta\frac{\partial F}{\partial N}$ is due to Effect B; the term $-\delta b$ reflects the contribution of Effect A. The characteristic equation is

$$\lambda^2 - a_1\lambda + a_2 = 0,$$

where

$$a_2 = \det J = (1-c)\frac{\partial F}{\partial I} + \delta\left(b\frac{\partial F}{\partial S} - (1-c)\frac{\partial F}{\partial N}\right)$$

and

$$a_1 = \mathrm{tr}J = \frac{\partial F}{\partial I} - \delta\frac{\partial F}{\partial N} + 1 - c - \frac{\partial F}{\partial S}.$$

The characteristic multipliers λ_1, λ_2 are complex conjugate if $D = a_1^2 - 4a_2 < 0$ holds. The fixed point Q^* reverses its stability when the pair of complex conjugate multipliers $\lambda, \bar{\lambda}$ crosses the unit circle in the complex plane, i.e. when $|\lambda| = 1$. This condition holds when $a_2 = 1$, that is at

$$\delta_{cr} = \frac{1 - (1-c)\frac{\partial F}{\partial I}}{b\frac{\partial F}{\partial S} - (1-c)\frac{\partial F}{\partial N}}. \tag{5.18}$$

At $\delta = \delta_{cr}$, $a_2 = 1$, and hence

$$\frac{\partial F}{\partial I} - \delta \frac{\partial F}{\partial N} = c\frac{\partial F}{\partial I} - \delta\left(b\frac{\partial F}{\partial S} + c\frac{\partial F}{\partial N}\right)$$

and

$$D(\delta_{cr}) = a_1^2 - 4a_2 = \left(1 - c\left(1 - \frac{\partial F}{\partial I}\right) - \delta c\frac{\partial F}{\partial N} - (1+\delta b)\frac{\partial F}{\partial S}\right)^2 - 4.$$

Therefore, $D < 0$ (and hence the multipliers λ_1, λ_2 are complex conjugate) if

$$\left|\delta c\frac{\partial F}{\partial N}\right| < 1 + (1+\delta b)\frac{\partial F}{\partial S} \tag{5.19}$$

holds at Q^*. This condition holds for all realistic models, since $\delta, c < 1$ and $\frac{\partial F}{\partial N} < \frac{\partial F}{\partial S}$ for all biologically feasible S, I and N, including Q^*. It is easy to see that this condition holds for all models given in Section 3..

Furthermore, $\dfrac{\partial F}{\partial N} \leq 0$ ensures $\dfrac{\partial a_2}{\partial \delta} > 0$, and hence the absolute value of the characteristic multipliers grows with δ. That is the bifurcation is supercritical (the fixed point loses its stability as δ grows).

This completes the proof. □

Theorem 5.2 states only that as δ increases, the stability of the fixed point Q^* of the system reverses. However, this theorem does not provide a necessary condition for a supercritical Hopf bifurcation, i.e. for existence of a stable limit cycle in the phase space of the system for $\delta > \delta_{cr}$. For the Hopf bifurcation to occur in the system (and for the limit cycle to appear) an additional condition, namely that at $\delta = \delta_{cr}$ the fixed point is a weak attractor [18, 19, p. 23], is necessary. In practice, this condition holds for robust systems [2, p. 93]. However, pathological cases, such that at $\delta = \delta_{cr}$ the fixed point is neutrally stable, are possible. Andronov's theorem [2, p. 93] states that for any structurally unstable system there are "close" structurally stable systems such that a supercritical Hopf bifurcation occurs at the same, or a close value of the bifurcation parameter.

While δ grows further beyond δ_{cr}, one more bifurcation of the fixed point Q^* can occur: an unstable focus can bifurcate into an unstable node.

6. Stability and Bifurcation of the Specific Models

Though Theorem 5.2 ensures that the positive value δ_{cr} exists for all disease transmission functions $F(S, I, N)$ satisfying conditions (4.7)–(4.11), only $\delta \leq 1$ is biologically realistic. For human populations $b, c \ll 1$, and the divisor in the equation (5.18), namely

$$b\frac{\partial F(S^*, I^*)}{\partial S} - (1-c)\frac{\partial F(S^*, I^*)}{\partial N},$$

is a very small value. For instance, for the mass action model, $S^* = N/R_0$, $I^* = (R_0 b - c)\, N/R_0$, and

$$\frac{\partial F(S^*, I^*)}{\partial I} = 1, \qquad \frac{\partial F(S^*, I^*)}{\partial S} = R_0 b - c, \qquad \frac{\partial F(S^*, I^*)}{\partial N} = -\frac{R_0 b - c}{R_0}.$$

Hence the divisor is

$$b(R_0b-c)+(1-c)\frac{R_0b-c}{R_0}=b+R_0b^2-2bc-\frac{c}{R_0}+\frac{c^2}{R_0}\approx b.$$

It can differ for other models, however it is easy to see that it is of the same order for all disease transmission functions mentioned in Section 3., and we may expect that it will be of the same order for all realistic disease transmission functions. Therefore, $\delta_{cr}\leq 1$ holds only for transmission functions $F(S,I,N)$ such that $1-(1-c)\frac{\partial F(S^*,I^*)}{\partial I}$ is of the same order as the denominator. Generally, δ_{cr} grows with the difference.

For the mass action model

$$a_2=(1-c)+\delta\frac{1}{R_0}(R_0b-c)\left(R_0b+1-c\right),$$

and

$$\delta_{cr}=\frac{R_0c}{(R_0b-c)^2+(R_0b-c)}.$$

It is easy to see that δ_{cr} depends on two constants, $A_1=R_0c$ and $A_2=R_0b-c$, and is independent of the population size N. Furthermore, δ_{cr} grows as c grows, and $\delta_{cr}=0$ when $c=0$. However, since we may expect that c does not exceed b, $\delta_{cr}<1$.

It is easy to see that for any model δ_{cr} grows monotonically with c, and hence δ_{cr} is minimal when $c=0$. In the case $c=0$, for the model with Poisson distribution of infective contacts

$$I^*=bN,\qquad S^*=\frac{bN}{1-\exp(-R_0b)},$$

and the disease transmission function satisfies

$$\begin{aligned}\frac{\partial F(S^*,I^*)}{\partial I} &= R_0b\frac{\exp(-R_0b)}{1-\exp(-R_0b)},\\ \frac{\partial F(S^*,I^*)}{\partial S} &= 1-\exp(-R_0b),\\ \frac{\partial F(S^*,I^*)}{\partial N} &= -R_0b^2\frac{\exp(-R_0b)}{1-\exp(-R_0b)}.\end{aligned}$$

(Note that the condition (5.19) that the multipliers are complex conjugate holds for this model.) Denoting $\sigma=\delta b$, $\sigma_{cr}=\delta_{cr}b$ and $\epsilon=R_0b$, we obtain

$$a_2=\epsilon(1+\sigma)\frac{\exp(-\epsilon)}{1-\exp(-\epsilon)}+\sigma(1-\exp(-\epsilon))$$

and

$$\sigma_{cr}=\frac{1-(1+\epsilon)\exp(-\epsilon)}{(1-\exp(-\epsilon))^2+\epsilon\exp(-\epsilon)}.$$

In the case $c=0$, a_2 and consequently δ_{cr} depend on the parameters b and R_0 only and this makes further calculations comparatively simple. The function $\sigma_{cr}(\epsilon)$ satisfies $\lim_{\epsilon\to 0}\sigma_{cr}=0$ and $\lim_{\epsilon\to\infty}\sigma_{cr}=1$, and increases monotonically on the positive semi-axes $\epsilon>0$ ensuring that there is a $\sigma_{cr}\in(0,1)$ for all $\epsilon>0$ (Fig. 5).

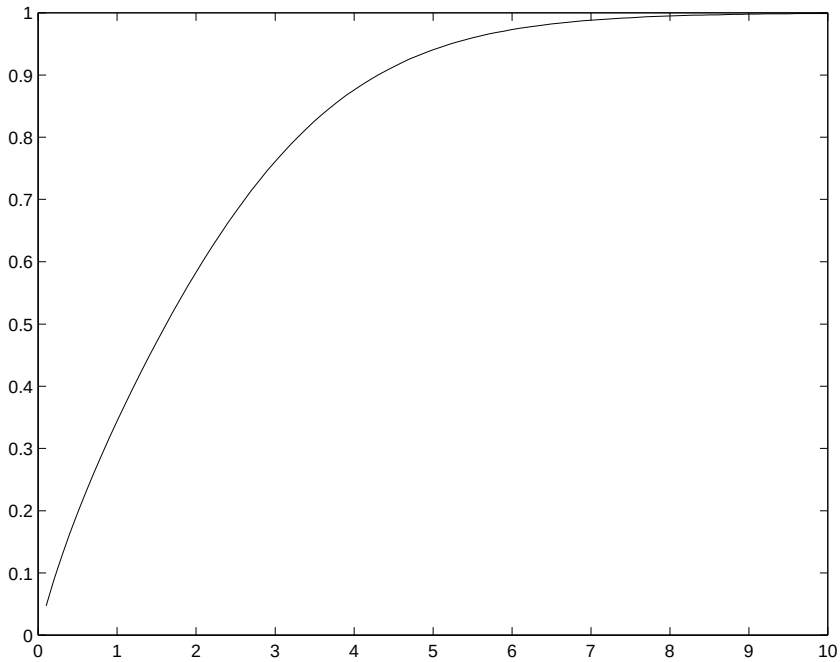

Figure 5. σ_{cr} versus ϵ for $c = 0$ for Poisson distribution of infective contacts.

However, since for the majority of human infections $b \ll 1$, only very small values of σ and ϵ are of the interest. In the vicinity of zero the estimation

$$\frac{1}{2}\epsilon - \frac{1}{3}\epsilon^2 < \sigma_{cr} < \frac{1}{2}\epsilon$$

holds. Consequently, for small values of ϵ, δ_{cr} is of the same order as R_0 which is too large a value for the typical mortality expectation δ. In fact, recalling that $R_0 \sim 10$, we come to the condition that, in the case of the Poisson distribution of infective contacts, $b \sim 10^{-1}$ should hold in order to ensure $\delta_{cr} \leq 1$. Such values of b are too high for the majority of human infections. For $c > 0$, δ_{cr} is even higher.

6.1. Negative Binomial Distribution

In the case of the negative binomial distribution of infective contacts for $c = 0$,

$$I^* = bN, \qquad S^* = \frac{bN}{1-(1+R_0 b/m)^{-m}},$$

and the transmission function satisfies

$$\begin{aligned}
\frac{\partial F(S^*,I^*)}{\partial I} &= R_0 b \left(1+\frac{R_0 b}{m}\right)^{-(m+1)} \Bigg/ \left(1-\left(1+\frac{R_0 b}{m}\right)^{-m}\right), \\
\frac{\partial F(S^*,I^*)}{\partial S} &= 1-\left(1+\frac{R_0 b}{m}\right)^{-m}, \\
\frac{\partial F(S^*,I^*)}{\partial N} &= -R_0 b \frac{S^*}{N}\left(1+\frac{R_0 b}{m}\right)^{-(m+1)} = -R_0 b^2 \frac{(1+R_0 b/m)^{-(m+1)}}{1-(1+R_0 b/m)^{-m}}.
\end{aligned}$$

Hence, using ϵ, σ notation,

$$a_2 = \epsilon(1+\sigma)\frac{(1+\epsilon/m)^{-(m+1)}}{1-(1+\epsilon/m)^{-m}} + \sigma\left(1-(1+\epsilon/m)^{-m}\right)$$

and

$$\sigma_{cr} = \frac{1-(1+\epsilon/m)^{-m} - \epsilon(1+\epsilon/m)^{-(m+1)}}{(1-(1+\epsilon/m)^{-m})^2 + \epsilon(1+\epsilon/m)^{-(m+1)}}.$$

Again as for the Poisson distribution both the parameters a_2 and δ_{cr} depend on the constants b and R_0 only which makes further calculations comparatively simple. As in the case of the Poisson distribution, the function $\sigma_{cr}(\epsilon)$ satisfies $\lim_{\epsilon\to 0}\sigma_{cr} = 0$ and $\lim_{\epsilon\to\infty}\sigma_{cr} = 1$. (In contrast with the Poisson distribution the function $\sigma_{cr}(\epsilon)$ does not grow monotonically reaching a maximum on the axes $\epsilon \in (0,\infty)$.) In the vicinity of zero for the function $\sigma_{cr}(\epsilon)$ the inequalities

$$\frac{\frac{1}{2}m(m+1)\epsilon - \frac{1}{3}(m+1)(m+2)\epsilon^2}{m^2} < \sigma_{cr} < \frac{1}{2}\frac{m+1}{m}\epsilon$$

hold. Therefore for small ϵ values in the case of the negative binomial distribution the value of δ_{cr} is even higher than for the Poisson distribution, approaching the latter as $m \to \infty$.

7. Discussion and Conclusion

In this paper we assume that a disease transmission function $F(S,I,N)$ satisfies the condition

$$\frac{\partial^2 F(S,I,N)}{\partial I^2} \le 0.$$

This condition ensures uniqueness and stability of the endemic equilibrium state of the models considered. We should stress that this result is valid for autonomous models with the assumption of constant population size.

It also follows from this result that to have an unstable equilibrium the transmission function $F(S,I,N)$ must necessarily be a convex function with respect to the variable I at least at some points. This leads us to the question whether a transmission function convex with respect to the variable I is biologically feasible. In the case of continuous-time models convexity of the incidence rate may be associated with some form of cooperation or community effect [16]. However for discrete-time models the situation is completely different: for such models to avoid a multiple infection and to have realistic limited infection probability (see Section 3.) a disease transmission function must necessarily be concave with respect to I (that is satisfy (4.10)). The same result, a concave disease transmission function, can be obtained by the introduction of a non-homogeneous population structure; for example, the negative binomial distribution is associated with a distinctively concave transmission function. It is remarkable that the properties of the steady-states are completely independent of how the transmission rate depends on the number of susceptibles.

We would like to note that the same result, that is stability of the endemic equilibrium states of models with incidence rates concave with respect to I, holds for continuous-time models as well [16].

In the case of the system (4.4), disease-induced mortality affects the system stability in two ways: through decrease of the total births due to the reduction of population size (Effect A) and through intensification of disease transmission due to the rise of the infective contact probability (Effect B). Though much more sophisticated models — continuous-time or discrete-time — can be considered, Effects A and B remain the most important factors for the system dynamics.

In the case of the system (4.4), by equation (5.18) the contributions of these two effects toward instability are $\delta b\frac{\partial F(S^*,I^*)}{\partial S}$ and $-\delta(1-c)\frac{\partial F(S^*,I^*)}{\partial N}$ (remember that $\frac{\partial F}{\partial N}<0$) respectively. For example, in the case of mass action (2.3) Effect A (birth rate decline) contributes $\delta b(R_0 b-c)$ toward instability, and Effect B (increase of infective contacts probability) adds $\delta(1-c)(b-c/R_0)$. For other possible disease transmission functions, such as those given in Section 3., the values of the partial derivatives $\frac{\partial F(S^*,I^*)}{\partial S}$ and $\frac{\partial F(S^*,I^*)}{\partial N}$ can differ from those for mass action, however they are of the same order (at least for the transmission functions given in Section 3.), and hence we can expect that the contribution of these Effects will be of the same order as well.

For human communities the birth ratio b is fairly small: humans reproduce with rate about 2–3% of a population size per annum while for the majority of infections there are tens of generations per year; that is $b\sim 10^{-3}$. Though for endemically persistent diseases the basic reproduction number $R_0>1$ always, it never reaches or exceeds 100. Consequently, for the majority of human diseases $R_0 b\sim 10^{-2}$ and $R_0 b\ll 1$; therefore for human communities and for the mass action model (2.3), of the two factors, Effect B (increase of the disease transmission) prevails. For the majority of domestic and wild animals the host reproduction number b is considerably higher than that for humans and can reach (for rodents) values of order 10^{-1}. Furthermore, for many social animals the disease reproduction number R_0 can be higher than that for humans. Then the impact of Effects A and B can be comparable, or even Effect A can prevail. Whether each of these two effects manifests itself in a specific case depends on the infection in question.

The analysis of specific models shows that for the Poisson distribution and negative binomial distribution δ_{cr} tends to be larger than one, whereas for mass action $\delta_{cr}\sim c/b$. As we already have mentioned, for animals a value of the divisor

$$b\frac{\partial F(S^*,I^*)}{\partial S}-(1-c)\frac{\partial F(S^*,I^*)}{\partial N}$$

is considerably higher than for humans, and since the probability of death due to a disease for animals is higher than that for humans, disease-induced mortality would more often lead to self-sustained oscillations in animal populations.

Bubonic plague is an example of infection when mortality can affect the system stability. Bubonic plague is in a fact a rat disease. Humans contact it as a consequence of disease outbreak in rat communities. For rats the host reproduction rate b as well as the basic reproduction number R_0 are much higher than for humans. Since the mortality ratio δ for bubonic plague is high (tends to 1.0), we can expect that high magnitude self-sustained oscillations caused by disease-induced mortality can occur in an infected rat community.

It is noteworthy that the characteristic multipliers of the system decrease and the critical value δ_{cr} grows as the susceptible mortality rate c increases. This can explain an observed phenomenon that, in spite of the difference in the quality of public health systems, in the

prevaccination era the magnitudes of measles epidemics in England and Wales were higher than in India and Bangladesh.

The approach applied in this paper can be used for more sophisticated discrete-time and continuous-time models. Though for specific models critical values of death expectation can differ, the qualitative result will be the same, namely that disease-induced mortality is a destabilising factor.

Appendix

We are interested in the stability of the system

$$\begin{aligned} S_{n+1} &= S_n - F(S_n, I_n, N_n) + bN_n - cS_n, \\ I_{n+1} &= F(S_n, I_n, N_n), \\ N_{n+1} &= N_n - \delta I_n = N_0 - \delta \sum_{i=0}^{n} I_i. \end{aligned}$$

It is easy to see that for an endemically persistent infection (that is for $I > 0$) this system has no fixed points for all $\delta \neq 0$. However, we may consider the stability of the phase orbit initiated at the point (S^*, I^*, N_0), where S^* and I^* are the coordinate of the endemic equilibrium state Q^* of the system with $\delta = 0$ (we will denote this orbit by γ_0).

It is obvious that for $\delta \neq 0$ the population size N monotonically decreases, and we are interested whether the phase orbits initiated near the point (S^*, I^*, N_0) will approach the orbit γ_0. Therefore, instead of stability of the three-dimensional system, we consider a projection of the system to the SI plane. The behaviour of such a projection is governed by the equations

$$\begin{aligned} S_{n+1} &= S_n - F\left(S_n, I_n, N_0 - \delta \sum_{i=0}^{n} I_i\right) + b\left(N_0 - \delta \sum_{i=0}^{n} I_i\right) - cS_n, \\ I_{n+1} &= F\left(S_n, I_n, N_0 - \delta \sum_{i=0}^{n} I_i\right). \end{aligned}$$

In is easy to see that these equations do not depend on N. Linearising this system in the vicinity of the orbit γ_0, we obtain the Jacobian (5.17) and Theorem 5.2.

References

[1] R.M. Anderson, R.M. May, *Infectious Diseases in Humans: Dynamics and Control*, Oxford University Press, Oxford (1991).

[2] A.A. Andronov, E.A. Leontovich, I.I. Gordon, A.G. Maier, *Theory of Bifurcations of Dynamic Systems on a Plane*, John Wiley and Sons, New York (1973).

[3] N.T.J. Bailey, *The Mathematical Theory of Infectious Diseases and its Applications*, Griffin, London (1975).

[4] M.S. Bartlett, The critical community size for measles in the United States, *J. Roy. Statist. Sos., A*, **123** (1) 37–44 (1960).

[5] Brown, G.C., Hasibuan, R., 1995. Conidial discharge and transmission efficiency of *Neozygites floridana*, an Entomopathogenic fungus infecting two-spotted spider mites under laboratory conditions. *Journal of invertebrate pathology*, **65**, 10–16.

[6] Busenberg, S., Cooke, K., 1993. *Vertically transmitted diseases: Models and Dynamics*, Springer, Berlin.

[7] Capasso, V., Serio, G., 1978. A generalisation of the Kermack-McKendrick deterministic epidemic model. M*ath. Biosci.* **42**, 43–61.

[8] R.M. Cullen, N.D. Ellis, W.J. Walker, A model of measles endemicity, *Nonlinear Analysis*, **35**, 191–198 (1999).

[9] R.M. Cullen, A. Korobeinikov, W.J. Walker, Seasonality and critical community size for infectious diseases, *ANZIAM J.*, **44**, 501–512 (2003).

[10] B.-S. Goh, *Management and Analysis of Biological Populations*, Elsevier Science, Amsterdam (1980).

[11] M.P. Hassell, *The Dynamics of Arthropod Predator-Prey Systems*, Princeton University Press, Princeton (1978).

[12] F.C. Hoppensteadt, *Mathematical Theories of Populations, Demographics, Genetics and Epidemics*, SIAM, Philadelphia (1975).

[13] F.C. Hoppensteadt, *Mathematical Methods of Population Biology*, New York University, New York (1976).

[14] F.C. Hoppensteadt, *Mathematics in Medicine and the Life Sciences*, Springer, New York (1992).

[15] M.J. Keeling, B.T. Grenfell, Disease extinction and community size: modeling the persistence of measles, *Science*, **275**, 65–67 (1997).

[16] A. Korobeinikov and P.K. Maini, Nonlinear incidence and stability of infectious disease models, *MMB IMA*, **22**, 113–128 (2005).

[17] A. Korobeinikov, P.K. Maini and W.J. Walker, Estimation of effective vaccination rate: pertussis in New Zealand as a case study, *J. Theor. Biol.*, **224**, 269–275 (2003).

[18] Kuznetsov Y.A., Elements of Applied Bifurcation Theory, Springer, New York (1995).

[19] J.E. Marsden, M.McCracken, *The Hopf Bifurcation and Its Applications*, Springer, New York (1976).

[20] J. Mena-Lorca, H.W. Hethcote, Dynamic models of infectious diseases as regulators of population sizes, *J. Math. Biol.*, **30**, 693–716 (1992).

[21] A. Nold, Heterogeneity in disease-transmission modeling, *Math. Biosci.*, **52**, 227–240 (1980).

[22] E.C. Pielou, *An Introduction to Mathematical Ecology*, Wiley-Interscience, New York (1969).

[23] H.E. Soper, Interpretation of periodicity in disease-prevalence. *J. R. Statist. Soc.*, **92**, 34–73 (1929).

In: Mathematical Biology Research Trends
Editor: Lachlan B. Wilson, pp. 261-273
ISBN 978-1-60456-141-8

Chapter 10

MATHEMATICAL STABILITY ANALYSIS IN BIOMECHANICAL APPLICATIONS

Peter Giesl[1*] ***and Heiko Wagner***[2]
[1]Department of Mathematics, University of Sussex, United Kingdom
[2]Biomechanics and Motion Science, WWU, Münster, Germany

Abstract

Human and animal locomotion represent a highly complex control problem. Internal and external disturbances increase these difficulties to maintain or achieve stability in static and dynamic situations. Two kinds of stability can be distinguished: on the one hand the stability is achieved by reflexes and control with neural feedback, and on the other hand stability is based on mechanical properties and the geometrical configuration of muscles and tendons within the musculoskeletal system. The present article is mainly interested in the latter one, which is called selfstability. Biological systems adapt the pure mechanical properties of muscles and passive structures to support stability and to cope with disturbances. In the following, we mainly restrict ourselves to one joint with a pair of antagonistic muscles; in particular, we will focus on the human elbow joint. We describe the most important mechanical properties of muscles and summarize them in a model of a general joint with antagonistic muscles. This model is a system of ordinary differential equations for the joint angle and its angular velocity.

If the antagonistic muscles are activated in a certain relation, then the joint is in an equilibrium state. The definition of stability in the mathematical sense is given using the framework of dynamical systems. The eigenvalues of the linearization at the equilibrium give a detailed characterization of solutions near the equilibrium: real and complex eigenvalues lead to qualitatively different behavior of solutions, and the absolute value of their real part tells us how fast the equilibrium state is approached after a small perturbation.

Can we quantify the stability of an equilibrium point? We would surely assume the equilibrium point to be the "more stable" the larger its basin of attraction is. The basin of attraction consists of all perturbations which are led back to the equilibrium. Is an equilibrium also the "more stable" the faster small perturbations are corrected? The mathematical analysis will show that the answer depends on the situation.

*E-mail address: p.a.giesl@sussex.ac.uk. (Corresponding author.)

Besides an overview over the problems and results of mathematical stability analyses in biomechanics, we apply the theory to a specific situation. More precisely, we consider a waiter holding a glass of water. The task is not to spill the water in the glass under perturbations. The question is, whether less water is spilled by a high or a low co-activation of the elbow muscles. The mathematical analysis will show that the answer depends on the position of the upper arm.

1. Introduction

Considering the large degree of freedom as well as the complexity of our locomotion system it seems to be hopeless for engineers to control bipedal walking machines. Internal and external disturbances increase these difficulties. One strategy to cope with disturbances is to change behavior, i.e. to change the motor program. But thinking about jogging on some uneven terrain one might imagine the enormous dataflow and the high demands on the accuracy which are necessary to cope with all variations via the central nervous system.

Therefore it seems to be advantageous to use an "intelligent" mechanical system which unburdens the central nervous system [2]. The mechanical system itself should be stable with respect to small perturbations, e.g. the mechanical arrangement of the three segments of legs supports the global stability of locomotion [15]. Human locomotion is based on muscular contractions. From this viewpoint, muscles are reduced to simple force generators. Within the last few years, however, several studies have shown that the musculoskeletal system acts not only as a simple force generator but as a controller which selfstabilizes the locomotion, cf. [19], [17], [4], [18], [22], [5], [13], [14], [23], [1] and [24].

First indications that the properties of muscles may stabilize an envisioned movement were achieved from simulation studies, cf. [21] and [3]. Here, the reactions of the system following a perturbation were more stable if physiological muscles were included in the model compared to simple moment driven models.

Several different models exist to describe the force production of musculoskeletal systems. They range from very simple models describing the muscles as springs up to highly complex models, cf. [9], [26], [11], or three-dimensional models based on finite elements theory FEM, cf. [20], [10], [12]. Therefore a model to describe an envisioned situation must be adapted properly to the situation.

To discuss stability in a mathematical sense we use the framework of dynamical systems and apply it to biological musculoskeletal systems. To investigate the selfstabilizing properties of single muscle contractions, quick-release contractions can be used as a simple perturbation test [16]. Here, a muscle contracts isometrically when suddenly the external load is released and the muscle contracts. From experiments and simulations we found that the muscle tends toward a new asymptotically stable equilibrium; the muscle properties provide a selfstabilized system because stability was achieved in experiments and in the model without neural feedback. As a next step, it is necessary to analyze the interaction between muscle properties and the geometry of a joint.

In this article, we are interested in the stabilizing properties of muscles and the skeleton in general. Therefore, we consider the most important components of muscle force production, i.e. force length relation f_l, force velocity relation H and the geometry of the joint h. The activation $E(t) = E$ of each muscle is assumed to remain constant for this article. We

study a general joint with one extensor and one flexor muscle, in particular we consider the human elbow joint. For a detailed description of the model and the dependency on a weight in the hand as a model for acrobatics cf. [6].

In this setting we give the mathematical definition of stability of an equilibrium point. By the mathematical tool of linearization around the equilibrium one can decide whether the equilibrium is stable. The eigenvalues of the linearization around the equilibrium will provide this information. Moreover, they give a more detailed characterization of solutions near the equilibrium: real and complex eigenvalues lead to qualitatively different behavior of solutions [25], and the absolute value of their real part tells us how fast the equilibrium state is approached after a small perturbation. The linearization, however, will not provide information about the basin of attraction consisting of all initial conditions of perturbation which will tend to the equilibrium point, since it can only give local information near the equilibrium. The basin of attraction of an equilibrium can be analyzed using a Lyapunov function [8] or with other methods [7].

As an interesting application we show that the optimal stability strategy may depend on the circumstances. As a simple example we consider a waiter with a glass filled with water. The task is not to spill the water in the glass under perturbations, and we ask for the optimal strategy of the waiter. One may think, that a high co-activation of the elbow muscles resulting in a stiff characteristic of the elbow joint is the best strategy to cope with perturbations. The mathematical analysis, however, will show that the answer depends on the position of the upper arm. In some situations a low co-activation of the elbow muscles minimizes the amount of spilled water. This simple example shows that the mathematical analysis of the stability in biomechanics is not only an important and interesting interdisciplinary subject, but also provides unexpected insights into the biomechanics of movements.

2. Model

We present a model for a general joint connecting two bones, in particular, we will consider the elbow joint. The model will be sketched here, for more details cf. [6]. The upper arm is assumed to be fixed, e.g. by other muscles, whereas the lower arm is assumed to be a solid rod of uniform density which can only move in a fixed plane. We will later consider the two cases of a plane parallel or orthogonal to the ground level, cf. Figure 1. Then the position of the system is totally described by the angle between upper and lower arm, which we denote by x, and its angular velocity $v = \dot{x}$. We obtain the following equation of motion:

$$\left\{ \begin{array}{rcl} \dot{x} & = & v \\ \dot{v} & = & \frac{1}{J}\tilde{T}(x,v) =: T(x,v) \end{array} \right. \tag{1}$$

where $J = \frac{1}{3}ml^2$ denotes the moment of inertia, m denotes the mass of the upper arm, and l is the length of the upper arm.

We assume that the joint has two antagonistic muscles (which may summarize groups of muscles), namely the extensor muscle extending the angle and the flexor muscle decreasing the angle. In the case of the elbow joint, the most important muscles are the extensor muscle triceps brachii and the flexor muscles biceps and brachioradialis. The torque

$$\tilde{T}(x,v) \quad = \quad \tilde{T}_{grav}(x) + \tilde{T}_e(x,v) + \tilde{T}_f(x,v) \tag{2}$$

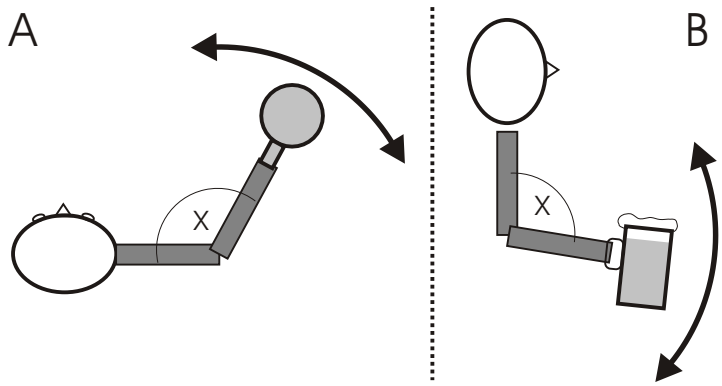

Figure 1. The task of a waiter is not to spill the water in the glass while walking. A. The movement is restricted to the horizontal plane. B. The arm movement is restricted to the sagittal plane. In both cases the flexion angle x describes the position of the arm.

consists of three parts corresponding to the gravitational force and to the forces generated by the extensor and the flexor muscles.

While the torque corresponding to the gravitational force depends on the position of the plane within which the upper arm is allowed to move, the torque for the flexor muscle is given by $\tilde{T}_f(x,v) = A_f \cdot f_{lf}(x) \cdot H_f(h_f(x)v) \cdot h_f(x)$, and similarily for the torque of the extensor muscle $\tilde{T}_e$. Here, f_l denotes the dependency of the muscle on its length, H denotes the Hill-function modelling the dependency of the muscle on its velocity $h_f(x)v$, and h denotes the effective moment arm, reflecting the geometry of the joint. The product $f_l(x) \cdot H(h(x)v) \cdot h(x)$ represents the maximal torque which can be generated, and $A \in [0,1]$ denotes the activation level of the muscle which is assumed to be constant. For the explicit formulas of the force-length function f_l, the Hill-function H and the effective moment arm h cf. [6].

3. Stability

In this section we analyze the conditions for stability as given in [23]. For a general system of differential equations as (1), the theory of dynamical systems defines an equilibrium point to be a solution which is constant in time. An equivalent condition for an equilibrium point (x_0, v_0) is that it is a zero of the right-hand side, i.e. in our case $v_0 = 0$ and $T(x_0, 0) = 0$. This corresponds to a situation, where the torques sum up to zero. In view of (2), this is equivalent to a certain dependency of the activation A_e on A_f cf. (3) or, alternatively, the other way round.

$$A_e(A_f) \;=\; -\frac{\tilde{T}_{grav}(x_0)}{f_{le}(x_0)H_e(0)h_e(x_0)} - \frac{f_{lf}(x_0)H_f(0)h_f(x_0)}{f_{le}(x_0)H_e(0)h_e(x_0)} \cdot A_f \qquad (3)$$

The concept of stability describes the behavior of solutions of the differential equation with initial conditions near the equilibrium. If the equilibrium is asymptotically stable,

then these solutions tend towards the equilibrium as time tends to infinity, and they stay near the equilibrium. This behavior corresponds to perturbations of the equilibrium which are corrected by the system, and thus describes a selfstable situation. If the equilibrium is unstable, then there are perturbations which lead away from the equilibrium. Hence, this would force the human to change the muscle activations in order to keep the equilibrium position.

Mathematically the stability of an equilibrium can be analyzed using the linearized system at the equilibrium or in other words the Jacobian matrix of first derivatives of the right hand side of the differential equation. The eigenvalues of this matrix give us the following information about the stability of the equilibrium and the behavior of solutions near the equilibrium:

- Stability: the equilibrium is asymptotically stable, if the real parts of all eigenvalues are strictly negative, and unstable, if the real part of at least one eigenvalue is strictly positive.

- Qualitative behavior: critically damped if the eigenvalues are real and oscillating if they are complex.

- Quantitative information: the largest real part of all eigenvalues, denoted by $\mathrm{Re}\lambda_1$, indicates how fast the equilibrium is approached $\approx \exp(t\mathrm{Re}\ \lambda_1)$. Note that the influence of the other eigenvalues is exponentially small compared to this term, if the eigenvalues are distinct.

In our case, we calculate the Jacobian of the right hand side of (1). It reads $\begin{pmatrix} 0 & 1 \\ T_x(x_0,0) & T_v(x_0,0) \end{pmatrix}$, where the subscripts x and v denote the respective partial derivatives (cf. Appendix). The eigenvalues of the matrix are given by $\lambda_{1,2} = \frac{1}{2}\left[T_v(x_0,0) \pm \sqrt{T_v(x_0,0)^2 + 4T_x(x_0,0)}\right]$. Because of (2), (3) and the negative slope of the Hill-function H (force-velocity relation), i.e. $H'(w) < 0$ for all $w \in \mathbb{R}$, we obtain $T_v(x,v) < 0$ for all x and v. Hence, in this special case we can distinguish between the different cases of stability and the qualitative behavior depending on $T_x(x_0,0)$ and $T_v(x_0,0)$:

- Stability: if $T_x(x_0,0) < 0$, then the equilibrium is asymptotically stable, and if $T_x(x_0,0) > 0$, then the equilibrium is unstable.

- Qualitative behavior: if $T_v(x_0,0)^2 + 4T_x(x_0,0) > 0$, then the behavior is critically damped, and if $T_v(x_0,0)^2 + 4T_x(x_0,0) < 0$, then the behavior is oscillating.

All these information are of local nature, i.e. they apply only to a possibly very small neighborhood of the equilibrium point. The mathematical reason is that they are properties of the linearized system, which is derived from the original, nonlinear one by means of linearization at the equilibrium.

4. Results

We distinguish between different cases by the angle of the (fixed) upper arm with respect to the ground (Figure 1). We consider only the two extreme cases, namely 0° and 90°. The corresponding equation of motion is of the form (1), where T_{grav} has to be chosen appropriately.

The first case corresponds to the upper arm extended to the side and the lower arm moves in the horizontal plane (Figure 1A). In this situation the task of spilling as few water as possible means to minimize the maximal acceleration of the arm, i.e. to minimize $\max_{t\geq 0} |\ddot{x}(t)|$. Indeed, consider a totally filled glass: no water is spilled for all angles x. Since, as a first approximation, the water surface is orthogonal on the vector of force given by the muscle and gravitational force, the amount of spilled water depends on the absolute value of acceleration $\ddot{x}$.

The second case corresponds to the upper arm near the body and the glass moving in the sagittal plane (Figure 1B). The task this time is to minimize the maximal deflection, i.e. to minimize $\max_{t\geq 0} |x(t) - x_0|$, where $(x_0, 0)$ is the equilibrium position. Again, the water surface is orthogonal on the acceleration vector. In this situation, however, as a first approximation, the acceleration caused by the muscle forces does not make the water fall out of the glass due to the position of the glass which is fixed to the lower arm by assumption. Only the gravitational force has an influence on the amount of spilled water, again due to the position of the glass: it depends monotonously on the deflection $|x(t)-x_0|$.

For the mathematical analysis (cf. Appendix) we fix an equilibrium point $(x_0, 0)$. The initial condition (x_0, v_0), where v_0 is small, is derived from a short pat to enable a comparison between the different situations. We deal with the linearized equations, since we consider an initial condition near the equilibrium, so that the derived tendency also holds for the original system for a neighborhood of the equilibrium. The proof for this fact uses that the equilibrium is asymptotically stable, i.e. that for $t \to \infty$ the solution tends towards the equilibrium point. For finite times we use the smoothness of the flow. In the following we denote $y(t) := x(t) - x_0$, such that $\dot{y} = \dot{x}$ and $\ddot{y} = \ddot{x}$.

How to minimize the maximal acceleration of the glass?

For the maximal acceleration $a_{max} := \max_{t\geq 0} |\ddot{x}(t)|$ we distinguish between the cases $T_x(x_0, 0) + T_v(x_0, 0)^2 \geq 0$ (case 1) and $T_x(x_0, 0) + T_v(x_0, 0)^2 < 0$ (case 2). In case 1 the eigenvalues can be either real or complex and in case 2 they are complex.

In case 1 the maximal acceleration is attained at the initial time $t = 0$, whereas in the case 2 the maximal acceleration is attained at a time $t > 0$. For typical evolutions of $\ddot{x} = \ddot{y}$, cf. Figure 2. The maximal acceleration a_{max} divided by the initial velocity is given by

$$\left|\frac{a_{max}}{v_0}\right| = |T_v(x_0, 0)| \text{ in case 1, and by}$$

$$\left|\frac{a_{max}}{v_0}\right| = \sqrt{T_x(x_0, 0)} \cdot \exp\left(\frac{T_v(x_0, 0)}{\omega} \arctan\left(-\frac{\omega(T_x(x_0, 0) + T_v(x_0, 0)^2)}{T_v(x_0, 0)(3T_x(x_0, 0) + T_v(x_0, 0)^2)}\right)\right) \text{ in case 2}$$

where we denote $\omega := \sqrt{-4T_x(x_0, 0) - T_v(x_0, 0)^2}$.

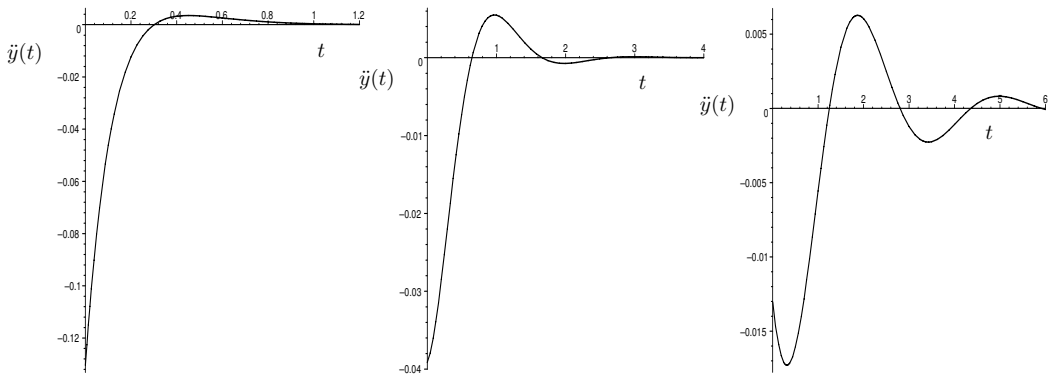

Figure 2. Schematical representation of typical reactions following a perturbation in arbitrary units (linearized equation). left: the acceleration $\ddot{y}(t) = \ddot{x}(t)$ if $4T_x(x_0,0) + T_v(x_0,0)^2 \geq 0$ (real, case 1); middle: the acceleration $\ddot{y}(t) = \ddot{x}(t)$ if $4T_x(x_0,0) + T_v(x_0,0)^2 < 0$ and $T_x(x_0,0) + T_v(x_0,0)^2 \geq 0$ (complex, case 1). For case 1 the maximal acceleration is attained for $t = 0$; right: the acceleration $\ddot{y}(t) = \ddot{x}(t)$ if $T_x(x_0,0) + T_v(x_0,0)^2 < 0$ (complex, case 2). The maximal acceleration is attained for $t > 0$.

How to minimize the maximal deflection of the glass?

Now we consider the maximal deflection d_{max}. We define $C := 1 + 4\frac{T_x(x_0,0)}{T_v(x_0,0)^2}$; note that $T_v(x_0,0) \neq 0$ due to the Hill-function in our model. The sign of C distinguishes between three different cases:

- $C > 0$: the eigenvalues of the matrix are real.
- $C < 0$: the eigenvalues are complex.
- $C = 0$: a double real eigenvalue.

The maximal deflection d_{max} divided by the initial velocity is given by

$$\begin{aligned}
\left|\frac{d_{max}}{v_0}\right| &= \frac{2}{|T_v(x_0,0)|}\left(1-\sqrt{C}\right)^{\frac{-1+1/\sqrt{C}}{2}}\left(1+\sqrt{C}\right)^{\frac{-1-1/\sqrt{C}}{2}} \text{ for } C>0\\
\left|\frac{d_{max}}{v_0}\right| &= \frac{2}{|T_v(x_0,0)|}\exp(-1) \text{ for } C=0\\
\left|\frac{d_{max}}{v_0}\right| &= \frac{1}{\sqrt{-T_x(x_0,0)}}\exp\left(-\frac{\arctan(\sqrt{-C})}{\sqrt{-C}}\right) \text{ for } C<0
\end{aligned}$$

For typical evolutions of $y(t) = x(t) - x_0$ in different cases, cf. Figure 3.

The only value a person can change at fixed angle is the co-activation of the muscles. More precisely, the angle x_0 and the flexor activation A_f determine the extensor activation A_e by the condition that $(x_0, 0)$ is an equilibrium, cf. (3). Thus, for the data of a person and a fixed angle x_0, we calculate the maximal deflection as a function of the flexor activation

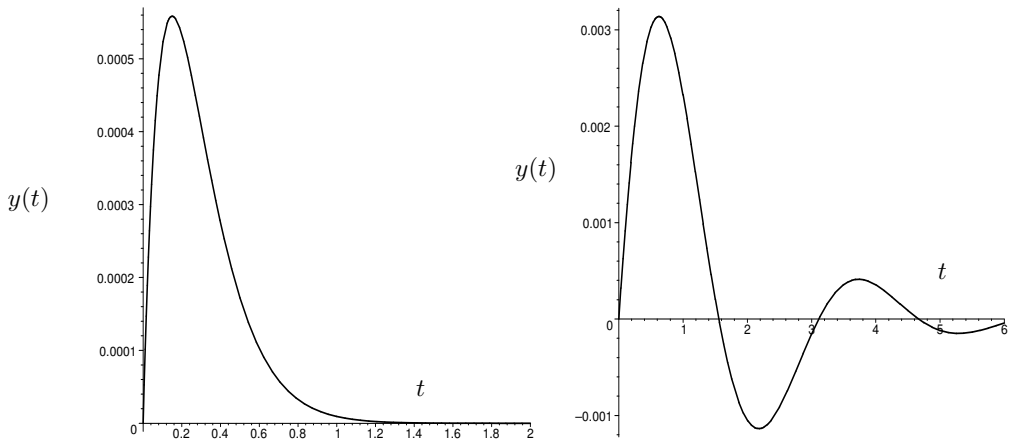

Figure 3. Schematical representation of typical reactions following a perturbation in arbitrary units (linearized equation). left: the deflection $y(t) = x(t) - x_0$ for $C > 0$ (real); right: the deflection $y(t) = x(t) - x_0$ for $C < 0$ (complex).

A_f (cf. Figure 4; for the data of the person cf. [6], we consider the movement in the sagittal plane, cf. Figure 1B). It turns out, that for the first situation the maximal acceleration is a strictly monotonously increasing function of the flexor activation. To minimize the spilled amount of water a low activation is optimal. For the second task, however, a similar analysis shows that the maximal deflection is a strictly monotonously decreasing function of the flexor activation (cf. Figure 5). To minimize the spilled amount of water in this situation a high activation is optimal.

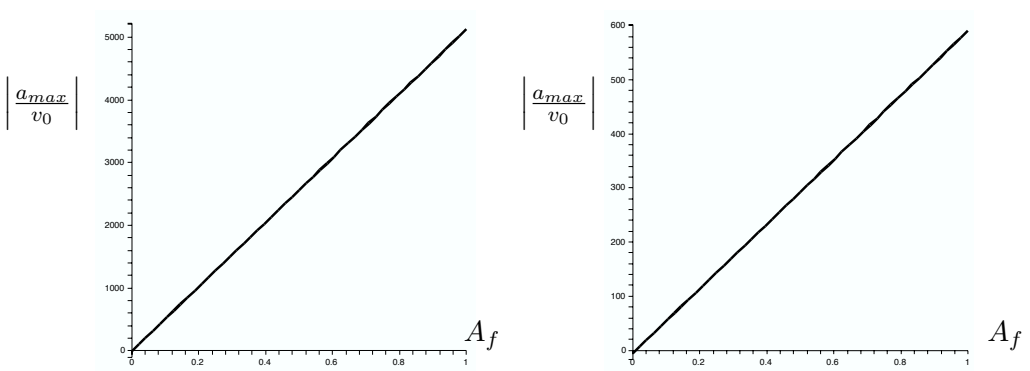

Figure 4. The maximal acceleration divided by the initial velocity $\left|\frac{a_{max}}{v_0}\right|$ depending on the flexor activation for the elbow angles left: $x_0 = 90°$ and right: $x_0 = 60°$. For both angles a low activation minimizes the maximal acceleration.

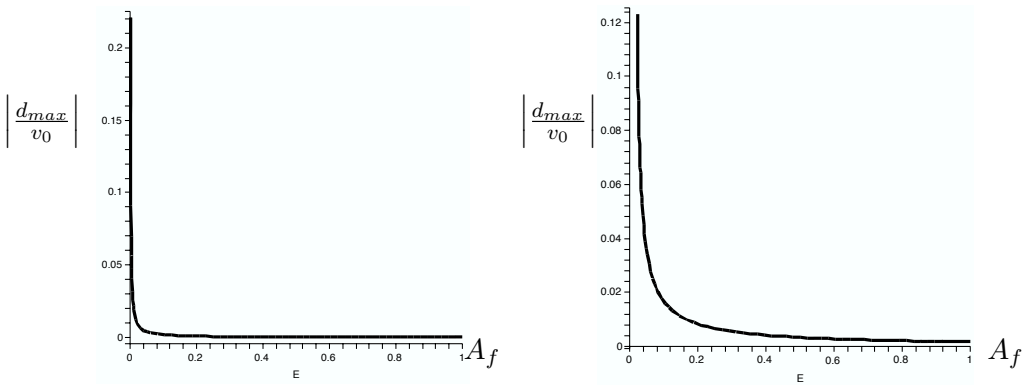

Figure 5. The maximal deflection divided by the initial velocity $\left|\frac{d_{max}}{v_0}\right|$ depending on the flexor activation for the elbow angles left: $x_0 = 90^\circ$ and right: $x_0 = 60^\circ$. For both angles a high activation minimizes the maximal deflection.

5. Discussion

In our biomechanical model we have described the force production of muscles, and the equation of motion for different experimental setups is used to study the stability of the systems. The question was, whether a high or a low co-activation of the elbow muscles should be used to minimize the maximal acceleration or deflection. Is an equilibrium point the "more stable" the faster small perturbations are corrected? On a first glance, the equilibrium might seem the "more stable", the faster small perturbations are corrected. But, as we have shown, this depends on the situation: a waiter with a glass will avoid spilling water and therefore will try to minimize the maximal acceleration or the maximal deflection, depending on the position of his upper arm. We have shown that, if the waiter holds the upper arm in the horizontal plane, a fast reaction means a high acceleration and thus here a lot of water will be spilled. The optimal behavior in this case is to come back to the original position as slowly as possible.

To understand the result, note that a high activation makes the arm stiff and causes a very fast reaction of the arm back to its original position. On the other hand, to minimize the spilled amount of water with the arm moving in the sagittal plane, a high activation is optimal. Therefore, the eigenvalues of a biomechanical model alone do not provide enough information for the optimal strategy concerning stability. This question can only be answered in relation to the movement task. If a subject is running on rough terrain with stiff legs, the head will perceive large deflections and accelerations. However, if the eigenvalues are negative but close to zero, the movement of the head is smooth, which is more comfortable [1].

If adapted to the envisioned task, the intrinsic properties of the musculoskeletal system are sufficient to generate self-stabilized movements, e.g. the negative slope of the force-velocity relation, the ascending limb of the force-length relation, co-activation of antagonistic muscles. The musculoskeletal system should not be reduced to a simple force generator. Both the intrinsic properties of the musculoskeletal system and the neural feedback system

provide the stability of the movement. In conclusion, the stability of biomechanical systems is an interesting and rich area. We have shown in a simple example that high stiffness in the sense of large (negative real parts of the) eigenvalues is not always the best strategy. In contrast, the optimal co-activation is task-dependent.

A. Appendix

We will derive the formulas of Section 3 and 4. We consider the solution of the linearized equation (set $y = x - x_0$)

$$\begin{pmatrix} \dot{y} \\ \dot{v} \end{pmatrix} = \begin{pmatrix} 0 & 1 \\ T_x & T_v \end{pmatrix} \begin{pmatrix} y \\ v \end{pmatrix}$$

with initial conditions $y(0) = 0$ and $v(0) = v_0$. Here and in the whole Appendix we use the abbreviations $T_x = T_x(x_0, 0)$ and $T_v = T_v(x_0, 0)$.

Real case

Let both eigenvalues of the above matrix $\lambda_{1,2}$, cf. Section 3., be real and distinct. Then the solution of the above initial value problem is given by $y(t) = \frac{v_0}{\lambda_1 - \lambda_2} (\exp(\lambda_1 t) - \exp(\lambda_2 t))$, where $0 > \lambda_1 > \lambda_2$ denote the eigenvalues. For the maximal acceleration we consider the border values $t = 0$ and $t \to \infty$ and we calculate the inner maxima via $\partial_t^3 y(t^*) = 0$. It turns out that $|\ddot{y}(t)|$ is maximal at $t = 0$: comparing $\ddot{y}(t^*) = -v_0 \lambda_1 \left|\frac{\lambda_1}{\lambda_2}\right|^{\frac{2\lambda_1+\lambda_2}{\lambda_2-\lambda_1}}$ with $\ddot{y}(0) = v_0(\lambda_1 + \lambda_2)$ we obtain the result since $\left|\frac{\lambda_1}{\lambda_2}\right| < 1$, $\frac{2\lambda_1+\lambda_2}{\lambda_2-\lambda_1} > 0$ and $|\lambda_1| < |\lambda_1 + \lambda_2|$ by the assumptions on the real case. The maximal deflection $|y(t)|$ is neither attained for $t = 0$ nor for $t \to \infty$ since in these cases y is equal to or tends to zero. In contrast, the maximum of the deflection is attained at $t^* = \frac{1}{\lambda_1 - \lambda_2} \ln \frac{\lambda_2}{\lambda_1}$.

Double eigenvalue

Note that in the case of a double eigenvalue, i.e. $\lambda_1 = \lambda_2$, the eigenspace is only one-dimensional. Hence, the solution of the initial value problem is given by $y(t) = v_0 t \exp(\frac{T_v}{2} t)$. For the maximal acceleration the procedure is the same as in the real case and the absolute value of the inner extremum, attained at $t^* = -\frac{6}{T_v}$, is smaller than $|\ddot{y}(0)|$. Concerning the maximal deflection $|y(t)|$, the maximum is attained at $t^* = -\frac{2}{T_v}$.

Complex case

In the complex case, we use the abbreviation $\omega = \sqrt{-4T_x - T_v^2}$ since $4T_x + T_v^2 < 0$. The solution of the initial value problem is then given by $y(t) = \frac{2v_0}{\omega} \exp\left(\frac{T_v}{2} t\right) \sin \frac{\omega}{2} t$. Here, local minima and maxima of $\ddot{y}(t)$ are attained at the points $t_k = \frac{2}{\omega} \left(\arctan\left(-\frac{\omega(T_x + T_v^2)}{T_v(3T_x + T_v^2)} \right) + k\pi \right)$ if $3T_x + T_v^2 \neq 0$ and at the points $t_k = \frac{2}{\omega} \left(\frac{\pi}{2} + k\pi \right)$ otherwise, where $k \in \mathbb{Z}$. It is clear that the absolute values of the inner extrema decrease as k increases, since the exponential term decreases.

If $T_x + T_v^2 < 0$, then $t_0 > 0$ and the absolute value of the first inner extremum is larger than $|\ddot{y}(0)|$ (complex, case 2). Otherwise (complex, case 1) the global maximal absolute value of the acceleration is attained at $t = 0$.

We first consider case 2, i.e. $T_x + T_v^2 < 0$, thus also $T_x < 0$ and $3T_x + T_v^2 < 0$, so that $\frac{T_x+T_v^2}{3T_x+T_v^2} > 0$ holds and we have $t_0 > 0$. The first inner extremum at t_0 is larger than $|\ddot{y}(0)|$, since $\ddot{y}(0)$ and $\partial_t^3 y(0)$ have the same sign.

In case 1, we compare $|\ddot{y}(0)| = |v_0 T_v|$ to $|\ddot{y}(t_k)| = |v_0|\sqrt{|T_x|}\exp\left(\frac{T_v}{2}t_k\right)$, $k = 0, 1$. Note that by case 1 we have $|T_v| \geq \sqrt{|T_x|}$. We consider the three subcases $3T_x + T_v^2 > 0$, $3T_x + T_v^2 = 0$ and $3T_x + T_v^2 < 0$. If $3T_x + T_v^2 > 0$, then $t_0 \geq 0$ and thus $\left|\frac{\ddot{y}(t_0)}{v_0}\right| \leq \sqrt{|T_x|} \leq |T_v|$. If $3T_x + T_v^2 = 0$, then $t_0 = \frac{\pi}{\omega}$ and thus $\left|\frac{\ddot{y}(t_0)}{v_0}\right| = \sqrt{|T_x|}\exp\left(\frac{T_v}{2\omega}\pi\right) < |T_v|$. If $3T_x + T_v^2 < 0$, then note that $t_0 \leq 0$ and $-\frac{\pi}{2} \leq \arctan\left(-\frac{\omega(T_x+T_v^2)}{T_v(3T_x+T_v^2)}\right) \leq \frac{\pi}{2}$, i.e. $\exp\left(\frac{T_v}{\omega}\left(\arctan\left(-\frac{\omega(T_x+T_v^2)}{T_v(3T_x+T_v^2)}\right)+\pi\right)\right) \leq \exp\left(\frac{T_v}{\omega}\frac{\pi}{2}\right) < 1$. Hence, $\left|\frac{\ddot{y}(t_1)}{v_0}\right| < \sqrt{|T_x|} \leq |T_v|$.

Concerning the maximal deflection, local minima and maxima of $y(t)$ are attained at the points $t_k = \frac{2}{\omega}[\arctan\left(-\frac{\omega}{T_v}\right) + k\pi]$ for $k = 0, 1, 2, \ldots$ and the global maximal value of $|y(t)|$ is attained at $t_0 = \frac{2}{\omega}\arctan\left(-\frac{\omega}{T_v}\right)$.

The dependency on the flexor activation

The formulas for $\tilde{T}_e(x, v)$ and $\tilde{T}_f(x, v)$ are, taking into account (3)

$$\begin{aligned}
\tilde{T}_f(x,v) &= A_f \cdot f_{lf}(x) \cdot H_f(h_f(x)v) \cdot h_f(x) \\
\tilde{T}_e(x,v) &= \left[-\frac{\tilde{T}_{grav}(x_0)}{f_{le}(x_0)\cdot H_e(0)\cdot h_e(x_0)} - \frac{f_{lf}(x_0)\cdot H_f(0)\cdot h_f(x_0)}{f_{le}(x_0)\cdot H_e(0)\cdot h_e(x_0)}\cdot A_f\right] \\
&\quad \cdot f_{le}(x)\cdot H_e(h_e(x)v)\cdot h_e(x)
\end{aligned}$$

Since the torque is given by

$$\begin{aligned}
JT(x,v) &= \tilde{T}_{grav}(x) + \tilde{T}_f(x,v) + \tilde{T}_e(x,v) \\
&= \tilde{T}_{grav}(x) - \frac{\tilde{T}_{grav}(x_0)}{f_{le}(x_0)\cdot H_e(0)\cdot h_e(x_0)}\cdot f_{le}(x)\cdot H_e(h_e(x)v)\cdot h_e(x) \\
&\quad + A_f\Bigg(f_{lf}(x)\cdot H_f(h_f(x)v)\cdot h_f(x) \\
&\qquad - \frac{f_{lf}(x_0)\cdot H_f(0)\cdot h_f(x_0)}{f_{le}(x_0)\cdot H_e(0)\cdot h_e(x_0)}\cdot f_{le}(x)\cdot H_e(h_e(x)v)\cdot h_e(x)\Bigg)
\end{aligned}$$

we obtain for the derivatives of T with respect to x and v, $T_x(x_0, 0)$ and $T_v(x_0, 0)$, respectively, where we denote by ∂_x and ∂_v the partial derivatives with respect to x, v.

$$\begin{aligned}
JT_x(x_0,0) &= \partial_x\tilde{T}_{grav}(x_0) - \frac{\tilde{T}_{grav}(x_0)}{f_{le}(x_0)\cdot H_e(0)\cdot h_e(x_0)} \\
&\quad \cdot[\partial_x f_{le}(x_0)\cdot H_e(0)\cdot h_e(x_0) + f_{le}(x_0)\cdot H_e(0)\cdot \partial_x h_e(x_0)] \\
&\quad + A_f\Bigg(\partial_x f_{lf}(x_0)\cdot H_f(0)\cdot h_f(x_0) + f_{lf}(x_0)\cdot H_f(0)\cdot \partial_x h_f(x_0) \\
&\quad - \frac{f_{lf}(x_0)\cdot H_f(0)\cdot h_f(x_0)}{f_{le}(x_0)\cdot H_e(0)\cdot h_e(x_0)}
\end{aligned}$$

$$\cdot[\partial_x f_{le}(x_0)\cdot H_e(0)\cdot h_e(x_0) + f_{le}(x_0)\cdot H_e(0)\cdot \partial_x h_e(x_0)]\Big)$$

$$\begin{aligned} JT_v(x_0,0) &= -\frac{\tilde{T}_{grav}(x_0)}{f_{le}(x_0)\cdot H_e(0)\cdot h_e(x_0)}\cdot f_{le}(x_0)\cdot H_e'(0)\cdot h_e^2(x_0) \\ &\quad + A_f\Big(f_{lf}(x_0)\cdot H_f'(0)\cdot h_f^2(x_0) \\ &\quad - \frac{f_{lf}(x_0)\cdot H_f(0)\cdot h_f(x_0)}{f_{le}(x_0)\cdot H_e(0)\cdot h_e(x_0)}\cdot f_{le}(x_0)\cdot H_e'(0)\cdot h_e^2(x_0)\Big) \end{aligned}$$

Note that in the first situation the arm is parallel to the ground, i.e. $\tilde{T}_{grav}(x) = 0$, whereas in the second situation the arm is orthogonal to the ground, i.e. $\tilde{T}_{grav}(x) = \frac{1}{2}glm\sin x$, where l denotes the length and m the mass of the upper arm, and g is the gravitational constant. For the formulas of the functions f_l, H and h as well as for the data, cf. [6].

References

[1] Blickhan, R., H. Wagner, et al., Brain or muscles? Recent Research Developments in Biomechanics, *Transworldresearch*, S. G. Pandalai. Trivandrum, India 1, 215–245 (2003).

[2] Blickhan, R., et al., Intelligence by mechanics, *Phil Trans R Soc A* **365**, 199–220 (2007).

[3] Brown, I. E. and G. E. Loeb, A reductionist approach to creating and using neuromusculoskeletal models, *Neuro-Control of posture and movement* (2000).

[4] Dariush, B., M. Parnianpour, et al., Stability and a control strategy of a multilink musculoskeletal model with applications in FES, *IEEE Trans Biomed Eng* **45**, 3–14 (1998).

[5] Dickinson, M. H., C. T. Farley, et al., How animals move: an integrative view, *Science* **288**, 100–106 (2000).

[6] Giesl, P., D. Meisel, et al., Stability analysis of the elbow with a load, *J Theor Biol* **228**, 115–125 (2004).

[7] Giesl, P. and H. Wagner, On the Determination of the Basin of Attraction for Stationary and Periodic Movements, in: Fast Motions in Biomechanics and Robotics, M. Diehl and K. Mombaur (eds.), Springer-Verlag, *LNCIS* **340**, 147–166 (2006).

[8] Giesl, P. and H. Wagner, Lyapunov functions and the basin of attraction for a single-joint muscle-skeletal model, *J Math Biol* **54(4)**, 453–464 (2007).

[9] Hatze, H., A Myocybernetic Control Model of Skeletal Muscle, *Biol Cybern* **25**, 103–119 (1977).

[10] Johansson, T., P. Meier, et al., A finite-element model for the mechanical analysis of skeletal muscles, *J Theor Biol* **206(1)**, 131–149 (2000).

[11] Ma, S. P. and G. I. Zahalak, A distribution-moment model of energetics in skeletal muscle, *J Biomech* **24**, 21–35 (1991).

[12] Meier, P. and R. Blickhan, FEM-Simulation of Skeletal Muscle: The Influence of Inertia During Activation and Deactivation, in: *Skeletal Muscle Mechanics: From Mechanismus to Funtion*, W. Herzog, John Wiley & Sons, 207–224 (2000).

[13] Schmitt, J. and P. Holmes, Mechanical models for insect locomotion: dynamics and stability in the horizontal plane I. Theory, *Biol Cybern* **83(6)**, 501–515 (2000).

[14] Schmitt, J. and P. Holmes, Mechanical models for insect locomotion: dynamics and stability in the horizontal plane II. Application, *Biol Cybern* **83(6)**, 517–527 (2000).

[15] Seyfarth, A., M. Günther, et al., Stable operation of an elastic three-segment leg, *Biol Cybern* **84**, 365–382 (2001).

[16] Siebert, T., H. Wagner, et al., Not all oscillations are rubbish: Forward simulation of quick-release experiments, *JMMB* **3(1)**, 107–122 (2003).

[17] Taga, G., A model of the neuro-musculo-skeletal system for human locomotion I. Emergence of basic gait, *Biol Cybern* **73(2)**, 97–111 (1995).

[18] Taga, G., A model of the neuro-musculo-skeletal system for anticipatory adjustment of human locomotion during obstacle avoidance, *Biol Cybern* **78(1)**, 9–17 (1998).

[19] Taga, G., Y. Yamaguchi, et al., Self-organized control of bipedal locomotion by neural oscillators in unpredictable environment, *Biol Cybern* **65(3)**, 147–159 (1991).

[20] van der Helm, F. C., A finite element musculoskeletal model of the shoulder mechanism, *J Biomech* **27**, 551–569 (1994).

[21] Van Soest, A. J. and M. F. Bobbert, The contribution of muscle properties in the control of explosive movements, *Biol Cybern* **69**, 195–204 (1993).

[22] Wagner, H. and R. Blickhan, Stabilizing function of skeletal muscles: an analytical investigation, *J Theor Biol* **199(2)**, 163–179 (1999).

[23] Wagner, H. and R. Blickhan, Stabilizing Function of Antagonistic Neuromusculoskeletal Systems – an Analytical Investigation, *Biol Cybern* **89**, 71–79 (2003).

[24] Wagner, H. and P. Giesl, Self-stability in Biological Systems – Studies based on Biomechanical Models, in: Fast Motions in Biomechanics and Robotics, M. Diehl and K. Mombaur (eds.), Springer-Verlag, *LNCIS* **340**, 403–410 (2006).

[25] Wagner, H., P. Giesl and R. Blickhan, Musculoskeletal stabilization of arm movements – complex or real, *JMMB* **7(3)**, 275–296 (2007).

[26] Zajac, F. E., Muscle and tendon: properties, models, scaling, and application to biomechanics and motor control, *Crit Rev Biomed Eng* **17(4)**, 359–411 (1989).

In: Mathematical Biology Research Trends
Editor: Lachlan B. Wilson, pp. 275-294
ISBN: 978-1-60456-141-8

Chapter 11

THE BEHAVIOUR OF THE LIPID VESICLE UNDER OSMOTIC STRESS

Dumitru Popescu[1,2], Liviu Movileanu[3,4*] and Alin Gabriel Popescu[5]

[1]Department of Neurobiology and Biophysics, Faculty of Biology, University of Bucharest, Spl. Independentei 91–95, Bucharest, Romania

[2]Institute of Mathematical Statistics and Applied Mathematics, Calea 13 Septembrie 13, Bucharest, Romania

[3]Department of Physics, Syracuse University, 201 Physics Building, Syracuse, New York 13244-1130, USA

[4]Structural Biology, Biochemistry, and Biophysics Program, Syracuse University, 111 College Place, Syracuse, New York 13244-4100, USA

[5]Faculty of Automatic Control and Computer Science, Polytechnic University of Bucharest, Spl. Independentei 313, Bucharest, Romania

Abstract

There is a great interest for a mechanistic understanding of molecular transport across biological and reconstituted membranes due to its potential applications to the development of news methodologies in medical biotechnology, such as gene therapy and drug delivery. In the first part of this paper, we present the behavior of the liposomes under osmotic stress. Because of the mechanical tension induced by osmotic flow, the liposomes expand, triggering transient lipidic pores that fluctuate at the nanoscopic level until their death. We report here that this is a periodic process. Such a liposome, also called a pulsatory liposome, is characterized by the number of successive pores, the time interval between two successive pores, and the amount of exchanged material through a single transmembrane pore. The diffusion of water through the liposomal membrane is analyzed in detail. In the second part of this paper, we develop a theoretical model for analyzing experimental data, facilitating information about the diffusion and exchange through spherical interfaces. The effects of experimental parameters, including the bilayer stiffness and the viscosity of the internal fluid, are analyzed and discussed as well.

* E-mail address: lmovilea@physics.syr.edu (The author to whom correspondence should be addressed)

Introduction

The transport of small molecules and macromolecules through transient transmembrane pores is a fundamental and ubiquitous process in modern cell biology. The large interest for the exploration of pores by experimental, computational and theoretical approaches is dramatically growing not only for a better understanding of molecular traffic across biomembranes, but also potential applications in medical biotechnology. In general, the transmembrane pores are either proteinaceous or lipidic. Here, our approach is devoted only for those pores that transiently appear in the lipid bilayer, and with their wall formed by phospholipids. Some pores can appear due to structural and dynamic properties of the lipid bilayer (Popescu et al., 1991; Popescu and Victor, 1991; Popescu and Rucareanu, 1992; Movileanu and Popescu, 1995, 1996, 1998; Movileanu et al., 1997, 1998; Popescu et al., 1997). These transient transmembrane pores have a stochastic nature (Popescu et al., 2003; Movileanu and Popescu, 2004; Movileanu et al., 2006). Recently, in vesicles stretched by induced tension, a single pore of several micrometers in diameter was observed (Karatekin et al., 2003). However, in the same vesicle, a few tens of transmembrane pores can appear successively. In this paper, we show a theoretical approach for demonstrating that a successive formation of pores can take place in a liposomal membrane.

There are two very interesting biotechnological applications that require the increase of membrane permeability: gene therapy and targeted drug delivery. In the first one, the transport of DNA fragments through cellular and nuclear membranes is requested (Varma and Somia, 1997). The second application uses drug molecules encapsulated in lipid vesicles, which have to be transported to a targeted place (Lasic and Needham, 1995; Zasadzinski, 1997). In the second application, the lipid vesicle has to release the drug molecules in a well-controlled and accurate fashion. The appearance of transient transmembrane pores may be stimulated using chemical and physical methods (Bar-Ziv et al., 1998; Saitoh et al., 1998; Bernard et al., 2000; Fournier et al., 2003). The chemical methods are based on the addition of an external agent (Debregeas et al., 1995; Dietrich et al., 1997; Dietrich et al., 1998). Using physical methods, including electroporation (Weaver and Chizmadzhev, 1996), osmotic shock (Dvolaitsky et al., 1993), temperature jump (Lasic, 1993), and adhesion on porous or decorated substrate (Guedeau-Boudeville et al., 1995), one can produce a stretch of the vesicle membrane, which eventually relaxes, forming transient pores. These pores may reach diameters up to 10 μm (Sandre et al., 1999).

The appearance of transient pores through the cellular membrane, which are caused by mechanical tension, is a possibility for the intracellular material to be transported outside the cell. In article, we present a formalism for analyzing the successively formed transient pores induced in a vesicle by osmotic stress, and the time interval between two successive pores. In the first part, we describe the transient pore dynamics. Then, the solute concentration inside the vesicle, depending on the time elapsed, was calculated. An interesting application in medicine is discussed: transient pores in liposomes could be used for compensation of neurotransmitter deficiency in the synaptic cleft. This article is consisted of four parts: 1) the phenomenological bases of pulsatory liposomes, 2) the internal chemical changes, 3) the pore dynamics and 4) the numerical results.

Phenomenological Bases of a Pulsatory Liposome

Let us consider a lipid vesicle filled with aqueous solution containing an impermeable solute. The vesicle is inserted into an aqueous hypotonic medium. Initially, the vesicle membrane is smooth and unstretched. Osmotic pressure created by the gradient of solute concentration determines an influx of water molecules through liposomal membrane. The supplementary water entered inside the liposome has two consequences: the dilution of the internal solution and the swelling of the liposome. Also, the surface tension increases in the same time with with liposomal expansion. The surface tension increases the pressure inside the cell. Under these experimental conditions, either the liposal membrane may be ruptured or one pore may appear through its lipid bilayer. If the swelling process is slow enough, the liposome increases up to a critical size, in which a transient transmembrane pore forms. This event is followed by two simultaneous processes: the pore dynamics and the leak out of the internal material of the vesicle, due to Laplace pressure. The pore dynamics consists of two phases: 1) the pore diameter increases up to the maximum radius, r_m, and 2) the pore diameter decreases until the closure of the pore (Fig. 1). Both phenomena, the increase in the pore diameter and the leakage of the internal liquid, determine the membrane relaxation due to the reduction in the mechanical tension of the membrane. As a matter of fact, the pore dynamics is driven by the difference between the membrane tension and line tension (Fig. 2).

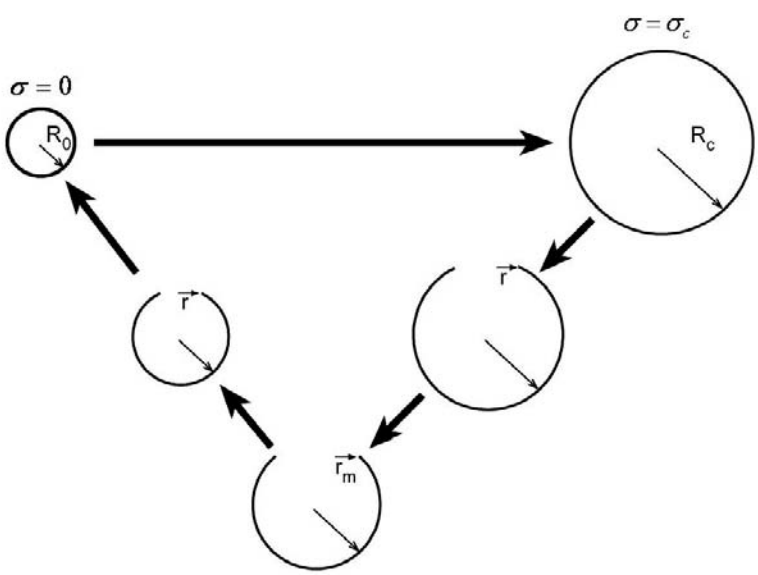

Figure 1. The evolution of a pulsatory liposome during a single cycle.

The membrane tension decreases until it becomes equal to the line tension of the membrane edge. The internal liquid continues to leak outside the liposome, even after the line tension equals to the membrane tension. From the time when the line tension equals to the membrane tension the second part of the pore dynamics starts, and so the pore radius reduces until the the closure of the pore. Therefore, the liposomes is in its initial size. We can envision that the dynamics of the vesicle described above can start over. This cyclic process ceases

when the osmotic gradient becomes smaller that a critical value, which will be discussed below.

The Change of the Chemical Composition of Internal Solution

Let us suppose at the beginning of its activity the lipid vesicle contains solute and water, with the molar concentrations c_{s0}, c_{w0}, respectively. Due to the influx of water, the vesicle swells itself and its radius increases from R_0 (the smooth and relaxed state) to R_c (just before the appearance of the transient pore) (Fig. 1). The quantity of water entered a lipid vesicle in each cycle is given by the following expression:

$$N^+ = \frac{4\pi\left(R_c^3 - R_0^3\right)}{3V_{\mu w}} = \frac{4\pi R_c^3}{3V_{\mu w}}\left(1 - \frac{R_0^3}{R_c^3}\right) = N\left(1 - f\right) \tag{1}$$

Where the molar volume of water is noted as $V_{\mu w}$. In the formula presented above, we introduced the following notations:

$$N = \frac{V_c}{V_{\mu w}} = \frac{4\pi R_c^3}{3V_{\mu w}} \tag{2}$$

which is the number of moles of water that would fill the stretched vesicle just before the appearance of the pore, if only water would be present.

Here,

$$\frac{1}{f} = \frac{V_c}{V_0} = \frac{R_c^3}{R_0^3} \tag{3}$$

is the reversal of swelling ratio, that is the ratio between the vesicle volumes in the stretched state (V_c), just before the pore formation, and in the relaxed state (V_0).

The Internal Liquid Composition after Each Cycle

So far, we noticed that in each cycle the liposome supports a swelling process followed by a relaxation process. Let us analyze the first cycle in both phases.

The swelling stage

At the beginning of the first cycle, the lipid vesicle contains $N_{s1} = c_{s0}V_0$ moles of solute and $N_{w1} = c_{w0}V_0$ moles of water. At the end of the swelling stage, just before the opening of

the pore, the same amount of solute is present in the lipid vesicle, but this contains a larger amount of water:

$$N_{w1} = N_{w1} + N^{+} = c_{w0}V_0 + N(1-f) \tag{4}$$

The new molar concentrations at the end of the first cycle are given by the following expressions:

$$c_{s1} = \frac{N_{s1}}{V_c} = \frac{c_{s0}V_0}{V_c} = fc_{s0} \tag{5}$$

$$c_{w1} = \frac{N_{w1}}{V_c} = \frac{\left(c_{w0}V_0 + N(1-f)\right)}{V_c} = fc_{w0} + \frac{1-f}{V_{\mu w}} \tag{6}$$

Relaxation stage

After the opening of the pore, the pore radius increases up to a maximum value, then it decreases, and eventually the pore closes. During this pore dynamics, an amount of internal liquid leaks out. At the beginning of the second cycle, which is the same with the end of the first cycle and, the lipid vesicle is in a relaxed state. In this state, the lipid vesicle contains the following amounts of solute and water, measured in moles:

$$N_{s2} = V_0 c_{s1} = fV_0 c_{s0} \tag{7}$$

$$N_{w2} = V_0 c_{w1} = fV_0 c_{w0} + \frac{V_0(1-f)}{V_{\mu w}} \tag{8}$$

Making the same reasoning as for the first cycle, one can find the following recurrent formula for characterizing the internal composition of the lipid vesicle at the end of the n^{th} cycle:

$$N_{sn} = f^n V_0 c_{s0};\ N_{wn} = f^n V_0 c_{w0} + \frac{V_0\left(1-f^n\right)}{V_{\mu w}} \tag{9}$$

$$c_{sn} = f^n c_{s0};\ c_{wn} = f^n c_{w0} + \frac{1-f^n}{V_{\mu w}} \tag{10}$$

The n cycles liposome programming

The driving force of a pulsatory liposome is generated by the osmotic gradient through the lipid bilayer. The internal concentration of the solute decreases along a cycle and with the cycle rank in sequence. Therefore, the osmotic pressure decreases as well. The lipid vesicle will swell up to its critical radius, only if the osmotic pressure at the end of the cycle is greater

than the excess Laplace pressure. Starting with this condition, we can programme a pulsatory liposome to have *n* cycles in its life activity by the following condition:

$$\sigma_0\left(1/\left(R-h\right)+1/\left(R+h\right)\right)\le \Re T\left(c_{sn}^{in}+c_{sn}^{out}\right) \tag{11}$$

where, c_{sn}^{in} and c_{sn}^{out} are the solute concentrations at the end of the swelling stage of the n-th cycle, inside and outside the liposome. Considering that at the beginning of the cycle, the external concentration of the solute is equal to zero, and the composition of the external medium is not affected by by the vesicle running, we can take c_{sn}^{out} =0. Taking into account that c_{sn}^{in} is equal to c_{sn}, the condition mentioned in equation (11) becames:

$$2\sigma_0 R/\left(R^2-h^2\right)\le \Re T f^n c_{son} \tag{12}$$

where *R* is the radius of the sphere between the two monolayers of the liposomal bilayer, σ_0 is the surface tension of the monolayer at the end of the cycle, and *2h* is the hydrophobic thickness of the bilayer. $\Re$ is the universal gas constant, and *T* is the absolute temperature. For the symmetry of the above formula, we take $R=R_c+h$. Therefore, the initial concentration of solute inside the liposome, c_{son} is equal to

$$c_{s0n}=\frac{2\sigma_0 R}{\Re T f^n\left(R^2-h^2\right)} \tag{13}$$

If the initial concentration is known, then we can calculate the number of cycles of liposome activity from formula (12).

The solute content of the pulse

We have named the quantity of internal material leaked out in a cycle as material pulse, or simply pulse. Achieving the difference between the solute contained inside the lipid vesicle after two successive cycles, we obtain the quantity of solute contained in the pulse of internal solution delivered between the two cycles. Assuming a liposome programmed for n cycles, the solute content of the p-th puls is:

$$\Delta N_{sp}=N_{s(p-1)}-N_{sp}=f^{p-1}\left(1-f\right)V_0 c_{s0n}=\frac{2\sigma_0 R V_0\left(1-f\right)}{\Re T f^{n-p+1}\left(R^2-h^2\right)} \tag{14}$$

The Swelling Time of the Vesicle

The length of a cycle is equal to the sum of the pore lifetime and the swelling time. Here, we calculate the swelling time of the lipid vesicle. Due to the tonicity difference between the two

adjacent media separated by the lipid bilayer, the water will diffuse through the lipid bilayer into the lipid vesicle, which swells up to a critical diameter. The increase of the volume of the lipid vesicle in a dt time interval is determined by the water molecules that entered the lipid vesicle. Thereforwe,

$$dV = J_w A V_{\mu w} dt \tag{15}$$

where, V is the internal volume of the lipid vesicle, J_w is the water flow through the internal surface of the lipid bilayer with area, A , $V_{\mu w}$ is the molar volume of water. The relation (15) may be rewritten as:

$$4\pi R^2 dR = J_{\mathbf{w}} 4\pi R^2 V_{\mu w} dt \tag{16}$$

which gives, after simplification, the differential equation for the radius of the lipid vesicle:

$$dR = J_w V_{\mu w} dt \tag{17}$$

Integrating the differential equation mentioned above from R_0 (when the lipid bilayer is not stretched, $\sigma_0 = 0$) to R_c (when the liposome is stretched, just before the pore formation) one can obtain:

$$R_c - R_0 = J_w V_{\mu w} \tau \tag{18}$$

where τ is the swelling time of the liposome, which is the time needed by the liposome to reach its critical state starting from the initial relaxed state. Now, we introduce a mean concentration of water molecules in the lipid bilayer after the p-th cycle as:

$$\overline{c}_w = \kappa\left(c_w^{out} + c_{wp}^{in}\right)/2 \tag{19}$$

where c_w^{out} and c_{wp}^{in} are the water concentration outside and inside the lipid vesicle at the beginning of the p-th cycle, respectively. The constant κ is the partition coefficient of water within the lipid domain of the vesicle. The flow of water across the lipid bilayer is equal to:

$$J_w = \overline{c}_w \mathrm{v} \tag{20}$$

where $\mathbf{v}$ is the mean transport velocity of water molecules through the lipid bilayer. Taking into account the relations (18), (19), and (20), the swelling time in the n-th cycle is given by:

$$\tau_n = \frac{2\left(R_c - R_0\right)}{\kappa \mathrm{v}\left(c_w^{out} + c_{wn}^{in}\right)V_{\mu w}} \tag{21}$$

But the c_w^{out} and c_{wn}^{in} are c_{we} and c_{wn}, respectively. Taking into account that:

$$c_{we}V_{\mu w} = 1 \tag{22}$$

and

$$c_{wn}V_{\mu w} + c_{sn}V_{\mu s} = 1 \tag{23}$$

and plugging them into the formula (21), one can obtain the expression for the swelling time in the n-th cycle of the dynamics of the lipid vesicle:

$$\tau_n = \frac{2\left(R_c - R_0\right)}{\kappa v\left(2 - c_{sn}V_{\mu s}\right)} \tag{24}$$

The swelling time from the period of pulsatory liposome

Introducing the c_{son} formula in the relation (24), one can obtain the formula for swelling time in the p-th cycle of a lipid vesicle programmed to evolve over n cycles:

$$\tau_p = \frac{R_c - R_0}{k\mathbf{v}\left[1 - \frac{\sigma_0 R V_{\mu s}}{\Re T f^{n-p}\left(R^2 - h^2\right)}\right]} \tag{25}$$

The Pore Dynamics

Energetical Conditions for Pore Appearance

Most of the models describing the formation of a single transient pore in membranes are based on a simple hypothesis proposed three decades ago by Litster (Litster, 1975). According to this hypothesis, the membrane free energy change due to the formation of a transmembrane pore is given by the Litster relation:

$$\Delta E_p = 2\pi r\gamma - \pi r^2\sigma \tag{26}$$

A stochastic pore may tend to open or close, depending on the forces acting on its boundary (Fig.2). The appearance of a circular pore of radius r, in a membrane with the surface tension coefficient σ, is determined by the presence of two competing energetic terms: a reduction in the free energy by a surface tension component ($-\pi r^2\sigma$), and an increase in free energy by a line tension component ($+2\pi r\gamma$). Here, γ is the line tension.

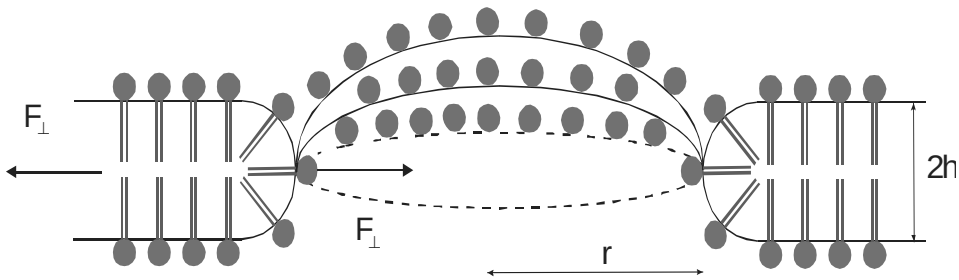

Figure 2. A cross-sectional view through a lipid bilayer containing a single transmembrane pore. Its dynamics is determined by the balance of two opposing forces. The opening of the pore is driven by the force F_σ generated by the membrane tension, whereas the closure of the pore is driven by the force F_γ due to the line tension.

The height of the free energy barrier is equal to:

$$\Delta E_{\max} = \pi \frac{\gamma^2}{\sigma} \tag{27}$$

and this is fulfilled for a critical pore radius,

$$r_0 = \frac{\gamma}{\sigma} \tag{28}$$

The line tension, γ, is caused by the hydrophobic property of phospholipids, and contributes to the free energy barrier that hinders pore formation. This component is favourable to the closing of the pore. The surface tension coefficient, σ, reduces the free energy barrier for the formation of the pore. This component drives an increase in the pore diameter.

The free energy change due to the bilayer deformation following the appearance of the pore is lost due to the internal viscosity of the lipid bilayer. Therefore, the free energy change due to the internal viscosity of the lipid bilayer is given by the following expression:

$$\Delta E_v = 4\pi r \eta_m h \frac{dr}{dt} \tag{29}$$

Equating the two energy changes of the lipid bilayer, one can obtain a differential equation for the pore radius:

$$\pi r^2 \sigma - 2\pi r \gamma = 2\pi r \eta_s \frac{dr}{dt} \tag{30}$$

$$r\sigma - 2\gamma = 2\eta_s \frac{dr}{dt} \tag{31}$$

Here, we introduce the surface viscosity, $\eta_s = 2h\eta_m$.

The equation (31) describes the pore dynamics. Unfortunately, it is difficult to solve this equation, because the membrane tension σ is not a constant. We consider a lipid vesicle in a relaxed state, when the membrane tension is nil ($\sigma = 0$), and its radius is R_0. If this lipid vesicle experiences a membrane tension, the radius will be dependent on the surface tension coefficient σ:

$$R(\sigma) = R_0\sqrt{1+\frac{\sigma}{E}} \tag{32}$$

where E is the elastic modulus for surface stretching or compression, and is equal to:

$$E = \frac{48\pi K_H^2}{R_0^2 kT} \tag{33}$$

In this formula, K_H is the Helfrich bending constant and kT is the thermal energy (Brochard et al., 1976; Brochard et al., 2000).

An analytical expression for the surface tension coefficient σ

Let us suppose that from the initial state with the surface tension coefficient $\sigma = 0$ and the radius R_0, the vesicle is stretched up to a critical state, just before the appearance of the pore. In this critical state, the lipid vesicle has the radius R_c, and the membrane tension is equal to σ_c. In any state between these ones, the vesicle is characterized by a radius R ($R_0 < R < R_c$), and a membrane tension σ ($0 < \sigma < \sigma_c$), which are related by the equation (32). The surface area in each of the three states is given by the following formulas:

$$A_0 = 4\pi R_0^2; \qquad A = 4\pi R^2 = 4\pi R_0^2\left(1+\frac{\sigma}{E}\right); \qquad A_c = 4\pi R_c^2 = 4\pi R_0^2\left(1+\frac{\sigma_c}{E}\right) \tag{34}$$

After its formation, the pore expands in the first part of its lifetime, then it decreases, and finally it closes. In the same time, membrane tension decreases from σ_c to zero. The membrane tension decreases due to two factors: 1) the growth of the pore and 2) the leakage of internal liquid due to the excess in Laplace pressure. We assume that the lipidic mass from the membrane is conserved during the pore lifetime. We can imagine a vesicle state at a given moment from its dynamics, when the pore radius is equal to *r*, and the lipid bilayer tension is σ. The following relation may be written:

$$4\pi R_c^{\,2} = 4\pi R_0^{\,2}\left(1+\frac{\sigma}{E}\right)+\pi r^2 \tag{35}$$

If one considers the case which internal liquid is gelified, therefore zero leakage, the pore reaches its maximum radius, named critical pore radius and marked as r_c. In this case, the lipid membrane is in a relaxed state ($\sigma = 0$), and the following relation is available:

$$4\pi R_c^{\,2} = 4\pi R_0^{\,2} + \pi r_c^2 \tag{36}$$

Combining the relations (34), (35), (36), an anlitical formula for the membrane tension can be obtained:

$$\frac{\sigma}{\sigma_c} = 1 - \frac{r^2}{r_c^2} - \frac{R_c^2 - R^2}{R_c^2 - R_0^2} \tag{37}$$

The pore hydrodynamics

After the appearance of the pore, the internal liquid comes out and the vesicle decreases in its size. The flow of the expelled liquid is: $Q = \pi r^2 v$, where r is the radius of the pore, and v is the mean leak-out velocity of the internal liquid. The flow divided by the time has to be equal to the rate of change of the volume of the lipid vesicle:

$$Q = \frac{\partial V_{vez}}{\partial R} \tag{38}$$

The internal liquid is pushed out through the transient pore by a Laplace pressure ΔP:

$$\Delta P = \frac{2\sigma}{R} \tag{39}$$

The force for pushing out is given by the following expression:

$$F_p = \Delta P \cdot \pi r^2 \tag{40}$$

This force may be equal to the shear viscosity force, which is involved in the outward flow:

$$F_v = 3\pi\eta_l r \,\mathrm{v} \tag{41}$$

Taking into account the above relations (39), (40) and (41), the outward flow velocity of the internal liquid is:

$$v = \frac{2\sigma r}{3R\eta_l} \tag{42}$$

Introducing the formula (42) in the relation (38), one can obtain an exact equation for the radius of the lipid vesicle:

$$\frac{2\pi\sigma r^3}{3R\eta_l} = 4\pi R^2 \frac{dR}{dt} \tag{43}$$

The pore dynamics is described by equations (31), (37) and (43). Hence, we will name them as dynamics pore equations. Their solutions are $r(t), \sigma(t)$ and $R(t)$.

Lifetime of the Pore

The lifetime of the pore is strongly dependent on the viscosity of the internal liquid of the lipid vesicle. If the viscosity of the internal liquid is low, then both the radius of the pore and the lifetime of the pore are small because the liquid is squeezed out very rapidly when the pore just opens. More interesting is the case when the internal liquid has a slow leakage. In the slow leak-out regime, both experimental results and theoretical predictions point out a dependence of the radius of the pore on time as that drawn in Fig. 3.

In this paper, we will use the dynamics pore equations for the calculation of the lifetime of the pore. The lifetime of the pore is equal with sum of time for pore expansion up to maximum value of its radius, and the time for its decrease up to its closure.

The expansion time

As one can see, the expansion time is very short. We assume that the internal liquid does not leak out from the vesicle in this short time. It results that the approximation $R \approx R_c$ is good and the bilayer tension is given by:

$$\frac{\sigma}{\sigma_c} \approx 1 - \frac{r^2}{r_c^2} \tag{44}$$

So the equation (31) becomes:

$$r\left(1 - \frac{r^2}{r_c^2}\right) = 2\eta_s \frac{dr}{dt} \tag{45}$$

Integrating this differential equation when the radius of the pore runs in the range $[r_0, r_m]$, one can find the expansion time t_e:

$$t_e = \tau\left(\ln\frac{r_m}{r_0} - \frac{1}{2}\ln\frac{r_c^2 - r_m^2}{r_c^2 - r_0^2}\right) \tag{46}$$

We used the following notations:

$$\tau = \frac{2\eta_s}{\sigma_0} \tag{47}$$

with the initial pore radius $$r_0 = \frac{\gamma}{\sigma_c} \tag{48}$$

and the maximum radius of the pore r_m

When the radius of the pore attains its maximum, $\sigma_m r_m = \gamma$, because $dr/dt = 0$.

It results an equation for r_m:

$$\frac{\gamma}{\sigma_c} \approx r_m \left(1 - \frac{r_m^2}{r_c^2}\right) \tag{49}$$

The solution of this equation is:

$$r_m \approx r_c - \frac{\gamma}{2\sigma_c} \tag{50}$$

The pore decrease time

After the radius of the pore reached its maximum, the liquid continues to leak out slowly and the driving force changes its direction: $\sigma r \le \gamma$. The liquid leaking out reduces the membrane tension, whereas the radius of the pore increases. This is the reason for which the driving force closing the pore is nearly equal to zero, and the membrane tension increases slowly:

$$\sigma \approx \frac{\gamma}{r} \tag{51}$$

Derivating the equation (37), and taking into account that $d\sigma/dt \approx 0$, one can obtain:

$$4R\frac{dR}{dt} = r\frac{dr}{dt} \tag{52}$$

Taking into account the relations (51) and (52), then the equation (31) for the pore dynamics becomes:

$$\frac{dr}{dt} \cong \frac{-2\gamma}{3\pi\eta_l}\frac{r}{R^2} \tag{53}$$

We integrate the equation (53):

$$\int_{r_m}^{r_0} \frac{dr}{r} = \frac{-2\gamma}{3\pi\eta_l R_0^2} \int_0^{t_d} dt \tag{54}$$

and we obtain the decrease time, for the second stage of its dynamics, noted with t_d :

$$t_d = \frac{3\pi\eta_l R_0^2}{2\gamma} \ln \frac{r_m}{r_0} \tag{55}$$

The closing time

When the radius of the pore has reached its inital value, the pore closes very quickly. In this state, the membrane tension is nearly equal to zero. The closing state is decribed by the equation (31), if we put $\sigma = 0$:

$$\frac{dr}{dt} \cong \frac{-\gamma}{2\eta_s} \tag{56}$$

The closing time results from the integration of the equation (56):

$$\int_{r_0}^{0} dr = \frac{-\gamma}{2\eta_s} \int_0^{t_c} dt \tag{57}$$

Therefore, the closing time t_c is:

$$t_c = \frac{2\eta_s r_0}{\gamma} \tag{58}$$

The Time of the N-Cycle of the Pulsatory Lipid Vesicle

It is easy to see that the periode of the cyclic process experienced by the lipid vesicle under osmotic stress is composed by the sum of the lifetime of the pore and the swelling time of the lipid vesicle. Therefore, a cycle with duration T_n is given by:

$$T_n = t_n + t_e + t_d + t_c \tag{59}$$

Replacing all the time intervals with their corresponding expressions, we obtain the time of the n-th cycle:

$$T_n = \frac{2\left(R_c - R_0\right)}{\kappa v\left(2 - c_{sn} V_{\mu s}\right)} + \tau\left(\ln\frac{r_m}{r_0} - \frac{1}{2}\ln\frac{r_c^2 - r_m^2}{r_c^2 - r_0^2}\right) + \frac{3\pi\eta_l R_0^2}{2\gamma}\ln\frac{r_m}{r_0} + \frac{2\eta_s r_0}{\gamma} \tag{60}$$

$$T_n = \frac{2\left(R_c - R_0\right)}{\kappa v\left(2 - c_{sn} V_{\mu s}\right)} - \frac{\tau}{2}\ln\frac{r_c^2 - r_m^2}{r_c^2 - r_0^2} + \left(\tau + \frac{3\pi\eta_l R_0^2}{2\gamma}\right)\ln\frac{r_m}{r_0} + \frac{2\eta_s r_0}{\gamma} \tag{61}$$

If the pore was programmed a priori to run n cycles, then the period of the p-th cycle of n-cycles programmed vesicle is:

$$T_{pn} = \frac{R_c - R_0}{k v\left[1 - \frac{\sigma_0 R V_{\mu s}}{\Re T f^{n-p}\left(R^2 - h^2\right)}\right]} - \frac{\tau}{2}\ln\frac{r_c^2 - r_m^2}{r_c^2 - r_0^2} + \left(\tau + \frac{3\pi\eta_l R_0^2}{2\gamma}\right)\ln\frac{r_m}{r_0} + \frac{2\eta_s r_0}{\gamma} \tag{63}$$

Numerical Results and Discussion

We apply our theoretical results mentioned above to the giant vesicles obtained experimentally (Karatekin et al., 2003). Such giant vesicle has the radius in relaxed state, R_0 = 19.7 μm and the value of the critical radius is R_c = 20.6 μm. The thicknees of the lipid bilayer is of 5 nm (Karatekin et al., 2003). Let us consider a vesicle in a closed chamber that contains water. The transport velocity through the lipid bilayer is $v = 10^5$ Å/s (Sackmann et al., 1978). The partition coefficient of water in the lipid bilayer is $\kappa = 64\ 10^{-6}$ (Lawaczeck 1979). In fact, κ must represent the partition coefficient of water in the hydrophobic core of the lipid bilayer. Also, we consider the maxim value of the bilayer tension, just before the formations of the pore $\sigma_0 = 10^{-5}$ N/m (Nardi et al., 1998).

The initial quantity of solute. If one introduces the above values in the formula (13), the initial concentration of solute inside the vesicle, measured in nM, if this runs over *n* cycles is:

$$N_{s0n} = \frac{12.45}{f^n} \tag{64}$$

The calculated value for the reversal swelling coefficient, *f*, is equal to 0.8746 for the considered vesicle. The dependence of the initial solute concentration on the programmed activity life, measured in cycles number is represented in Fig. 3.

Because the fraction $\frac{\sigma_0}{\Re T}$ appears in all formulae, we have calculated it separately and its value is equal to $4 * 10^{-9}\, mol.m^{-2}$.

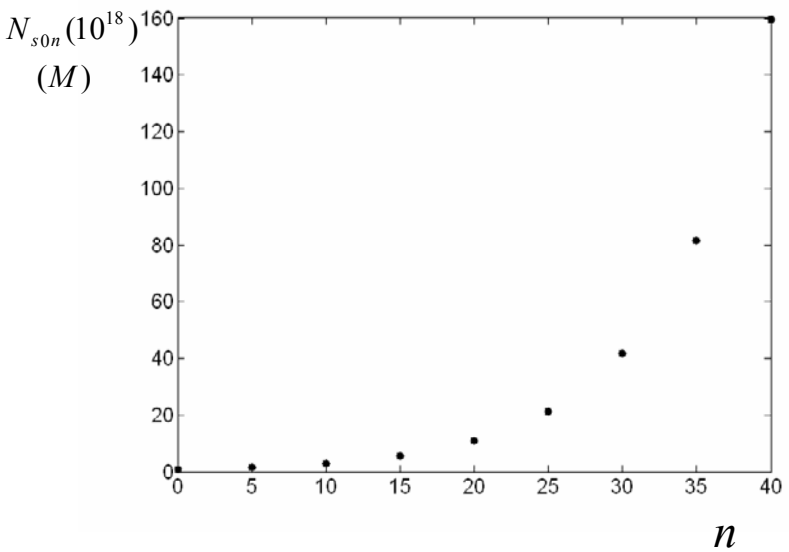

Figure 3. The dependence of the initial solute concentration on the programmed activity life, measured in cycles number.

The amount of solute delivered through a single transient pore

We think that it is useful to express the amount of solute delivered through a single pore in number of molecules than in mols. Introducing all data in formula (14) one obtain:

$$\Delta N_{sp} = \frac{425(1-f)10^4}{f^{n-p}} \tag{65}$$

We chose a liposome armed to work n cycles. The number of solute molecules leaked out from liposome through the p^{th} pore of n-sequence is given by formula (65). For a pulsatory liposome programmed to have 40 cycles, the solute quantity delivered versus p is represented in Fig. 4.

The activity life of a pulsatory liposome

It is obviously that the pulsatory lipozome life with the sum of all time length cycles. Therefore, for an n-cycle liposome its life, t_n is equal to:

$$t_n = \sum_{p=1}^{n} T_{np} \tag{66}$$

We assume that the pore life time does not depend on the pore rank in the sequence, although the pore lifetime is influenced by the viscosity of the internal liquid that changes with the solute dilution. The pore life time is up to 10 sec. For the pulsatory liposome selected here, the time, measured in minutes, of the p-th cycle is:

$$\tau_{np} = \frac{375}{16\left(1 - \frac{2*10^{-4} V_{\mu s}}{f^{n-p+1}}\right)} \tag{67}$$

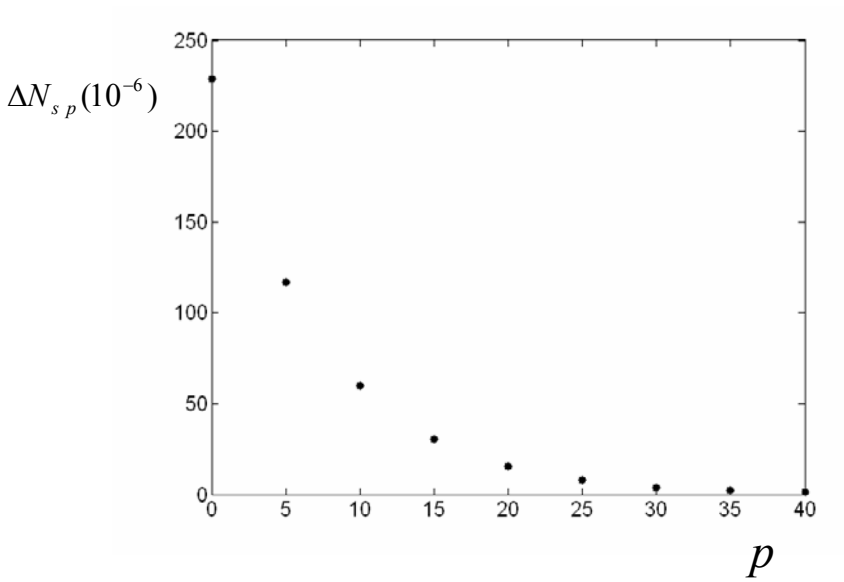

Figure 4. For a pulsatory liposome programmed to have 40 cycles, the solute quantity delivered versus p.

It is known that the water pass through the lipid bilayer with a very low probability due to a high free energy barrier for crossing the membrane. We find this situation at the beginning of the each individual cycle, but more than likely that the water molecules pass through lipid bilayer the reason that the bilayer is composed from a mixture of lipid molecules. For this reason, the bilayer is heterogeneous in its own nature, containing microclusters determined by the selective dynamic association of lipid molecules (Popescu and Victor 1990; Popescu 1993; Movileanu et al., 1997, 1998). The bilayer is neither smooth, nor static, and has a heterogeneous thickness. As a consequence, the vesicle is deformable in the relaxed state from the beginning of each cycle. Therfore, it is very possible that very small structural defects appear in the membrane, and these are used by the water molecules to come into the lipid vesicle. On the other hand, the pores are very large, up to 10 μm (Karatekin et al., 2003). Larger molecules, or greater amount of the internal liquid can leak out the lipid vesicle. A very interesting application of the pulsatory liposomes filled with drugs is in the case of hepatic cells. The endotethelial pores (also known as fenestrae) control the exchange of fluids, solutes and particles between the sinusoidal blood and the space of Disse. The free pulsatory liposomes or those included in other lipid vesicles may reach the hepatocyte due to hydrodynamic effects of blood circulation (Popescu et al., 2000). The transient pores in liposomes could be used for compensation of neurotransmitter deficiency in the synaptic cleft as well (Popescu et al., 2006).

Acknowledgments

The authors thank Cornel Zaharia and Viorel Paun for stimulating discussions. The authors are also grateful to Stelian Ion for his help during the preliminary stage of this study. LM acknowledges funding by Syracuse University start-up funds, and the US National Science Foundation DMR-706517.

References

Bar-Ziv, R., Nelson, P., Moses, E., 1998. Dynamic excitations in membranes induced by optical tweezers. *Biophys. J*. **75294**-320.

Bernard, A.-L., Guedeau-Boudeville, M.-A., Sandre, O., Palacin, S., di Meglio, J.-M., Jullien, L., 2000. Permeation through lipid bilayers by adhesion of giant vesicles on decorated surfaces. *Langmuir* **16**, 6801-6808.

Brochard, F., de Gennes, P. G., Pfeuty, P., 1976. Surface tension and deformations of membrane structures : relation to two dimensional phase transitions, *J.Phys. I (France)* **37**, 1099–1103.

Brochard, F., de Gennes, P. G., Sandre, O., 2000. Transient pores in stretched vesicles : role of leak–out, *Physica A* **278**, 32–51.

Debregeas, G., Martin, P., Brochard-Wyart, F., 1995.Viscous bursting of suspended films. *Phys.Rev.Lett*. **75**, 3886-3889.

Dietrich, A., Bahr, G., Winterhalter, M., 1998. Influence of polylisine on the rupture of negatively charged membranes. *Langmuir* **14**, 4597-4605.

Dietrich, A., Angelova, M., Pouligny, B., 1997. Adhesion of latex spheres to giant phospholipids vesicles: statics and dynamics. *J. Phys. II (Paris)* **7**, 1651-1682.

Dvolaitsky, M., de Gennes, P. G., Guedeau, M.-A., Jullien, L., 1993. *C.R. Acad. Sci. Paris* **316** (II), 1687-1690.

Fournier, L., Joos, B., 2003. Lattice model for the kinetics of rupture of fluid bilayer membranes. *Phys. Rev. E* **67**, 5190-5197.

Guedeau-Boudeville M-A, Jullien L and Di Meglio J-M., 1995 Drug delivery piercing vesicles by their adsorption onto a porous medium *Proc. Natl. Acad. Sci. USA* **92**, 9590–9592.

Karatekin E, Sandre O, Guitouni H, Borghi N, Puech P-H., Brochard-Wyart, F., 2003. Cascades of Pores in Giant Vesicles: Line tension and transport. *Biophys. J.* **84**, 1734-1749.

Lasic, D. D., Needham, D., 1995. The "Stealth" liposome: a prototypical biomaterial. *Chem. Rev*. **95**, 2601-2628.

Lasic D. D., 1993. *From Physic to Application in Liposomes*, Elsevir, Amsterdam, 318-321.

Lawaczeck, R., 1979. On the permeability of water molecules across vesicular lipid bilayers. *J. Membrane Biol*. **51**, 229-261.

Litster, J. D., 1975. Stability of Lipid Bilayers and Red Blood–Cell Membranes, *Phys. Letters A* **53**, 193–194.

Movileanu, L., Popescu, D., 1995, Differential length effects into a binary mixture of single-chain amphiphiles in planar monolayers. A three-dimensional approach. *BioSystems* **36**, 43-53.

Movileanu, L., Popescu, D., 1996, Global ratio of efficiency in a single chain binary mixture. *J. Biol. Systems* **4**, 425-432.

Movileanu, L., Popescu, D., Victor, G., Turcu, G., 1997. Selective association of phospholipids as a clue for the passive flip-flop diffusion through bilayer lipid membranes. *BioSystems* **40**, 263-275.

Movileanu, L., Popescu, D., Flonta, M.L., 1998. The hydrophobic acyl-chain effect in the lipid domains appearance through phospholipid bilayers. *J. Mol. Struct. (THEOCHEM)* **434**, 213-227.

Movileanu, L., Popescu, D., 1998. A theoretical model for the association probabilities of saturated phospholipids from two-component bilayer lipid membranes. *Acta Biotheor.* **46**, 347-368.

Movileanu, L., Popescu, D., 2004. The birth, life and death of statistical pores into a bilayer membrane. In: *Recent Research Developments in Biophysics* (chapter 4), vol. 3, Part I, Transworld Research Network, Kerala, pp. 61-86.

Movileanu, L., Popescu, D., Ion, S., Popescu, A., 2006. Stochastic pores appearance in BLMs. *Bulletin of Mathematical Biology* **68**, 1231-1255.

Nardi, J., Bruinsma, R., Sackmann, E., 1998. Adhesion-induced reorganization of charged fluid membranes. *Phys. Rev. E Stat. Phys. Plasmas Fluids Relat Interdisp Top*. **58**, 6340-6354.

Popescu, D., Victor, G., 1990. Association probabilities between the single chain amphiphiles into a binary mixture *Biochim. Biophys. Acta* **1030**, 238-250.

Popescu, D., Rucareanu, C., Victor, G., 1991. A model for the appearance of the statistical pores in membranes due to the selfoscillations *Bioelectrochem. Bioenerg.* **25**, 91-105.

Popescu, D., Victor, G., 1991. The Transversal Diffusion-Coefficient of Phospholipid Molecules Through Black Lipid-Membranes. *Bioelectrochem. Bioenerg*. **25**, 105-108.

Popescu, D., Rucareanu, C., 1992. Membrane selfoscillations model for the transbilayer statistical pores and flip–flop diffusion. *Mol. Cryst. Liquid Cryst.* **25**, 339-348.

Popescu, D., 1993. Association probabilities between single chain amphiphiles into a binary mixture in plan monolayers (II). *Biochim. Biophys. Acta* **1152**, 35-43.

Popescu, D., Movileanu, L., Victor, G., Turcu, G., 1997. Stability and instability properties of aggregation of single-chain amphiphiles into binary mixtures. *Bull. Math. Biol*. **59**, 43-61.

Popescu, D., Movileanu, L., Ion, S., Flonta, M. L., 2000. Hydrodynamic effects on the solutes transport across endothelial pores and hepatocytes membranes. *Phys. Med. Biol.* **45**, N157- 165.

Popescu, D., Ion, S., Popescu, A.I., Movileanu, L., 2003, Elastic properties of bilayer lipid membranes and pore formation. In: *Membrane Science and Technology Series* (vol. 7), Planar Lipid Bilayers (BLMs) and Their Applications, H. Ti Tien and A. Ottova (Eds.), Elsevier Science Publishers, Amsterdam, pp. 173-204.

Popescu, D., Zaharia, C. N., Ion, S., Flonta, M. L., 2006. Compensation of the neurotransmitters deficiency in the synaptic cleft. *Romanian J. Biophys*. **16**. 189-204.

Sackmann, E., Albrecht, O., Gruler, H., 1978. Polymorphism of phospholipid monolayers, *J. Physique* **39**, 301–313.

Saitoh, A., Takiguchi, K., Tanaka, Y., Hotani, H., 1998. Openimg up of liposomal membranes by talin. *Proc. Natl. Acad. Sci. USA* **95**, 1026-1031.

Sandre, O., Moreaux, L., Brochard-Wyart, F., 1999. Dynamics of transient pores in streched vesicles. *Proc. Natl. Acad. Sci. USA* **96**, 10591-10596.

Verma, I.M., Somia, M., 1997. Gene therapy–promises, problemes and prospects. *Nature (London)* **389**, 239-242.

Zasadzinski, J.A., 1997. Novel approaches to lipid based drug delivery. *Curr. Opin. Solid State Mat. Sci.* **2,** 345-349.

Weaver, J.C., Chizmadzhev, Y., 1996. Theory of electroporation: A review. *Bioelectrochem. Bioenerg*. **41**, 135-160.

INDEX

A

B

C

D

E

F

G

H

I

J

K

L

M

N

O

P

Q

R

S

T

U

V

W

X

Y

Z